



University
of Glasgow

Muinonen-Martin, Andrew James (2013) Melanoma cells induce LPA gradients that drive chemotactic dispersal and invasion. PhD

<http://theses.gla.ac.uk/4836/>

Copyright and moral rights for this thesis are retained by the author

A copy can be downloaded for personal non-commercial research or study, without prior permission or charge

This thesis cannot be reproduced or quoted extensively from without first obtaining permission in writing from the Author

The content must not be changed in any way or sold commercially in any format or medium without the formal permission of the Author

When referring to this work, full bibliographic details including the author, title, awarding institution and date of the thesis must be given.

Melanoma cells induce LPA gradients that drive chemotactic dispersal and invasion

Andrew James Muinonen-Martin

MBChB, MRCP(UK)

**Thesis submitted in fulfilment of the requirements
for the Degree of Doctor of Philosophy in the
Faculty of Medicine**

Beatson Institute for Cancer Research

College of Medical, Veterinary and Life Sciences

University of Glasgow

August 2013

Abstract

Melanoma is notoriously resistant to immuno- and even targeted chemotherapeutic strategies despite recent advances in drug development. The overall mortality of melanoma correlates with its ability to metastasise. Breslow thickness or the depth of invasion remains the most useful prognostic indicator, thereby linking the ability of the cells to invade with their propensity to metastasise. Invasion occurs early during tumour development, but the factors driving this process remain poorly understood. There is a growing appreciation that chemotaxis plays an important role in driving the migration and invasion of melanoma cells, but the key stimuli are not known.

Through the generation and validation of an improved chamber for cancer cell chemotaxis, melanoma cells are shown to create chemotactic gradients that drive or disperse themselves outwards with remarkable efficiency. This process is driven by strikingly positive chemotaxis and depends on the melanoma reaching a critical density to generate the gradient. The principal attractant is the inflammatory signal lysophosphatidic acid (LPA). Unexpectedly, it is active across all stages of melanoma evolution and LPA is both necessary and sufficient for chemotaxis in 2D & 3D assays. Growth Factors were previously considered to play essential roles in driving directed migration, but instead facilitate LPA chemotaxis. Sampling across the margins of melanomas *in vivo*, gradients of LPA are reliably identified, which are capable of driving accurate chemotaxis. This not only confirms the physiological importance of the results, but also is the first time a chemoattractant gradient has been measured *in vivo*.

The corollary of these findings is that, provided with an external homogenous source of LPA, a large enough melanoma will degrade the local LPA to generate an outward gradient. Therefore it is the ability to degrade the gradient that acts as the signal to drive chemotaxis and invasion rather than the presence of LPA *per se*. In the chambers, cells are observed dispersing in a wave and in addition to driving efficient melanoma invasion, this may be responsible for the patterning of melanocytes across the skin during embryogenesis. Ultimately, identifying key aspects of and targeting the LPA-axis may prove a novel prognostic indicator and therapeutic target for invasion and metastasis.

Dedication

During the course of my PhD studies, I have drawn inspiration from patients, friends and family affected by cancer. I dedicate this thesis to them.

Acknowledgements

There are many people who have contributed towards making this thesis a success and I am indebted to all of them. I apologise unreservedly to anyone who I have missed out. Firstly, I must thank my supervisor Robert Insall for the ideas, debate and enthusiasm that have inspired me. Support, guidance and wisdom were also provided by my advisor Rob Jones, as well as my clinical supervisor Robert Herd. I am also indebted to Laura Machesky for her guidance throughout informal meetings and lab meetings. I am grateful to all the members of the Insall and Machesky labs and a special mention must go to Pete Thomason and Heather Spence for their teaching of scientific procedures and assays. In addition: Michael Carnell for developing the stitching plugin; Douwe Veltman for designing the processing spreadsheet that aided every experiment I performed; Visiting Prof. Dave Knecht, whose approach made me consider every practical step in detail; and Jason King for many discussions and constructive criticism.

Also at the Beatson Institute, I am grateful to Don MacBean for producing the chamber cassettes and for drilling every chamber used throughout this thesis (and Epigem for manufacturing the chambers and adapting subsequent models); Owen Sansom, Liam Faller and Colin Lindsay for invaluable support with the murine work; Margaret O'Prey and Tom Gilbey for superb technical microscopy support to generate high quality images; Colin Nixon and histology services for processing organotypic and murine tissue. For help with the organotypic assays, I am grateful to members of Kurt Anderson's lab and in particular, Paul Timpson and Shereen Kadir, not to mention Mike Edward and Jean Quinn from the University of Glasgow.

A special mention must go to Dot Bennett (St. George's) for all her help and close collaboration from cell line provision to expert guidance on the project, cell culture techniques and advice on seeking ethical approval for collecting fresh primary melanoma tissue. The collection of human tissue was made possible through considerable effort provided in particular by Colin Moyes (Cons Pathologist) and Jane Hair (GGC Biobank) - along with her team. The support from Alan Lyell Centre for Dermatology and the West of Scotland Plastic Surgery service has also made this possible.

Finally, I am grateful to my wife and proofreader Liis who has offered love and support, especially during many absences at all hours and during, occasional, grumpy times. My wee daughters - Iris and Alice - have provided inspiration throughout. A special thank you too to my parents for their support, dedication and love from the beginning.

This work was initially supported by a Cancer Research UK Core Fellowship, which enabled me to gather the necessary data to successfully win a Wellcome Trust Research Training Fellowship.

Author's Declaration

I declare that the work described in this thesis was carried out personally unless otherwise stated and has not been submitted in full or in part for consideration for any other degree or qualification.

Andrew Muinonen-Martin

Definitions/ Abbreviations

BM	Basement membrane
BSA	Bovine serum albumin
cAMP	Cyclic adenosine monophosphate
CGM	Complete growth media
CI	Chemotaxis index
CM	Conditioned media
CO ₂	Carbon dioxide
CRE	Cre-recombinase
CSF-1	Colony stimulating factor-1
CTCs	Circulating tumour cells
°C	Degree centigrade
DIC	Differential interference contrast
DMSO	Dimethyl sulphoxide
DNA	Deoxyribonucleic acid
E	Embryonic day
ECM	Extracellular matrix
EDTA	Ethylenediaminetetraacetic acid
EGF	Epidermal growth factor
EGFR	Epidermal growth factor receptor
EMT	Epithelial-mesenchymal transition
EMU	Epidermal melanin unit
ET-3	Endothelin-3
FBS	Foetal bovine serum
FBSE	Full body skin examination
FFPE	Formalin fixed paraffin embedded
FN	Fibronectin
GFP	Green fluorescent protein
GF	Growth Factor
H&E	Haematoxylin and eosin
HGF	Hepatocyte growth factor/ scatter factor
HPLC	High-performance liquid chromatography
IHC	Immunohistochemistry
Kd	Dissociation constant
LC-MS	Liquid chromatography - mass spectrometry
LM	Lentigo maligna
LMM	Lentigo maligna melanoma
LPA	Lysophosphatidic acid
LPC	Lysophosphatidylcholine
LPP	Lipid phosphate phosphatase
LPAR	Lysophosphatidic acid receptor
LUT	Lookup table
MAG	Mono-acylglycerol
MAPK	Mitogen-activated protein kinase
MC1R	Melanocortin-1 receptor
MITF	Micropthalmia-associated transcription factor
MEM	Minimum Essential Medium
MIS	Melanoma in situ
MM	Metastatic Melanoma
µL	Microlitre
mg	Milligram

mL	Millilitre
mM	Millimolar
M	Molar
NA	Numerical aperture
nm	Nanometre
NM	Nodular melanoma
NMSC	Non-melanoma skin cancer
PBS	Phosphate buffered saline
PCR	Polymerase chain reaction
PDGF	Platelet derived growth factor
PFS	Perfect focus system
PA	Phosphatidic acid
PI3K	Phosphatidylinositol (4,5)-bisphosphate 3-kinases
PIP ₃	Phosphatidylinositol (3,4,5)-trisphosphate
PTX	Pertussis toxin
PTEN	Phosphatase and tensin homolog
PTX	Pertussis toxin
qPCR	Quantitative polymerase chain reaction
RCF	Relative centrifugal force
RGP	Radial growth phase
SC	Subcutaneous
SCF	Stem cell factor
SDF-1	Stromal cell derived factor-1
SEM	Standard error of the mean
sPLA ₂	Secretory-type phospholipase A ₂
SSM	Superficial spreading melanoma
TSSE	Total skin self-examination
Tyr	Tyrosinase
UV	Ultraviolet
UVA	Ultraviolet wavelength A
UVB	Ultraviolet wavelength B
UVR	Ultraviolet radiation
VEGF	Vascular endothelial growth factor
VGP	Vertical growth phase

Table of Contents

Chapter 1: Introduction	16
Cutaneous melanoma.....	18
1.1.1 <i>Introduction</i>	18
1.1.2 <i>Melanocyte development & homeostasis</i>	19
1.1.3 <i>Melanoma initiation</i>	23
1.1.4 <i>Melanoma progression model</i>	26
1.1.5 <i>Diagnosing melanoma</i>	29
1.1.6 <i>Treating cutaneous melanoma</i>	32
1.1.7 <i>Future directions</i>	34
Cancer cell metastasis	36
1.1.8 <i>Metastasis</i>	36
1.1.9 <i>Models of metastasis</i>	37
1.1.10 <i>Invasion & cell motility</i>	37
1.1.11 <i>Impact of the microenvironment on motility</i>	38
1.1.12 <i>Metastasis as a therapeutic target</i>	42
Chemotaxis.....	44
1.1.13 <i>Background</i>	44
1.1.14 <i>Dictyostelium discoideum: the chemotaxis role model</i>	44
1.1.15 <i>Translating the chemotactic signal to directional movement</i>	45
1.1.16 <i>Measuring chemotaxis</i>	46
Chemotaxis as a mechanism for cancer cell invasion	53
1.1.17 <i>The importance of cancer cell chemotaxis</i>	53
1.1.18 <i>Correlation of chemotaxis with metastatic ability</i>	55
1.1.19 <i>Cancer cell chemotaxis: membrane receptor signal transduction</i>	56
1.1.20 <i>Modelling chemotaxis of cancer cells with melanoma</i>	60
Lysophosphatidic acid (LPA).....	63
1.1.21 <i>Background</i>	63
1.1.22 <i>Structure & biological activity</i>	63
1.1.23 <i>LPA homeostasis</i>	64
1.1.24 <i>LPA signal transduction</i>	66
1.1.25 <i>Role of LPA signalling in vivo</i>	68
Aims of this study	70
Chapter 2: Materials & Methods	71
Materials.....	72
Cell biology	72
2.1.1 <i>Cell lines</i>	72
2.1.2 <i>Cell Culture</i>	73
2.1.3 <i>Cell Passaging & Counting</i>	73
2.1.4 <i>Cell preservation and recovery</i>	73
2.1.5 <i>Transfection</i>	74
Cell Motility Assays	74
2.1.6 <i>Insall chamber chemotaxis assay</i>	74
2.1.7 <i>Quantification of chemotaxis and statistical analysis</i>	80
2.1.8 <i>Random motility assay</i>	83
2.1.9 <i>Organotypic invasion assay</i>	83
Imaging	87
2.1.10 <i>Live cell imaging</i>	87
2.1.11 <i>Nikon Perfect Focus System (PFS)</i>	88
2.1.12 <i>Insall chamber validation</i>	88
In vivo studies: fresh melanoma tissue collection	89
2.1.13 <i>Fresh murine melanoma tissue collection</i>	89
2.1.14 <i>Fresh human melanoma tissue collection</i>	90
2.1.15 <i>Conditioned media & fresh melanoma LPA quantification</i>	93

Chapter 3: Development, Optimisation & Validation of an Efficient Assay for Cancer Cell Chemotaxis	95
Introduction.....	96
Chamber Development & optimisation	98
3.1.1 Chamber design	98
3.1.2 Extracellular matrix (ECM) coating	98
3.1.3 Handling and securing the coverslip	99
3.1.4 Reverse filling of the outer chemoattractant well.....	100
3.1.5 Gradients with simple orientations.....	100
3.1.6 Gradients with different steepnesses	101
3.1.7 Ongoing chamber evolution	101
Validation	103
3.1.8 Gradient stability and linearity	103
Capturing cell images & image processing	105
3.1.9 Phase & DIC microscopy.....	105
3.1.10 Fluorescence microscopy.....	105
3.1.11 Capturing and processing multiple images	107
Metastatic melanoma cells perform accurate chemotaxis towards 10% FBS	109
Insall chamber assay refinement	111
3.1.12 Starvation	111
3.1.13 Cell density	111
3.1.14 Best time window for analysis	113
Discussion	113
3.1.15 Conclusion.....	114
Chapter 4: The Inflammatory Signal LPA Drives Melanoma Chemotaxis and Invasion	116
Introduction.....	117
4.1.1 WM239A metastatic melanoma cells perform chemotaxis with a high degree of accuracy towards 10% FBS.....	118
Serum chemotaxis is universal across all stages	120
4.1.2 Serum chemotaxis is accurate across all stages.....	120
4.1.3 Speed is stage dependent.....	122
Identifying the chemoattractant(s) in serum	123
4.1.4 Growth factors drive chemokinesis	124
4.1.5 LPA is sufficient to drive chemotaxis with efficiency approaching that of 10% FCS	127
LPA is the dominant attractant in 2D & 3D assays	130
4.1.6 LPA is necessary to drive chemotaxis towards serum in WM239A metastatic melanoma cells.....	131
4.1.7 LPA is necessary to drive chemotaxis to serum consistently across multiple melanoma cell lines	136
4.1.8 LPA is necessary for invasion into 3D organotypic assays	140
The role of Growth factors in LPA chemotaxis	141
4.1.9 Growth factors act as accessory factors to enhance LPA chemotaxis	141
Discussion	144
4.1.10 Conclusion.....	146
Chapter 5: The Self-Generation of LPA Gradients Drives Melanoma Cell Dispersal	147
Introduction.....	148
Melanoma cells disperse in serum by positive chemotaxis	150
5.1.1 Melanoma cells disperse in uniform 10% FBS media.....	150
5.1.2 Melanoma cells do not disperse by contact inhibition of locomotion in 2D or 3D	152
5.1.3 Melanoma cell dispersal is density dependent	155
5.1.4 Melanoma cell dispersal is overwhelmingly driven by positive chemotaxis through depletion of a serum factor(s)	156

Melanoma cells degrade LPA to generate gradients driving dispersal	158
5.1.5 <i>Degradation of a serum factor(s) drives chemotaxis</i>	158
5.1.6 <i>LPA is depleted in melanoma cell conditioned medium</i>	159
5.1.7 <i>Biologically active LPA species are preferentially depleted</i>	161
5.1.8 <i>LPA is sufficient to generate a dispersal effect</i>	162
5.1.9 <i>LPA is necessary to generate a dispersal effect</i>	163
Fibroblasts and keratinocytes also degrade LPA	164
Patterning associated with self-generated gradients	166
5.1.10 <i>A wave precedes the patterning of the bridge with evenly spaced cells</i>	166
Discussion	166
5.1.11 <i>Conclusion</i> :.....	169
Chapter 6: The Identification of LPA Gradients Across The Margins of Melanomas <i>In Vivo</i>	171
Introduction.....	172
The generation of murine melanomas	173
6.1.1 <i>The Tyr::CreER^{T2} BRAF^{V600E/+} PTEN^{lox/+} mouse melanoma model</i>	173
6.1.2 <i>Suitability & characterisation of the Tyr::CreER^{T2} BRAF^{V600E/+} PTEN^{lox/+} mouse melanoma model for sampling LPA gradients</i>	173
6.1.3 <i>Incorporation of the 3Rs: replacement, reduction and refinement</i>	174
Sampling & quantifying LPA <i>in vivo</i>	175
6.1.4 <i>Quantification of LPA</i>	175
6.1.5 <i>Sampling methodology</i>	175
The identification of LPA gradients across murine melanomas.....	177
6.1.6 <i>LPA gradients exists across the margins of non-ulcerated murine melanomas</i> 177	
6.1.7 <i>Inverse LPA gradients exists across the margins of ulcerated murine melanomas</i>	179
6.1.8 <i>Steady LPA levels exist across normal murine skin</i>	181
The identification of LPA gradients across a human melanoma	183
Discussion	184
6.1.9 <i>Conclusion</i>	187
Chapter 7: Discussion	188
A summary of key findings generated by this thesis.....	189
7.1.1 <i>The Insall chamber is a robust assay for investigating chemotaxis</i>	189
7.1.2 <i>LPA chemotaxis is a key driver of melanoma dispersal and invasion across all stages</i> 189	
7.1.3 <i>Growth factors act as accessory factors enhancing LPA chemotaxis</i>	189
7.1.4 <i>Melanoma cells perform positive chemotaxis through the self-generation of outward gradients</i>	190
Key questions & future perspectives.....	190
7.1.5 <i>The role of platelets in LPA generation and metastasis</i>	191
7.1.6 <i>The LPA-axis as a potential prognostic and or therapeutic target for metastasis</i>	197
7.1.7 <i>A biological explanation for the adverse prognosis associated with melanoma ulceration</i>	201
7.1.8 <i>Implications for diagnosis & treatment</i>	203
7.1.9 <i>Self-generated gradients: a universal model for cell dispersal in morphogenesis and disease?</i>	204
Model for melanoma invasion	208
Summary.....	208
References	210
Appendix	255

List of Figures

Figure 1-1 Melanocyte development and homeostasis.	22
Figure 1-2 The major signalling pathways in melanoma initiation	24
Figure 1-3 The biological stages of melanoma development.....	28
Figure 1-4 AJCC survival curves for primary and metastatic melanoma.....	33
Figure 1-5 Comparison of Mark 2 Insall chamber features.....	49
Figure 1-6 Paracrine and autocrine chemotactic driven tumour cell invasion. ..	54
Figure 1-7 Representative comparisons of RTK and GPCR transduced chemotaxis.	58
Figure 1-8 Two pathways to LPA production and its structure.....	65
Figure 1-9 Key pathways in LPAR 1-5 signal transduction	68
Figure 3-1 Bridge heights in Insall and Dunn chambers during use.	99
Figure 3-2 Mark 4 Insall Chamber features.	102
Figure 3-3 Stability of linear gradients.	104
Figure 3-4 Insall chamber imaging modalities.	106
Figure 3-5 Insall chamber imaging set-up.	108
Figure 3-6 Quantification and statistical analysis.	110
Figure 3-7 Insall chamber assay refinement.	112
Figure 4-1 Characterisation of the chemotactic response of the WM239A metastatic melanoma cell line towards 10% FBS.	119
Figure 4-2 An investigation of the chemotaxis responses of melanoma cells from all biological stages.	121
Figure 4-3 Chemotaxis index and speed filtered by melanoma stage.....	123
Figure 4-4 The effect of gradients of GFs on melanoma cell motility.	125
Figure 4-5 Quantification of the effect of gradients of GFs on melanoma cell motility.	126
Figure 4-6 Characterisation of the chemotaxis response induced by LPA.	129
Figure 4-7 Analysis of speed during LPA chemotaxis.	130
Figure 4-8 Confirmation of the effect of Ki16425 on LPA chemotaxis.	132
Figure 4-9 The effect of Ki16425 on WM239A serum chemotaxis.....	133
Figure 4-10 The quantitative effect of Ki16425 on WM239A serum chemotaxis.	134
Figure 4-11 The effect of Ki16425 on the speed of cells.....	135
Figure 4-12 The effect of Ki16425 on primary melanoma chemotaxis.....	137
Figure 4-13 The effect of Ki16425 on metastatic melanoma chemotaxis.	138
Figure 4-14 The quantitative effect of Ki16425 on chemotaxis of primary and metastatic melanoma cells.	139
Figure 4-15 LPA is necessary for invasion into 3D organotypic assays.	141
Figure 4-16 The effect of combining GFs with LPA on melanoma cell chemotaxis.	143
Figure 4-17 The effect of combining GFs with LPA on melanoma cell speed..	144
Figure 5-1 Observing the behaviour of cells in uniform serum.....	149
Figure 5-2 Two Insall chamber assays for investigating chemotaxis.	151
Figure 5-3 Cell migration in the centre-well assay	152
Figure 5-4 Observing the mode of migration in 2D.....	153
Figure 5-5 Observing the mode of migration in 3D.....	155
Figure 5-6 The effect of increasing cell density on autonomous cell dispersal.	156
Figure 5-7 Examining the mechanism of dispersal +/- 10% FBS gradient.	157
Figure 5-8 The effect of conditioning media on the dispersal effect of serum.	159
Figure 5-9 LC-MS quantification of the [LPA] within media conditioned by WM239A cells.	160
Figure 5-10 Examining the ability of 1 μ M LPA to generate an “edge-effect”..	162

Figure 5-11 Examining the effect of Ki16425 on the “edge-effect”	163
Figure 5-12 Investigating the effect of keratinocyte and fibroblast conditioned media on the dispersal of melanoma cells.....	165
Figure 6-1 Schematic of in vivo melanoma sampling methodology.....	176
Figure 6-2 Quantification of [LPA] across the margins of non-ulcerated murine melanomas.....	178
Figure 6-3 Quantification of [LPA] across the margins of ulcerated murine melanomas.....	180
Figure 6-4 Quantification of [LPA] in normal murine skin in vivo.	182
Figure 6-5 Quantification of [LPA] across the margin of a human melanoma. .	184
Figure 7-1 Development of an orthotopic mouse metastasis model	195
Figure 7-2 Model for LPA driven melanoma invasion	209
Figure 9-1 Appendix: Cell line characterisation	256
Figure 9-2 Appendix: R&D project approval	257
Figure 9-3 Appendix: Declaration of Helsinki	261
Figure 9-4 Appendix: Melanoma tissue collection advert with inclusion criteria	262
Figure 9-5 Appendix: WM239A dispersal in conditioned media - all time-points	263
Figure 9-6 Appendix: Individual murine melanoma LPA quantification.....	264

List of Tables

Table 1. Relative risk for the main melanoma risk factors.....	30
----------------------------------------------------------------	----

List of Supplementary Movies

- Movie S1. MV3 Melanoma cells migrating in SFM-10% FBS
- Movie S2. MV3 Melanoma cells migrating in SFM-SFM
- Movie S3. WM35 melanoma cells (RGP) migrating in SFM-10% FBS
- Movie S4. WM98-1 melanoma cells (VGP) migrating in SFM-10% FBS
- Movie S5. WM239A melanoma cells (MM) migrating in SFM-10% FBS
- Movie S6. WM239A melanoma cells migrating in SFM-1 μ M LPA
- Movie S7. WM239A melanoma cells migrating in SFM-10% FBS+Vehicle
- Movie S8. WM239A melanoma cells migrating in SFM-10% FBS+Ki16425
- Movie S9. WM239A melanoma cells migrating in SFM-EGF+PDGF+1 μ M LPA
- Movie S10. WM1158 MM cells migrating in uniform 5% FBS in the standard assay
- Movie S11. WM239A MM cells migrating in uniform 10% FBS in the centre well assay over 72 hours - performed by Olivia Susanto
- Movie S12. WM239A MM cells migrating in SFM-10% FBS in the centre well assay over 72 hours - performed by Olivia Susanto
- Movie S13. WM1158 MM cells migrating in uniform 10% FBS in the centre well assay - demonstrating chain-like dispersal
- Movie S14. WM239A MM cells migrating in conditioned media T0-T0
- Movie S15. WM239A MM cells migrating in conditioned media T0-T48
- Movie S16. WM239A MM cells migrating in uniform 10% FBS + vehicle in the standard assay
- Movie S17. WM239A MM cells migrating in uniform 10% FBS + Ki16425 in the standard assay
- Movie S18. Dictyostelium cells migrating in uniform folate in the under agar assay - performed by Dave Knecht

List of Publications

Muinonen-Martin, A.J. et al. (2013) Measuring Chemotaxis Using Direct Visualisation Microscope Chambers. *Methods Mol Biol*, 1046:307-21 (Ed, Coutts AS) Springer

Muinonen-Martin, A.J. et al. (2010) An improved chamber for direct visualisation of chemotaxis. *PLoS One*, 5, e15309.

Chapter 1:

Introduction

Preface

This thesis has been written from the perspective of both a dermatologist and clinician-scientist and I have therefore chosen to divide the introductory chapter into two parts. The first part is written primarily from a clinical perspective and aims to provide an overview of the key clinical and biological aspects of cutaneous melanoma. This covers topics varying from its development to metastasis and provides background to the disease. It also reviews the clinical management of melanoma aimed to reduce the risk of metastasis and highlights important translational developments and areas of unmet need. The second part focuses on cell biology, reviewing the literature directly related to this thesis, starting from chemotaxis and progressing to an in-depth review of the chemotaxis-driven invasion paradigm and the inflammatory signal lysophosphatidic acid (LPA). There is, inevitably, some overlap between the two parts, although a gulf exists between the clinical management of melanoma and research into the biology underpinning the disease. Therefore, the final chapter will attempt to address this issue by highlighting the key findings and translating these to clinical implications and areas for further focused research.

Part 1

Cutaneous melanoma

1.1.1 Introduction

Early-stage cutaneous melanoma is curable, but advanced, metastatic melanoma is almost uniformly fatal (Zbytek et al., 2008). Patients with such advanced disease have a median survival of only 6-9 months (Gogas et al., 2007).

Melanoma is responsible for 75-80% skin cancer deaths despite being only responsible for 4% of skin cancers and is the 6th most common cancer type in the UK in 2010 (CRUK, 2013; Lee and Herlyn, 2007; Sladden et al., 2009). Cutaneous melanoma therefore remains a disease with high unmet need.

Not only is melanoma characterised by its aggressiveness, but the incidence rates in Europe, Australasia and North America have been rising since the mid 1970s (Coory et al., 2006; de Vries and Coebergh, 2004; Swetter et al., 2005). This unmet need is therefore acutely exacerbated by the ongoing “melanoma epidemic” (Dennis, 1999; Schaffer et al., 2004). The rising incidence is only tempered by the less dramatic rise in mortality, possibly due to the success of public awareness campaigns (Doherty and MacKie, 1988; Tucker, 2009).

Detecting and excising melanoma early is key to improving survival but melanoma is characterised by clinical and biological heterogeneity (Herlyn, 2009; Lachiewicz et al., 2008; Lee and Weinstock, 2009). This creates complex challenges for professionals involved in the management of melanoma; strategically for both public health physicians and policy makers in the delivery of patient awareness messages and, clinically, for dermatologists and pathologists in the diagnosis of malignant disease, and for oncologists in the successful treatment of disseminated cancer. Furthermore, melanoma is notoriously resistant to both chemo- and immunotherapeutic strategies (Vultur and Herlyn, 2009). Until very recently, the best current treatment - dacarbazine - offered only a 4% durable remission (Eton et al., 1998).

There are, however, major translational success stories emerging for this disease with the advent of personalised medicine, and tools to aid accurate diagnosis

are now in routine use (Flaherty et al., 2012c; Guitera and Menzies, 2011). That said, major hurdles lie ahead and further translational success depends on the successful interplay between physicians and surgeons managing the disease and scientists researching the biological mechanisms that underpin it (Wich et al., 2009).

One of the key questions this thesis addresses is: what drives melanoma cells to metastasise? We do not know why two patients exhibiting the same degree of invasion in their primary lesion - Breslow thickness, the most powerful prognostic predictor of subsequent metastasis - can demonstrate such biological variability. One may be cured with simple excisional surgery and yet another may present with, or go on to develop, widespread metastases (Balch et al., 2009). Although clinico-pathological parameters can to some extent identify those tumours at high risk of dissemination, the cellular mechanisms underlying this ability to metastasise early are poorly understood (Slingsluff and Seigler, 1992). There is therefore a great need to understand this difference in biological behaviour and develop novel prognostic and therapeutic targets.

1.1.2 Melanocyte development & homeostasis

1.1.2.1 Melanoblasts & morphogenesis

Melanocytes are derived from highly migratory precursors called melanoblasts and much of the knowledge about pigment cell embryogenesis has been derived from murine studies. In these murine models, melanoblasts appear from the neural crest around embryonic day 8.5 (E8.5; Fig. 1A). They travel along the dorsolateral pathway between the dermatome and overlying ectoderm, before redirecting through the dermis (E10.5), and “invade” the epidermis through the developing basement membrane around E14.5 (Jordan and Jackson, 2000a; Mayer, 1973). This pathway involves considerable axial mixing along with predominantly lateral migration (Wilkie et al., 2002). The modes of motility and invasion required for this process have been associated with the paradigm of epithelial-mesenchymal transition (EMT; Micalizzi et al., 2010; Theveneau and Mayor, 2012).

Very few molecules have been implicated in directing melanoblast dispersal and migration along the dorsolateral pathway and currently the mechanism by which melanoblasts traverse this pathway is poorly understood (Kelsh et al., 2009; Larue et al., 2012). The most well-studied is Stem Cell Factor (SCF), the Kit-receptor ligand, which plays a critical role in permitting the survival of Kit-expressing melanoblasts (Jordan and Jackson, 2000b; Wehrle-Haller, 2003). SCF has also been shown to drive increased migration into hair follicles through enhancing migration speed (chemokinesis) rather than directed migration towards SCF (chemotaxis). Other ligands (and their respective receptors) known to be involved in co-ordinating melanoblast migration include Endothelin-3 (ET-3)/ Endothelin receptor B2 (EDNRB2) signalling, with disruption of this pathway in mouse models demonstrating spotting phenotypes (Baynash et al., 1994). The chemokine-receptor axis SDF-1/ CXCR4 is implicated in the motility of cells within the hair follicle during cycles of hair growth (Belmadani et al., 2005; Belmadani et al., 2009). Niche localisation is further guided by spatially and temporally directed micro environmental cues in the expression of cadherins (Nishimura et al., 1999). Contact inhibition of locomotion may play a role in the patterning of melanocytes in zebra fish (Inaba et al., 2012; Kondo and Miura, 2010; Nakamasu et al., 2009; Theveneau et al., 2010). Contact inhibition of locomotion was first described by Abercrombie who observed the inhibition of continuing forward locomotion when two cells meet while migrating toward one another (Abercrombie, 1970).

Although these signals have been implicated in driving melanoblast migration, a clear model integrating the key pathways remains elusive and chemotaxis has yet to be shown to play a role in directing what is a tightly temporally and spatially controlled process. The reactivation of dormant embryonic pathways is considered to be an essential mechanism by which cancer cells invade and metastasise (Gupta et al., 2005; Lee and Herlyn, 2007). The extraordinary journey undertaken by melanoblasts during development/embryogenesis may, therefore, explain why melanoma has the ability to invade and metastasise so effectively.

1.1.2.2 Melanocyte homeostasis

Melanocytes are the mature pigment producing cells of the skin (Uong and Zon, 2010). They reside in the basal layer of the epidermis (Fig. 1B) in a symbiotic relationship with keratinocytes in an epidermal melanin unit (EMU) (Fitzpatrick and Breathnach, 1963; Seiberg, 2001). In 3 dimensions (3D) this highly ordered unit consists of approximately 36 keratinocytes associated with the dendritic processes of 1 (Meier et al., 2000) melanocyte. In 2D, this results in a distribution of melanocytes along the basement membrane with keratinocytes in a ratio of 1:5. The EMU is only disrupted to allow melanocyte proliferation, either to enable growth of skin in childhood or the development of a naevus or melanoma (Haass and Herlyn, 2005). E-Cadherin is a key regulator of melanocyte homing and plays a pivotal role in maintaining melanocyte homeostasis and is expressed on the surface of both melanocytes and keratinocytes (Tang et al., 1994). The melanocytes are further spatially regulated through CCN3 mediated basement membrane localisation via the discoidin domain receptor 1 (DDR1) that binds the basement membrane specific protein collagen 4 (Fukunaga-Kalabis et al., 2006).

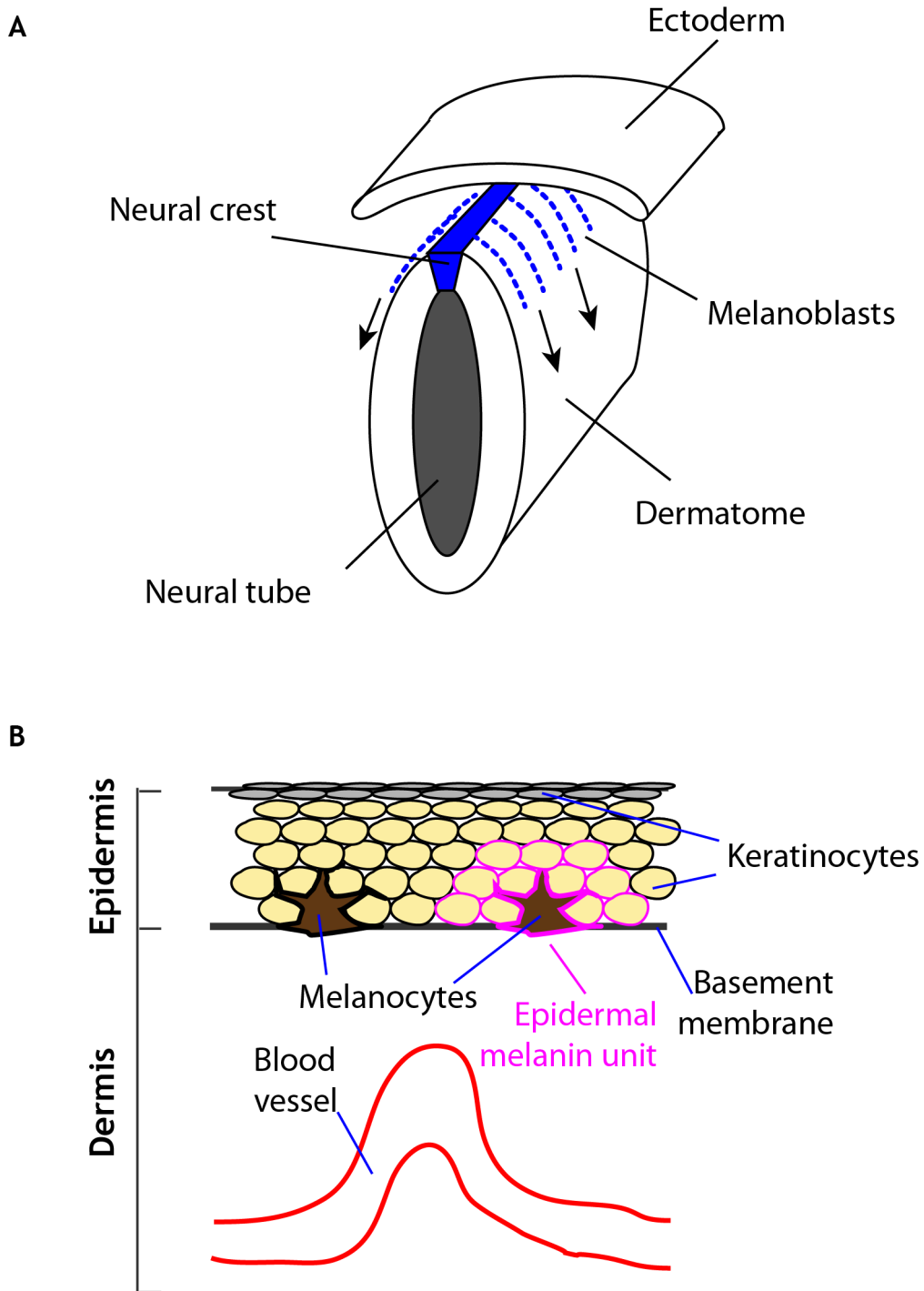


Figure 1-1 Melanocyte development and homeostasis.

A Melanoblasts are melanocyte pre-cursors, which migrate out laterally from the dorsally located neural crest between the dermatome and ectoderm to cover the entire trunk, before invading up into the epidermis. Adapted from Anne's Rat Page. **B** A simplified schematic of the architecture of the skin, composed of two main layers, the dermis and more superficial epidermis. It shows the relationship of melanocytes with keratinocytes in the epidermis during homeostasis. One melanocyte contacts approximately 36 keratinocytes through its dendritic processes, forming an Epidermal Melanin Unit. Keratinocytes mature as they rise through the epidermis, becoming flatter and losing their nuclei. Melanocytes reside on the basement membrane, separating the epidermis from the vascular dermis below. Adapted from (Haass and Herlyn, 2005).

1.1.2.3 The role of melanocytes

Melanocytes are photoprotective against the harmful effects of ultraviolet radiation-induced (UVR) damage (Brenner and Hearing, 2008). Epidemiological data support the photoprotective role of melanin with the observation that there is an inverse correlation with the risk of skin cancer and skin pigmentation (Gilchrest et al., 1999). Melanocytes synthesise melanin, which is transported within melanosomes via dendrites to adjacent keratinocytes. The melanin aggregates to form perinuclear protective caps in both cell types, thereby directly shielding the DNA from UV-induced photodamage (Warren et al., 1991). This reduces the impact of photodamage from UVR. The UVR spectrum includes the two most important wavelengths for melanomagenesis, UVA (315-400 nm) (280-315 nm) and UVB. On reaching the earth's surface, UVB is preferentially absorbed by the epidermis, compared to 80% of UVA, which penetrates beyond the basement membrane to the upper papillary dermis (Svobodova and Vostalova, 2010). UVR within the UVB wavelength range is particularly implicated in generating carcinogenic DNA damage, in the form of highly specific CC→TT and C→T nucleotide substitutions, which are described as classic UV fingerprint mutations (Brash et al., 1991). This is important because a recent genome wide screen for somatic mutations in melanoma found that many of the 33,000 mutations discovered had the hallmark of a UV fingerprint mutation (Plesance et al., 2009). UVA is also capable of producing DNA damage via photosensitised reactions that result in oxygen radical species (Peak and Peak, 1991).

1.1.3 Melanoma initiation

1.1.3.1 Melanoma driver mutations

Several key signalling pathways are deregulated in melanoma but of these it is the mitogen-activated protein kinase (MAPK) pathway (Fig. 2) mediating cellular responses to growth signals that appears pivotal in the early development of melanoma (Blokx et al., 2010; Haass and Herlyn, 2005).

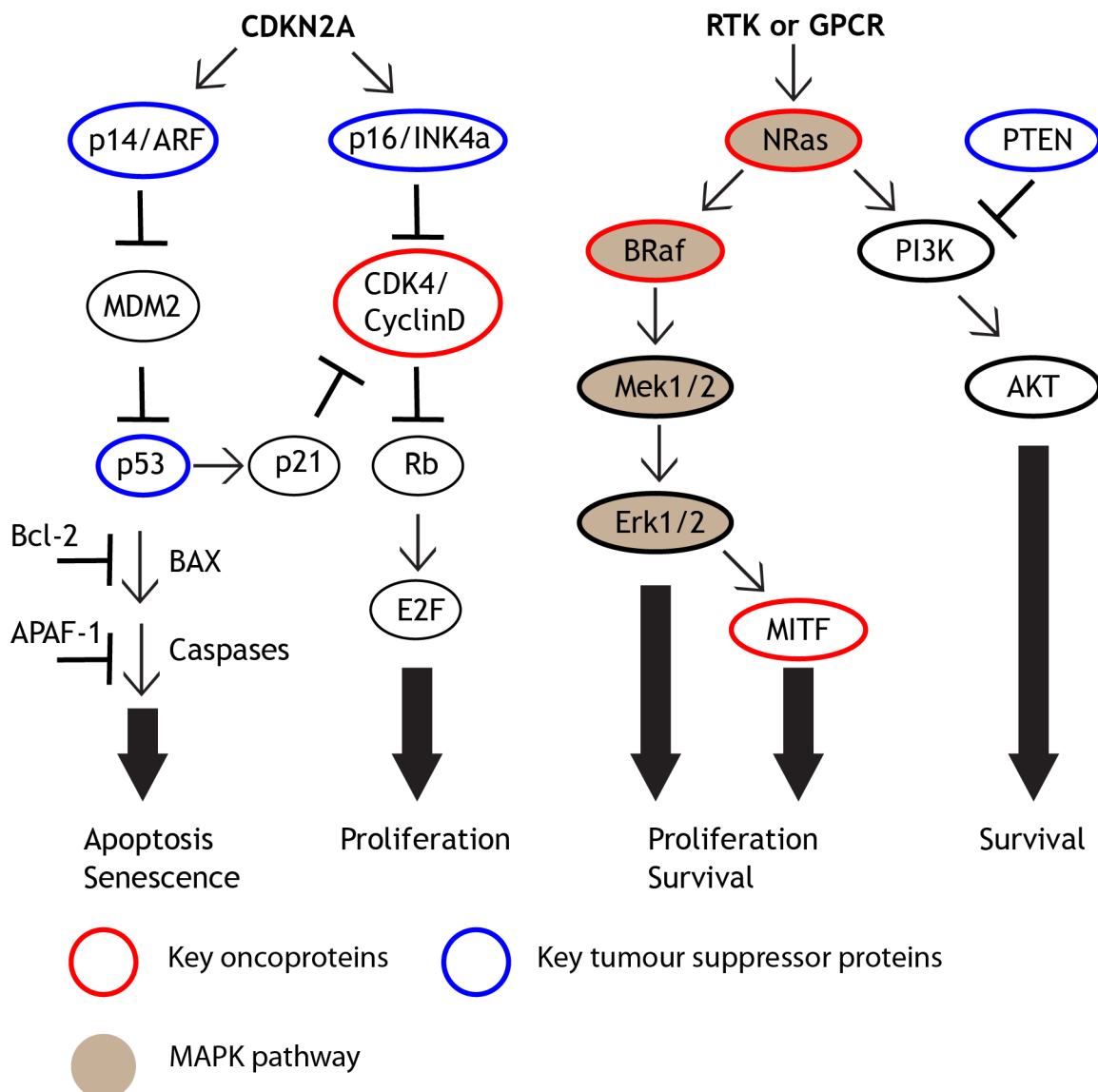


Figure 1-2 The major signalling pathways in melanoma initiation

The major signalling pathways in melanoma development are represented in this schematic, with the two key genetic networks involved in melanoma initiation, progression and maintenance. The CDKN2A locus, through alternate reading frames, encodes two separate tumour suppressors, p16 and ARF, and deletion of this locus leads to evasion from apoptosis and senescence and uncontrolled tumour growth. NRAS/BRAF and PI3K/AKT3 pathways are mainly implicated in melanoma proliferation, survival, and progression. The oncoproteins are indicated in red and tumour suppressors in blue and the MAPK pathway is shaded in light brown. Adapted from (Ji et al., 2010).

In 2002, the MAPK pathway was shown to be oncogenically mutated in melanomas, with the BRAF^{V600E} (a single valine to glutamic acid substitution) mutation accounting for 80% of mutations in the BRAF protein (Davies et al., 2002). This key step involved in the development of a naevus is also found in 50% of melanomas making it the most frequently activated oncogene (Flaherty et al., 2012a). Despite the mutation, naevi very rarely progress to melanoma due to activation of classical oncogene-induced senescence with the induction of

both p16 (INK4a) and senescence-associated acidic beta-galactosidase activity (Dhomen et al., 2009; Michaloglou et al., 2005). Interestingly, although 80% of acquired naevi are BRAF driven, 80% of congenital naevi are NRAS driven (Alikhan et al., 2012; Pollock et al., 2003).

NRAS driven tumours are the other major group and constitute 15% of all tumours that arise in a mutually exclusive pattern with respect to BRAF mutations (Devitt et al., 2011). Activation of NRAS driver mutations also signal through the MAPK pathway.

Although UVR from sunlight is generally accepted as a major risk factor for melanomagenesis, mechanistic evidence has been lacking (Garibyan and Fisher, 2010). The recurrent base mutations that produce oncogenic NRAS and BRAF mutations are not C > T transitions indicative of UVB mutagenesis (Hodis et al., 2012). Tumour genome sequencing has now produced new contenders for driver mutations. The identification of statistically significant “hot spot” mutations in RAC1 is particularly appealing, as it provides genomic evidence linking UVB mutagenesis mechanistically to this malignancy, with all samples tested exhibiting the C>T transition. Hodis et al. discovered this mutation in 4% of melanomas and another group confirmed its presence as the third most common mutation in sun exposed melanomas (Krauthammer et al., 2012). This mutation is particularly interesting from a metastasis perspective as it is the first mutation that has been shown to be involved in cellular migration (Insall and Machesky, 2009a).

This year, 74% of human melanoma cell lines were shown to exhibit recurrent UV signature mutations in the telomerase reverse transcriptase (TERT) promoter region (Horn et al., 2013). These mutations were found even more frequently than BRAF or NRAS mutations and CDKN2A. Concomitant mutations were found at a higher rate than expected by chance together, suggesting that these are driver rather than passenger events.

1.1.3.2 Tumour suppressor genes

CDKN2A, and the less common CDK4/6, (Fig. 2) are considered high-risk melanoma tumour suppressor genes (Box et al., 2001; Palmer et al., 2000).

Mutations in these genes were identified in melanoma-prone kindreds conferring a risk of multiple melanomas across the kindred, multiple primary melanomas arising in individuals and melanomas arising at an earlier age (Lin et al., 2008). The CDKN2A gene encodes two tumour suppressor proteins, produced through alternative splicing: p16/INK4a and p14/ARF. Downstream, these proteins signal via the Retinoblastoma (Rb) and p53 pathways and are proteins with critical roles in growth regulation and apoptosis respectively (Hsieh et al., 2012; Ji et al., 2010). Although these pathways are very important, they will not be discussed further as they do not directly feature in this thesis.

1.1.4 Melanoma progression model

To generate a melanoma, melanocytes must undergo at least three key changes. Firstly, clonal expansion, secondly, immortalisation through overcoming melanocyte senescence, and thirdly, suppression of apoptosis (Bennett, 2003; Bennett, 2008). There are then two key primary melanoma stages recognised biologically: radial growth phase (RGP), in which melanoma cells are capable of spreading along the basement membrane but remain keratinocyte dependent, and vertical growth phase (VGP), in which melanoma cells develop the ability to invade and survive in the dermis. This latter stage alone is considered to be metastasis competent (Bennett, 2008).

The melanoma progression model was described as a simple model of progression through 6 steps (1) common acquired melanocytic naevus; (2) melanocytic naevus with lentiginous melanocytic hyperplasia, i.e., aberrant differentiation; (3) melanocytic naevus with aberrant differentiation, and melanocytic nuclear atypia, i.e., melanocytic dysplasia; (4) the RGP of primary melanoma; (5) the VGP of primary melanoma; and (6) metastatic melanoma (Clark et al., 1984) This model belies the true complexity of melanoma in addition to the fact that less than half of sporadic melanomas are believed to arise through a naevus precursor (Clark et al., 1969; Haass and Herlyn, 2005). Figure 3 presents a simplified model of progression.

In vitro, VGP and MM cells exhibit constitutive activation of Erk1/2 (Satyamoorthy et al., 2003). This switch to growth factor independence distinguishes non-tumorigenic RGP from tumorigenic VGP primary melanomas

and appears to be closely related to tumorigenicity and metastatic potential (Haass and Herlyn, 2005). The mutual exclusivity of BRAF and NRAS mutations suggests that they are signalling through the same essential pathway (Davies et al., 2002). Melanocyte localising mechanisms are also disrupted. VGP melanomas (*in vitro* and *in vivo*) express markedly reduced levels of E- and P-cadherin, and exhibit decreased affinity for normal keratinocytes *in vitro*, suggesting that loss of cadherins may play a role in melanoma metastasis (Sanders et al., 1999; Tang et al., 1994). Knockdown of CCN3 or DDR1, which are essential for melanocyte localisation, result in dispersal of cells upwards into the epidermal layers of 3D skin reconstructs or downwards into the dermis (Fukunaga-Kalabis et al., 2006).

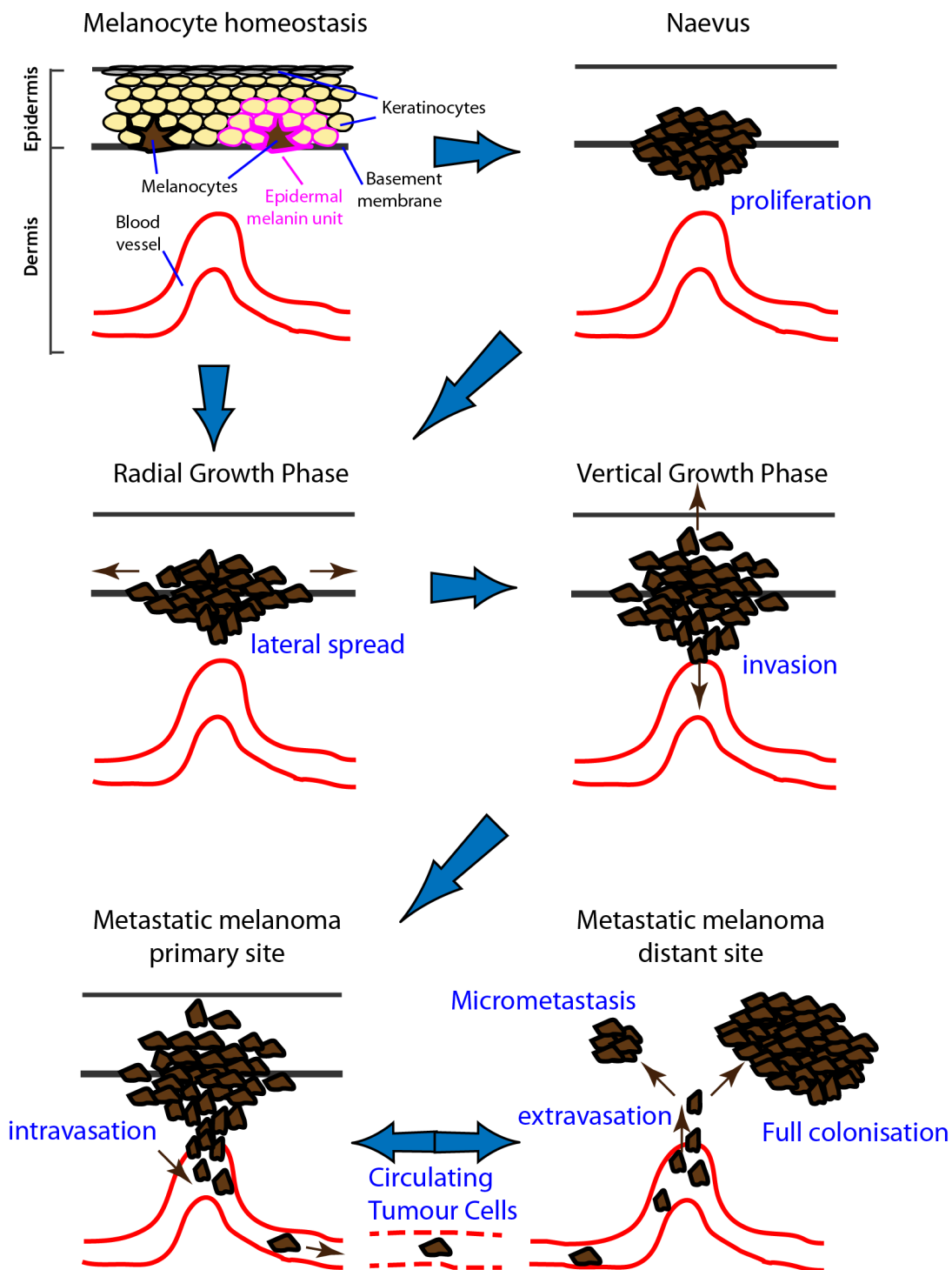


Figure 1-3 The biological stages of melanoma development.

The stepwise progression of melanoma through various growth stages is presented from left to right. Less than 50% of melanomas progress through the naevus stage and some tumours exhibit minimal radial growth phase. Importantly, cells move away or disperse from the tumour, this is best exhibited by the pagetoid spread of melanoma cells up into the epidermis. This dispersal is shown by small brown arrows. Circulating tumour cells may progress in a non-linear fashion and return to niche of the primary site, in addition to extravasating at distant sites to form metastases. Adapted from (Gaggioli and Sahai, 2007).

1.1.5 Diagnosing melanoma

1.1.5.1 Clinical phenotypes with increased risk of melanoma

Cutaneous melanoma is primarily a disease of pale-skinned populations and evidence from meta-analyses clearly shows UVR to be an important risk factor (Gandini et al., 2005b; Lancaster, 1956). The mechanism is complex, with intermittent sun exposure with a history of sunburn during childhood increasing risk in more northern latitudes and a role for chronic sun exposure in lower latitudes (Chang et al., 2009). This observation is supported with the finding that polymorphisms in the MC1R gene confer an increased risk of melanoma. MC1R encodes the receptor coordinating the pigmentation phenotype and is therefore an important gene in melanocyte biology and polymorphisms result in the red hair and fair skin phenotype (Makova and Norton, 2005; Valverde et al., 1995). Genome-wide association studies have also implicated other pigmentation genes as key susceptibility loci, including ASIP, encoding the agouti signalling protein upstream of MC1R, and TYR, encoding the tyrosinase related protein down stream of MC1R (Bishop et al., 2009; Gudbjartsson et al., 2008).

Whilst these phenotypes confer increased risk, by far in a way the most important risk factor is the presence of increased numbers of naevi and naevus atypia: the presence of 101-120 naevi compared with <15 (pooled relative risk (RR) = 6.89; 95% Confidence interval (CI): 4.63, 10.25) and for the number of atypical naevi (RR = 6.36 95%; CI: 3.80, 10.33; for 5 versus 0) (Gandini et al., 2005a). Although naevus number has a genetic basis, evidence has recently emerged that increase in naevus number is associated with UVR exposure (Falchi et al., 2009; Newton-Bishop et al., 2010). A list of relative risks can be found in Table 1.

Other groups at high risk that are beyond the scope of this thesis include patients with giant congenital naevi and individuals with a family history of three or more cases of melanoma, or of pancreatic cancer (Marsden et al., 2010).

Risk Factor	RR	95%CI
Multiple naevi	6.89	4.63-10.25
Atypical naevi	6.36	3.80-10.33
Pre-malignant & skin cancer lesions	4.28	2.80-6.55
Red Hair	3.64	2.56-5.37
Freckles	2.10	1.80-2.45
FH melanoma	1.74	1.41-2.14

Table 1. Relative risk for the main melanoma risk factors

A series of three systematic meta-analyses of observational studies for the relative risk of the main melanoma risk factors is summarised. Adapted from (Gandini et al., 2005a; Gandini et al., 2005b; Gandini et al., 2005c)

1.1.5.2 Early clinical diagnosis

By virtue of its heterogeneous nature, melanoma is characterised by a wide variety of clinical presentations, from small curable primary lesions, which can be cured by simple excision surgery, through to disease, which is widely disseminated at the time of initial diagnosis (Jerant et al., 2000). Early melanoma diagnosis is the key factor in reducing mortality, by detecting melanomas before they have metastasised (Rigel et al., 2010)

Most melanomas are detected based on their macroscopic appearance and with the “ABCD” or “7-point checklist” tools (Friedman et al., 1985; Healsmith et al., 1994). These risk assessment tools have proved a useful paradigm in enhancing early diagnosis. Some melanomas however lack these criteria, particularly in the early stages. For example, 15% of all melanomas are nonpigmented/amelanotic (Giuliano et al., 1982) and signs such as the “ugly duckling” sign have evolved to aid the diagnosis of these more atypical lesions (Scope et al., 2008). Despite these criteria, no one tool is perfect and clinical experience remains an important criterion for accurate diagnosis (Morton and Mackie, 1998).

The dermatoscope is a handheld non-invasive *in vivo* imaging device with 10x magnification that is used by dermatologists to enhance diagnostic accuracy by visualising biological processes in the epidermis and upper dermis (Kittler et al., 2002). This results in fewer biopsies of benign lesions and more accurate

detection of early stages of melanoma (Argenziano et al., 2012). Despite dermatoscopy and the advent of confocal microscopy in a research setting, there are no clinical markers for metastatic melanoma (Longo et al., 2013). Following identification of a suspicious lesion, an initial excision with a 2mm margin is recommended to enable an accurate pathological assessment (McCarthy and Scolyer, 2004).

1.1.5.3 Prognosis, histological features and risk of metastasis

The histological examination of the primary melanoma is central to providing accurate prognostic information as it guides ongoing clinical management and informs patients and physicians alike about the likely outcomes (Scolyer et al., 2012). However, melanoma remains one of the most challenging and controversial fields in diagnostic histopathology, and it is one of the leading causes for litigation against pathologists (Troxel, 2004). This is due largely to the wide morphological spectrum and often only subtle differentiating architectural, cytological and host response features, with potential for both under- as well as overdiagnosis of melanoma (Brenn, 2012; Metcalf, 1996).

No one feature alone is diagnostic and therefore the differentiation between benign naevus cells and infiltrating melanoma cells can be extremely subtle (Mackie et al., 1989). These features can also be complicated by trauma to the lesion, pregnancy, topical treatment or recent UV exposure (McCarthy and Scolyer, 2004). The diagnosis usually rests on a correlation of histopathological and clinical factors and an expert review may be necessary if there is discordance between the clinician and pathologist (Scolyer et al., 2012; Van Dijk et al., 2008).

Melanoma was initially categorised into three main groups based on a clinico-pathological classification: superficial spreading melanoma (SSM), nodular melanoma and lentigo maligna melanoma. The fourth, acral lentiginous melanoma, was added later and now forms part of the World Health Organisation's classification (Arrington et al., 1977; Clark et al., 1969). This approach has been criticised because it carries no independent prognostic significance (Romano et al., 2011; Weyers et al., 1999).

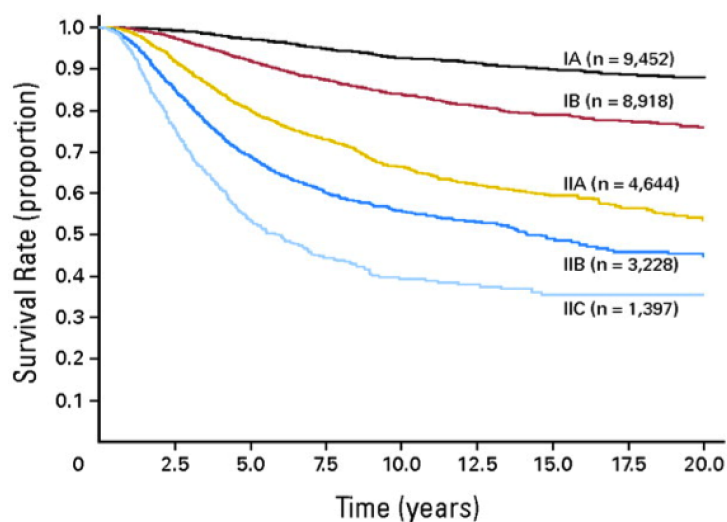
The melanoma AJCC staging and classification guidance was recently updated and provides valuable information regarding prognostic features that are also histologically identified from the primary lesion (Balch et al., 2009). These parameters include: *primary tumour thickness* (Breslow thickness), *primary tumour ulceration* and *primary tumour mitotic rate*, which replaces the biological level of invasion. These three factors are the dominant prognostic markers, with Breslow thickness the single most important marker. For stage III disease the number and volume of metastases remain important and for stage IV disease LDH is the key marker with lung metastasis providing a slightly better prognosis than other visceral metastases. The extent of the impact of these factors on 5-year survival can be seen on these graphs for localised and metastatic disease (Fig. 4). It is clear from the graphs that the presence of metastasis is the major difference between patients surviving or not. Based on these graphs, patients with stage IA melanoma (<1mm Breslow thickness, with no ulceration) have a greater than 95% 5-year survival and Stage IVC disease (metastasis to non-pulmonary viscera) have around a 10% 5-year survival rate.

1.1.6 Treating cutaneous melanoma

1.1.6.1 Primary melanoma: Treatment with curative intent

Following identification of a suspicious lesion, an initial excision with a 2mm margin is recommended to enable an accurate pathological assessment and ensure the entire primary lesion is excised in its entirety (Marsden et al., 2010). Once the Breslow thickness has been calculated, a definitive wide local excision can be performed to excise any micro-metastases that have escaped the primary melanoma (Marsden et al., 2010; Sladden et al., 2009). Recent UK guidance also takes into account the relatively benign biological nature of <1mm thick melanomas and these patients now only require a 1-year follow up period rather than the 5 years previously recommended. Surgical excision currently remains the only curative treatment for cutaneous melanoma.

A



B

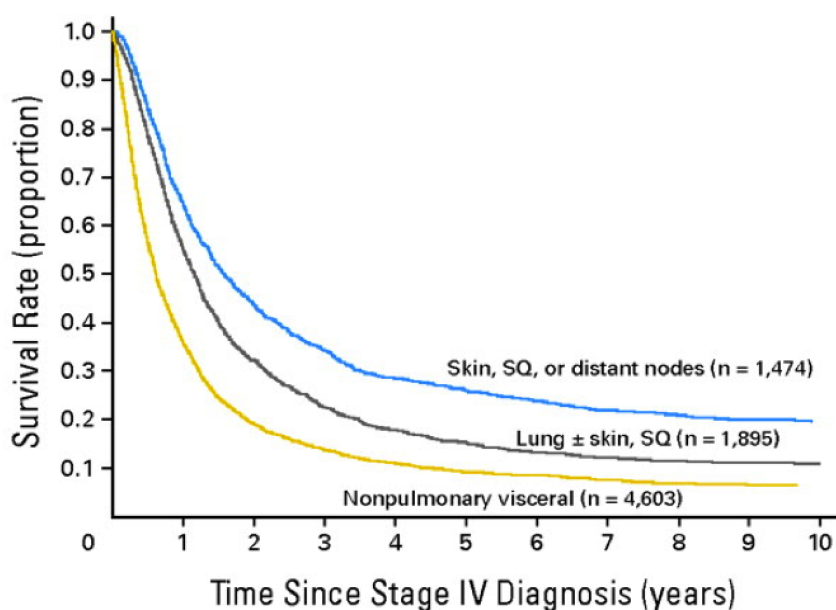


Figure 1-4 AJCC survival curves for primary and metastatic melanoma.

A Survival curves from the American Joint Committee on Cancer Melanoma Staging Database comparing the stage groupings for stages I and II melanoma. **B** Survival curves of 7,635 patients with metastatic melanomas at distant sites (stage IV) subdivided by the site of metastatic disease. Adapted from (Balch et al., 2009).

1.1.6.2 Metastatic melanoma: Treatments pre-2011

Prior to 2011, only an occasional patient would experience long-term benefit from therapy (Atkins, 1997) with the treatment mainstay, dacarbazine (DTIC), giving a 6-year survival rate of <2% (Eton et al., 1998; Gogas et al., 2007). Three decades of phase 2 trials showed virtually no difference in the response rates between DTIC and any other agent investigated (Korn et al., 2008).

1.1.6.3 Metastatic melanoma: Current treatments

2011 was lauded as a landmark year for the treatment of melanoma with two new agents conferring a survival benefit: the immune-stimulatory anti-CTLA4 antibody ipilimumab and the BRAF inhibitor vemurafenib (Hoos et al., 2010; Rebecca et al., 2012).

Modelled around the success of trastuzumab (a monoclonal antibody used in the treatment of breast cancer) and with a biomarker, vemurafenib fulfils the paradigm of a personalised medicine (Slamon et al., 2001). It was shown to demonstrate exquisite sensitivity against the V600E oncogene in pre-clinical studies enabling the rapid establishment of Phase 1 trials (Korn et al., 2008). In a subsequent Phase 3 trial, patients with previously untreated melanoma carrying the V600E mutation were randomised to receive either vemurafenib or dacarbazine. There were response rates of 48% for vemurafenib and 5% for dacarbazine, with median survival increased from 1.6 to 5.3 months in the vemurafenib arm (Chapman et al., 2011). Remarkably, it has taken only 10 years to translate the molecular biology to a licensed treatment to the clinic (Machesky and Sansom, 2012). Despite the initial success of vemurafenib, resistance rapidly became problematic and, in addition, up to 25% of patients develop squamous cell carcinomas (SCCs). Patients with increased sun exposure are at particular risk of developing SCCs. Even though vemurafenib inhibits MAPK signalling in BRAF mutant cells, it is postulated that this increase in SCCs arises through paradoxical activation of pre-existing RAS mutations in keratinocytes (Oberholzer et al., 2012; Sinha et al., 2012).

1.1.7 Future directions

1.1.7.1 Improving diagnostic accuracy and early detection

Prevention and early detection are essential in the battle against the rising incidence of melanoma. Dermatoscopy and the advent of modern *in vivo* imaging techniques such as confocal microscopy and multi-photon microscopy may offer new insights into the biology of melanoma through careful clinico-pathological-molecular correlation (Dimitrow et al., 2009; Longo et al., 2013).

1.1.7.2 Classification

Following the identification of key driver mutations and with the development of targeted therapies there is a move towards a genetic-morphologic classification: BRAF driven tumours are more common in SSM and show more pagetoid spread (upward migration into the epidermis), nest formation in the epidermis, epidermal thickening, greater pigmentation, a preponderance in younger population and a tendency to metastasise to the lymph nodes (although overall survival was not affected; Viros et al., 2008). By contrast, NRAS tumours presented with a greater Breslow thickness, a higher mitotic rate and evidence of a shorter melanoma specific survival, but these tumours could not be identified by morphological features (Devitt et al., 2011; Viros et al., 2008). cKIT has recently been shown to be mutated in acral lentiginous melanomas (Carvajal et al., 2011). These findings suggest that driver mutations can confer distinct pathological characteristics and further work is required to delineate and confirm these findings.

1.1.7.3 Improving efficacy of targeted therapies

The initial treatment successes have been tempered by the inherently heterogeneous and chemo-resistant nature of melanoma (Vultur and Herlyn, 2009). Importantly, it appears that the resistant tumours are still reliant on the MAPK pathway and therefore combining BRAF with MEK inhibition further downstream may go some way to abrogating this response (Smalley and Sondak, 2010). A Phase 1 and 2 clinical trial comparing this combination therapy with BRAF inhibition monotherapy found improvement in progression free survival and a Phase 3 trial is currently underway (Flaherty et al., 2012b). There remains a pressing need for more effective agents, which, either alone or in combination with agents that may abrogate resistance and agents that may impact collateral pathways in a rational manner, may achieve a more significant impact on this disease (Gogas et al., 2007). The heterogeneity of melanoma is being methodically deconstructed and now BRAF V600E mutations predict clinical efficacy of RAF inhibitors such as vemurafenib; activating KIT aberrations may predict response to tyrosine kinase inhibitors such as imatinib, nilotinib, or dasatinib, and some NRAS mutant tumours may exhibit sensitivity to MEK inhibition (Hodis et al., 2012).

New drugs studies should be carefully evaluated to show benefit in sub-groups of patients (Stewart et al., 2010). Smarter clinical trial design will therefore be important and methods like enrichment strategies will prove more successful when the specific mutation is known and large gains can be expected in a subset of patients (Mandrekar and Sargent, 2011). Based on current thinking and research, it is likely that in future patients will be given targeted therapies or combinations thereof based on the individual molecular profile of their tumours.

1.1.7.4 Biomarkers for metastasis

Currently, no single biomarker is prognostic for future metastatic relapse. Improving our understanding of the mechanisms of metastasis and identifying biomarkers associated with melanoma invasion and metastasis may also aid the development of novel therapeutic targets. In recent years, studies have investigated gene expression signatures based on mRNA levels in melanomas (Bittner et al., 2000). However, due to translational and post-translational alterations, these signatures cannot accurately reflect the protein levels *in vivo*. Therefore modern techniques such as proteomics screening tools may identify relevant and significant changes in protein expression (Huang et al., 2009). Given that metastasis is the most important cause of mortality, there remains an unmet need for a useful molecular marker of metastatic potential (Mackie, 2000).

Cancer cell metastasis

1.1.8 Metastasis

Cancer cell metastasis, the ability of tumour cells to spread from the primary to a distant site is the major cause of death in cancer patients, accounts for over 90% of cancer related mortality (Sethi and Kang, 2011). Most remarkable is the tortuous journey taken by a cancer cell to reach its site of metastasis. This is a complex and multi-stage process for which the cancer cell has to overcome many barriers and unfavourable environments (Steeg and Theodorescu, 2008). Thus, only a few cells end up completing this journey (Fig. 3). These cells are likely to be derived from a sub-population within the primary tumour and one would therefore hypothesise that the heterogeneity, characteristic of melanoma, may enhance its chances of success (Fidler, 2003).

1.1.9 Models of metastasis

One mechanistic theory is based on the anatomical/ mechanical model, whereby cells passively enter the blood stream or lymphatic system and grow in the first draining organ (Langley and Fidler, 2011). Gastric cancers have a predilection for the liver, which has a rich blood supply via the portal vein. Uveal melanoma by comparison also has a predilection for the liver, but it is unlikely that this organ bias arises simply through a direct filtering effect. This organ-tropism suggests that there are sites that present desirable features for cancer cells. These are known as pre-metastatic niches.

The first appreciation of the importance of such microenvironments was published in 1889, with the observation that breast cancer did not spread randomly. Instead the fastidious cancer cell “seed” depends on the fertility of a particular organ “soil” (Paget, 1889). Experimental evidence supporting the seed and soil hypothesis eventually emerged in the 1980s with the demonstration that melanoma allografts would metastasise to transplanted lungs and ovaries, but not kidneys, despite the passive spread and arrest of cells at different sites, confirmed with radiolabelling (Fidler and Nicolson, 1976). There is evidence that this is a highly co-ordinated event mediated by chemotaxis. Recently, Kim et al., revealed that metastasis is a multi-directional process with melanoma circulating tumour cells (CTCs) able to re-seed the site of the primary (Kim et al., 2009). Two interesting observations from this study include the role of chemotaxis in actively directing cells to this site and the role of the motility protein fascin in facilitating the process.

1.1.10 Invasion & cell motility

Underlying the invasive behaviour is increased motility caused by genetic alterations, changes in cytoskeletal organisation and altered contacts with the extracellular matrix (Gaggioli and Sahai, 2007). Cell motility can be deconstructed into a series of co-ordinated processes requiring cell protrusion, adhesion, contraction and de-adhesion. Movement is generated through alterations in the actin cytoskeleton with cycles of actin polymerisation, cell adhesion and acto-myosin contraction (Olson and Sahai, 2009). For efficient

motility, cells must co-ordinate these movements. Small GTPases of the Rho family are central to regulating both protrusion and contraction.

Key regulators of the motility have been shown to be up-regulated in a subset of motile cancer cells (Condeelis et al., 2005). The recent finding that Rac1, a small GTPase of the Rho family, is a driver mutation in melanoma also implicates dysregulated motility as a mechanism of cancer progression (Hodis et al., 2012). P-Rex1, a Rac-specific Rho GTPase, has been shown to drive invasion and is elevated in the majority of human melanomas, implicating a role in melanoblast migration and cancer progression to metastasis in mice and humans (Lindsay et al., 2011).

In an invasion model proposed by Liotta, cells must first attach to the extracellular matrix (ECM) and then degrade the matrix locally before commencing forward cellular migration. Adhesion to ECM components present in the basement membrane and underlying stroma is an essential factor in the ability of cells to invade and ultimately metastasise (Klominck et al., 1997). The second stage involves a programme of basement membrane transmigration, and first, cells must actively degrade this structure. One key programme involves degradation through the membrane anchored matrix metalloprotease (MT1-MMP) (Hotary et al., 2006), which can be delivered by invadopodia, invasive actin-dependent protrusions (Desmarais et al., 2009). Cells then actively migrate through the surrounding stromal tissue, stimulated by interactions with cytokines, growth factors, motility factors and ECM components (Klominck et al., 1997).

Melanoma is capable of spreading haematogenously and via the lymphatic channels. There is also evidence supporting an angiotropic, extravascular migratory mechanism (Lugassy et al., 2007).

1.1.11 *Impact of the microenvironment on motility*

1.1.11.1 *Role of the microenvironment*

“An often over-looked facet of tumour biology research is the involvement of the surrounding tumour microenvironment” (Lee and Herlyn, 2007). There is

increasing evidence to support a major role for stromal components in all stages of tumorigenesis including initiation, progression and metastasis.

The influence of the microenvironment became clear with studies showing that changes in tissue structure were critical for the expression of the malignant phenotype and that ECM receptors are important modulators of this effect. Despite the malignant genotype, cellular and tissue architecture are considered to act as the most dominant tumour-suppressor of all (Weaver et al., 1997). For example, the formation of a basement membrane has been shown to be accompanied by the cessation of growth and observations in melanomas *in vivo* concur with this hypothesis (Mackie et al., 1989). Analysis of histological human melanoma samples show that breaks in and thinning of the normally continuous line of type IV collagen and laminin at the dermo-epidermal junction are seen in association with areas of melanocytic proliferation, either with the junctional activity of benign naevi or in melanomas in association with invasive tumour cells.

1.1.11.2 2D v 3D motility

One of the observations and challenges in studying cell motility has been the differing motility mechanisms seen in 2D and 3D models (Pinner and Sahai, 2008). It is therefore important to reflect on how the cells respond to the 3D environment they inhabit *in vivo*. For example, RhoA activity during invasion, demonstrates significant differences in the subcellular spatial regulation of RhoA in 3 dimensions compared with standard 2-dimensional culture models (Timpson et al., 2011). There is increasing evidence that 2D and 3D migration utilise the actin cytoskeletal machinery differently, although structures such as invadopodia can be visualised in 3D as well as 2D (Magalhaes et al., 2011; Tang et al., 2013).

Mechanistic findings from standardised 2D assays can advance understanding of malignant transformation, but it is important to analyse the results in the context of the tumour microenvironment (Lee and Herlyn, 2007). The majority of research is performed using 2D platforms yet solid tumours do not exist in monolayers and in 3D cells also have to detach from a tumour (Wells, 2000). It may therefore not be a surprise that 90% of drugs exhibiting preclinical activity

fail given that a tumour is a mass of heterogeneous cells distributed within an ECM structure comprising a complex array of stromal components. The invasion “gold standard” is pathologically identified invasion of tumours in *in vivo*. This is currently largely unattainable for mechanistic studies in humans although animal models are providing important insights (Wells, 2000). Interweaving the complexity of the 3D environment with the fundamental mechanisms displayed in 2D promises to result in more effective therapeutic approaches and enhance the overall success rate of drugs in the clinic (Lee and Herlyn, 2007).

1.1.11.3 Single cell v collective migration

Cells explanted for tissue culture often flatten and lose their differentiation markers, but when placed back into 3D culture conditions, will regain their *in vivo* morphology (Yamada and Cukierman, 2007). This difference in cell culture morphology can translate to differences in cancer cell migration phenotypes in 3D matrices: single cell and collective migration.

Two main types of single cell motility have been described: amoeboid and mesenchymal (Olson and Sahai, 2009; Sanz-Moreno et al., 2011). “Amoeboid” is similar to leucocyte migration with an amorphous phenotype. This has been likened to the appearance of single cell migration *in vivo* with rapidly changing morphology. It bears similarities with the blebbing morphology witnessed occasionally in the amoeba *Dictyostelium* and in cancer cells treated with proteases (Wolf et al., 2003). Conversely, MDA-MB-231 carcinoma cells exhibit a constitutive protease dependent “mesenchymal” movement. The phenotype is integrin dependent, involving cellular elongation with a tendency to polarise the binding end of the cell and it is the main mode of motility by which *Dictyostelium* migrate. Cancer cells can transition between phenotypes without loss of speed (Smirnova and Segall, 2007).

Alternatively, cancer cells can migrate collectively and this form of migration has been likened to the Epithelial-Mesenchymal Transition (EMT) and the reverse Mesenchymal-Epithelial Transition (MET; Micalizzi et al., 2010). EMT is proposed to occur around the time of delamination during melanoblast migration, providing additional flexibility and is considered to be an important stage of metastasis (Theveneau and Mayor, 2012). Melanoma demonstrates both forms of

invasion histologically (Friedl and Gilmour, 2009). Friedl demonstrated that melanoma cells migrating out of an explant collectively would switch to single cell “amoeboid” motility in a β -1 integrin dependent manner, suggesting efficient cellular and molecular plasticity in tumour cell migration strategies in response to microenvironmental cues (Hegerfeldt et al., 2002).

1.1.11.4 Melanoma & the microenvironment

Melanocytes or melanomas are surrounded by a range of cells from keratinocytes, fibroblasts, endothelial cells and immune cells (Lee and Herlyn, 2007). Under normal conditions, the proliferation of epidermal melanocytes is controlled by the surrounding keratinocytes (Herlyn and Shih, 1994). Following invasion, the ability of melanoma cells to survive in the dermis appears to be dependent upon expression of cell-ECM adhesion molecules such as the integrins (Haass and Herlyn, 2005). An important ligand is fibronectin, an ECM glycoprotein consisting of 220-250 kDa sub-units linked by disulphide bonds, which is widely distributed throughout plasma and tissue in dimeric and multimeric forms respectively (Aota et al., 1991). Its main function involves promoting cell attachment and spreading, and is stimulated primarily by a tetrapeptide sequence, Arg-Gly-Asp-Ser (RGDS) (Aota et al., 1991; Pierschbacher and Ruoslahti, 1984).

The phenotype-switching paradigm involves changes in the local microenvironment driving transcriptional changes in melanoma cells (Hoek and Goding, 2010). This argues that metastases arise because of microenvironment-driven changes to a melanoma cell’s phenotype, leading to some cells acquiring a slow proliferating, stem cell-like phenotype with invasive potential. Following migration, cells can switch back to a proliferative state. There is data to support this via the action of TGF- β , regulating the Microphthalmia-associated transcription factor (MITF; Pinner et al., 2009). Through intravital imaging, cells were visualised migrating in a low pigmented de-differentiated state. Secondary site cells were differentiated in a high pigment state. This challenges previous models of melanoma progression that evoke one-way changes in gene expression and provides a more rational context for explaining observed melanoma biology (Hoek et al., 2008).

1.1.12 Metastasis as a therapeutic target

Drugs which target cancer cell invasion and metastasis have proven difficult to develop (Moustafa and Nicolson, 1997). Unfortunately, conducting and designing clinical trials for the prevention of metastasis remains a controversial area. One strategy to overcome this challenge may involve targeting metastatic colonisation in the adjuvant setting. However the trials will be large, long, expensive and with a lack of hard intermediate endpoints. Funding and carrying through with these trials will be challenging. There are the ethical and practical questions of whether a patient with for example, thick melanoma and no signs of metastatic disease, should undergo potentially toxic treatment. Conversely, is it ethical to treat patients to prevent metastasis, when many may have already developed metastases at presentation? How long should they be treated for? Arguably, the most ethically sound cohort to target, and with the greatest chance of trial success, are high-risk groups with stage III melanoma who have regional lymph node disease, but no detectable visceral metastases. It is not yet known if metastatic colonisation is an important therapeutic target and it will be challenging to validate this (Steege and Theodorescu, 2008). There is also evidence to support the use of drugs targeting pre-invasive conditions to prevent subsequent invasion. An example of this is the use of Cyclooxygenase-2 inhibitors in preventing the progression of familial adenomatous polyposis from benign colonic polyps to invasive carcinoma (Taketo, 2012).

The problem of validating success is complicated by our relative lack of understanding about the basic biology underlying the metastatic process. One of the many challenges is to enhance this understanding to identify novel biomarkers (Wells, 2000). One potential avenue could involve detecting CTCs as biomarkers for metastasis. One trial using a filtration technique detected a statistically significant difference in CTCs present between primary invasive (18 of 62, 29%) and metastatic melanoma patients (5 of 8, 62.5%), whereas controls were negative (De Giorgi et al., 2010). An alternative strategy involves seeking molecular biomarkers from the primary tumour and/or its microenvironment. Another potential biomarker is fascin, an actin bundling protein, involved in melanoma motility. Fascin, upregulated in advanced disease, has also been proposed as a potential therapeutic target (Mackesky and Li, 2010). The potential key driver mutation discovered in Rac1 is also linked to cell motility

and potentially metastasis (Li et al., 2012). These biomarkers could have three key uses: firstly, to predict response to specific therapies; secondly, to identify patients at high risk of metastasis; and finally, to measure response to therapy.

Various strategies could be employed in developing targets and either the tumour or host cells could be targeted (Steeg and Theodorescu, 2008). There is also clinical trial evidence supporting the use of dual agents, targeting growth and metastasis (Tortora et al., 2008). Combining therapies that inhibit different signalling pathways has the potential to be more effective than inhibition of a single pathway. For example, anti-VEGF treatment with anti-EGFR therapy has been shown to overcome EGFR resistance in pre-clinical trials and this combined treatment has shown benefit over standard chemotherapy. The challenge for the analysis of treatments targeting metastasis is deconstructing what effects are induced either by host or tumour cells in this setting because both may express the target receptor, but targeting both cell types may of course prove beneficial. These novel approaches will require further clinical trials to determine the benefit. However, in order to progress to clinical trials, it is critical to understand and investigate the underlying biology driving invasion in order to seek novel targets. Understanding the biology is critical for the successful development of new therapeutic compounds. In the 1990s, multiple large-scale clinical trials using matrix metalloproteinase (MMP) inhibitors did not show any benefit despite *in vitro* work to support their success. These failed for a combination of factors ranging from unclear end-points to a lack of understanding about the ability of MMPs to exert a range of anti- as well as pro-tumour effects (Fingleton, 2006). Fully appreciating the targets is therefore essential in ensuring the likely success of new compounds.

Part 2

Chemotaxis

1.1.13 **Background**

Chemotaxis is the process by which cells perform directed migration towards gradients of soluble molecules (Insall, 2010a). This is distinct from chemokinesis, the activated random migration of cells in response to an extracellular signal (T, 1995). Chemotaxis is a very ancient evolutionary mechanism has been observed across species, from amoebas to eukaryotic cells (Van Haastert and Devreotes, 2004). It is likely to have emerged from our single-celled ancestors and been preserved due to its essential role in survival, with key roles in fundamental physiological processes including cell division, embryogenesis and wound repair (King and Insall, 2009). Importantly, it has key roles in pathophysiological processes and examples pertinent to this thesis include the homing of immune cells to pathogens and inflammatory mediators and the invasion of cancer cells (Smirnova et al., 2012; Zigmond and Hirsch, 1973).

1.1.14 ***Dictyostelium discoideum: the chemotaxis role model***

Chemotactic cell migration is orchestrated through a complex set of interacting processes. These include detecting the chemoattractant, transducing the signal and resolving the information about the source's direction whilst transmitting the information to the cell's motility machinery to bias the direction of migration (King and Insall, 2009). To deconstruct this process, researchers have studied the underlying principles of the process with the amoeba *Dictyostelium discoideum*.

This unicellular organism has allowed the dissection and greater appreciation of the multiple and intertwined signalling pathways in an experimentally friendly model. Significant understanding about chemotaxis has been derived from this organism due to its simpler genetics. The relatively small genome was sequenced in 2005 showing that it had retained more of the diversity of the ancestral genome than plants, animals or fungi (Eichinger et al., 2005). As a eukaryote, many of the cellular mechanisms mirror those of mammalian cells.

Axenic strains grown with defined media have been generated for laboratory investigation (Franke and Kessin, 1977; Sussman et al., 1967).

Dictyostelium depends on chemotaxis for survival. It performs chemotaxis to direct itself towards folate secreted by its bacterial food source. During starvation it secretes cAMP in an autocrine fashion, which causes the cells to stream together to form a multicellular aggregate. Both these processes resemble neutrophil chemotaxis and involve signal transduction through G-protein coupled receptors (GPCRs).

This form of motility is mediated through actin polymerisation and resembles mesenchymal migration. *Dictyostelium* also migrate using an amoeboid morphology dependent on osmotic pressure (Yoshida and Soldati, 2006). Importantly, this means that as well as being an excellent model for GPCR transduced chemotaxis, it can model two of the key modes of motility exhibited by cancer cells (Sahai and Marshall, 2003).

1.1.15 Translating the chemotactic signal to directional movement

To generate directional movement the cell must bias its direction of migration towards the chemoattractant. The paradigm involves sensing the gradient through cell surface receptors uniformly distributed along the cell surface (Van Haastert and Devreotes, 2004). *Dictyostelium* and breast cancer cells will migrate efficiently towards the source until the concentration saturates the receptors (Bailly et al., 1998). This (mesenchymal) motility is induced by the projection of a pseudopod. There are two current hypotheses for steering cells: the “compass or signal-centred” and “pseudopod-centred” models. The former is based on the concept of the cell first resolving the direction of the signal and then generating a pseudopod in that direction. Experiments have confirmed that cells can respond spatially to localised high concentrations of chemoattractants (Gerisch and Keller, 1981). The latter model supports the idea of pseudopod protrusion independent of a chemoattractant signal. Instead the signal simply biases the lifetime of the pseudopod, thereby biasing the direction of migration (Andrew and Insall, 2007). This model is predicted to produce a greater variety of motility responses, allowing greater adaptation to

and integration of the signals produced in the 3D environment inhabited by cancer cells (Insall, 2010a). The co-existence of both models will allow cells to respond to a wide range of chemoattractant concentrations.

Intracellular signalling driving chemotaxis remains poorly understood. Following directional sensing based on receptor occupancy, one hypothesis supports the notion of a short-range pseudopod permissive signal (eg. phosphatidylinositol (3,4,5)-trisphosphate (PIP₃) and a longer range antagonistic global inhibitory signal (eg. cGMP) (Kay et al., 2008). In *Dictyostelium*, following GPCR occupancy, a PIP₃ gradient is formed that is amplified in relation to the external gradient (Onsum and Rao, 2007). This PIP₃ gradient is generated either by the activation of the catalyst phosphatidylinositol (4,5)-bisphosphate 3-kinases (PI3K) or by the loss of Phosphatase and tensin homolog (PTEN) from the membrane in the same region. However, recent knock out experiments of either PI3K or PTEN, individually or in combination, results in almost no reduction in their ability to perform chemotaxis, with accuracy continuing to approach that of wild-type cells (Hoeller and Kay, 2007) although their motility is impaired with slower chemotactic or random migration.

The knowledge from *Dictyostelium* and neutrophil chemotaxis models therefore suggests that chemotaxis is transduced through at least two interconnected signalling networks. This is an area of on going research and will not be discussed further. The two main classes of cell surface receptors that transduce the extracellular signal, will be discussed later in this chapter.

1.1.16 Measuring chemotaxis

1.1.16.1 Background

Despite its significance, chemotaxis is challenging to study due the highly dynamic and complex process of cell movement (Insall and Machesky, 2009b; Insall, 2010b). This is further complicated by the great variety of biological and microenvironmental variables that can affect both cell movement and chemotaxis.

Direct visualisation allows cells to be observed migrating using time-lapse microscopy (if needed) in real-time and bridge chambers are considered the gold

standard assay for investigating chemotaxis (Wells, 2000). With the application of a consistent and measured gradient they are capable of accurately quantifying chemotaxis in a tightly controlled system. The copious data generated are traditionally laborious to process, but offer detailed mechanistic insight into the behaviour of individual cells. Logically, laboratories with an interest in the processes underlying chemotaxis therefore often favour these assays.

One approach to managing the complexity of chemotaxis has been to use simplified indirect assays. They are generally useful for screening chemoattractants and rapidly performing multiple simultaneous experiments. Zicha and Dunn propose that the evidence for any substance acting as a direct chemoattractant should also be carefully validated in a direct observation chamber (Zicha and Dunn, 1995).

This section aims to review the key assays that are available to quantify or infer chemotaxis either directly or indirectly. It considers their design relative to the study of cancer cell chemotaxis and focuses on 2D direct visualisation bridge chambers and their development as this formed the basis to the development of Insall chamber assay discussed in detail in chapter 3. For brevity, the other types of important direct visualisation assays that exist including the under agarose (Ibarra et al., 2006), pipette (Gerisch and Keller, 1981) and microfluidic chamber assays (Li Jeon et al., 2002) are not discussed. But the same principles of balancing ease, information and precision apply.

1.1.16.2 2-Dimensional Assays:

Bridge chambers provide a visualisation platform for observing the behaviour of cells between the two wells. The cells are plated onto cover slips, which are then inverted leaving a small gap between the bridge and the cover slip. Cells can then be observed using an inverted time-lapse microscope. This means that individual chemotactic parameters can be recorded as well as separating the steps of the motility cycle, for example lamellipod protrusion and detachment of the rear aspect of the cell (Bailly et al., 1998; Maheshwari and Lauffenburger, 1998).

The Zigmond chamber was the original direct visualisation platform and was designed for studying the process of neutrophil chemotaxis in detail. The eponymous chamber allowed Sally Zigmond to obtain unparalleled insight into the basis of chemotaxis through the study of neutrophil migration in the presence of chemoattractant gradients. For example, she was able to demonstrate that these cells could orient in a gradient with only a 1% change in concentration across their length and this becomes efficient with a 10% change (Zigmond, 1977). Importantly, she also demonstrated that the ability to sense shallow gradients was optimal in the region of the dissociation constant K_d of the receptor (Zigmond, 1977). This observation has been confirmed for tyrosine kinase signalling in addition to GPCR signalling (Sourjik and Berg, 2002). This is logical because for a cell to chemotax, it must detect the change in concentration by a change in occupancy of its chemoattractant receptors. The change in occupancy is greatest when the gradient is steepest and is well below the receptor saturation level. Experimenting with progressively higher concentrations of chemoattractant solutions have demonstrated that chemotaxis accuracy tails off, supporting the adaptive process of receptor down regulation and saturation (Li Jeon et al., 2002). It therefore follows that around the K_d of a specific receptor, a small change in the concentration of the chemoattractant results in the maximal change in the percentage of receptors occupied, giving optimal orientation (Zigmond et al., 2001).

The Zigmond chamber was a great improvement on under agarose assays, due to its improved optical properties and near steady state linear gradient stable for 30-90 minutes - perfectly adequate for assessing neutrophils, capable of rapidly migrating at speeds of up to 30 $\mu\text{m}/\text{min}$. The chamber was designed with two medium-filled reservoirs, connected by a 1 mm wide, 20 μm deep, optically clear bridge (Fig. 4A).

This 20 μm gap is large enough to allow the migration of cells, but small enough to ensure there is no flow and the only mechanism of mass transport over the bridge is diffusion (Zicha et al., 1991). Therefore, adding a chemoattractant to one well will diffuse across the bridge, establishing a linear gradient. This design also limits convection currents to the wells, which beneficially stirs the contents.

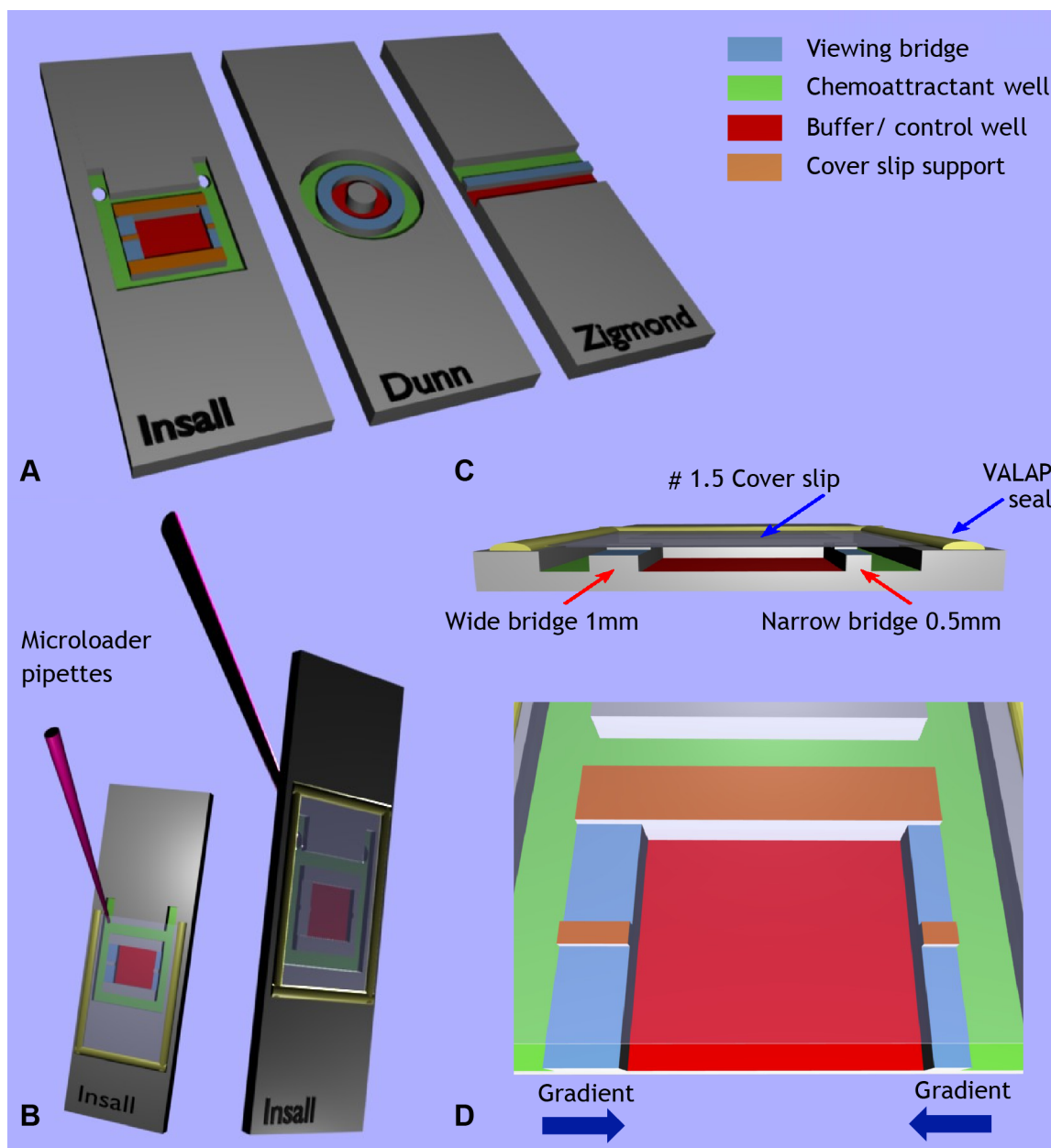


Figure 1-4 Comparison of Mark 2 Insall chamber features.

A Schematic showing the Insall Mark 2, Dunn and Zigmond chambers. The chemoattractant and buffer/control wells have been colour coded for direct comparison, along with the viewing bridges and cover slip supports. Note that the central cylindrical block on the Dunn chamber is the same height as the bridge and therefore offers no support to the cover slip. **B** demonstrates the versatility of the chamber with front or reverse side chemoattractant loading with no requirement for metal clips, unlike the Zigmond chamber. The latter technique involves loading after the cover slip has been secured and sealed in place with VALAP, producing a tight seal that reduces the risk of evaporation during experiments over one hour's duration. **C** Cross section through the Insall chamber highlighting one key feature – the ability to use thin (#1.5, 0.16–0.18 mm) cover slips that permit high NA oil immersion microscopy. Bridges of differing widths provide different gradient steepnesses. **D** provides a close-up of the Insall chamber and demonstrates the directions of the two chemotactic gradients, which are unidirectional across each bridge.

The design included non-sealed ends and a large bridge relative to the source and sink meaning that gradients are short-lived. It is therefore not suited to the study of cancer cells, which move significantly more slowly than neutrophils and

therefore require longer periods of observation to allow movement to occur. Another major flaw with this chamber design when considering its use for investigating cancer cells is the variable gap between the bridge and cover slip. This arises as a result of the cover slip being held in place by temperature sensitive springs, which are capable of deforming the chamber, leading to unpredictable gradient variability both during and between experiments (Zicha et al., 1991).

Published in 1991, and based on essentially the same bridge dimensions, the Dunn chamber was essentially an evolved version of the Zigmond chamber for the investigation of fibroblast chemotaxis (Fig 4A; Zicha et al., 1991). These cells migrate significantly more slowly than neutrophils, at speeds of 0.42-1.25 $\mu\text{m}/\text{min}$, (Ware et al., 1998). The chamber design circumvented the problem of a variable gap between bridge and cover slip by seating a thick (#3, 0.25-0.35 mm thickness) cover slip over a relatively inflexible glass chamber with annular wells of precise geometry. Gradient characterisation experiments for this chamber found it was able to form a linear gradient within one hour of setting up the chamber. One down side to this chamber design compared to similarly designed flow chambers is the delay in developing the linear profile (Li Jeon et al., 2002). With proportionately less bridge compared to the volume of the wells and a stable gap between the cover slip and bridge, it generated a constant linear gradient for 12 hours and a significant gradient for 48 hours. The reliable prediction and long-term stability of this chamber make it suitable for investigating the slower fibroblasts, which migrate at speeds similar to cancer cells that move around 1 $\mu\text{m}/\text{min}$ (Friedl et al., 1997). An important limitation of this particular assay concerns data analysis, which is complicated by the annular bridge design resulting in a variable chemoattractant gradient orientation (Monypenny et al., 2009).

In 2010, we described the Insall chamber, as an improved tool for measuring cancer cell chemotaxis (Fig 4A; Muinonen-Martin et al., 2010). This was a further refinement of the Zigmond and Dunn chambers and specifically designed for high quality imaging techniques for cancer cell chemotaxis, with attributes including ease of use and simplified gradient orientations. The precise details and critique can be found in chapter 3: development, optimisation & validation of an efficient assay for cancer cell chemotaxis. Modelling cancer cell migration

in an enhanced 2D chemotaxis assay should enable even greater appreciation of the diverse migratory behaviours exhibited *in vivo* (Soon, 2007).

1.1.16.3 3-Dimensional Assays:

The most commonly employed indirect assay is the high throughput Boyden chamber/ Transwell assay. The design again uses 2-chambers, but the compartments are separated by a microporous filter onto which cells are seeded (Toetsch et al., 2009). Chemoattractant gradients are established either side of a filter membrane in a 96-well plate and the cells are given a defined period of typically 3-4 hours to migrate. Quantitative data is gained by counting cells that have migrated to the chemoattractant well. A key difference is that this assay provides a limited 3D environment for cell migration. It has been reported as a chemoinvasion assay with the simple addition of an acellular extracellular matrix, and this has been shown to correlate with invasion *in vivo* (Albini et al., 1987). It can be modified, for example, by exchanging the filter with a mammalian peritoneal basement membrane (Schachtner et al., 2013). This has the benefit of providing a more realistic environment, and generating a physical barrier that requires active degradation.

Quantification of cell migration can be improved by performing a checkerboard analysis, which attempts to separate the relative effects of chemokinesis and chemotaxis. To produce these data, the chemoattractant is methodically added at differing concentrations both above and below the filter. A chemokinetic agent will enhance speed if the concentrations are equal both sides of the filter but a chemotactic agent will enhance the count only when there is a gradient (Zigmond and Hirsch, 1973). This can reliably quantify cell movement, but it is not able to unequivocally distinguish chemotaxis from chemokinesis (Rhodes, 1982). Boyden chambers are subject to a wide range of artefacts including an unknown concentration gradient over time and the effects of gradient dependent differential speeds with the net result that accurate analysis of chemotaxis is further hampered (Zigmond and Hirsch, 1973).

With this closed design, cells cannot be directly imaged during the assay and therefore it does not provide detailed mechanistic understanding about

chemotaxis. Detail including cell speed, cell polarity, pseudopod generation and turning rate are missed (Andrew and Insall, 2007).

Tumour spheroid assays assess the invasion of embedded multicellular tumour spheroids into collagen. Under the correct conditions melanoma cells will develop into smaller or even necrotic quiescent cells inside the spheroid and larger proliferating invasive cells outside, establishing a gradient of oxygen and nutrients and recapitulating the heterogeneity of tumour growth (Mueller-Klieser, 2000). Cells from the different biological stages will respond with an invasive phenotype indicative of their stage (Lee and Herlyn, 2007). Typically this assay is used as a tumour model for drug resistance in discovery assays and is not easily adapted into an easily decipherable chemoinvasive assay (Naber et al., 2011).

Driven by the need to develop assays more accurately reflecting the complexity and physiological nature of the *in vivo* environment, organotypic collagen assays are now commonly used to bridge the gap between *in vitro* and *in vivo* work (Berking and Herlyn, 2001). They consist of collagen, extracted from rat tails, and polymerised in combination with human fibroblasts, with the latter contracting the gel into a rigid 3D coin like structure. Cells can be seeded on top of the gel and invasion is believed to occur with the generation of a chemoattractant gradient, once the gel is lifted up to the air liquid interface. These gels have the capacity to recapitulate human melanoma initiation (Kiowski et al., 2011). Studies analysing the growth patterns of melanoma cells from different stages using these gels have also been shown to faithfully recapitulate progression across the biological stages (Meier et al., 2000). The host fibroblasts have been shown to play an important role in enhancing invasion (Ridky et al., 2010). This is a malleable platform acting as a dermal equivalent assay with the option of assessing the invasion of cells from fresh tumour explants, thereby investigating a heterogeneous population of cells, rather than a clonal subpopulation (Commandeur et al., 2009).

Finally, invasion can be quantified correcting for any growth defects that may occur with inhibitory drug treatments (Nystrom et al., 2005).

1.1.16.4 *In Vivo Assays*

It is possible to study the effects of chemotaxis on cancer cell motility *in vivo* (Wyckoff et al., 2000b). Implanting a needle containing a chemoattractant into a tumour in a murine model, cells can be collected that actively migrate into the lumen. Wyckoff *et al.* used EGF as a chemoattractant to collect breast cancer cells from a primary tumour. The cells can then be isolated and subjected to microarray analysis, and the results have contributed to the concept of a gene invasion signature (Wang et al., 2004). Cells have also been shown to polarise towards blood vessels, a presumed rich source of chemoattractants (Pollard, 2008; Wyckoff et al., 2004). With advances in imaging technology, the field of cancer cell motility research is now focusing more on intravital imaging techniques with clear demonstrations of individual melanoma cells migrating/chemotaxing during invasion (Pinner et al., 2009).

This diversity of experimental models is reflected by the many pros and cons of each, with no one approach superior. The choice of experimental system therefore depends on the question to be answered and ideally one would employ a combination of 2D, 3D and *in vivo* approaches to validate the physiological relevance of any mechanistic observations.

Chemotaxis as a mechanism for cancer cell invasion

1.1.17 *The importance of cancer cell chemotaxis*

The last decade has seen the emergence of chemotaxis as an important player in the field of cancer migration, invasion and metastasis (Condeelis et al., 2005; Wang et al., 2002). Many of the proteins that regulate motility are involved in chemotaxis and are also markers for metastasis and poor patient outcomes (Hodgson et al., 2003; Stathopoulos et al., 2008). One chemotaxis pathway that has been interrogated in particular detail involves the invasion of breast cancer cells (Fig. 6). In this model, tumour cells establish paracrine signalling with macrophages by secreting CSF-1 and sensing EGF,

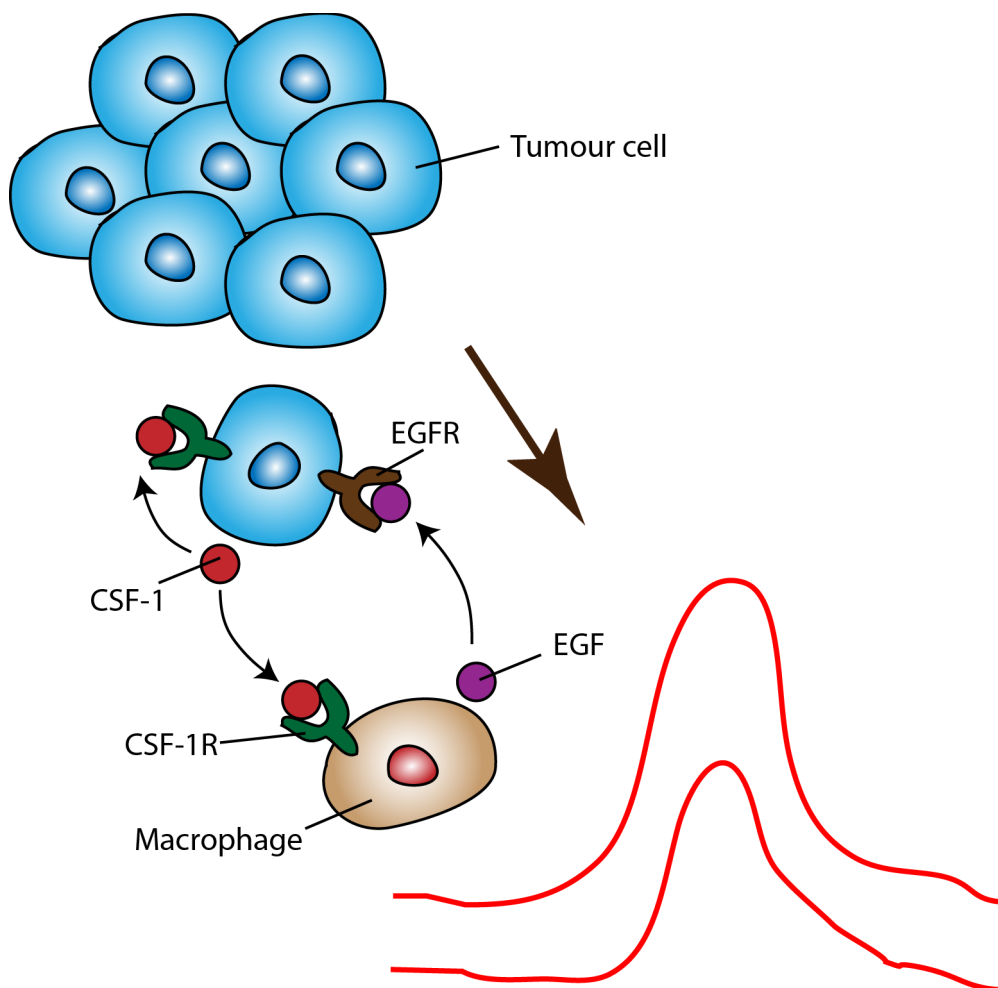


Figure 1-6 Paracrine and autocrine chemotactic driven tumour cell invasion. A schematic of breast cancer cell driven invasion driven by chemotactic gradients of EGF generated by macrophages. This are recruited through paracrine signalling by tumour cells with CSF-1. CSF-1 acts in an autocrine fashion to promote a more aggressive metastatic phenotype. Adapted from (Patsialou et al., 2009).

whereas the macrophages secrete EGF and sense CSF-1. In addition, tumour cells also sense CSF-1 and this autocrine signalling contributes to the aggressive phenotype of human breast cancer cells (Patsialou et al., 2009).

These results combined with the finding that cells polarise towards blood vessels has have been central to the development of the chemotaxis driven invasion paradigm *in vivo* and the concept that invasion is most efficient during active chemotaxis (Roussos et al., 2011a). The metastatic signature generated from these studies is enlightening, but it is not clear whether tumour chemotaxis can be predicted from such gene expression patterns. Currently, the physiological relevance of this work can only be inferred, as there are no available methods for quantifying actual levels of EGF *in vivo*.

The challenge now is to use this knowledge to increase our understanding of the role of chemotaxis in cancer cell metastasis. This may enable the prioritisation of better drug targets, better drugs, appropriate patient selection and smarter early clinical study design.

1.1.18 Correlation of chemotaxis with metastatic ability

Liotta proposed that the various metastatic stages of tumour invasion require three distinct steps. 1) Tumour cell attachment to the extracellular matrix 2) Local degradation and 3) tumour cell locomotion into the region of the matrix modified by proteolysis (Liotta, 1986). Several studies have focused on the third step and investigated the relationship between the metastatic ability of cells *in vivo* and cell motility responses displayed *in vitro* (Raz and Ben-Ze'ev, 1987). These have been performed in general using pairs of related cell lines with differing degrees of metastatic potential. These studies have supported the enhanced motility of highly metastatic cell lines. Volk et al reported that poorly metastatic murine melanoma cells were slower with greater focal adhesion plaques, formed strong intercellular connections and *in vivo* formed compact tumours. Conversely, highly metastatic lines were poorly adherent, with loose intercellular connections, but faster (Mean speed $5.0 \pm 2.2 \mu\text{m/hr}$) and, *in vivo*, easily detached and dispersed from the tumour (Volk et al., 1984).

Murata et al investigated the chemotactic response to fibronectin using Boyden chambers and found both renal and melanoma high metastatic potential lines were approximately three times more chemotactic than low metastatic potential lines, although haptotactic migration (motility towards a bound substrate) remained unchanged (Murata et al., 1992). With their *in vivo* chemoinvasion assay, Wyckoff et al collected cells of high metastatic potential with approximately 15-fold higher efficiency compared with low metastatic potential tumours (Wyckoff et al., 2000a). This process was enhanced with the addition of either EGF or 10% Foetal Bovine Serum (FBS). The current literature therefore supports significant differences in chemokinesis and chemotactic ability between cells of differing metastatic potential. None of these studies were investigated with direct visualisation assays and therefore it is difficult to make robust conclusions about the relative roles of chemokinesis and chemotaxis.

1.1.19 Cancer cell chemotaxis: membrane receptor signal transduction

1.1.19.1 Background

There are myriad factors known to stimulate motility. One large group of motility factors corresponds to the ECM proteins (Bogenrieder and Herlyn, 2003). These can either be solubilised by cleavage and stimulate chemotaxis or when bound they can stimulate haptotaxis. These factors include fibronectin, laminin, collagens type 1 and 4 and thrombospondin, all of which have been shown to stimulate motility in melanoma cells through integrin receptors (Kleinman et al., 1982; Klominek et al., 1997). Despite these data, integrin mediated chemotaxis is not even mentioned in several reviews by leaders in the field of chemotaxis research. Due to the paucity of data, this section will therefore focus on the two main classes of receptors that have been well studied and are known to mediate chemotactic signals activating cell motility pathways acting through the actin cytoskeleton: signal transduction via receptor tyrosine kinases (RTKs) and G-protein coupled receptors (GPCRs).

1.1.19.2 Receptor tyrosine kinase driven chemotaxis

RTKs are membrane bound receptors with an extracellular ligand binding domain, a single transmembrane helix and a cytoplasmic region containing the protein tyrosine kinase (TK) domain plus additional carboxy terminal and juxtamembrane regulatory regions (Lemmon and Schlessinger, 2010). The ligand, a growth factor (GF), binds and induces receptor dimerisation, thereby transducing signalling by stimulating tyrosine kinase activity through autophosphorylation at the cytoplasmic domain (Ullrich and Schlessinger, 1990). This phosphorylation increases its efficiency by 50-200 fold and this site acts as an assembly point for downstream signalling molecules. Amongst many others, PI3K is the major protein associated with the activated receptor and this is stimulated through CSF-1 binding to macrophage RTKs (Kanagasundaram et al., 1996).

The most studied chemotactic signalling pathway in cancer cell chemotaxis, is via EGF and the EGF receptor (EGFR). Importantly expression of epidermal growth factor receptor has been shown to correlate with invasive and metastatic

potential in animal models and human cancer (Pryczynicz et al., 2008). EGF is a strong chemokinetic agent, but chemotactic signalling in fibroblasts is delayed for a 4 hour window following stimulation with EGF (Ware et al., 1998). EGFR overexpression enhances the ability of MTLn3 mammary adenocarcinoma cells to intravasate and metastasise to the lung after mammary fat pad injection through the paracrine and autocrine loops with macrophages recently discussed (Patsialou et al., 2009; Xue et al., 2006). This particular loop highlights the ability of cancer cells to hijack the body's host response to enhance their chance of successful metastasis. It thereby implicates the inflammatory response in metastasis, with macrophages shown to generate a chronic inflammatory response in malignancy (Wyckoff et al., 2007).

Examples of the chemotactic responses induced by EGF are presented in this figure (Fig. 7A,B). In a direct visualisation pipette assay, the chemotaxis index is high, with a mean 0.55, and this calculation is based on the average displacement of roughly one cell's length. The significance of this will be discussed further (Soon et al., 2005). The Rose plot in Fig. 7B demonstrates the representative moderate bias in directionality induced by PDGF and IGF in a highly metastatic cell line, with a broad spread of end point positions relative to the chemoattractant (Zicha and Dunn, 1995).

Other clinically relevant chemoattractants implicated in cancer cell chemotaxis activating RTKs include the motility receptor c-Met, which has been shown to drive bony metastasis (Ono et al., 2006), and signals through its ligand hepatocyte growth factor (HGF, scatter factor; Steeg and Theodorescu, 2008). The paracrine action of PDGF plays an important role on the tumour stroma and fibroblasts in particular on tumour progression, but it has also been implicated in autocrine PDGFR signalling promoting breast cancer metastasis (Jechlinger et al., 2006). Not only are chemoattractants produced by host cells that attract malignant cells, but there is a substantial literature describing the role melanoma cells play in secreting chemotactic factors that attract host cells and thereby promote metastasis. One recent example reported the maintenance of human mesenchymal stem cells in the melanoma tumour microenvironment. This arises through chemotaxis and invasion of these multipotent stem cells towards the tumour, and this migratory effect appears to be mediated in part through secretion of FGF2 by melanoma cells (Watts and Cui, 2012).

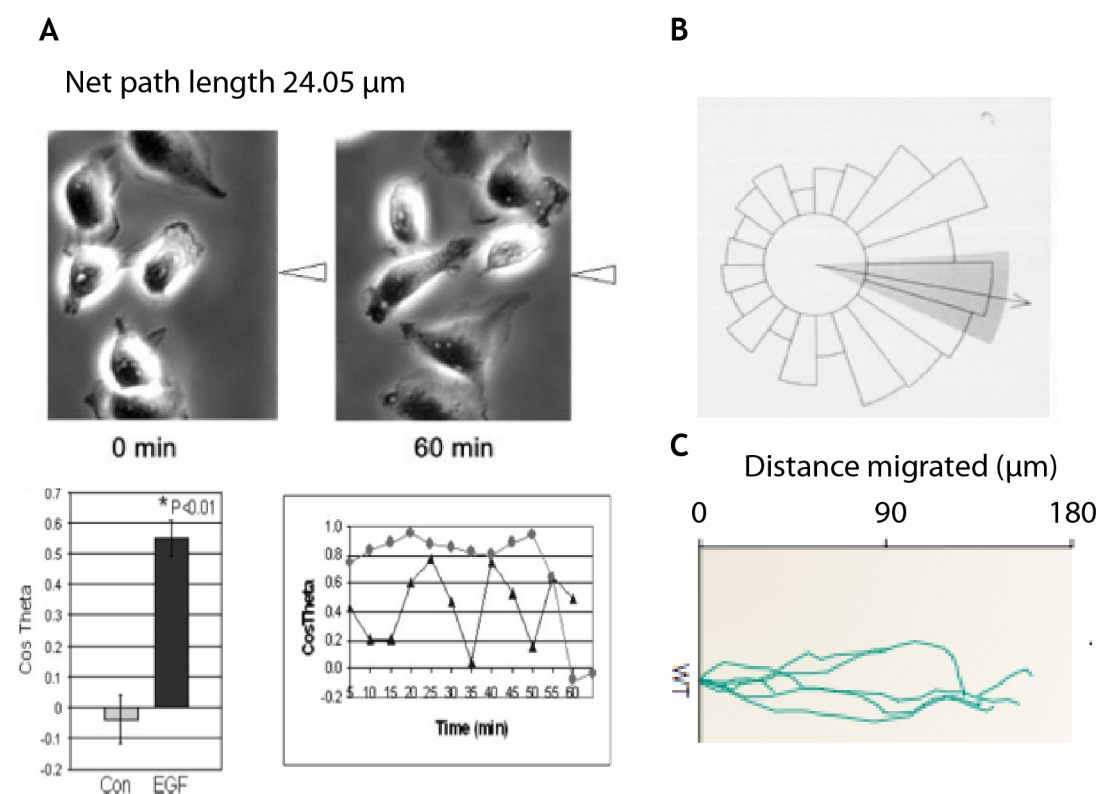


Figure 1-7 Representative comparisons of RTK and GPCR transduced chemotaxis.

The chemoattractants are located on the right in all images. **A** Phase contrast imaging of MTLn3 breast carcinoma cells showing polarisation and motility towards the micropipette (arrowhead) containing EGF over 1 hour. The chemotaxis index end-point and continual plots are also presented (Published by (Soon et al., 2005)). **B** Rose plot of highly metastatic rat T15 cells chemotaxing towards IGF and PDGF over 16 hours (Published by (Zicha et al., 1991)). **C** Murine neutrophil cells chemotaxing towards the chemotactic peptide fMLP, generating a chemotaxis index of approximately 0.95 (Published by (Kay et al., 2008)).

1.1.19.3 G-protein coupled receptor driven chemotaxis

GPCRs are composed of seven-transmembrane α -helices. With more than 800 members, GPCRs represent by far the largest family of cell-surface molecules involved in signal transduction, accounting for >2% of the total genes encoded by the human genome and they currently represent the target of over half of all current therapeutic agents (Dorsam and Gutkind, 2007). Following binding with their ligand, GPCRs undergo conformational change and expose intracellular sites involved in the interaction with the G-protein hetero-trimer, which contains α , β and γ subunits. This catalyses the dissociation of GDP for GTP thereby initiating several downstream signalling networks. These include several second-messenger-generating systems including small GTPases of the Ras and Rho families, and signalling pathways.

GPCRs were directly implicated in transducing extracellular chemotaxis signals with the generation of a G-B null *Dictyostelium* mutant (Wu et al., 1995). Although this mutant displayed normal motility it failed to perform chemotaxis, which was also the phenotype of a G- α protein subunit mutant (Kumagai et al., 1989). A complex array of chemokines, as well as bio-active lipids such as lysophosphatidic acid (LPA) and sphingosine-1-phosphate (S1P) are implicated in aberrant cell proliferation in a wide range of cancer cells (Dorsam and Gutkind, 2007). Chemokines are one of the main classes of cues that initiate chemotaxis in tumour cells and they act via GPCRs. One of their key roles in cancer metastasis has been shown to be the homing of cells to specific organs through chemotaxis but they have also been implicated in tumour growth and invasion (Payne and Cornelius, 2002). There are many that have been shown to play a role in disease progression and these have been reviewed in detail (Payne and Cornelius, 2002; Roussos et al., 2011b). From a melanoma perspective, CCR7 signalling has been associated with directed growth towards lymphatic tissue via secretion of its ligand (CCL21) from lymphatic endothelial cells (Emmett et al., 2011). This has been confirmed in other studies and a soluble inhibitor of the ligand has been developed that showed promise in a study, confirming this as a potential therapeutic target and also confirming that lymphatic spread appears to be a chemokine dependent process (Lanati et al., 2010). There is evidence to implicate the CXCL9/CXCR3 axis in transendothelial melanoma cell migration (Amatschek et al., 2011).

One of the most widely studied examples of GPCR mediated chemotaxis is the stromal cell-derived factor 1 (SDF-1/ also known as CXCL12)/chemokine receptor 4 (CXCR4) axis. This has been linked to many cancers, but appears to play a critical role in mediating metastasis of a chemoresistant tumour subpopulation toward a lymphatic niche in specific target organs, regional lymph nodes and lungs (Kim et al., 2010). SDF-1 is also an autocrine chemoattractant produced by melanoma cells to attract cytotoxic T lymphocytes, and the author argues that the expression of CXCR4 by the T-cells may be a beneficial prognostic marker (Zhang et al., 2006). A typical example of GPCR chemotaxis (Fig. 7C) by neutrophils is presented, reflecting the long, straight and highly accurate tracks towards the chemoattractant (Kay et al., 2008). These accurate tracks reflect the high chemotaxis indices generated by GPCR mediated chemotaxis compared

to the lower chemotaxis indices generated by RTK mediated chemotaxis described earlier.

1.1.20 *Modelling chemotaxis of cancer cells with melanoma*

1.1.20.1 The relevance of melanoma

Melanoma is a particularly relevant cancer sub-type for researching the mechanisms and the role of chemotaxis in cancer cell metastasis for several reasons. Firstly, studies have already shown that melanoma cell lines are chemotactic to soluble extracellular matrix components found particularly in basement membranes (Hodgson et al., 2003; Saito et al., 2009). This work led some groups to begin to look at the interplay between haptotaxis, (directed migration on extracellular matrices), and chemotaxis. As yet, no one has investigated the relative roles of these migration mechanisms in one experimental model (Aznavoorian et al., 1990; Hodgson et al., 2003; Klominek et al., 1997; Saito et al., 2009). Secondly, based on the paradigm of cancer cell reactivation of embryonic pathways, and considering the journey taken by melanoblasts, melanoma cells should exhibit highly motile behaviour (Friedl and Gilmour, 2009). This in turn makes melanoma an appealing experimental tool for the investigation of their chemotactic behaviour. Finally, melanoma has clinico-pathologically distinct growth phases and a panel of primary and metastatic melanoma cells from all stages with representative mutations are available for study (See appendix 1; Satyamoorthy et al., 1997).

1.1.20.2 Murine models of melanoma

Fresh melanoma tissue for investigation can be derived from different mammalian models and humans. The challenges of accessing primary melanoma tissue for research have been discussed (Wich et al., 2009). Here I will present two key mouse models that are available for study locally and have a body of literature that supports their ability to recapitulate many of the features of human melanoma (Walker et al., 2011).

One important caveat relates to the differences in architecture between mouse and human skin. Human melanocytes are found primarily in the inter-follicular regions of the basal layer of the epidermis, and in the hair follicle. In mice, the

melanocytes reside in the hair follicle, upper dermis and less typically in the inter-follicular basal epidermis. Therefore the melanomas generated will arise from different environmental niches, which is problematic for many of the reasons already discussed and tends to generate melanomas resembling nodular melanoma rather than SSM. Noonan et al generated a mouse overexpressing hepatocyte growth factor/scatter factor (HGF/SF), generating inter-follicular melanocytes like human skin and melanomas are generated recapitulating the growth characteristics of SSM following irradiation (Noonan et al., 2001). Assimilating these factors, combining cell lines, mouse and human melanoma models is considered the ideal paradigm to achieve physiological relevance (Herlyn and Fukunaga-Kalabis, 2010).

There are murine models that are highly representative of the main genetic determinants of human melanoma and encompass the four most common driver and tumour suppressor mutations. These include activation of BRAF^{V600E} or NRAS^{Q61K}, and deletion of PTEN or CDKN2A (the INK4a locus encodes both p16INK4a and p19 (ARF)). McMahon et al discovered that activating BRAF^{V600E} alone in a heterozygous or homozygous manner generated naevi, but PTEN deletion was necessary for melanomagenesis (Dankort et al., 2009). Another BRAF^{V600E} model, using a different source of alleles, generated melanomas without the requirement for PTEN deletion (Dhomen et al., 2009).

Ackermann et al described the N-Ras^{Q61K} INK4a^{-/-} transgenic mouse model (Ackermann et al., 2005). This generated melanomas metastasising to viscera but not with the efficiency of the BRAF^{V600E} PTEN^{-/-} models suggesting that PTEN mutations are more likely to cause metastasis.

1.1.20.3 Three key mechanisms of tumour dispersal

In vivo, melanomas not only invade downwards, but they exhibit signs of dispersal, with spread above the tumour and lateral migration away from the tumour into a less (cancer cell) dense area (Wells, 2000). This global outward migration suggests the cells are dispersing and I have presented evidence to support this as an active rather than mechanical process. There are three key mechanisms by which a tumour could actively disperse: positive chemotaxis, negative chemotaxis and contact inhibition of locomotion.

Contact inhibition of locomotion, is exemplified by the migration of neural crest cells towards their final destination (Theveneau et al., 2010). This can operate as a mechanism of pseudo-chemoattraction, whereby attractants such as Sdf1 amplify and stabilise contact-dependent cell polarity, resulting in directional collective migration. In the cancer setting, Friedl et al postulate, that contact inhibition of locomotion may maintain a high degree of polarity in cells invading collectively and this process would contribute to the directional persistence of motility even in the absence of a chemotactic gradient (Friedl et al., 1995).

External factors such as chemorepellents (negative chemotaxis) and chemoattractants (positive chemotaxis) have been proposed to confer directionality on migratory cell populations (Kay et al., 2008). I have discussed the role and evidence for positive chemotaxis in driving cancer cell and melanoma migration under the direction of a gradient. Other than release of soluble factors via host cells, this could be mediated in a “sequestrine” manner by the appearance of new haptotactic or soluble chemotactic factors following invasive degradation (Wells et al., 1998). However, little is known about how this, or other attractive signals, can be integrated by a migratory group (Theveneau et al., 2010).

Negative chemotaxis is illustrated by the paradigm of *Entamoeba histolytica* cell movement (Zaki et al., 2006). This organism is responsible for amoebic dysentery and its invasion through the mucosa of the gastrointestinal tract is postulated to be pathogenically driven by its motility response to the production of ethanol, which acts as a chemorepellent. The closely related but non-pathogenic *Entamoeba dispar* conversely fails to respond to ethanol.

These three mechanisms of tumour dispersal therefore require close interrogation, especially because at present the relative influence of each is not known.

Lysophosphatidic acid (LPA)

1.1.21 *Background*

LPA (monoacyl-glycerol-3-phosphate) is a naturally occurring bioactive lysophospholipid eliciting growth-factor-like activities that signals through GPCRs (Van Corven et al., 1989; Moolenaar, 1994). Its simple structure belies its critical roles in physiological and pathophysiological processes (Moolenaar and Hla, 2012). Early studies demonstrated its bioactivity with the induction of smooth muscle contraction and platelet aggregation.

1.1.22 *Structure & biological activity*

1.1.22.1 *Structure & sub-species*

LPA consists of a single fatty acid chain, a glycerol backbone and a free phosphate group and compared to other phospholipids is water-soluble. It is present in numerous chemically distinct species with considerable variation in the length and degree of saturation of the fatty acid chain (Choi et al., 2010). The most abundant forms in plasma are 16:0, 18:1 (the most commonly used laboratory reagent) and 18:2 (Sano et al., 2002). It is esterified at the sn-1 or sn-2 position of the glycerol backbone (Fig.7).

1.1.22.2 *Biological activity*

Jalink et al, investigated the biological function of differing LPA structures on the ability of LPA to act as an agonist, activating phospholipase C-mediated Ca^{2+} mobilisation in human A431 carcinoma cells (Jalink et al., 1995). Increasing biological activity was shown to correlate with longer acyl chain lengths (C16-C20) and the short-chain species (<C14) are almost completely biologically inactive (Jalink et al., 1995; Van Corven et al., 1992). For a given chain length, unsaturated LPA is more potent than the saturated species, but there is no further correlation with increasing double bonds and LPA's potency. Deletion of the glycerol backbone reduces potency by a factor of 1000 and the phosphate group is critical for function.

In the current model for ligand-receptor interaction, the acyl chain and glycerol backbone anchors the LPA molecule to present the negatively charged phosphate

group to the positively charged residues in the extracellular domain of the LPA receptor. Binding of the phosphate group triggers a conformational change that activates the receptor (Jalink et al., 1995).

1.1.22.3 Role of albumin and carrier proteins

In 1992, LPA was shown to bind to BSA (Van der Bend et al., 1992), and was biologically active in this form (Eichholtz et al., 1993) Further biological support for this was derived from studies with fibroblasts, whereby serum induced a stress-fibre response with albumin bound LPA and albumin also aids the delivery of LPA to cells within stroma (Meerschaert et al., 1998; Ridley and Hall, 1992). It is not known at the receptor ligand level whether the dissociation of LPA from albumin is necessary for its activation (Tigyi and Miledi, 1992).

1.1.23 LPA homeostasis

1.1.23.1 There are two main pathways to LPA production

A natural exogenous source of LPA was first identified in 1993, with platelets shown to release LPA following activation with thrombin. It was identified in mammalian serum bound to albumin at concentrations ranging from 1-5 μM , but is $<100\text{nM}$ in plasma (Eichholtz et al., 1993). Lysophosphatidylcholine (LPC) a precursor of LPA is by comparison found in abundance in the plasma. LPA is fairly water-soluble with a critical micelle concentration ranging from 70 μM -1mM, high enough to permit its presence in serum. Aoki et al investigated this finding and found that half the LPA in serum is produced via a platelet-dependent pathway. The two main pathways (Fig. 8) for LPA production were identified with thrombin induced platelet activation (Aoki et al., 2002). In addition to platelets, fibroblasts, adipocytes and ovarian cancer cells have been shown to produce LPA.

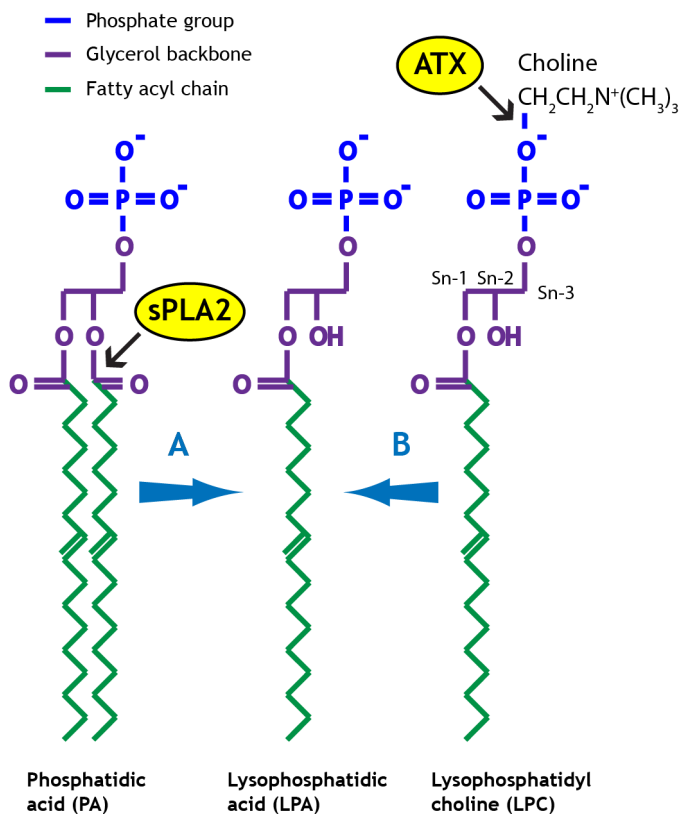


Figure 1-8 Two pathways to LPA production and its structure.

A hydrolysis of phosphatidic acid (PA) by soluble phospholipase A2 (sPLA2), which cleaves the fatty acyl chain at the sn-2 position of the glycerol backbone; **B** hydrolysis of lysophosphatidylcholine (LPC) by ATX, which liberates the hydrophilic headgroup (choline). LPC is produced by the action of PLA1 or PLA2 on membrane phosphatidylcholine. Adapted from (Mills and Moolenaar, 2003).

LPA can be produced by at least two distinct enzymatic mechanisms: hydrolysis of phosphatidic acid (PA) by soluble phospholipase A2 (sPLA2), which cleaves the fatty acyl chain at the sn-2 position, or hydrolysis by phospholipase A1 (PLA1), which cleaves the fatty acyl chain at the sn-1 position of the glycerol backbone; or hydrolysis of lysophosphatidylcholine (LPC) by ATX/lyso PLD, which liberates the hydrophilic headgroup (choline). LPC is produced by the action of PLA1 or PLA2 on membrane phosphatidylcholine. Published by Mills & Moolenaar 2003

In serum or plasma, LPA is predominantly produced in a two-step process. LPC is present in abundance in plasma and is generated by secretory-type Phospholipase A₂ (sPLA₂) and sPLA₁. In the second step, LPC is hydrolysed by autotaxin (ATX) to produce LPA (Aoki et al., 2002). sPLA₁ and sPLA₂ are enzymes catalysing the release of fatty acids from the sn-1 and sn-2 positions of fatty acids (respectively). sPLA₂ has been identified in the epidermis but both sPLA₁ and sPLA₂ are released in abundance from activated platelets (and to a lesser

degree, by red blood cells) (Maury et al., 2000). The ATX pathway generates the majority of LPA in blood. This was established in experiments with ATX knockout mice, with ATX heterozygote mice having half of the normal ATX activity and plasma LPA levels. From this paper, it was also clear that ATX activity and LPA production are essential factors in angiogenesis during development with ATX null mice dying at E9.5 with severe vascular defects (Van Meeteren et al., 2006).

LPA is identical in structure to phosphatidic acid (PA), but possesses only a single acyl chain, therefore the second pathway involves the straightforward cleavage of this second chain from PA by the action of sPLA₂ (Aoki et al., 2008).

1.1.23.2 Degradation

Extracellular LPA concentrations are tightly and rapidly controlled mainly by the balance of ATX and lipid phosphate phosphatase (LPP) activities producing a circulating half-life of only 3 minutes (Samadi et al., 2011). Each LPP consists of six transmembrane domains and is an ecto-enzyme with its active site on the outer surface of the plasma membrane (Brindley, 2004; Moolenaar et al., 2004). There are three LPPs and four LPP-related proteins (LPRs, or plasticity-related genes, PRGs). Dephosphorylation of extracellular LPA by the ecto-activities of the LPPs yields the minimally biologically active mono-acylglycerol (MAG) and rapidly terminates the signalling action of LPA (Smyth et al., 2003; Brindley and Pilquill, 2009). Thus the balance between production and degradation spatially and temporally determines the concentration of extracellular LPA.

1.1.24 LPA signal transduction

Six LPA self-surface receptors (LPARs) have been identified belonging to the GPCR family (Choi et al., 2010). GPCR signalling was initially implicated through the ability of pertussis toxin (PTX) to inhibit the mitogenic effects of LPA (Van Corven et al., 1989). The LPARs were identified in 1992, in cells known to be LPA sensitive by photoaffinity labelling (Van der Bend et al., 1992). LPAR 1 was first cloned in 1996 and following overexpression in a neuroblast cell line the cells rounded in a serum-dependent manner that was reproducible with the sole addition of LPA (Hecht et al., 1996). LPAR 2 and LPAR 3 are also closely

related and two additional, distantly related receptors, LPAR 4 and LPAR 5, which belong to a purino-receptor family, are also activated by LPA (Ohuchi et al., 2008). LPAR 6 was recently identified in hair follicles and has a key role regulating hair follicle development, with LPA generation in a novel pathway catalysed by PA-PLA1a (Inoue et al., 2011). Bandoh demonstrated that both LPARs 1 and 2 have broad ligand specificities, although LPAR 3 is less sensitive to 18:1 LPA (Bandoh et al., 2000).

Cellular signalling by the LPA receptors is relatively redundant, and extremely complicated with numerous downstream effectors known to be activated, including those driven by Ras, Rho and Rac1. These effectors are known to be activated by at least three G-subunits and may explain the variety of biological responses (Mills and Moolenaar, 2003). These include $G_{12/13}$, G_i , and G_q , and possibly G_s (Moolenaar and Perrakis, 2011; Ohuchi et al., 2008). The outcome of this signalling will depend on the LPAR expression signature (Fig. 9). The receptors show distinct genetic and physiological properties. LPA has been shown to induce transient elevation of cytosolic free Ca^{2+} and this response has been used as a quantitative read out for LPAR signalling (Ohta et al., 2003). One of the key phenotypic changes induced by LPA are the acute and marked changes in the actin cytoskeleton. In fibroblasts, LPA stimulated the production of stress fibres and focal adhesion formation within 2 minutes (Ridley and Hall, 1992). In PC12 cells it triggers rapid growth cone collapse, neurite retraction and transient rounding of the cell body (Tigyi and Miledi, 1992; Jalink et al., 1994).

During a search for its ability to induce chemotaxis in invertebrate cells, LPA was also shown to induce a weak response in *Dictyostelium*, independent of cAMP formation and secretion (Jalink et al., 1993) in μM concentrations by LPA and no other (lyso) lipids. It was hypothesised that this function may have arisen in evolutionary terms as an alternative chemoattractant to cAMP, produced by bacteria at a different stage in the lifecycle, and signalling through an independent pathway (Jalink et al., 1993; Schenk et al., 2001).

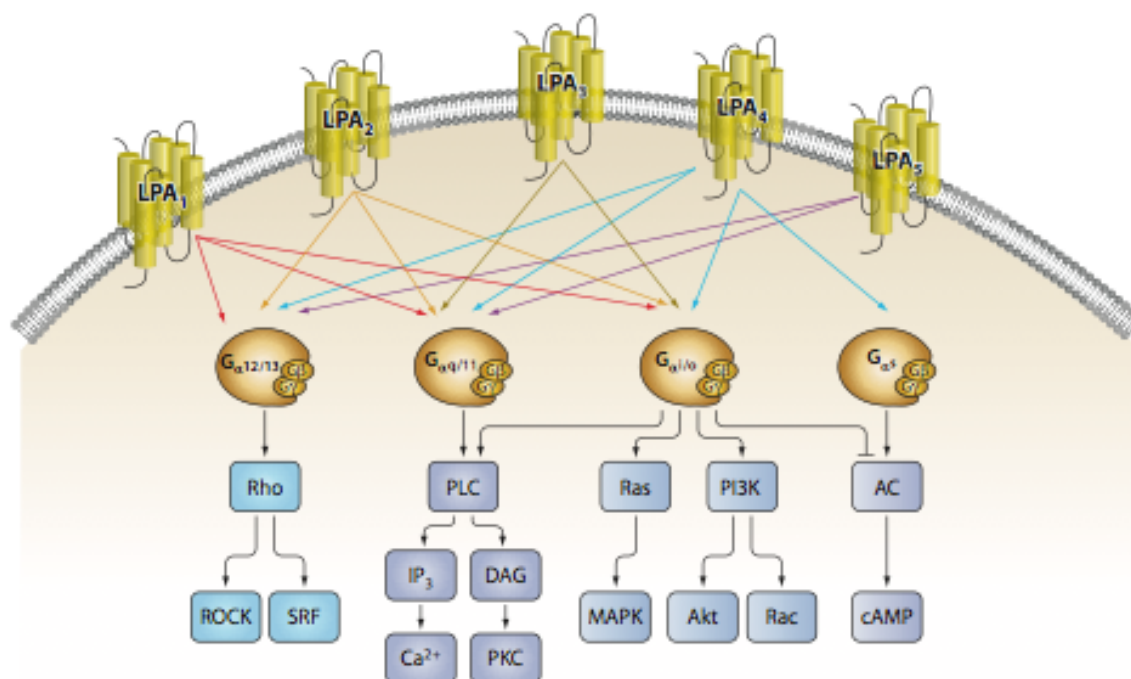


Figure 1-9 Key pathways in LPAR 1-5 signal transduction

The broad range of signalling pathways activated by the five known LPARs. Published by (Choi et al., 2010).

1.1.25 Role of LPA signalling in vivo

1.1.25.1 LPA signalling in health & disease

LPA has diverse biological functions. In the skin, LPA has important pathophysiological functions promoting wound (Mazereeuw-Hautier et al., 2005; Sauer et al., 2004) and corneal ulcer healing (Xu et al., 2007). It also promotes the terminal differentiation of keratinocytes and thickening of the epidermis (Piazza et al., 1995). It has a role in inflammatory and fibrosing conditions, resulting in radiation pneumonitis, lung and kidney fibrosis and scleroderma (Rancoule et al., 2011). As already described, it has a key role in vascular development and the generation of atherosclerosis. LPA is therefore essential for many biological processes but aberrant signalling results in pathological states within that organ system.

1.1.25.2 Role of LPA signalling in cancer

A melanoma “autocrine motility factor” was identified in A2058 melanoma cell conditioned medium and subsequently identified as ATX (Liotta et al., 1986;

Stracke et al., 1992). This induced random and directed motility in Boyden chambers in a PTX-sensitive G protein manner through autocrine secretion (Nam et al., 2000). ATX is reported to increase the aggressiveness and invasiveness of transformed cells, and ATX levels directly correlate with tumour stage and grade in several human malignancies including melanoma (Saunders et al., 2008). LPA was also reported to be involved in cancer cell motility during the investigation of the role of serum in hepatoma and small cell lung cancer cell motility and invasion into mesothelial cell monolayers (Imamura et al., 1993). Serum was shown to be necessary for the invasive response and could be substituted by LPA in these two cell lines.

Over the last decade there has been a growing appreciation that LPA plays an important role in cancer progression (Mills and Moolenaar, 2003). Activation of LPARs induces a host of GPCR induced responses favourable to cancer progression. LPA has been shown to be present at high concentrations in the plasma and ascites of ovarian cancer patients in advanced disease thus is regarded as a potential biomarker for epithelial ovarian cancer (Dorsam and Gutkind, 2007; Huang et al., 2008). There is evidence to support that the primary effect of LPA in promoting cancer progression is primarily due to enhanced cell motility, rather than cell proliferation (Imamura et al., 1993; Stahle et al., 2003).

Most carcinoma cells express more than one LPA receptor subtype, and the expression levels and responses to LPA vary among the different subtypes. It has been reported that the migration of fibroblasts and multiple cancer cells is mediated by LPAR 1. The migratory response of fibroblasts from LPAR 1 $-/-$ mice was diminished and with a LPAR 1 and 3 antagonist (Ki16425), there was a “loss of migratory response” across multiple cancer cell lines in Boyden chamber assays (Hama et al., 2004). Signalling through LPAR 1 was shown to activate both Rac1 and RhoA. The importance of LPAR 1 mediated cell motility has also been reported in: colon cancer (Lee and Yun, 2010; Shida et al., 2003) and pancreatic cancer (Stahle et al., 2003; Lv et al., 2011; Yamada et al., 2004). There are also data to support a role in LPAR 1 mediated cell-cell dissociation and dispersal, an early step of cancer invasion and metastasis (Jourquin et al., 2006; Shin et al., 2009).

Aims of this study

Melanoma is a heterogeneous disease and, despite recent advances, remains resistant to chemo- and immunotherapeutic strategies, with multiple signalling pathways constitutively activated. Current opinion suggests that more than one critical pathway will have to be targeted to induce an enhanced period of remission or cure. This chapter is a review of the current scientific literature, highlighting the available knowledge of the key pathways driving metastasis. There is a growing but currently limited body of evidence to support the paradigm of chemotaxis driven invasion. As metastasis is the major cause of mortality in cancer and the most important signalling pathways are not known, investigating chemotaxis is paramount.

This thesis aims to clarify the role of chemotaxis in melanoma invasion through a detailed examination of the chemotactic responses of melanoma cells using a direct visualisation approach. Due to the plasticity of motility responses exhibited by melanoma cells in different environments, a combination of melanoma models will be used to validate the findings. The aims of the thesis are as follows:

1. To develop a robust assay for cancer cell chemotaxis
2. To comprehensively explore the relationship between the chemotactic behaviour of melanoma cells at different stages of progression
3. To identify the key drivers of melanoma cell chemotaxis
4. To identify novel melanoma prognostic and therapeutic markers

Chapter 2:
Materials & Methods

Materials

All materials are listed by technique or assay. Laboratory plastic ware is from Nucleon, Thermo Scientific and all reagents are prepared and stored at room temperature (unless indicated otherwise). When disposing of all materials, Beatson Institute regulations were strictly adhered to.

Cell biology

All procedures were carried out at room temperature unless otherwise specified.

2.1.1 Cell lines

2.1.1.1 Melanoma

All melanoma cell lines used are listed by biological stage of derivation and were transferred from the Wellcome Trust Genomics Cell Bank unless marked (*), in collaboration with Prof Dot Bennett (Biomedical Sciences Research Centre, St George's, University of London; See Appendix 1 for characterisation).

Radial Growth Phase (RGP) melanoma

WM35 (Herlyn, 1990)

Vertical Growth Phase (VGP) melanoma

WM98-1 (Herlyn et al., 1985b)
WM278 (Satyamoorthy et al., 1997)

Metastatic melanoma (MM)

WM239A (Herlyn et al., 1985a)
WM852 (Herlyn et al., 1990)
WM1158 (Easty et al., 1995)
MV3* (Friedl et al., 1997; Van Muijen et al., 1991), Prof. Laura Machesky (Beatson Institute for Cancer Research, Glasgow)

2.1.1.2 Non-melanoma

The following cells were kindly donated:

HaCaT: immortalised keratinocytes (Boukamp et al., 1988), Dr Gareth Inman (Beatson Institute for Cancer Research, Glasgow)

Human primary fibroblasts, Passage 3, Dr Mike Edward (Glasgow University)

hTert-immortalised foetal foreskin fibroblasts (Tiff; Munro et al., 2001), Prof Bradford Ozanne (Beatson Institute for Cancer Research, Glasgow)

2.1.2 Cell Culture

All Cells were maintained in complete growth media (CGM): WM cell lines, HaCaT cells and Tiff fibroblasts were nourished with Roswell Park Memorial Institute (RPMI, Invitrogen) 1640 medium, supplemented with 10% Foetal Bovine Serum (FBS; PAA Labs) and 2 mM L-Glutamine (Gibco, Invitrogen) and 1% penicillin and streptomycin (Gibco, Invitrogen) and stored at 4°C. MV3 cells were grown in Dulbecco's Modified Eagle's Medium (DMEM, Invitrogen) and the same supplements, minus the additional Glutamine. All melanoma cell lines were incubated at 37°C in a 5% CO₂ incubator until approximately 80% confluence was reached.

2.1.3 Cell Passaging & Counting

With the appropriate degree of confluence, the cells were passaged. Cells were washed with Phosphate Buffered Saline (137mM NaCl, 2.68mM KCl, 7.98mM Na₂HPO₄, 1.47mM KH₂PO₄, pH7.2) and incubated at 37°C in a 5% CO₂ incubator for five minutes with Trypsin-EDTA (Sigma-Aldrich). After detachment, the Trypsin was deactivated by re-suspending the cells in CGM.

For experiments, cells were counted automatically using a CASY counter (Roche). 400 µl of cell suspension was diluted with 19.6 mL Casyton prior to counting. The cells were then seeded and the cell colony was maintained by diluting the remaining cells 1:5 with fresh CGM.

2.1.4 Cell preservation and recovery

To preserve cell stocks, cells were pelleted by centrifugation at 1000rpm for five minutes at the cell counting stage described above. The pellet was re-

suspended in the preservation mix (10% Dimethyl sulfoxide (DMSO), 40% FBS & 50% CGM). 1 mL (2×10^6 cells) cryovial aliquots were placed in a chilled freezing container, Nalgene® Mr. Frosty and transferred to a -80°C freezer for storage.

Cells were recovered by defrosting them in a 37°C water bath and immediately diluting them in 9 mL warmed CGM in a 10cm Petri-dish. Following cell attachment and within 24 hours, the cells were washed with PBS and the media was replaced with fresh CGM. Using this method the cells would reach the appropriate confluency for experiments within 48-72 hours.

2.1.5 Transfection

MV3 cells were transfected with the GFP-Lifeact fusion construct containing a neomycin resistance gene (kindly donated by Laura Machesky/ Roland Wedlich-Soldner). The cells were transfected by nucleofection with the Amaxa Nucleofection Kit (Lonza) V. The manufacturers' protocol was adhered to throughout. In brief, 2×10^6 MV3 cells were centrifuged and the pellet was re-suspended in 100 μL Nucleofector solution, warmed to room temperature. 2 μg GFP-Lifeact DNA was combined with the mixture. Once transferred to a cuvette the cells were transfected using a Nucleofector device programme (P020).

Approximately 80% of cells survived the transfection and allowed to recover for 48 hours in CGM. After this the GFP-Lifeact cells were selected by adding G418 (Stock solution 50 mg/mL, Sigma) diluted to 1 $\mu\text{g}/\text{mL}$ in the CGM (G418-CGM). The cells were maintained in G 418-CGM too maintain the stably transfected cell line.

Cell Motility Assays

2.1.6 Insall chamber chemotaxis assay

2.1.6.1 Chambers and related materials

The Insall chambers were originally designed by my supervisor Robert Insall. They were manufactured using microfabrication techniques by Epigem Ltd. (Redcar, UK). The chamber is a two-layer structure made from an optically clear and non-polarising layer of polymethylacrylate (PMMA) coated with a

second thin 20 μm layer of SU8 photoresist. To generate cover slip supports, UV light was used to cross-link the SU8 at the desired locations before generating the bridges by photo-etching the full 20 μm layer of SU8. The wells were then produced by mechanically milling to a depth of 1mm around the edge of the bridges and supports, as described (Muinonen-Martin et al., 2010; Muinonen-Martin et al., In Press).

VALAP sealant (Vaseline, Lanolin and Paraffin) was prepared by combining the three components together in a weight ratio 1:1:1 and melting at 100°C on a heat block. A fine artist's paint brush was used to apply the VALAP. A micropipette with P200 pipette tips were used to exchange media in the Mark 4 chamber and ultrafine pipette tips, Microloader (Eppendorf) in the Mark 2 assay. 22 x 22 mm #1.5 coverslips (VWR International). 1M HCl was pre-prepared in a 50 mL stock for acid washing. Absolute ethanol for sterilising and storing coverslips. 18G needle and coverslip forceps for handling the coverslips. Blu Tack® (Bostick Inc.) and chamber holder cassette.

2.1.6.2 Chamber reagents

Human Fibronectin (BD Biosciences): prepared according to the manufacturer's instructions by dissolving in distilled water to make a 1 mg/mL stock solution before storing aliquots at -20°C. A working solution of 20 $\mu\text{g}/\text{mL}$ was used throughout, generating an adsorbed concentration of 4.17 $\mu\text{g}/\text{cm}^2$ in the range of 1-5 $\mu\text{g}/\text{cm}^2$ as suggested by the manufacturer.

0.5% (w/v) BSA solution in PBS: cell culture grade Bovine Serum Albumin (BSA; Sigma-Aldrich) was heat denatured at 85°C for 13 min and allowed to cool to room temperature. It was passed through a 0.45 μm sterile filter (Minisart, Sigma-Aldrich) and stored for a maximum of 1 week at 4°C. A BSA coating is applied to block non-specific binding using heat-denatured BSA after laying down the ECM. The BSA is heat denatured to generate large β -sheet structures that enhance its ability to coat the non-ECM covered sites. It binds to the glass that is not occupied by fibronectin and prevents cell adhesion at these sites and is considered important for studies of cell motility (DiMilla, 1992; Grinnell and Feld, 1979; Wetzel et al., 1980). A 1% (w/v) BSA stock solution in PBS was

generated and diluted 1:20 in the chemoattractant solution to act as a carrier protein.

Chemoattractant solutions: based on the appropriate Serum Free Medium (SFM), RPMI for WM cells and DMEM for MV3 cells. Chemoattractant (*e.g.*, 10% FBS) was added to the medium as required. Addition of HEPES buffer to the media in the sealed chamber is essential to buffer the pH of the media throughout the experiment. This sulfonic buffer is superior to bicarbonate buffers at maintaining the pH in the physiological range whilst the carbon dioxide concentration increases as a result of cellular respiration (Baicu and Taylor, 2002). A 1M HEPES solution (PAA Labs) was added to both buffer (SFM-H) and chemoattractant solution (*eg.* FBS-H) to a final working concentration of 5 mM.

Lysophosphatidic acid (LPA) (Sigma, L7260): dissolved in a 1:1 ratio of distilled water: absolute ethanol to generate a 1mM stock solution and stored at -20°C. To use as a chemoattractant, BSA was diluted to a final concentration of 0.05% (w/v) to SFM-H (SFM-HB) and then 1 µL LPA was added to 1 mL to generate a 1 µM LPA solution.

EGF (Peprotech, AF-100-15): dissolved in PBS to a stock concentration of 100 µg/mL and stored at -20°C. In chemotaxis experiments two working concentrations were used after diluting in SFM-HB: Low (6.25 ng/mL) and High (25 ng/mL).

PDGF, BB Homodimer (Merck, Calbiochem, 521225): dissolved in PBS to a stock concentration of 10µg/mL and stored at -20°C. In chemotaxis experiments three working concentrations were used after diluting in SFM-HB: Low (25 ng/mL), Mid (25 ng/mL) and High (100 ng/mL).

HGF/ Scatter Factor (Peprotech, 100-39): dissolved in PBS to a stock concentration of 10 µg/mL and stored at -20°C. In chemotaxis experiments two working concentrations were used after diluting in SFM-HB: Low (6.25 ng/mL) and High (25 ng/mL).

SDF-1α/ CXCL12 (Peprotech, 250-20A): dissolved in PBS to a stock concentration of 100 µg/mL and stored at -20°C. In chemotaxis experiments two working

concentrations were used after diluting in SFM-HB: Low (100 ng/mL) and High (300 ng/mL).

Ki16425 (Cayman, Cambridge Bio): stored in absolute ethanol at a stock concentration of 10mM as per the manufacturer's instructions. In Insall chamber assays, cells were pre-incubated for 5 minutes with a 10 μ M solution before combining with reagents in the chamber at the same concentration.

2.1.6.3 Pre-assay cover slip preparation

Acid washing coverslips. It is not uncommon for coverslips to be contaminated with a fine layer of grease, and to remove this layer, routine acid washing is recommended (Fischer et al., 2008). Approximately 20 coverslips were etched with 1M HCl for 15 min in a 300 mL glass beaker and rinsed extensively for at least 15 min in a constant stream of water and stored in ethanol until use.

Fibronectin coating. Coverslips were air dried in a tissue culture hood and diluted from the 1 mg/mL fibronectin stock to a 20 μ g/mL working solution with PBS. Each coverslip was submerged with 1.5 mL of the fibronectin working solution in a six-well dish for 1 hour at room temperature or overnight at 4°C.

BSA blocking. The fibronectin solution was aspirated from the coverslips and washed three times with distilled water. Coverslips were coated with 2 mL 0.5% BSA solution in each well for 1 hr.

2.1.6.4 Insall chamber setup for standard cancer cell chemotaxis assay

Chamber preparation. The chambers were drilled in advance with a 1.3 mm drill bit using an overhead drill press. During drilling, the chamber was secured in a small machine vice sitting inside a V-block at 45° and a hole was drilled into each 'rabbit ear' of the outer well to allow reverse filling.

Cell seeding (T-minus 24 hrs). The BSA solution was aspirated from the coverslips and washed thrice with PBS. Cells were seeded at a density of 5.5x10⁴ cells/mL in CGM. Each cover slip was coated with 2 mL of the seeding suspension. After seeding cells, the six-well dish was shaken in the x and then y planes for five seconds each and placed in a CO₂ incubator at 37°C on top of a

shock absorbent base to prevent vibration induced patterns of cell accumulation.

Cell starvation (T-minus 14 hrs). CGM was aspirated and washed thrice with PBS. Add 2 mL SFM and continue to incubate at 37°C.

Reagent preparation (T-minus 1 hr). The microscope chamber holder cassette, and reagents in 1.5 mL centrifuge tubes, were pre-warmed to 37°C in a heating block. Chambers were washed thoroughly under a stream of water to remove debris and then immersed in ethanol before blotting with a lint free cloth (Kimwipes, Kimtech) and left to air-dry. VALAP mixture was warmed to 100°C for 10 min.

Chamber assembly (T-minus 30 min). The centre well of the Mark 2 or Mark 4 Insall chamber was filled with control medium (SFM-H) - 12.5 µL or 45 µL respectively. The exact medium depended on the precise experiment. A cell-coated coverslip was picked up and held vertically to gently blot excess medium at the edge. The coverslip was gently lowered onto the chamber ensuring it did not slip and was centrally placed. The VALAP mixture was gently applied along the edges with the fine paintbrush to seal the chamber. Residue was wiped off the coverslip from the centre with a cotton bud or swab to prevent crystals forming.

The chemoattractant solution e.g., FBS-H, was drawn up using a micropipette with a microloader tip for the Mark 2 and a 200 µL tip for the Mark 4 chamber and the outer wells were slowly filled from the reverse side. The tip was either: (1) placed just inside the drilled hole allowing the outer well to fill by capillary action, or (2) inserted slightly further to form a seal between the hole and the pipette tip before gently pushing the solution through. Either way, care should be taken not to insert the tip too far and push on the inner surface of the coverslip, which will result in fluid flowing between the coverslip and the chamber thereby disturbing the integrity of the chamber and the quality of the linear gradients.

As the outer well filled, the chamber was gently moved to allow air bubbles to rise towards the outlet hole as the solution passed each corner. The Mark 2

outer chamber held approximately 80 μL and the Mark4 chamber 145 μL . Once full, a further 40 μL was added to ensure any control medium that leaked from the centre well was washed out of the chamber. Excess solution was blotted from the outlet holes before sealing with electrical tape. The chamber was labelled and secured to the microscope cassette with Blu Tack® before incubating at 37°C until up to four chambers were assembled and secured in the cassette.

2.1.6.5 Insall chamber setup for centre-well cancer cell chemotaxis assay

Coverslips and chambers were prepared as described above.

Cell Culture and seeding. Cells were grown until 50-80% confluent. The medium was aspirated and the cells washed with PBSx3 and then incubated overnight in SFM. The slightly rounded and less adherent cells were detached by triturating them with a 1,000 μL micropipette before harvesting them into a 15 mL centrifuge tube. A portion of cells was counted and the rest were pelleted at 1000 rpm for 5 min at room temperature. The cell pellet was re-suspended in SFM-H to a density of $5 \times 10^5/\text{mL}$.

Chamber assembly. 40 μL of cells were added to the centre-well of a Mark 4 Insall chamber. After removing as much excess liquid as possible from the fibronectin/ BSA coated coverslip, it was secured onto the chamber. The medium was allowed to spread by capillary action to secure the coverslip and then gently (so as not to allow the coverslip to move) the chamber was flipped over and placed in the microscope cassette. The chambers were placed in a 37°C incubator for 10-15 min to allow the cells to settle and attach to the coverslip. After incubation, the cells remained round, but loosely attached to the surface. The cassette was removed from the incubator and each chamber was carefully flipped over and sealed with VALAP. As with the standard assay, the coverslips were cleaned and the outer wells filled with chemoattractant eg. FBS-H. The outlets were sealed with electrical tape and each chamber was secured in the microscope cassette with Blu Tack®.

2.1.6.6 Conditioned media preparation for chemotaxis assays

Conditioned media were generated as follows. A sub-confluent 10 cm petri dish of WM239A cells was washed with PBSx3. Following the protocol for cell passaging, the cells were split in a 1:5 ratio into five new 10 cm petri dishes and combined with fresh CGM to a final volume of 10 mL. The conditioned media were then harvested from one dish per time-point, staggered between 0-48 hours (Marked T0, T6 etc). All 10ml was aliquoted into 10x1ml eppendorf tubes. The samples were immediately frozen on dry ice before storing at -80°C. The cells in each dish were then counted. Tiff fibroblast and HaCaT keratinocyte conditioned media were also generated using the same method.

Aliquots of conditioned media were thawed in a 37°C waterbath and centrifuged at max ($\approx 16,000$ rcf) for 10 mins using a lab top centrifuge (5415, eppendorf) to remove debris. After decanting and filtering with a sterile 0.2 μm filter, the conditioned media were tested in the Insall chamber standard chemotaxis assay. I added T0 (mock) conditioned medium to the centre-well and a conditioned medium (from the various collection intervals eg. T6, T12 etc) was added to the outer well. I then followed the protocol for the standard cancer cell chemotaxis assay.

2.1.7 Quantification of chemotaxis and statistical analysis

In order to quantify chemotaxis it was necessary to track the migration of cells in the presence of the chemoattractant gradient.

2.1.7.1 Imaging processing

The following software and plugins were used:

1. ImageJ: <http://rsb.info.nih.gov/ij/>.
2. LOCI: <http://rsbweb.nih.gov/ij/plugins/index.html>.
3. Image stabilizer: (http://www.kangli.org/code/Image_Stabilizer.html).

Imagej was used to process all the work in this thesis, along with freely open-access software unless otherwise stated. First, the tiff image sequences were imported using the Bio-formats importer found within the LOCI plugin. Chamber movement during imaging occurred occasionally, resulting in the image gradually

drifting, most often in the y-plane. Nearly all images could be corrected for this drift, by running the image sequence through the Image stabilizer plugin. Very occasionally, due to a large shift, it was necessary to split the image sequence into two or three smaller stacks to minimise the drift per stack. These stacks could then be stabilised individually as described above before concatenating the image sequence again into one movie.

Adjacent images were then stitched using a plugin generated by a former Insall lab PhD student, Michael Carnell, and the cells were individually tracked using MtrackJ. The images were calibrated and stamped with time and distance. The calibration was performed by measuring a set distance on a graticule and converting this distance to pixels.

If the image of the bridge was not perfectly aligned to the screen, it was necessary to rotate the image to ensure that each bridge was perpendicular to the chemotactic gradient. For consistency, all chemoattractant gradients were orientated from low (buffer) on the left to high (chemoattractant) on the right.

2.1.7.2 Cell tracking

For consistency, I attempted to track a minimum of 40 cells in every chamber assay and in most cases this was sufficient to ensure statistical significance. Regardless of the cell lines tested, all cells were tracked using the ImageJ plugin MTrackJ (<http://www.imagescience.org/meijering/software/mtrackj/>) and the track followed the path of the cell nucleus (Soon et al., 2005). The following criteria were used for deciding which cells to track:

- Cells that moved more than 1 cell length in 24 hours
- Tracked continuously until the end of the experiment or until the cell migrated off the bridge or rounded up in preparation for mitosis
- Tracked only cells that started on the bridge and excluded those that migrate onto the bridge during the experiment
- Avoided tracking post-mitotic cells

2.1.7.3 Quantification of migration and chemotaxis parameters

An abundance of tabulated chemotaxis data was generated in the tracking process that was readily exported from Mtrackj. I developed an excel spreadsheet (written by Drs DM Veltman & AJ Muinonen-Martin) to facilitate the processing, analysis and quantification. It has since been used as a tool by other lab members and other groups researching chemotaxis out with the Beatson (McCarty Lab, University of Oregon; Chapple Lab, University of Birmingham).

This spreadsheet automatically produced spider plots, speed and chemotaxis index data over time. A time window was selected (*e.g.*, 6-12 hrs for melanoma cells) and values zeroed within this window to produce end-point data. Chemotaxis index ($\cos\theta$) plots are presented as mean \pm SEM (Soon et al., 2005). $\cos\theta$ is a function of the distance migrated in the direction of the gradient divided by the euclidian distance (the linear distance between the start and end position of the cell). $\cos\theta$ therefore equals +1 for migration directly up the gradient and equals -1 for migration directly away from the gradient. The relative degree chemotaxis between experiments could then be compared between experiments. These data were also processed in the Circstat toolbox for MATLAB by Dr Gabriela Kalna (Beatson Institute) (Berens, 2009). This generated rose and polar plots with 95% confidence intervals and a Rayleigh test.

It is important to know whether the end point positions of the cells are distributed uniformly suggestive of randomly motility or are not distributed uniformly, predicted with chemotactic migration (Berens, 2009). Due to the circular nature of directional data, standard statistical tests cannot be used to analyse these data. The Rayleigh test (Circstat toolbox) is the most powerful and well used circular statistical test for detecting a unimodal deviation from uniformity.

Absolute chemotaxis was defined by meeting the following two criteria: (a) the presence of a significant Rayleigh test, to determine whether there was statistical support for unimodal cell movement and (b) cell movement in the direction of the chemoattractant gradient (*i.e.*, the actual direction of the

attractant gradient had to fall within the 95% confidence interval for the direction of the cell migration) (Muinonen-Martin et al., In Press).

2.1.8 Random motility assay

Six-well glass bottom dishes were coated with fibronectin serially diluted from the 1 mg/mL stock solution and then blocked with BSA as per the method described for Insall chamber cover slip preparation. The following concentrations were used: 100, 30, 10, 3 and 1 µg/ml. Cells were counted and seeded at a density of 1×10^4 /mL in 2mL CGM. This ensured the cells were evenly spread but were not contacting one-another. At least three sites from each well were imaged by time-lapse microscopy with a 10x objective using the Nikon Perfect Focus System (described in detail in chapter 3) at a frame rate of one per 15 mins for 24 hours.

2.1.9 Organotypic invasion assay

This method was provided by Dr Mike Edward, Glasgow University, Dept of Dermatology.

2.1.9.1 Collagen extraction

The tendons from approximately 15 rat tails (Glasgow University) were extracted using toothed forceps and then bathed in 70% ethanol. After blotting dry, the collagen was extracted for 48 hours in 2 L 0.5M acetic acid whilst stirring at 4°C. The extract was centrifuged to remove debris and an equal volume of 10% NaCl (w/v) was added to the supernatant to re-precipitate the collagen before stirring for 30 mins. The sample was centrifuged again, the supernatant discarded and the precipitate was re-dissolved over 48 hours in 0.25M acetic acid, whilst stirring at 4°C. The collagen solution was dialysed against 4-6 changes of 17.5mM acetic acid and then centrifuged at 20,000g for 2hrs at 4°C. The final solution was adjusted with 1:1000 acetic acid to ensure the gels contracted over 6-7 days. The final collagen solution had an approximate concentration of 2mg/ mL and was stored at 4°C.

2.1.9.2 Collagen gel preparation

The collagen gels were prepared by combining the collagen solution, 10x Minimum Essential Medium (MEM, Invitrogen) and 0.22M NaOH in a ratio 8:1:1. The pH was finely adjusted to pH 7.2 with the 0.22M NaOH (this step is critical as fibroblasts are extremely sensitive to alkaline conditions). All solutions were chilled to 4°C before combining to ensure the collagen did not polymerise prematurely. 1 volume of FBS containing 7.5×10^5 primary human skin fibroblasts (passage 5-7) was immediately combined with 10 mL of the gel mixture on ice. After pipetting well, 2.5 mL of the gel and cell mixture was added to each 35 mm petri dish. The gels were then placed in a humidified incubator with 5% CO₂ to set for 15-30 minutes. A further 1 mL MEM was added to each petri dish and the gels were carefully detached to enable gel contraction in the same incubator. The media was changed every 3 days. After 6/7 days the gels measured approximately 1.5 cm in diameter and were transferred to a 24-well dish ready for tumour cell seeding. The gels were typically made in batches of 12 requiring 24 ml collagen solution and one confluent T75 flask (Nunclon) of fibroblasts.

2.1.9.3 Tumour cell seeding

A simple organotypic invasion assay involved seeding only tumour cells onto the surface of each gel. $1-2 \times 10^5$ tumour cells were counted and allowed to seed on the surface of each gel. Alternatively, a skin organotypic assay was generated by combining the melanoma cells with keratinocytes in a ratio 1:5 (Berking and Herlyn, 2001; Santiago-Walker et al., 2009). 48 hours after cell seeding, the organotypic invasion assay was ready to commence the experiment.

2.1.9.4 Organotypic invasion assay

The gel was carefully transferred with forceps to an elevated stainless steel grid (Sigma, Screens for CD-1, Size: 40 mesh, S0770-5EA) and placed in a 6cm petri dish and this was denoted Day 0. CGM was added to cover the grid and was then carefully aspirated to leave a meniscus around the base of each gel, thereby generating an air-liquid interface. Three gels were loaded onto each grid and the medium was changed three times weekly. In experiments using Ki16425, the gels with adherent cells were pre-incubated for 5 minutes with 10 µM Ki16425 in

the CGM before raising the gels to the air-liquid interface. 10 μ M Ki16425 was maintained in the CGM throughout the experiment with thrice weekly media changes as before. A typical experiment lasted 7-12 days.

2.1.9.5 Organotypic invasion assay fixation, embedding and sectioning

At the end of the invasion assay, each gel was carefully divided into two with a scalpel and placed in 4% Paraformaldehyde at 4°C. The embedding, sectioning, histology and IHC techniques were all carried out by staff at the Histology Service (Beatson Institute). The following protocol was provided by Colin Nixon.

In brief, after overnight fixation, the samples were processed the following day on a Thermo Excelsior tissue processor using a day cycle program. The samples were passed through a sequence of six graded alcohols (70%, 90%, 95%, 3 x 100%), then through three changes of xylene before undergoing three changes of molten histology wax under pressure. After this, the organotypics were transferred to a heated chamber where upon they were immersed and orientated correctly in molten histology wax and allowed to harden to form a wax block of the tissue. 4 μ m sections were taken from this tissue block and placed upon polylysine coated glass slides to allow subsequent staining for tissue identification to take place. These sections were baked onto the slides for at least 1 hour at 60°C before being stained with a Haematoxylin and Eosin stain.

2.1.9.6 Histology and Immunohistochemistry (IHC)

Haematoxylin and Eosin (H&E) staining performed on a Leica Autostainer

Reagent	Time
Xylene	4 min
Xylene	2 min
100% EtoH	1 min
100% EtoH	1 min
70% EtoH	1 min
Water	1 min
Gills Haematoxylin	13 min
Water	1 min
1% Acid Alcohol	2 secs
Water	1 min
Scotts Tap Water Substitute	2 min
Water	30 secs
Eosin	3min 15 secs

Water	30 secs
70% EtoH	30 secs
100% EtoH	30 secs
100% Etoh	30 secs
Xylene	1 min
Xylene	1 min
Xylene	1 min
Coverslip applied with DPX	

S100 staining by IHC

Sections were cut to the appropriate thickness and placed in an oven at 60°C overnight. The following protocol was performed on a Dako Autostainer and a Gut parcel was used as a positive control.

Place sections in Xylene	5 mins
Place sections in Ethanol	1 min
Place sections in Ethanol	1 min
Place sections in 70% Ethanol	1 min
Wash sections in Tris Buffered Tween (TbT) (Thermo, TA-999-TT)	5 mins
Block endogenous peroxidase (Dako, S2023)	5 mins
Wash sections in TbT	1 washes
S100 Rabbit polyclonal Ig (Dako, Z0311) Diluted 1/100 with Primary Ig Diluent (Dako, S2022)	35 mins
Wash sections in TbT	2 washes
Rabbit EnVision (Dako, K4003)	30 mins
Wash sections in TbT	2 washes
3,3'-Diaminobenzidine tetrahydrochloride (Dako, K4011)	10 mins
Wash sections in deionised water	1 mins
Haematoxylin Z (Cell Path, RBA-4201-00A)	7 mins
Wash sections in deionised water	1 min
1% Acid Alcohol	2 dips
Wash sections in deionised water	30 seconds
Scotts Tap Water Substitute	1 min
Wash sections in deionised water	1 min
Dehydrate, clear and mount sections with DPX	

2.1.9.7 Quantification of invasion

Invasion was quantified by generating an invasion index from images captured with 10x or 20x objectives. This was calculated as the ratio of cells in the organotypic gel that invaded beyond approximately 30 µm as a ratio of all the cells on top and within the gel. This corrected for any changes in cell number due to the drug treatment. At least three different, but representative,

locations on each gel are analysed. Mean +/- SEM is tested for statistical difference using the unpaired student t test. Over 2000 cells were counted for each condition.

Imaging

2.1.10 *Live cell imaging*

2.1.10.1 *Time-lapse Microscopy*

I used a Nikon TE2000-E inverted time-lapse microscope equipped with a motorised stage (Prior) and Perfect Focus System (PFS) to prevent focal drift due to thermal fluctuations. The entire microscope was enclosed in a plexiglass box, humidified and maintained at 37°C with 5% CO₂. The Insall chamber experiments did not require the addition of supplementary CO₂. The microscope system was driven by Metamorph software (Molecular Devices) and the x, y positions were manually selected and pre-loaded.

2.1.10.2 *Imaging cells using phase, DIC or fluorescence microscopy*

For Insall chamber assays, the inverted chambers were secured in the holding cassette. Objectives used to capture images included Nikon achroplan x10 and x60. For most cell tracking, a 10x objective was used as it enabled the entire width of the bridge to be imaged as well as a few cell widths either side into the wells.

Fluorescent images were acquired using a 60x, 1.45NA achroplan objective, and a digital camera controlled by metamorph software. Differential interference contrast (DIC) images were acquired using a Zeiss Axiovert 200 M inverted time-lapse microscope equipped with a 37°C incubation chamber and motorised stage.

During fluorescence microscopy it is essential to image using as small an illuminated field as possible to reduce the fluorescent illumination on the cells of interest and neighbouring cells. This reduces the phototoxic effect of reactive oxygen species produced by excited fluorophores (Nishigaki et al., 2006). To optimise the duration of imaging and the quality of the images the condenser was therefore focussed and the shutter aperture minimised. For

consistency, imaging always moved clockwise, starting from the bottom left corner of each chamber. Great care was taken to always image each corner to ensure verification of the chamber orientation and hence the gradient direction during processing.

For cell tracking, frame rates and imaging duration depended on the cell speed, but generally frame rates between 15 min to 1 hr were adequate for cancer cell chemotaxis for a duration of 24-36 hrs.

2.1.11 Nikon Perfect Focus System (PFS)

PFS (or a similar system) has proved an essential system, providing real time focus correction for focus drift arising during time-lapse experiments as a result of thermal and mechanical effects. This drift occurred despite allowing the chambers to acclimatise for 30-60 minutes and securing them in the holding cassette with Blu-Tack. The system eradicated the need to perpetually reset the focus, thereby enabling prolonged time-lapse experiments, without the need to image in multiple planes simultaneously (Peters, 2008).

2.1.12 Insall chamber validation

2.1.12.1 Confocal microscopy

The concentration gradient profile was characterised using 100 μM fluorescein isothiocyanate in 100 mM Tris.Cl pH 8.0 in the outer chemoattractant well and 100 mM Tris.Cl pH 8.0 in the inner control well. Images were captured using a Leica confocal microscope with excitation by a 488 nm laser and an emission filter within the 502-542 nm spectra. The laser intensity was determined prior to capturing each image using a peri-saturating power for the chemoattractant well by referring to a Lookup Table (LUT) with a high contrasting upper limit (Glow (Over & Under), LUT, Leica). This was determined by reducing the laser intensity until just below the upper saturating limit. 16 bit greyscale images were acquired at intervals during 24 hours and pixel intensity across the bridge was quantified using the imagej plot profile function. In brief, a representative section across the bridge was sampled and a line plotted perpendicular to the bridge. Using the plot profile command, tabulated pixel intensity data relative to location along the line was acquired and extracted for processing.

In vivo studies: fresh melanoma tissue collection

2.1.13 Fresh murine melanoma tissue collection

2.1.13.1 Murine melanoma tissue

I used the inducible Tyr::CreER^{T2} BRAF^{V600E/+} PTEN^{lox/-} melanoma model, in which the melanomas were all generated in mixed background mice from 6-12 weeks of age (Dankort et al., 2009). This model was generated through the breeding programme of Prof Sansom and Prof Ozanne at the Beatson Institute by Dr Lindsay and Dr Faller. All work was performed with the appropriate personal and project licences under the UK Home Office guidelines.

The alleles used were as follows: Tyr::CreER^{T2} (Bosenberg et al., 2006) BRAF^{V600E/+} (Mercer et al., 2005) PTEN^{lox/-} (Lesche et al., 2002). After activating Cre-recombinase, this model generated a melanocyte-specific expression of one copy of BRAF^{V600E/+} and melanocyte-specific deletion of one copy of PTEN.

To induce recombination in the Tyr::CreERT2 mice, animals were treated with 2 mg tamoxifen topically to shaved back skin daily for 5 days. There was no discernable phenotype until naevi or primary melanomas started developing 6-8 weeks after induction predominantly on the treated area. Typical grooming behaviour spread the tamoxifen to other parts of the skin and/ or was ingested leading to activation in other cutaneous regions.

All mice used were part of my collaborators' cohort study. Before they were sacrificed, all mice had reached the primary or secondary end-points of their designated study.

2.1.13.2 Tumour sample collection

Suitable mice were identified with at least one and up to four tumours, ideally located on the back. 4x4 mm was the smallest tumour size to enable at least 2 areas to be sampled. The mice were all sacrificed using the Schedule one home office protocol. Once the mice were sacrificed, the skin containing the tumours was rapidly dissected off the back and pinned slightly taut to paper overlying a

corkboard. Where possible, the samples were photographed before and after sampling.

To sample the tumours, sterile Punch Biopsy tools (Stiefel) were used to punch circular samples from the tumour and surrounding skin. The size of punch biopsy depended on the tumour size and varied from 3-6 mm in diameter.

Samples were taken at various locations across the tumour and were coded as follows: within the tumour (A), across the margin (B), 5 mm from the margin (C), 10 mm from the margin (D), 15mm from the margin (E), >20mm from the margin (Distant) and subcutaneous tissue (SC).

Samples were immediately snap frozen in liquid nitrogen in eppendorf 2 ml safe-lock micro tubes (Sigma). The samples were then transferred to a -80°C freezer for storage.

2.1.13.3 Control samples

Control samples of normal appearing skin in the same melanoma model activated with tamoxifen were used to calculate the basal level of LPA. Each section of mouse skin underwent a series of nine punch biopsies (A, B and C in 3 replicate series).

2.1.14 *Fresh human melanoma tissue collection*

2.1.14.1 Ethical approval for a melanoma tissue collection programme

A great deal of consideration was given to the challenges of collecting fresh melanoma tissue and in particular the primary lesions. Support and advice from Prof Dot Bennett and Dr Julia Soo, (St. George's, London) was instrumental in providing the framework for the application, given their recent successful primary melanoma tissue collection programme.

Ethical approval for the collection of melanoma tissue was originally granted through the West of Scotland Research Ethics Service in February 2010. NHS Greater Glasgow & Clyde (GGC) granted management approval in June 2010 (Appendix 2). The study was in accordance with "Good Clinical Practice" and

the World Medical Association's Declaration of Helsinki (1964) and its' revisions (Tokyo 1978, Venice 1983, Hong Kong 1989, South Africa 1996 and Edinburgh 2000). (Appendix 3) A minimum primary melanoma size of 10 mm was agreed with the GGC lead skin pathologist, Dr Karen Blessing. Key extracts from the protocol highlighting the tissue approved for collection is as follows:

“5.1 Collection of Tumour samples

5.1.1 Collection of fresh tumour samples

Samples of both suspected primary and secondary melanoma will be collected at the point of excision and carried immediately to the Department of Pathology at the corresponding hospital site. Tissue deemed excess to diagnostic requirements will be identified and prepared by, or under the supervision of, a member of the pathology department. This will then be transported to the Beatson Institute for Cancer Research or another laboratory.

5.1.2 Collection of archival tumour samples

All patients included in the fresh tumour sample collection programme will be asked to consent to retrieval of paraffin embedded, formalin fixed tissue from the pathology archive where there is sufficient in excess of diagnostic requirement (as decided by the responsible pathologist). In addition, excess tissue held in the archive from other patients meeting the appropriate eligibility criteria will be retrieved by appropriately trained healthcare workers in the department of pathology.

No additional visits will be required for any subjects taking part in this study.”

Tissue collection commenced in November 2012. By this time, the 2006 Human Tissue Act legislation in Scotland had been altered, following the 2011 update. This led to the formation of NHS Research Scotland and I therefore reapplied to the local representative, the GGC NHS Bio-repository, to seek project approval

to allow the project to proceed using the framework from the initial approved application.

The terms were renegotiated with the new GGC lead consultant skin pathologist, Dr Colin Moyes. The major change re-negotiated was an increase in the size of the primary melanoma from 10 to 25 mm to ensure there was no risk of harming the accuracy of the diagnosis or prognosis. In addition, it was agreed a consultant pathologist would attend the procedure to decide whether tissue excess to diagnostic requirements could be provided.

2.1.14.2 Tumour identification

A pilot of between three and five samples was agreed with the GGC Bio-repository. Samples were identified through plastic surgery and dermatology skin cancer clinics, in addition to support from the multi-disciplinary teams leads across the region and the staff at the Bio-bank who actively searched through pre-operative lists. The study was advertised through presentations and dissemination of a 1-page summary (Appendix 4) to all plastic surgeons and dermatologists involved in melanoma care across the West of Scotland.

2.1.14.3 Tumour sample collection

Following identification, potential samples were screened both by Dr Moyes and myself. Informed consent was obtained using the appropriate bio-bank form. The lesion was photographed with and without a dermatoscopic lens following informed consent. Immediately following excision of the lesion, Dr. Moyes determined if samples were permitted to be taken across the lesion with a 3 or 4 mm punch biopsy tool. These samples were labelled with the letter coding as per the mouse samples.

The samples were immediately snap frozen in liquid nitrogen and as per the mouse samples, stored at -80°C

2.1.15 Conditioned media & fresh melanoma LPA quantification

2.1.15.1 Tumour weighing

To generate a concentration of LPA within the tissue, the frozen tumour core was first weighed to the nearest mg.

2.1.15.2 Liquid chromatography-mass spectrometry (LC-MS)

The LPA was extracted and quantified at my collaborator's laboratory (Prof Wakelam, Lipidomics Mass Spectrometry Laboratory, Babraham Institute, Cambridge). The frozen conditioned media samples and tumour cores were posted next-day delivery in a copious bath of dry-ice. The following protocol was provided by my collaborators.

Mice and human melanoma/ skin samples (1-20mg) were pulverised after thoroughly cooling with liquid nitrogen. The pulverised powder was suspended in 750 μ L water then used for LPA extraction. For cell culture media samples, 750 μ L of cell culture media was used for LPA extraction. Media or tissue samples were spiked with 50 ng of 17:0-LPA as an internal standard before extraction. LPA was extracted with 1 mL n-butanol three times at room temperature.

The combined LPA extract was dried under vacuum with SpeedVac (Thermo) and re-dissolved in 60 μ L chloroform/methanol/water 2:5:1. 14 μ L was injected for liquid-chromatography with tandem mass spectrometry (LC-MS/MS) analysis. For LC-MS/MS analysis, we used a Thermo Orbitrap Elite system (Thermo Fisher) hyphenated with a five-channel online degasser, four-pump, column oven, and autosampler with cooler Shimadzu Prominence HPLC system (Shimadzu) for lipids analysis. High resolution / accurate mass and tandem MS were used for molecular species identification and quantification. The identity of the lipid subspecies was further confirmed by reference to appropriate lipids standards. All the solvents used for lipid extraction and LC-MS/MS analysis were LC-MS grade from Fisher Scientific.

2.1.15.3 Quantification & statistical analysis

The final amount of LPA (ng) is presented as a concentration per 750 mL of conditioned media analysed or per mg tissue. The data is represented graphically plotting mean \pm SEM for the concentration of LPA v conditioning time (for conditioned media samples); and distance from tumour margin (for tumour samples). Samples were normalised to position "A" for comparison between tissue samples.

Chapter 3:

Development, Optimisation & Validation of an Efficient Assay for Cancer Cell Chemotaxis

Introduction

The current challenge is to build on the knowledge developed through studying chemotaxis in model organisms like *Dictyostelium* to enhance our understanding of the role of chemotaxis in human cancer. The introductory chapter contained a review of the growing body of evidence that chemotaxis plays an important role in the invasion and metastasis of cancer cells. Drugs which target cancer cell invasion and metastasis have proven difficult to develop, so an improved understanding of the detailed mechanism of chemotaxis may enable the prioritisation of better drug targets, better drugs, appropriate patient selection and smarter early clinical study design (Kedrin et al., 2007).

Research into the field of cancer chemotaxis is still in its infancy. The introductory chapter reviewed the investigative tools that have had to be developed for investigating chemotaxis. In the introduction, I outlined two of these key tools in detail, the Zigmond and Dunn chambers. These tools were initially designed for investigating rapidly moving cells like neutrophils and *Dictyostelium* and so require refinement in order to study cancer cell chemotaxis. To recap, these direct visualisation bridge chambers use a two-well design whereby cells are seeded between one well containing a control or buffer substance and the other the chemoattractant. In standard assays, the cells lying within the gradient are free to migrate between them.

Direct visualisation chambers are considered the gold standard assay for investigating the behaviour of cells whilst performing chemotaxis due to the defined conditions and the wealth of data generated (Wells, 2000). However, this assay is challenging, due to the delicate assembly and short-lived gradient, compounded by non-perpendicular gradients complicating analysis. These factors render the observation of slowly-moving cells unfeasible or almost impossible (Zengel et al., 2011). We therefore established a user-friendly, robust assay for cancer cell chemotaxis in order to comprehensively explore the chemotactic behaviour of melanoma cells.

In developing the assay, it was important to consider the various advantages, disadvantages and caveats of existing direct and indirect visualisation assays and these were dissected in some detail in the introductory chapter. There were

several attributes of the Dunn chamber that were considered important for the new and improved chamber, and most important, was reproducing a similar gap of 20 μm between bridge and cover slip to reproduce a stable linear gradient over 24 hours allowing slowly-moving cells to be tracked. Previous chamber designs including the Dunn and Zigmond chambers were intentionally designed for use with thick (#3, 0.25-0.35 mm thickness) cover slips. This “dictates that high-power, non-immersion objectives with a fixed compensation for the standard (#1.5) coverslips (0.16–0.18 mm) should not be used for critical work” (Zicha et al., 1991). Therefore the use of high numerical aperture (NA) oil immersion objectives for the critical work of investigating the mechanisms of chemotaxis with fluorescently tagged proteins in known gradients has been very technically challenging. In addition, changing the gradient in Dunn chambers is inefficient due to the method of sealing the chambers.

In 2010, we described the Insall chamber as an improved tool for measuring cancer cell chemotaxis (Muinonen-Martin et al., 2010). It was designed, by my supervisor, as a refined derivative of the Dunn chemotaxis chamber. Particular advantages include easy handling, simple perpendicular gradient orientations, and two different gradient steepnesses in the same assay, and above all the ability to use standard thin (#1.5) cover slips, allowing the use of high NA oil immersion lenses. Using this improved (Mark 2) chamber and a further evolved (Mark 4) model.

This chapter charts the development, optimisation and validation of the Insall chamber. Although the chamber has been optimised for use with melanoma cells throughout this body of work, it is equally at home as a tool for cancer cell chemotaxis in general or with other slow moving cells such as fibroblasts. I outline the “standard assay”, which is comparable with typical Zigmond or Dunn assays, with cells spread throughout the linear chemoattractant gradient (Zicha et al., 1997; Zigmond, 1977). This assay allows cells to move freely in any direction within the gradient, with the caveat that cells may locally modify the gradient through autocrine or paracrine effects, or as yet unidentified mechanisms (Wyckoff et al., 2004; Zicha and Dunn, 1995). We have described protocols for this assay in a published detailed methods paper (Muinonen-Martin et al., 2013).

Chamber Development & optimisation

3.1.1 Chamber design

As discussed, previous chamber designs were designed for use with #3 cover slips and therefore did not include support structures. Without any extra structural support, the #1.5 coverslips we desired to use bow, causing occlusion of the chamber. This interferes with the gradient formation across the bridge with resultant intra- and inter-chamber gradient inconsistencies. Careful consideration was therefore given to the positioning of supporting material within the bridges to minimise the distance that the cover slip spans (Fig. 1-5A,D). By ensuring that the supports were the same height as the surrounding chamber, the thin coverslip was provided with enough support to ensure that the bridge height did not fluctuate more than 1µm anywhere across the bridge (Fig. 1). Additional supports were also included for the cover slip at the upper and lower ends of the chamber. This had the benefit of further supporting the coverslip and reducing the wasteful diffusion of chemoattractant from the source.

3.1.2 Extracellular matrix (ECM) coating

ECM coating is important to enhance the adhesion to hydrophobic surfaces such as glass (DiMilla, 1992). Throughout the experiments, fibronectin has been used as the ECM for melanoma cell chemotaxis. The introduction highlighted how ubiquitously expressed this protein is in stromal tissue. This coating is beneficial to allow better attachment of cells to enhance motility, although cells have been shown to chemotax with only minimal adherence (Aznavoorian et al., 1990). It is important to determine the ideal concentration of fibronectin to maximise the migration speed to increase the number of cells that can be quantified in a given Insall chamber assay. This is due to the biphasic migration speed response with varying attachment strength, with maximal migration at an intermediate level of cell-substratum adhesiveness (DiMilla et al., 1993). The optimal concentration should be determined after performing a serial dilution of the ECM and testing which concentration enables the fastest random motility of cells in a 6-well dish. This experiment was performed with varying concentrations of fibronectin between 25 µg/ml and 2.5 µg/ml and 5 µg/ml was

visually identified as the optimal concentration for MV3 melanoma cells. For consistency, this concentration was used throughout all the experiments.

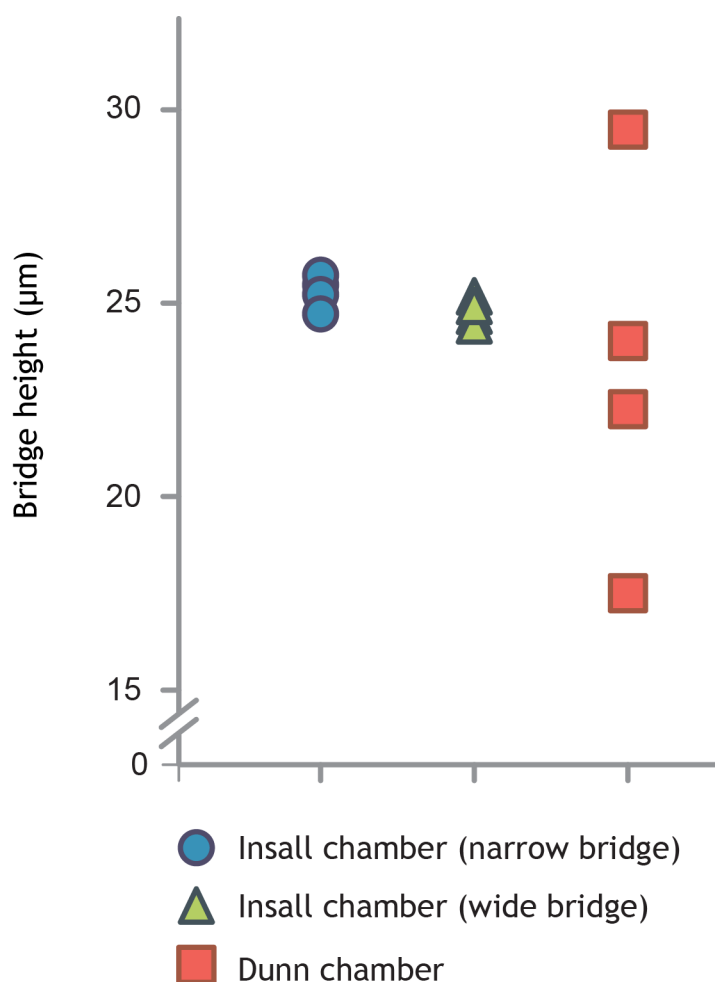


Figure 3-1 Bridge heights in Insall and Dunn chambers during use.

Bridge heights are measured in μm at four locations across the Insall chamber narrow and wide bridges and the Dunn chamber using a #1.5, 0.16–0.18 mm cover slip. Chambers were filled with fluorescein and images were taken in a z-stack using 1 mm intervals to calculate the distance between the bridge and cover slip. The bridge height was consistent at all sites in the Insall chamber with less than 1 mm variation demonstrating that thin cover slips can be used without affecting the geometry of the chamber and hence the diffusion profile.

3.1.3 Handling and securing the coverslip

As the cells are adherent to the cover slip, any movement can be potentially harmful to cells by either exerting shear stresses on them or crushing them against the supports. The coverslip is secured in place to both ensure that there is no movement relative to the chamber and no evaporation of chamber contents during imaging for around 24 hours in a 37°C environment. This is particularly

essential to avoid in the centre-well assay described later because in addition to cellular damage it will move cells relative to the origins of the bridge. A second important factor is the need to prevent evaporation of chamber contents, which is noticeable within 30-60 minutes even at room temperature. This problem became apparent whilst trialling Zigmond chamber clips to secure the coverslip in the early stages of development (Zigmond et al., 2001). The clips also exerted tension on the chamber with a resultant bowing deformation leading to a variable interface between the cover slip and chamber. After experimentation with nail polish and beeswax, a published VALAP formula was used with great success to seal the coverslip to the chamber avoiding the complications of shearing cells, evaporation of contents or chamber deformation (Sluder et al., 2007).

3.1.4 Reverse filling of the outer chemoattractant well

With a similar principle and methodology, the chamber handling is similar to the Dunn chamber, but with a few advantages. The “rabbit ears” at the top of the external well (Fig. 1-5A,B & 3A) facilitate the filling and refilling of the external well. These can if desired be drilled to allow the contents of the chemoattractant/outer well to be changed in situ by reverse filling (Fig. 1-5B). To investigate slow moving cancer cells over longer time frames it is imperative to seal the chamber effectively and this necessitates the drilling of all chambers to enable reverse filling.

The other advantage of this technique and one, which is still in the theoretical stages of development, is the possibility of pumping fresh chemoattractant solution through the drilled holes using a micropump (Toetsch et al., 2009). This is a useful technique to explore the response to a new chemoattractant/inhibitor or to ensure that any local effects generated by the cells is negated by the constant flow of fresh media.

3.1.5 Gradients with simple orientations

The microfabrication techniques used enabled the design of a square bridge or viewing platform. The Dunn chamber, in particular, was manufactured by grinding glass and hence they produced a circular bridge. This complicates the

calculation of chemotaxis index, which to be accurate must always be corrected for the angle of the gradient at that point. The square geometry across all the bridges provides a simple and consistent chemoattractant gradient orientation perpendicular to the bridge. This makes the analysis of chemotaxis parameters considerably easier than for Dunn chambers (Zicha et al., 1997; Fig. 1-5D).

The only essential consideration to bear in mind when preparing to analyse the data is the orientation of the inner and outer wells that are diametrically opposite depending on which side of the chamber is being viewed. To ensure this error is avoided, I always systematically imaged the four corners of the chamber. The corners possess a curved inner edge in all versions of the chamber, which enables the easy orientation of the images relative to the gradient direction.

3.1.6 Gradients with different steepnesses

Dunn chambers were milled from glass and only one 1 mm bridge width could be incorporated into the design. Due to the fabrication technique of the Insall chambers, it was straightforward to create different bridge widths in the two sides of the device (Fig. 1-5C, D). As the concentrations of attractant in the inner and outer wells are constant, this translates into two different steepnesses of gradients. With an automated XY stage it is thus possible to track cells chemotaxing in both gradients simultaneously. In the Mark 2 version of the chamber shown here bridge widths of 0.5 mm and 1.0 mm were constructed.

3.1.7 Ongoing chamber evolution

The Mark 2 chamber provided an improved platform from which to start investigating cancer cell chemotaxis. It became clear with use that the design required further improvement to simplify the filling of the outer well, further increase the stability of the gradient over time and improve the data yield from each experiment. The Mark 3 design attempted to address these issues but failed and will not be discussed further.

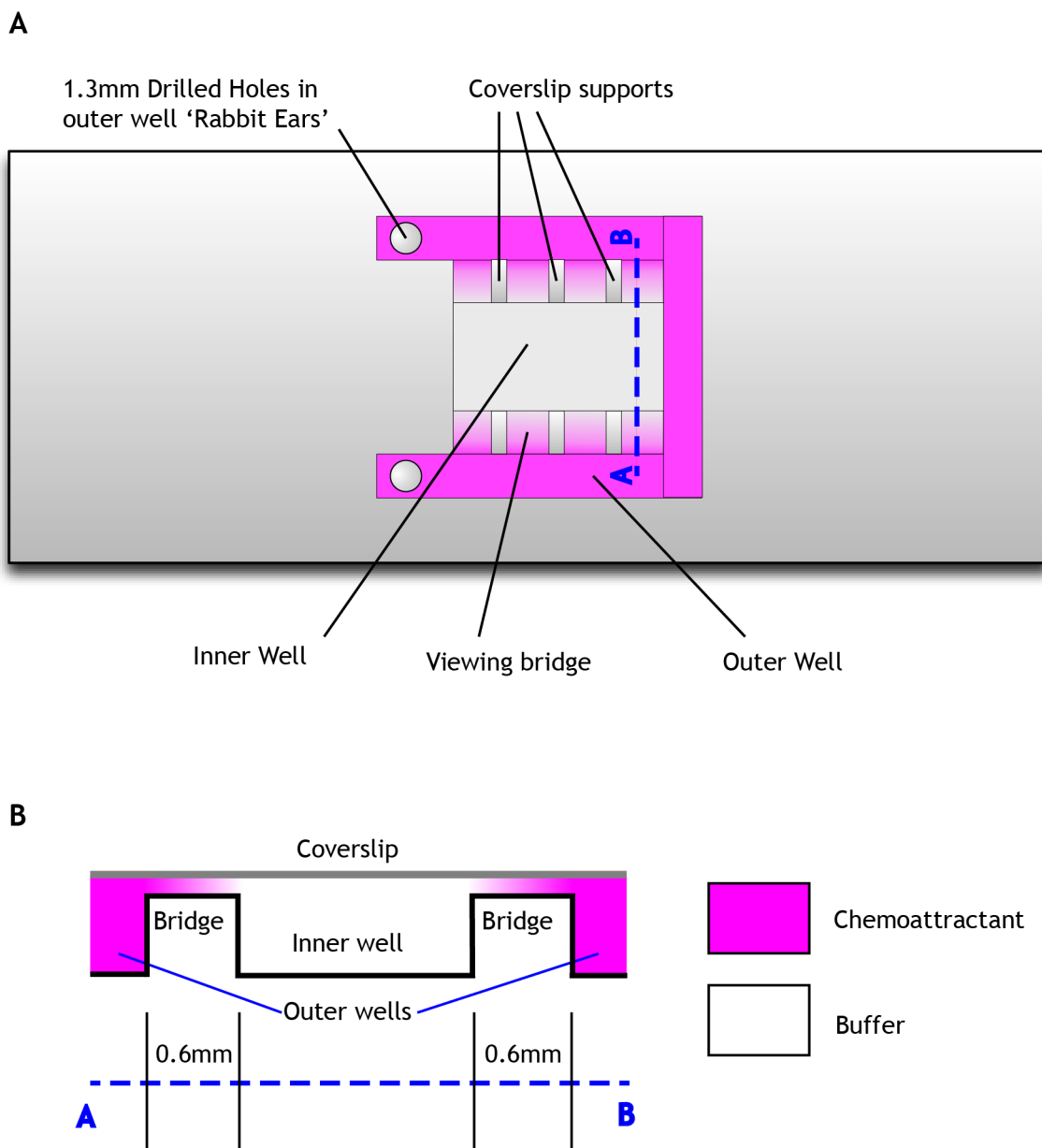


Figure 3-2 Mark 4 Insall Chamber features.

A Schematic of a Mark 4 Insall chamber from above highlighting the key features. Drilled holes in the 'rabbit ears' necessary for >1 hour experiments to allow reverse side filling in order to seal the chamber and prevent evaporation. The inner buffer well and outer chemoattractant wells along with the 8 viewing bridges are also emphasised. Magenta highlights the location and intensity of the chemoattractant. **B** A cross-section along the blue dashed line in **A** highlights the chamber shape, the 0.6mm bridges throughout and the resultant linear chemoattractant gradient (again in magenta) produced towards the outer wells.

The Mark 4 design proved a great success and has been used for all the work presented in this thesis unless otherwise stated. The outer well was designed with a U rather than an A shape (Fig. 2A). This meant it was no longer necessary to fill the well with a microloader pipette and instead a standard pipette tip attached to a P200 pipette could be used to fill the entire outer well in one load. Importantly, this reduced the number of experiments lost due to bacterial contamination and reduced the presence of trapped air bubbles due to the A-

frame design. Air bubbles expand once inside the incubator, affecting the pressure inside the chamber and potentially the rate of diffusion of the chemoattractant (Jowhar et al., 2010). The bridges were all manufactured to 0.6mm in diameter (Fig. 2B) to allow enough distance for cells to migrate over with a steep enough gradient to enable efficient chemotaxis. Both the inner and outer wells were increased in size to enhance the stability of the gradient by increasing the source and the sink (Torisawa et al., 2010). To increase the data yield, the number of bridges was doubled to eight in total. Due to the random nature of cell seeding, it is not uncommon to see some bridges with low density and almost no cells and others with too high a density and nearly all cells contacting one another.

The latest incarnation, the Mark 5 chamber, is identical to the Mark 4 chamber but has two chambers per slide allowing a control or duplicate experiment to be performed in exactly the same conditions. In the future it will also be possible to automate the replacement of buffer in the outer chamber, with improvements in the possible range of experiments.

Validation

3.1.8 Gradient stability and linearity

Gradient formation was directly observed using fluorescein as a diffusible marker, which demonstrated that the profiles of both gradients remain stable for 24 hours (Fig. 3A,B). These validation experiments were carried out with the assistance of Douwe Veltman. In the Mark 2 chamber, the narrow (0.5 mm width; Fig. 3A) bridge produced a linear gradient and the wide (1.0 mm; Fig. 3B) bridge a less steep gradient, but both remain relatively stable throughout the 24 hour period, although with time, the steepness of both gradients gently reduce. Interestingly, the wider (1 mm width) bridge produced a stable linear gradient again with gentle reduction in steepness, but only over the two-thirds of the bridge nearest the buffer following initial stabilisation. I therefore concluded that the central area of the wide bridge should be imaged for consistency. The gradient generated in the Mark 4 chamber was validated using the same method and as predicted, the resulting gradient is more linear and stable over the 24 hour window than either gradient generated in the Mark 2 chamber (Fig. 3C).

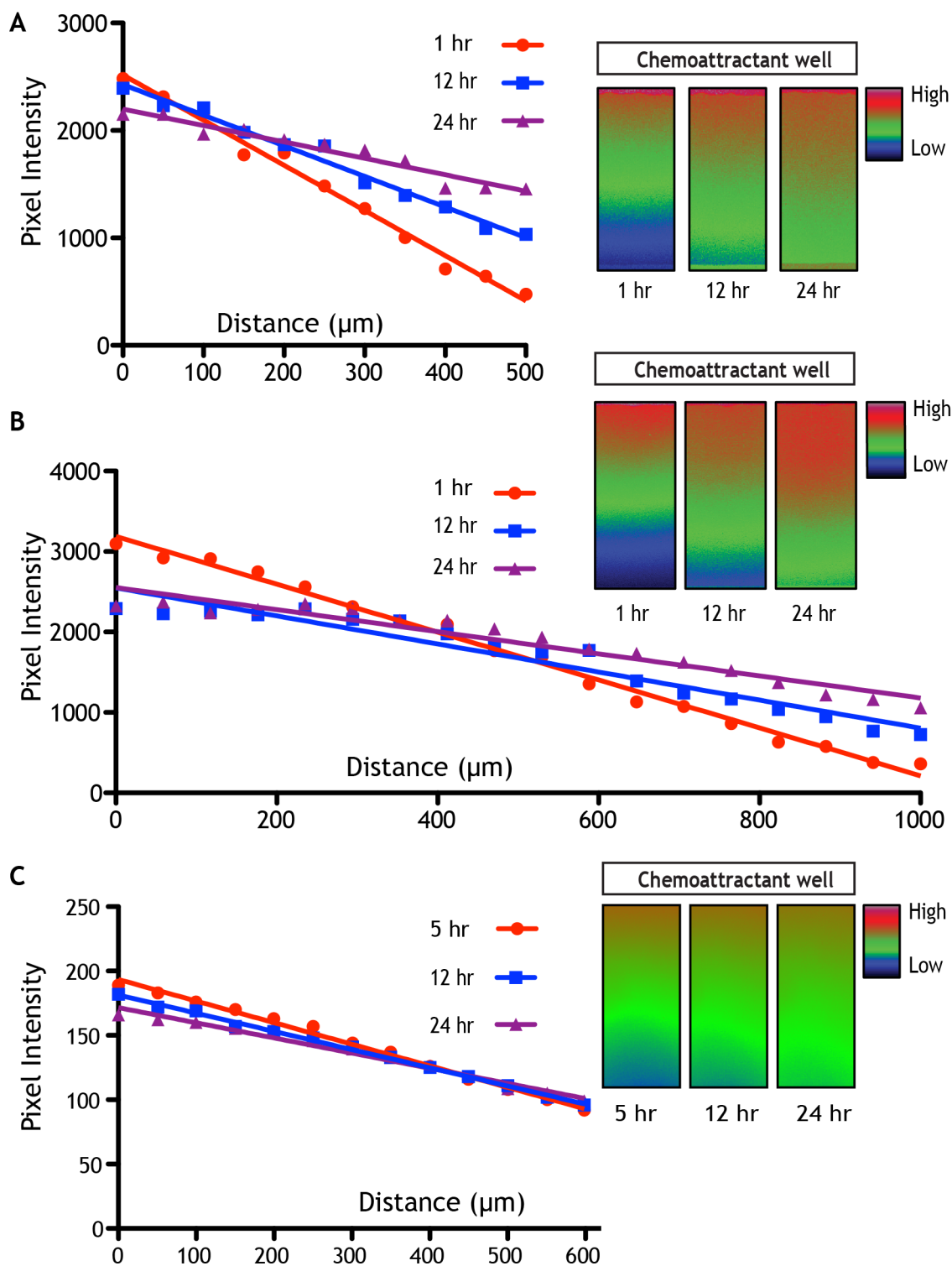


Figure 3-3 Stability of linear gradients.

Gradients were established for between 1 and 24 hours across the **(A)** narrow and **(B)** wide bridges in the Mark 2 Insall chamber and the **(C)** standard 0.6mm bridge in the Mark 4 Insall chamber. The outer chemoattractant chamber was loaded with 100 mM fluorescein in 100 mM Tris-Cl pH 8.0 and the inner control chamber with 100 mM Tris-Cl pH 8.0. Confocal images were acquired at various intervals and quantification of the gradient was performed by measuring pixel intensity from the fluorescence signal as it diffused across the respective bridges. The pixel intensities across the bridges in **(A-C)** are represented by the respective colour panel inserts.

Capturing cell images & image processing

Time-lapse microscopy was performed to capture the chemotactic responses of the relatively slow moving cancer cells. A motorised x, y stage allows multiple positions to be imaged during the course of an experiment. All microscopes used were controlled using metamorph software. A major benefit of the Insall chamber over previous chamber designs is the ability to use differential interference contrast (DIC) microscopy and high NA oil immersion microscopy to provide the highest quality fluorescence images. I was therefore able to capture high resolution images using phase, DIC and fluorescence microscopy.

3.1.9 Phase & DIC microscopy

With phase microscopy, I have been able to successfully demonstrate the chemotaxis of MV3 melanoma cells towards a 10% Foetal Bovine Serum (FBS) gradient. This can be successfully and reliably performed using a range of objectives from 10x to 60x magnification (Fig. 4A). The use of nonpolarising substrates in the chamber fabrication means that DIC microscopy may also be used, which is not possible with many plastic devices (Fig. 4B). Due to limited PFS compatible objectives, it has not been possible to use PFS with DIC microscopy. DIC imaging, therefore involved selecting images from a vertical series (z-stack). When reviewing the images, the in focus z-planes were then selected for onward processing. Movies were generated by concatenating the focussed images, which was a laborious process and is one of the key reasons I did not pursue this technique, despite the detailed images it can produce.

3.1.10 Fluorescence microscopy

Due to the thin cover slips high NA oil immersion microscopy is also possible and I demonstrated the chemotaxis of Lifeact-GFP transfected MV3 metastatic melanoma cells over 24 hours using fluorescence microscopy with a 60x 1.45NA oil immersion objective (Fig. 4C). Two daughter cells can be seen emerging from mitosis, polarising and then chemotaxing towards the FBS gradient. Their paths are highlighted by the red and yellow tracking lines.

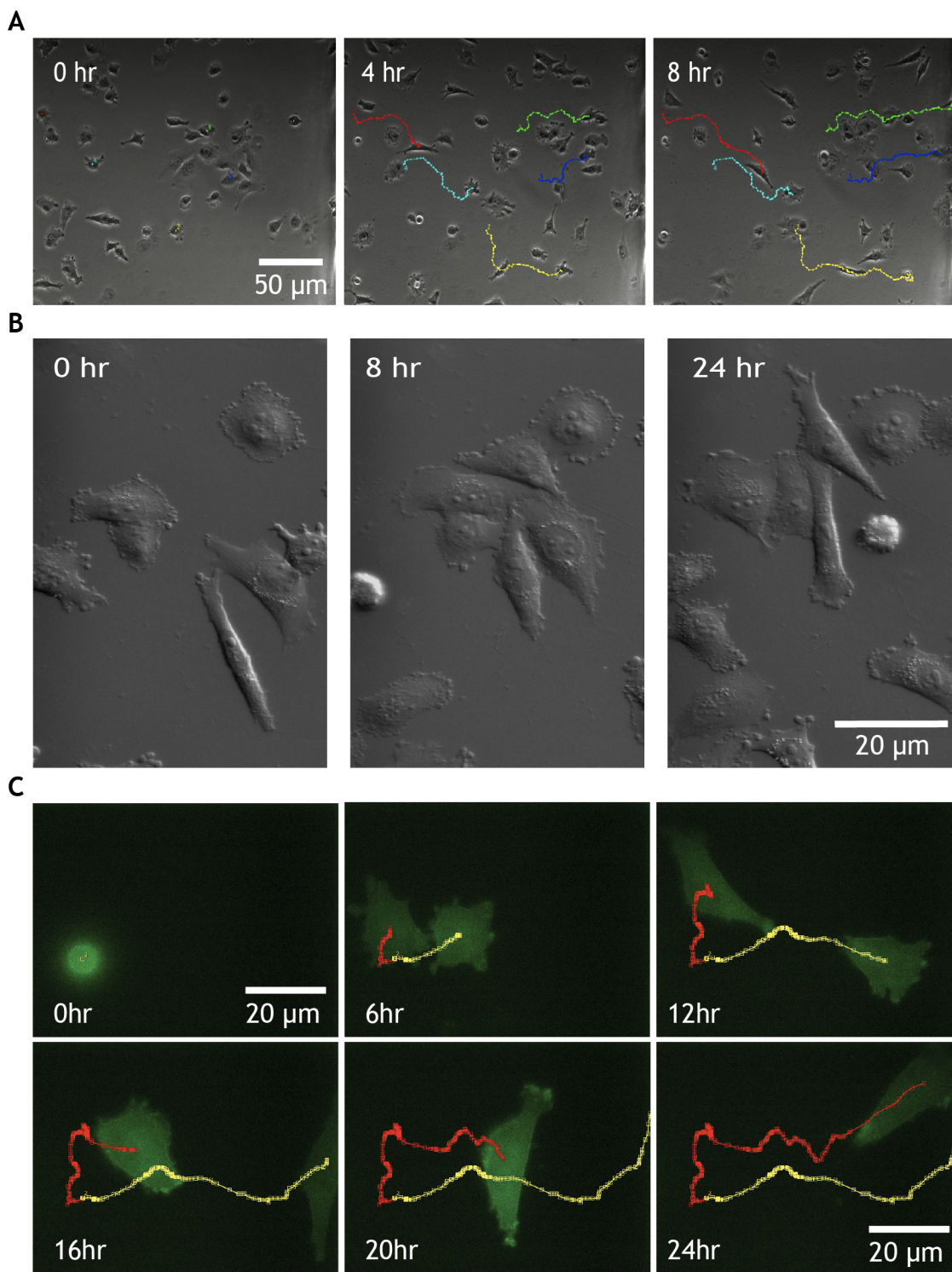


Figure 3-4 Insall chamber imaging modalities.

A shows chemotaxis of MV3 melanoma cells towards a 10% FBS gradient on the right of each image and imaged using inverted phase contrast microscopy with a 10x phase objective with time-lapse imaging. Cell tracking lines have been created using the ImageJ MTrackJ plugin. **B** DIC imaging of melanoma chemotaxis. MV3 melanoma cells migrating towards a 10% FBS chemoattractant at the top of the image(s) over the course of 24 hours were imaged in differential image contrast using a 40x 1.3NA objective. **C** Live cell fluorescence microscopy using high-NA objective. Insall chamber chemotaxis assay with identical set-up and analysis to experiment in Fig. 2, but the MV3 cells are stably transfected with GFP-Lifeact. Time-lapse images are taken using a 60x, 1.4NA oil immersion objective.

3.1.11 *Capturing and processing multiple images*

The PFS system not only ensured a focussed image at one site throughout a 24 hour time-lapse movie, but importantly, it allowed images at multiple x, y positions to be captured reliably. Two 10x overlapping images on the Mark 4 chamber covered one entire bridge. Stitching these two images (Fig. 5A) was helpful to provide an overview of the responses of all the cells across the entire bridge and to track some cells that passed between one field of view and another (McCluggage, 2006).

With eight bridges per chamber, all 16 positions could be imaged (Fig. 5A). The yield and consistency between experiments was significantly enhanced by designing a cassette that was capable of holding 4 chamber slides per microscope (Fig. 5B). Using the Mark 4 chamber, it was therefore possible to image all 32 (8x4 Insall chambers) bridges in one time-lapse experiment. This was a major improvement from early experiments with the Mark 2 chamber where images of only 4 bridges could be captured during any one experiment.

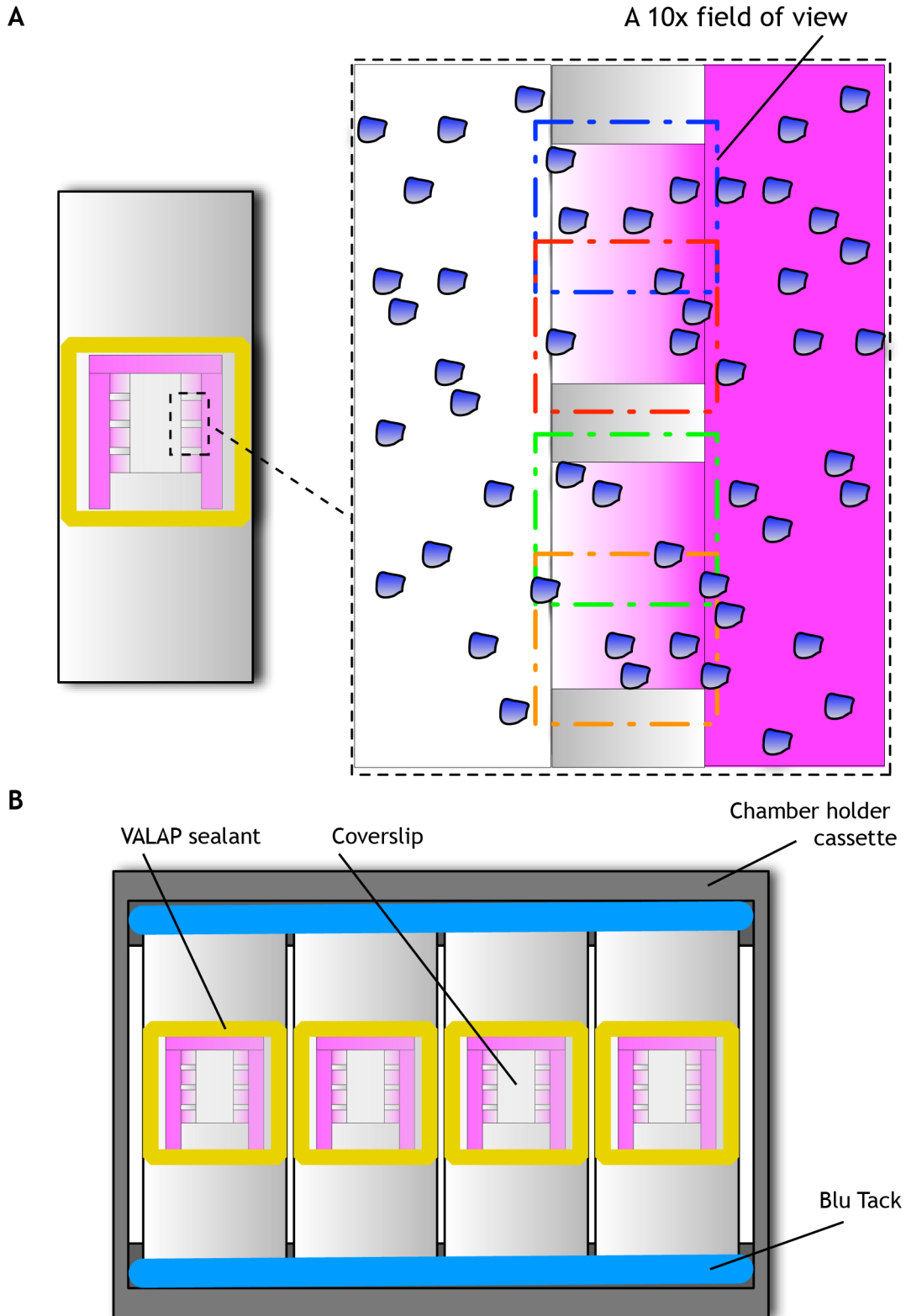


Figure 3-5 Insall chamber imaging set-up.

A The rectangular area over the viewing bridges in **A** is exploded. The coloured dashed squares represent the field of view for a 10x objective showing that the entire width of the bridge can be viewed. Two overlapping images can be stitched together to provide footage of the entire bridge between the coverslip supports. **B** Up to four chambers can be positioned inverted on a purpose built aluminium cassette. The chambers are secured in place with Blu Tack®.

Metastatic melanoma cells perform accurate chemotaxis towards 10% FBS

Having developed, optimised and validated the Insall chamber, I first asked the question, are metastatic melanoma cells chemotactic to serum? To answer this, I employed the standard assay and analysed the cell tracks of 43 MV3 metastatic melanoma cells in the presence of a 10% FBS gradient (SFM inner well: 10% FBS outer well - denoted as SFM: FBS) and 46 cells without a 10% FBS gradient (SFM inner well: SFM outer well - denoted as SFM: SFM) migrating on the narrow bridge of a Mark 2 Insall chamber (Movie S1 and Movie S2).

The quantification and analysis of the data demonstrating chemotaxis in the presence of 10% FBS and random migration with no chemotactic gradient can be seen in (Fig. 6). Rose plots (A & B) demonstrate that cells migrated randomly in the absence of FBS but predominantly up the gradient in the chemoattractant experiment. Polar plots use end-point data to plot points on a unit circle and the red line indicates the direction and magnitude of the resultant mean vector. The polar plots for the control experiment (C) reveal a short mean resultant vector for the control experiment with the cells so randomly spread that it was not possible to calculate a 95% confidence interval. Conversely, the cells in a chemoattractant gradient demonstrate a much longer mean resultant vector with a narrow 95% confidence interval falling directly over the direction of the chemoattractant (D). The evidence for directed migration is further supported by a highly significant Rayleigh test ($p = 2.30 \times 10^{-9}$) demonstrating a unimodal deviation from uniformity (or non-random migration). The paths of individual cells in the spider plots highlight a strong bias for migration towards FBS.

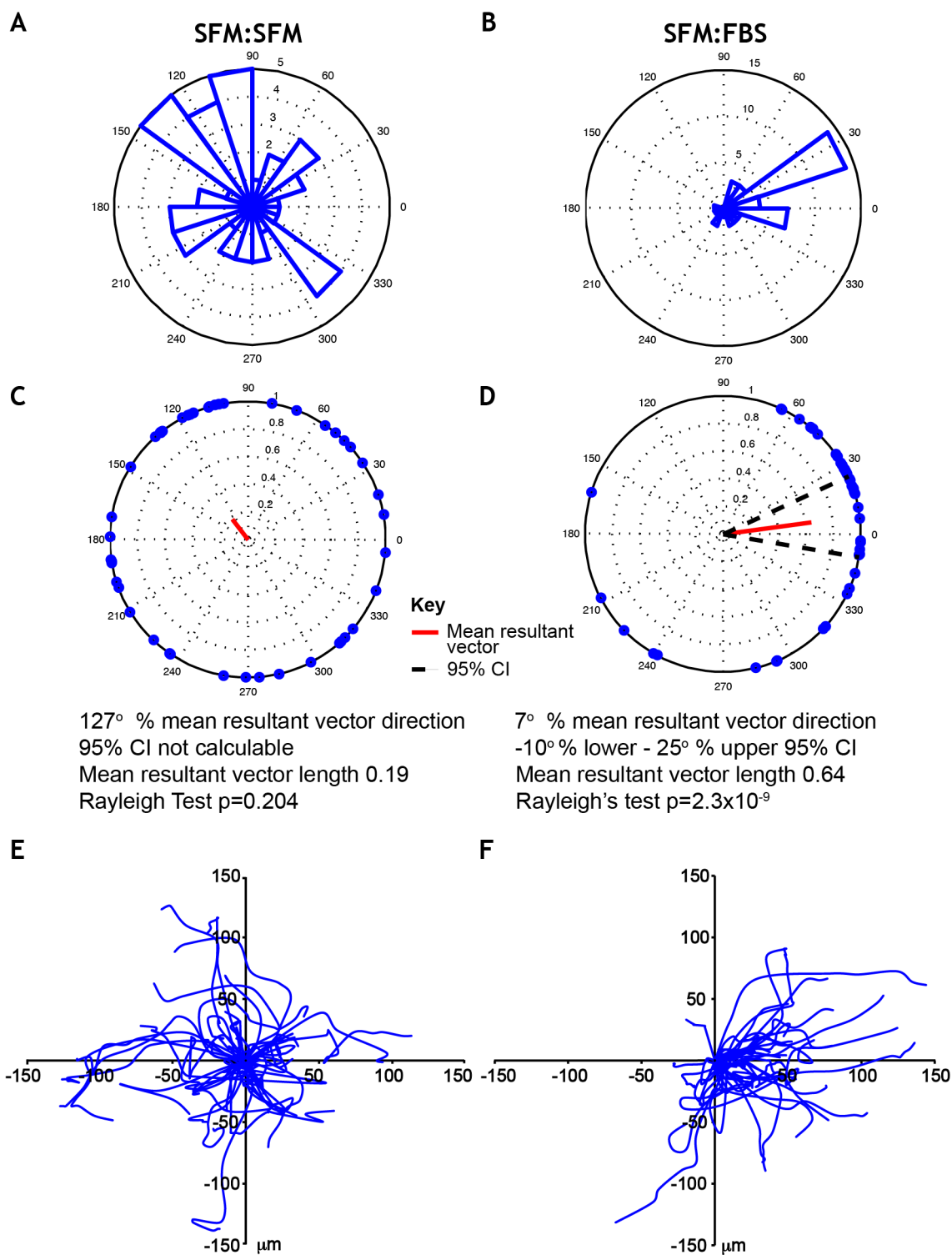


Figure 3-6 Quantification and statistical analysis.

(A, C, E) represent the results for the migration of all 46 MV3 cells tracked in a control experiment (SFM:SFM) and (B, D, F) represent the results for the migration of all 43 MV3 cells in the presence of a chemoattractant (SFM:FBS) both across the narrow bridge of a Mark 2 Insall chamber over 12 hours. In the chemoattractant experiment the chemoattractant is to the right. Rose plots (A, B) and polar plots (C, D) use end-point data to demonstrate the final position of cells relative to their starting position. Below these, Mean resultant vector, 95% CI and Rayleigh tests provide evidence for directed migration. (E, F) The paths of individual cells during the experiment are presented in the spider plots.

Insall chamber assay refinement

3.1.12 Starvation

Serum starving cells is frequently performed to enhance cell responses. This provides a period of cellular stress that drives a multitude of cellular responses. The effects are known to be variable and cell-type specific but it has been shown to be important for example in promoting cancer cell invasion by recycling receptors and upregulating EGFR signalling and forcing cells into a “survival state” (Ye et al., 2012). It is also regarded as an important step to provide reproducible experimental conditions by eliminating the variation that is found in different batches of FBS (Pirkmajer and Chibalin, 2011).

Recognising that the effects of starvation are experiment and cell type-specific, the length of starvation should be experimentally determined to optimise chemotaxis. The results of a serum starvation experiment using the WM239A metastatic melanoma cell line are summarised (Fig. 7A). The speed and chemotactic responses were compared over time for cells undergoing starvation for 0 hr, 6 hrs and 14 hrs. Both speed and chemotactic index (CI) are greatest after a period of 14 hrs starvation. This period of starvation was therefore used consistently throughout this thesis.

3.1.13 Cell density

Early experiments with <10 cells per bridge produced results with minimal if any movement or chemotaxis. Optimising the cell density to produce an even spread of cells, near but without contacting one another, reliably produced good chemotaxis. This meant seeding 5.5×10^4 cells/ml in 2 ml growth media and this density was used consistently throughout the thesis.

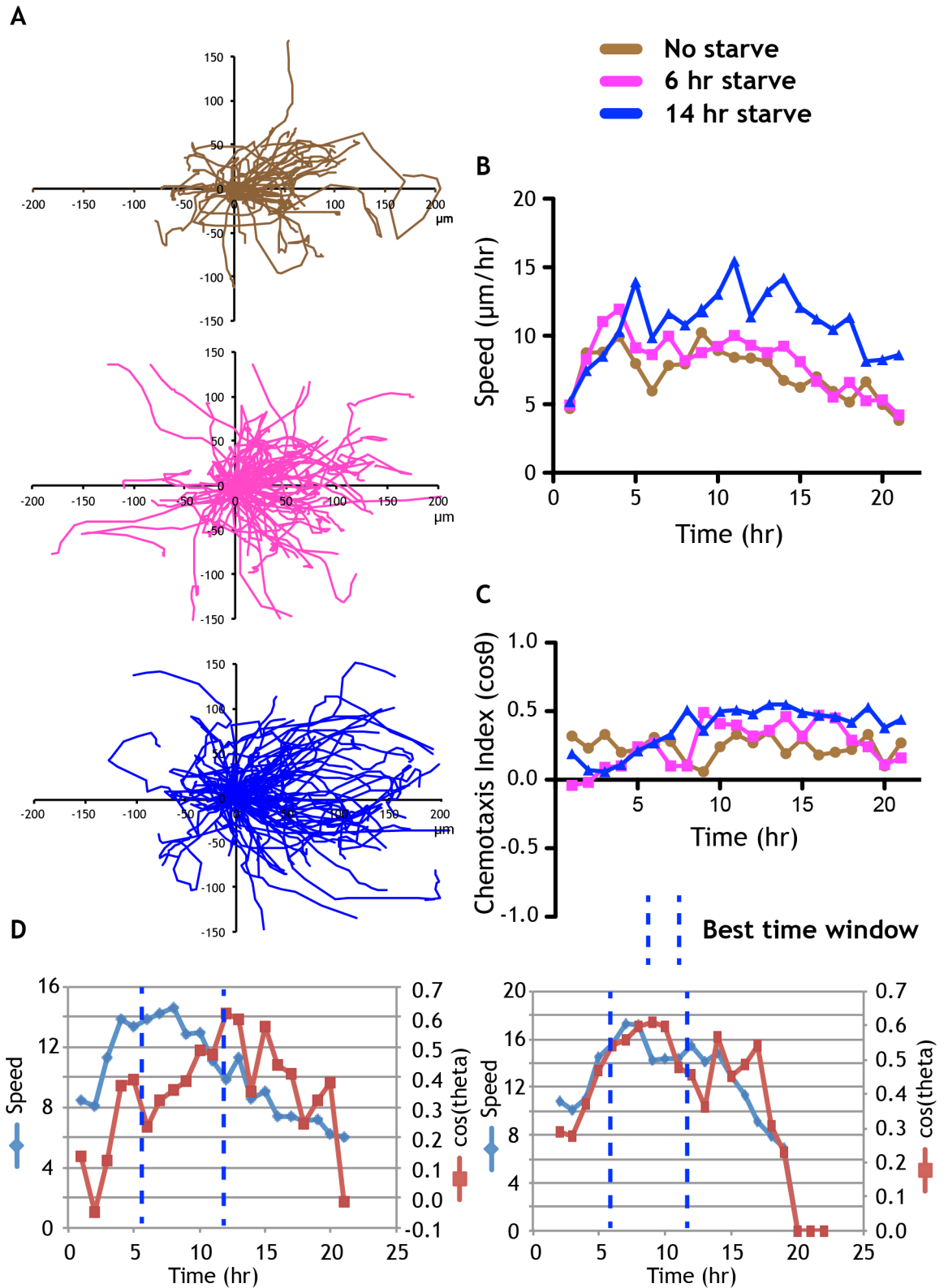


Figure 3-7 Insall chamber assay refinement.

A Spider plots for three parallel Insall chamber standard assay 10% FBS chemotaxis experiments with WM239A metastatic melanoma cells. Starvation times were varied: 0 hr starvation (brown), 6 hr magenta, 14 hr blue. **B** Speed and **C** chemotaxis index plots respectively for the three starvation experiments plotted against time. **D** two separate experiments for WM239A cells performing serum chemotaxis with speed and chemotaxis index plotted on the same graphs with the best time window chosen for analysis.

3.1.14 Best time window for analysis

In order to obtain consistent data, it is necessary to select a time window for analysis because the chemotactic parameters evolve. In the initial stages of any assay, the cells are sensing the gradient, polarising and accelerating (Veltman and Van Haastert, 2008). Following a period during which CI and cell speed plateau, there follows a gradual fall in these parameters almost certainly due to the limited supply of nutrients and oxygen in the chamber.

To choose the best time window for analysis I reviewed the speed and CI data over time from separate assays performed on different days. The representative graphs all clearly show a period of acceleration and increasing CI that starts to level out after approximately six hours (Fig. 7B,C). This period is maintained for another six hours before chemotaxis consistently starts to decline. This 6-12 hr window was therefore selected to generate end-point data for analysis and is used consistently throughout all experiments unless otherwise stated.

Discussion

This chapter has charted the development, optimisation and validation of the Insall chamber. I have argued why this is a significant improvement over existing direct visualisation bridge chambers. The latest versions have further enhanced the assay by stabilising the gradient for longer and increasing the data yield. The chamber continues to evolve and the latest version contains two chambers on one slide. This allows the imaging of up to eight assays on one microscope to facilitate the multiplexing of experiments and associated controls in identical environments.

The major challenge with the Insall chamber assay, despite its relative ease of use, arises as a complication of its strength. From generating very large movie files to processing the images, requires suitable storage hardware and presents a logistical and time-consuming challenge respectively. To ease this process, it will be important to develop automated cell processing and stitching packages combined with automated cell tracking software. Nevertheless the development of the chemotaxis processing spreadsheet used throughout this work has enabled the rapid processing of cell tracking data.

Most remarkable is the striking accuracy with which MV3 metastatic melanoma cells perform chemotaxis towards 10% FBS. Chemotaxis of melanoma cells to serum has been reported in Boyden chamber assays (Lanati et al., 2010), but never before in direct visualisation chambers. Reviewing the literature for cancer cell chemotaxis I observe the most accurate chemotaxis over the longest time frame (Bailly et al., 1998; T, 1995; Jensen et al., 2011; Sturge et al., 2003; Wang et al., 2004). The chemotactic accuracy is more akin to the behaviour of haemopoietic lineage cells (Kay et al., 2008; Zicha et al., 1998) and this poses the question of whether they share similar signalling pathways?

Saadi et al investigated chemotaxis of MDA-MB-231 cells in their parallel-gradient microfluidic chamber in response to linear and polynomial EGF gradient profiles (Saadi et al., 2006). Their data suggested linear gradients were not effective at inducing chemotaxis whereas polynomial gradients did induce a chemotactic response. This is contrary to my data that show robust chemotaxis in linear gradient profiles. The effect of differing gradient profiles on cancer cell chemotaxis is therefore an area that merits further research. Their result may be explained by the relatively short three hour assay period, which is also often used for transwell assays, but only allows time for the cells to move a few cell lengths. This may produce a false negative result due to time taken to initiate movement (Maheshwari et al., 1999) as confirmed during my optimisation studies. This further justifies the use of a relatively long (8-24 hour) assay period, especially for slowly moving cells. Other assays have required steep gradients to induce chemotaxis, but again have been limited by a short experimental duration (Soon et al., 2005). The ability to chemotax in less steep, linear profiles may therefore require a greater time window and raises the question of whether cells are actively modifying the linear gradient?

3.1.15 Conclusion

In conclusion, we have created a significantly improved chemotaxis chamber and processing package for studying cancer cell chemotaxis. The Insall chamber satisfies our design criteria and, most importantly, it allows us to track and investigate cancer cell chemotaxis for at least 24 hours.

We have demonstrated that utilising the Insall chamber in the standard assay format, provides a new opportunity for this robust and powerful system to probe the chemotactic behaviour of slow-moving cancer cells in detail. My data reveal that metastatic melanoma cells are capable of performing chemotaxis with a degree of accuracy not previously appreciated. The factor(s) and mechanism(s) driving this therefore require careful investigation. I will therefore describe my investigation of this in the following chapters.

Chapter 4:

The Inflammatory Signal LPA Drives Melanoma Chemotaxis and Invasion

Introduction

Having demonstrated MV3 metastatic melanoma cells performing strong chemotaxis towards serum, I wished to validate this result by testing another metastatic melanoma cell line. The standard cell line used by many researchers over the years as a melanoma model has been the B16 family of mouse melanoma cell lines (Bobek et al., 2010; Fang et al., 2008; Hirayama et al., 1984). The B16-f10 line has been highly selected for its ability to metastasise to lung in an intra-cardiac/ IV injection model and was characterised by Fidler et al during the 1970s as a model for metastasis research (Fidler and Nicolson, 1976) but concern has been raised about its use as a melanoma model due to its failure to reflect many of the molecular attributes of the human disease (Herlyn and Fukunaga-Kalabis, 2010).

The WM239A cell line, by contrast, is derived from a human metastatic melanoma. It is held by the Wellcome Trust genomics cell bank at St George's in London and freely available through collaboration with the curator, Prof Dot Bennett. The advantage of using this cell line is that it is part of a larger collection of human melanoma cells derived from different biological stages of development. These cells have been tested and shown to maintain many of the biological and molecular characteristics of human melanomas relevant to each stage (Herlyn et al., 1985; Herlyn, 1990). This collection therefore provides a powerful tool for understanding the responses exhibited by melanoma cells across the various stages of melanoma development.

A multitude of chemoattractants have been targeted for study, and there are reviews that attempt to order these as a list of serum factors that have chemotactic properties (Roussos et al., 2011). From a translational perspective, this catalogue is a starting point but it is not clear what the key chemotaxis pathways are. Melanoma is an aggressive cancer that metastasises early during tumour evolution, contributing greatly to its high mortality (Broekaert et al., 2010; Zbytek et al., 2008). So an understanding of the factors driving this process is essential, especially the chemotactic factors involved in the essential invasive step, which are poorly delineated (Payne and Cornelius, 2002). Reviews have gathered together those chemoattractants that are known to be involved in

the process (Roussos et al., 2011). However, it is unknown which of these factors are key to driving cancer cell invasion.

Identifying the key driver(s) of melanoma cell chemotaxis could be an important step in developing novel therapeutic and/ or prognostic targets. There are reports attempting to characterise the motility of melanoma cells towards various chemoattractants using Boyden chambers and pipette assays but it is unknown which is the most potent, or physiologically relevant (Dong et al., 2002; Quinones and Garcia-Castro, 2004). The robust chemotactic response of the MV3 cell line to serum provides a clear starting point from where to begin this explorative process. This chapter begins by validating this finding by fully characterising the chemotactic response of the WM239A metastatic melanoma cell line towards 10% FBS.

4.1.1 WM239A metastatic melanoma cells perform chemotaxis with a high degree of accuracy towards 10% FBS

In the absence of a chemoattractant, WM239A cells migrate randomly as shown in Fig 1A. In the presence of 10% FBS, the cell tracks clearly orientate in the direction of the gradient over the same 21 hour experimental period. The presence of serum also elicits a strong chemokinetic effect, increasing the cell speed by approximately 1 $\mu\text{m/hr}$ ($p=0.0004$; Fig. 1B). Although the cells in SFM are moving slower, a similar proportion of cells are migrating as those in 10% FBS. The absence of chemotaxis cannot therefore be occurring due to a lack of cellular motility.

To fully characterise the chemotactic response of the cells, a multifaceted approach was utilised. Cell tracking data is presented as both spider and rose plots for a visual representation of chemotaxis. Quantifiable data is presented with the Rayleigh test and chemotaxis index (CI) plot (Mean \pm SEM). The former provides a degree of certainty with which the cells are migrating in a unimodal fashion and the CI plot describes the mean degree of chemotaxis and permits a simple graphical comparison between experiments.

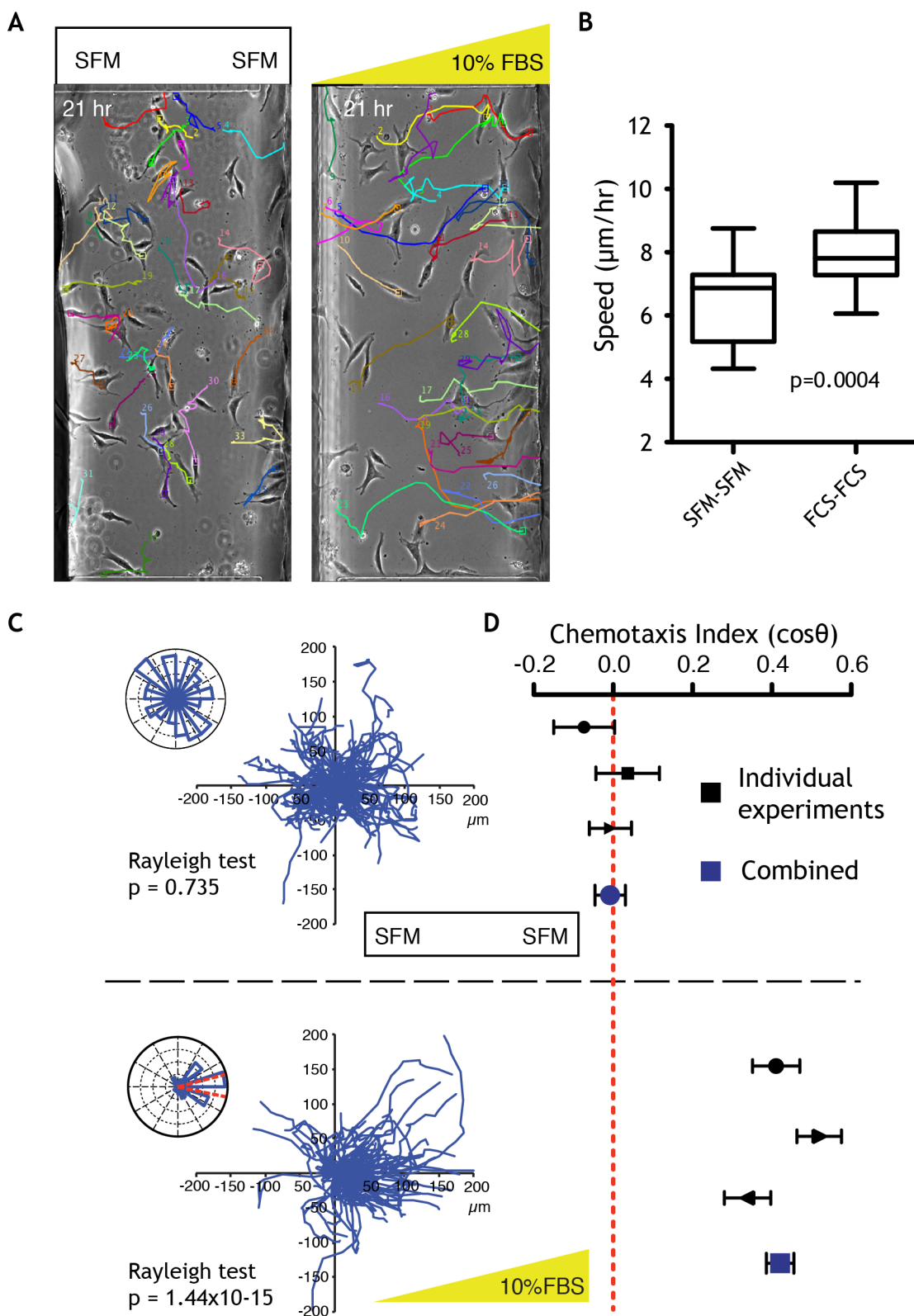


Figure 4-1 Characterisation of the chemotactic response of the WM239A metastatic melanoma cell line towards 10% FBS.

A Still images of standard Insall chamber standard assays were acquired after 21 hours with a SFM control on the left and a 10% FBS gradient experiment on the right. Cell tracks are generated using the mtrackj plugin. **B** Box and whisker plots comparing speed of cells using data from tracking >100 cells in 3 independent experiments for both conditions. The means are statistically compared with a 2-tailed t-test. **C** Spider plots for these SFM (upper panel) and 10% FBS (lower panel) experiments in **A**. Using 6-12 hour window data generated from all 3 experiments, I quantified the speed (**B**) and chemotactic responses using a combination of rose plots (with red dashed lines representing the 95% confidence interval) and a confirmatory Rayleigh test. **D** Chemotaxis index plots (Mean \pm SEM) were generated using the same window data for SFM (upper panel) and 10% FBS (lower panel). The individual experiments are marked in black and the combined data for each condition is marked in blue.

The spider plots each represent the cell tracks from one Insall chamber experiment, with data collected from >1 viewing bridge (Fig. 1C). In the SFM experiment, the tracks centre around the origin (0, 0) and this is supported by a rose plot with migration in all directions during the peak window for chemotaxis and it was not possible to calculate a 95% confidence interval. Numerical data generated from 3 experimental repeats confirms the absence of chemotaxis. These include an insignificant Rayleigh test (Fig. 1C; $p=0.735$) and a combined CI ≈ 0.0 (Fig. 1D). Conversely, the data for the 10% FBS experiment(s) supports a very strong chemotactic response. The spider plot is overwhelmingly biased towards the direction of the chemoattractant gradient (Fig. 1C). This is also reflected in the rose plot with the majority of cells in the 10% FBS group tightly distributed (red dashed lines in the rose plot represent the 95% confidence interval) in the direction of the gradient. The Rayleigh test is highly significant ($p=1.44 \times 10^{-15}$) and again the experimental repeats in the CI plot show a high degree of uniformity, producing an overall CI ≈ 0.4 , with a narrow SEM (Fig. 1D).

These data again demonstrate the robustness of the Insall chamber standard assay in producing high quality consistent data. Importantly, I show another metastatic melanoma cell line is capable of performing accurate chemotaxis towards 10% FBS (also referred to as serum in subsequent text).

Serum chemotaxis is universal across all stages

I have demonstrated that both human MV3 and WM239A MM cells perform highly accurate chemotaxis towards 10% FBS. This poses the question of whether metastases arise when non-chemotactic cells acquire chemotactic ability?

4.1.2 Serum chemotaxis is accurate across all stages

To investigate this question, I tested the chemotactic ability of human melanoma cell lines from primary (RGP & VGP) as well as metastatic (MM) stages, using the battery of melanoma cells donated by collaborator Prof. Dot Bennett. These included: WM-35 (RGP), WM98-1 & WM278 (VGP) and WM852 & WM1158 (MM).

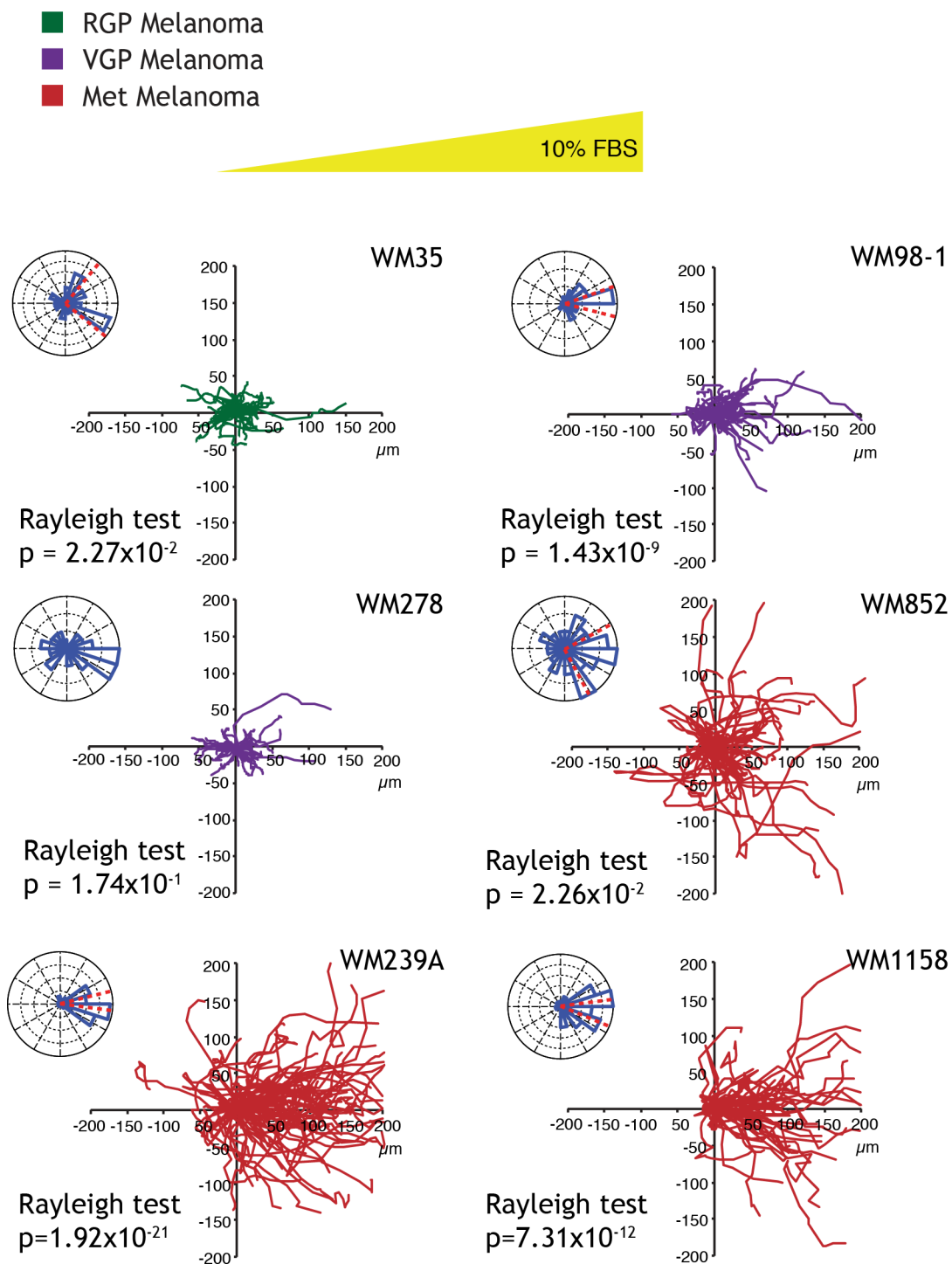


Figure 4-2 An investigation of the chemotaxis responses of melanoma cells from all biological stages.

Insall chamber standard assay experimental data presented with spider and rose plots with Rayleigh tests from six different melanoma cell lines from the three biological melanoma stages: RGP (green), VGP (purple) and MM (red). The data is generated from tracking at least 45 cells per cell line using 10% FBS as the chemoattractant.

Using the Insall chamber, all cell lines tested demonstrated a chemotactic response towards serum (Fig. 2). The spider plots all show a bias towards serum, although this is more subtle in the WM35 and WM278 cell lines due to the shorter

track lengths. The rose plots all show a biased migration towards the chemoattractant with 95% confidence intervals comfortably falling over the direction of the gradient. The exception is the WM278 line, which demonstrates the weakest chemotaxis response to serum. Although a 95% confidence interval was not calculable for this cell line, the rose plot suggests biased migration, but with a smaller proportion of cells moving towards the gradient.

By grouping the data by melanoma stage (Fig. 3A & Movie S3 (RGP), Movie S4 (VGP) & Movie S5 (MM)), I show that chemotactic accuracy increases with progressive disease stage, with a weakly significant increase in CI between RGP and MM cells was confirmed ($p=0.044$). However, even early stage cells possesses considerable chemotactic accuracy towards serum (CI plot) and with a significant one sample t test.

4.1.3 Speed is stage dependent

The dominant change in motility parameters between these biological stages is speed. Whilst RGP and VGP cells are indistinguishable, MM cells are moving with approximately double the speed (Fig. 3B).

It has been suggested that metastases arise when non-chemotactic cells acquire chemotactic ability. However, my data instead show that melanoma cell chemotaxis to serum is almost universal and even RGP cells possess significant chemotactic ability. Rather, the main difference between metastatic and non-metastatic cells is the doubling of speed between the primary and metastatic stages.

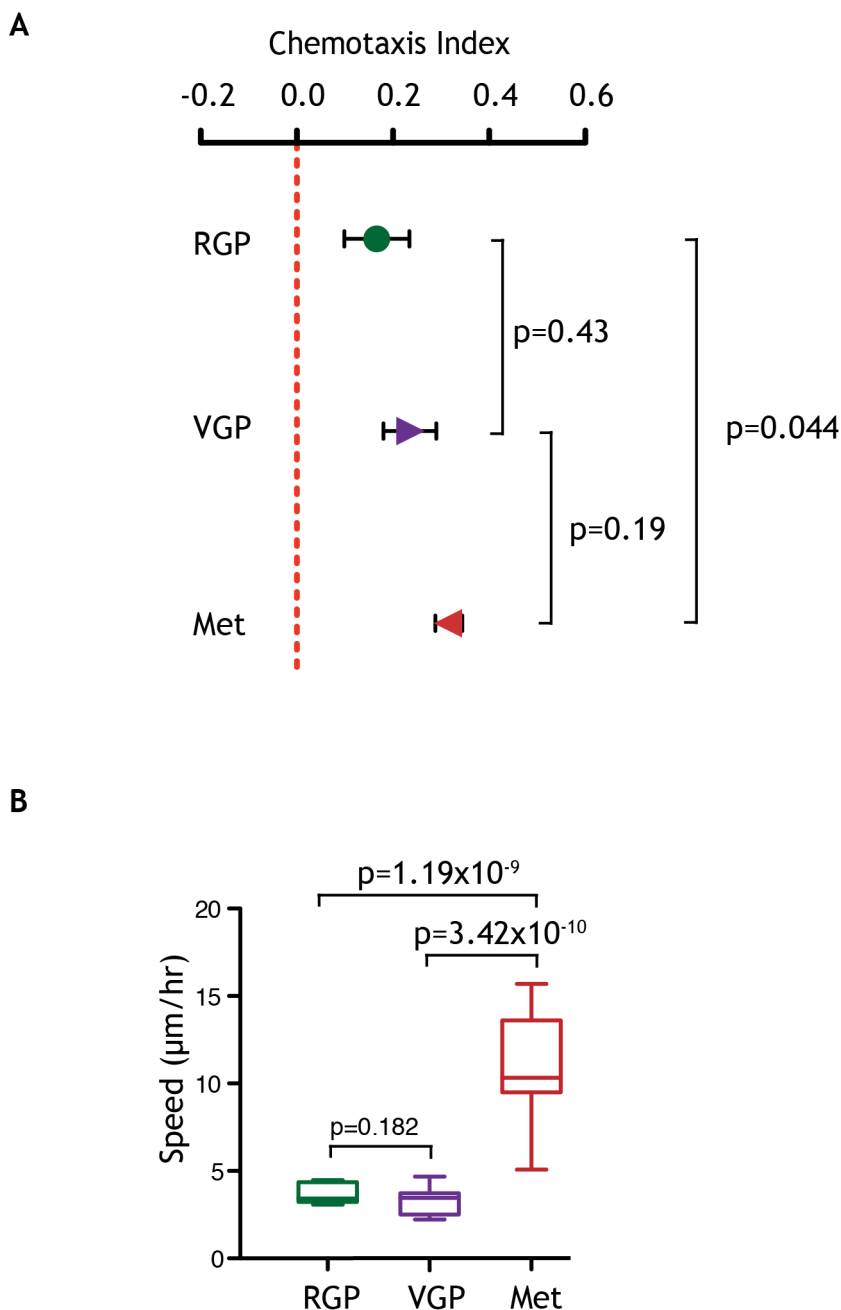


Figure 4-3 Chemotaxis index and speed filtered by melanoma stage.

Sub-analysing the data generated for Fig. 2. **A** Pooled chemotaxis index plots generated by melanoma stage. **B** Pooled box and whisker plots of speed against melanoma stage. Data generated in A and B has been compared statistically using the student's unpaired t-test.

Identifying the chemoattractant(s) in serum

Current evidence suggests that chemotactic signalling occurs through two major classes of receptors Receptor Tyrosine Kinases (RTKs) or G-protein coupled receptors (GPCRs) by GFs or chemokines respectively (Smirnova and Segall, 2007). Given the chemotactic accuracy of melanoma cells across all stages of

disease progression, I next asked whether a single agent within serum was capable of reproducing this effect?

4.1.4 Growth factors drive chemokinesis

There is a wealth of literature supporting the role of growth factor signalling via RTKs in chemotaxis both *in vitro* and *in vivo* (Goswami et al., 2005; Haugh et al., 1999; Patsialou et al., 2009; Stracke et al., 1989; Wells, 2000). Many different growth factors and their receptors have been shown to be upregulated in cancer cells and human tumours (Easty et al., 2011; Otsuka et al., 1998; Goswami et al., 2005; Pierce et al., 1991; Philippar et al., 2008). I reviewed the key growth factors known to stimulate cell motility and tumour invasion, with most evidence supporting EGFR signalling in breast cancer (Desmarais et al., 2009; Smirnova et al., 2012; Wang et al., 2004; Wyckoff et al., 2004).

I selected a number of GFs as putative cancer cell chemoattractants based on the literature review to perform a detailed assessment of their ability to induce chemotaxis in melanoma cells. GFs bind to their receptors within a narrow range, and binding is complicated by further complexity in the receptor conformation, with biphasic affinities for the same receptor ligand combination (Bjorkelund et al., 2011). I therefore used both low and high concentrations known to stimulate motility in melanoma or cancer cells. The GFs and their concentrations used in the assay included: EGF (6.25 & 25 ng/mL), PDGF (25 & 100 ng/mL), HGF (6.25 & 25 ng/mL) and SCF (10 & 100 ng/mL). The chemokine SDF-1 (100 & 300 ng/mL) was also tested. (Belmadani et al., 2009; Bjorkelund et al., 2011; Deuel et al., 1981; Jensen et al., 2011; Jourquin et al., 2006; Kwok et al., 2012; Monypenny et al., 2009; Taylor et al., 2001; Zicha and Dunn, 1995)

The results of testing the putative GF chemoattractants are presented in Figures 4 and 5. The spider plots demonstrate no evidence of bias in migration in the direction of the gradient for any of the potential attractants under investigation. The rose plots highlight more subtle biases, and for PDGF (high/ low) and EGF (low), they demonstrate slight reverse chemotaxis with the 95% confidence intervals orientated away from the gradient. However, this does not reach statistical significance in the Rayleigh test for PDGF and there is a low level of significance for EGF (low; $p=2.47 \times 10^{-2}$).

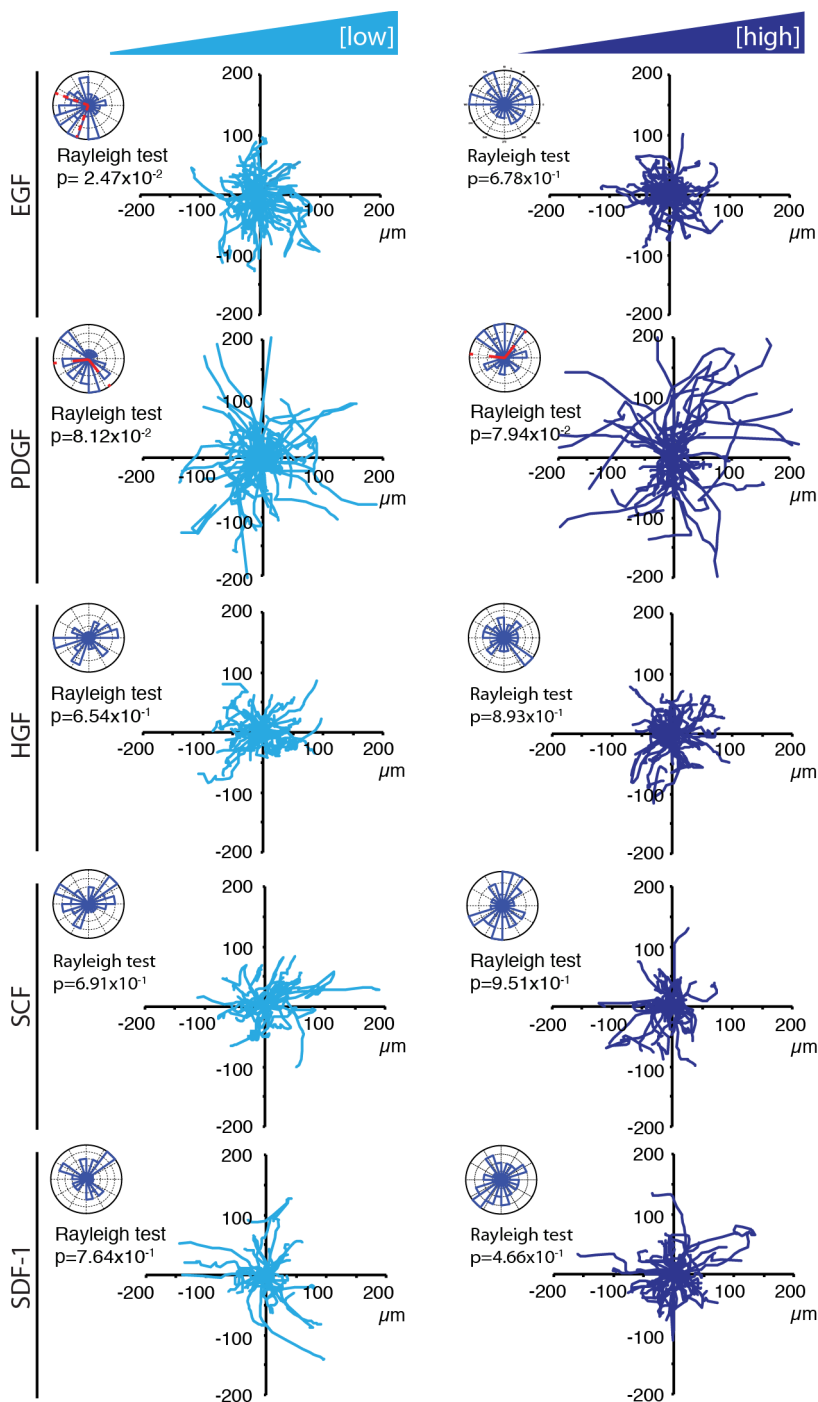


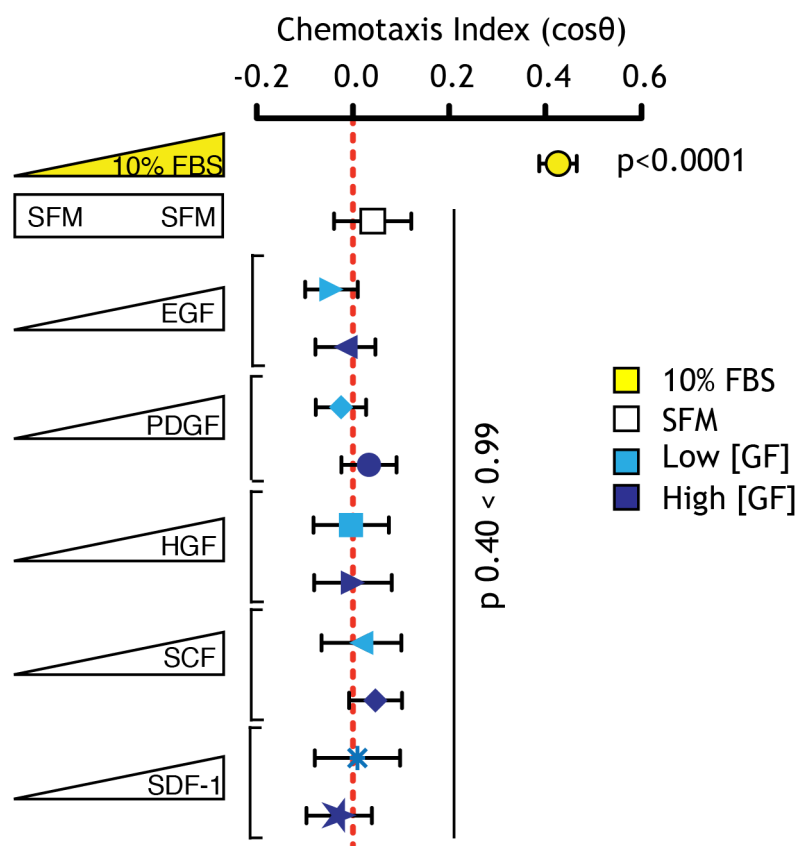
Figure 4-4 The effect of gradients of GFs on melanoma cell motility.

Spider and Rose plots with Rayleigh tests performed on WM239A cells migrating in the presence of low (left panel) and high gradients (right panel) of growth factors (GFs) in the Insall chamber standard assay. More than 40 cells were tracked for each condition. GFs included EGF (6.25 & 25 ng/mL), PDGF (25 & 100 ng/mL), HGF (6.25 & 25 ng/mL) and SCF (10 & 100 ng/mL). The chemokine SDF-1 (100 & 300 ng/mL) was also tested.

This interesting observation is consistent with another study investigating the chemoattractant effects of PDGF and IGF on two sarcoma cell lines through direct observation (Zicha and Dunn, 1995). They discovered that the direction of biased migration could deviate as much as 170° from the gradient orientation.

They conclude that GFs induced the autocrine release of a chemoattractant and question whether GFs are ever genuinely chemotactic. In the same paper, this was supported by the finding that the proposed released chemoattractant could act in a paracrine manner on cells that were poorly responsive to GFs.

A



B

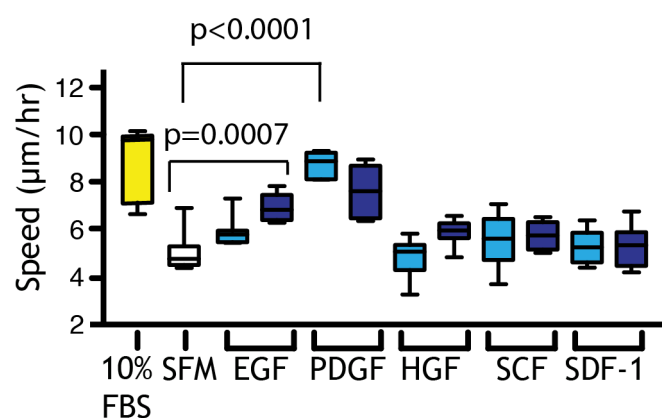


Figure 4-5 Quantification of the effect of gradients of GFs on melanoma cell motility.

A Chemotaxis indices plotted with SFM and 10% FBS controls for the Insall chamber standard assays performed in Fig. 15. One sample t tests are highlighted. **B** Box and whisker plots of speed are plotted with SFM and 10% FBS controls. EGF and PDGF demonstrated the greatest chemokinetic effects. Statistical comparisons are performed using the unpaired student t test.

The other main observation is the spider track lengths that clearly vary between the low and high concentrations of GFs suggesting that the two concentrations of factors are exhibiting differing chemokinetic responses.

Viewing the graph of chemotaxis index in Fig. 5A, none of the GFs, regardless of concentration, induce any significant chemotaxis. However, although directionality was unaffected by GFs, they consistently increased speed in a dose-dependent manner. The spider plot track length variation between the low and high concentrations of GFs is clearly mirrored with varying speeds induced by the different factors and concentrations used (Fig. 5B). All the factors tested ranged between the SFM and 10% FBS control experiments. The greatest difference is seen between the SFM control and the low concentration of PDGF ($p < 0.0001$) with EGF (high) also exerting a marked increase in chemokinesis ($p = 0.0007$).

The spider or rose plots from previous direct visualisation studies of chemotaxis to GFs often show more subtle biases and not the degree of chemotaxis exhibited by melanoma cells in my assay chemotaxing towards serum (Sturge et al., 2003; Wang et al., 2004). One of the key reasons that RTK signalling fails to produce such accurate chemotaxis is due to its method of signal transduction. Following the binding of the ligand to its receptor, the ligand-receptor complex is internalised and signalling continues even during transit within the cytosol (Haugh et al., 1999). The result of this is reduced spatial sensing and an increased receptor off time with a likely net effect of a blunted chemotactic response.

These data strongly suggest that GFs are primarily regulators of speed, with EGF and PDGF demonstrating the greatest chemokinetic effects, and are not responsible for the chemotaxis response generated by serum.

4.1.5 LPA is sufficient to drive chemotaxis with efficiency approaching that of 10% FCS

Single agents such as fMLP drive highly accurate chemotaxis of neutrophils and cAMP in *Dictyostelium*, binding and transducing their signals through GPCRs (Kay et al., 2008). In evolutionary terms, their ability to respond to chemotactic cues

is essential for the survival of the mammal or amoeba respectively. This “do or die” response has therefore evolved with the ability to react rapidly and accurately (Van Haastert and Devreotes, 2004). Given the accuracy of serum chemotaxis and the failure of GFs to induce chemotaxis, I asked whether the signalling is occurring through GPCRs?

In 1992, LPA was identified as a key factor found within serum, which was able to rapidly induce a conformational change in the actin cytoskeleton and signals through GPCRs (Bathena et al., 2011; Bot et al., 2013; Ridley and Hall, 1992; Swaney et al., 2010; Xue et al., 2010). LPA was therefore chosen as a putative chemoattractant based on the data supporting its signalling pathway, and its reported effects on motility and cancer cell invasion. These attributes therefore make LPA an ideal candidate for investigation. I used a chemoattractant concentration of 1 μ M LPA, which is within the 1-5 μ M range found within serum (Eichholtz et al., 1993; Tigyi and Miledi, 1992).

The results of three independent experiments are summarised (Fig. 6A). Across multiple independent experiments, the WM239A cells consistently chemotaxed towards LPA (Movie S6). This statistically significant chemotaxis is reflected in both the spider and rose plots.

The track pattern of WM239A cells migrating in a 1 μ M LPA gradient is very similar to the pattern when migrating towards the 10% FBS positive control (Fig. 6B). The comparison of the response compared to serum can be seen most clearly on the CI plot (Fig. 6C). I therefore conclude that 1 μ M LPA is sufficient to produce chemotaxis with accuracy approaching that of 10% FBS.

Analysing the speed data during the 6-12 hour window shows mild inter-experimental variation although the pooled data were not statistically different from the pooled 10% FBS control (Fig. 7A). Although, analysing the speed over time (Fig. 7B) did show a trend towards the cells slowing towards the last half of the time window in the LPA gradient.

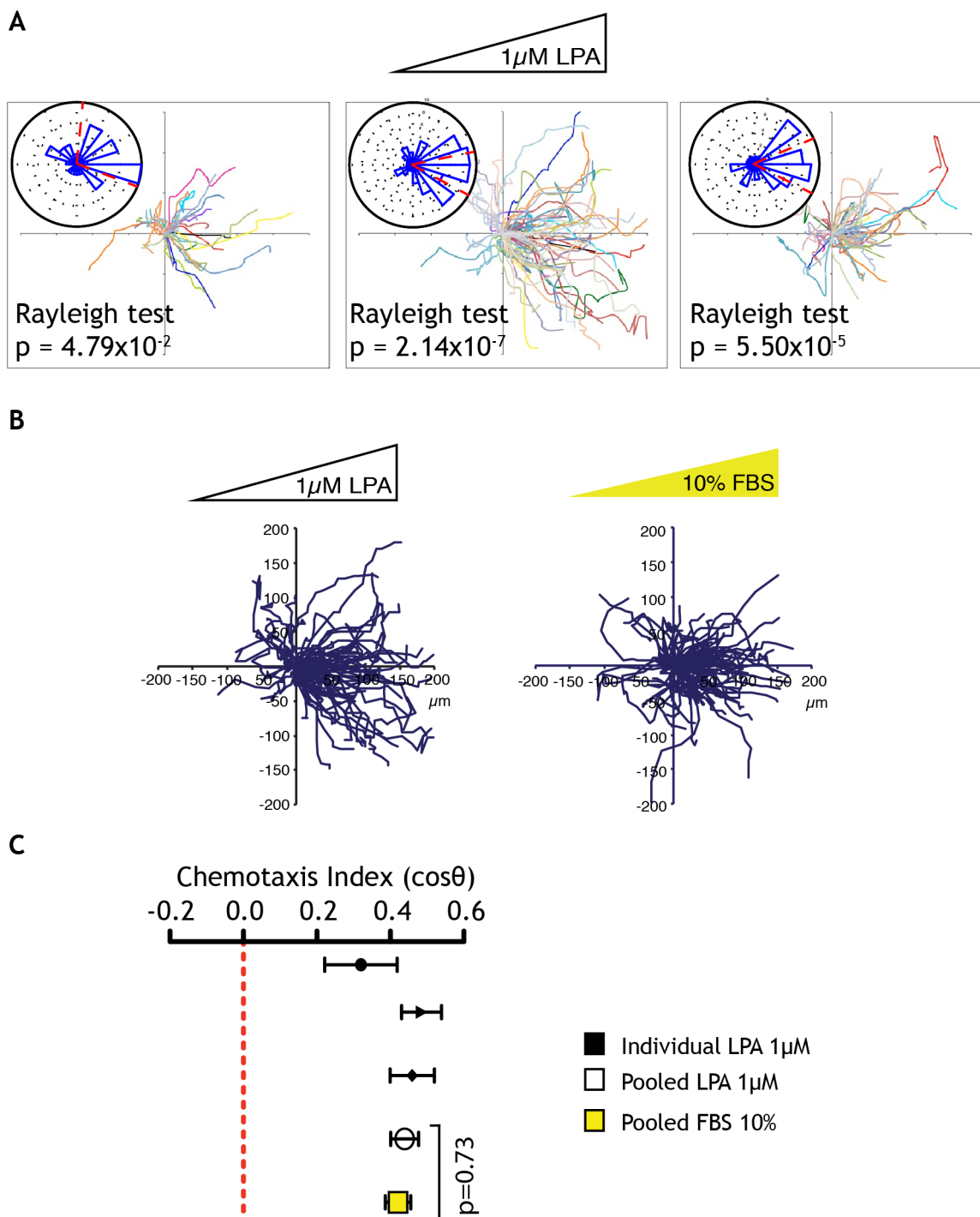
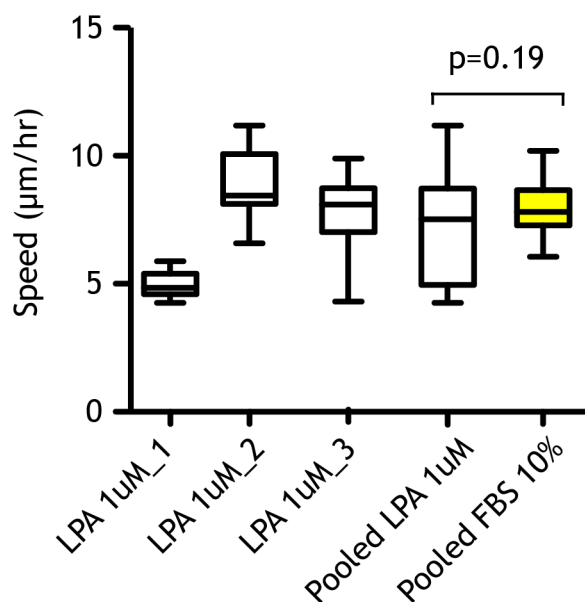


Figure 4-6 Characterisation of the chemotaxis response induced by LPA.

In all chamber standard assay data generated from tracking over 160 cells in 3 independent experiments investigating the chemotaxis responses of WM239A MM cells using 1 μ M LPA as the chemoattractant. **A** Spider and rose plots with Rayleigh tests by experimental repeat from left to right. **B** Spider plots of cells chemotaxing in the presence of a 1 μ M LPA gradient and a 10% FBS gradient control. **C** Chemotaxis index plots for the experiments in A. The pooled responses of cells chemotaxing towards 1 μ M LPA and 10% FBS are statistically compared using an unpaired t test.

A



B

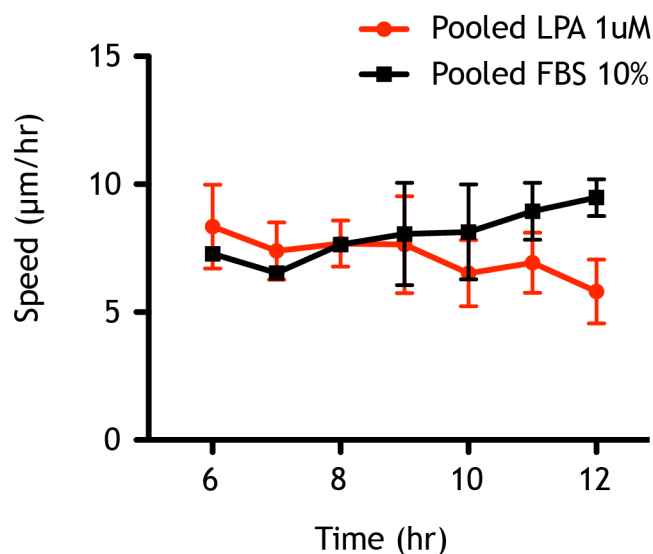


Figure 4-7 Analysis of speed during LPA chemotaxis.

The data from figure 4 has been further analysed to generate speed data. **A** 6-12 hour window speed for individual experiments and pooled and presented as box and whisker plots. The pooled LPA response is compared to the pooled 10% FBS response using an unpaired t test. **B** The pooled data from A is presented over the 6-12 hour window time frame.

LPA is the dominant attractant in 2D & 3D assays

The previous experiments suggest that this naturally occurring lipid may be responsible for the majority of serum chemotaxis identified in 2D chemotaxis assays. Serum contains many potential chemoattractants and I therefore ask the question of whether LPA is necessary as well as sufficient for serum chemotaxis?

4.1.6 LPA is necessary to drive chemotaxis towards serum in WM239A metastatic melanoma cells

To determine if LPA is the major chemoattractant in serum, the first approach I took was to attempt to strip the serum of LPA using charcoal. Attempts were made to strip the serum using a protocol described with activated charcoal (Gaetano et al., 2009). Unfortunately, this gave no alteration to the serum chemotaxis phenotype and this may have been due to the failure of charcoal to strip the serum of LPA (although I was not able to quantify this at the time), or due to the ability of serum to re-generate LPA through autotaxin (Aoki et al., 2008; Moolenaar and Perrakis, 2011). Given the potential complexity of subsequently depleting autotaxin I pursued an inhibitor strategy.

I previously discussed the LPAR receptors that are known to be important in cancer cell motility and LPAR1 emerged as a clear favourite to target initially. There are several commercially available LPA receptor (LPAR) antagonists that have been well characterised (Choi et al., 2010). I chose to use the inhibitor Ki16425 because its inhibition profile was most specific for antagonising LPAR 1. It inhibits LPAR 3 to a lesser extent, and it has 20 times less affinity for LPAR 2 (Ohta et al., 2003). There is also a growing body of literature for its use *in vivo* (Boucharaba et al., 2006; Pradere et al., 2007; Subramanian et al., 2010).

Ki16425 is a readily available competitive antagonist discovered after a screen of 150,000 low-molecular weight compounds that selectively inhibited the LPARs. The inhibition profile described above was calculated for a 10 μ M concentration of inhibitor. Importantly, it was shown to exhibit excellent LPAR specificity without any appreciable agonistic or antagonistic effect on EGF and PDGF receptors (Ohta et al., 2003).

To confirm that Ki16425 is operating through antagonism of LPA receptors, its effect was studied in the presence of a 1 μ M LPA gradient and compared to vehicle (Fig. 8). The three chemotaxis parameters presented here (spider plots, rose plots and Rayleigh test) all confirm complete inhibition of LPA chemotaxis. This experimental evidence supports the conclusion that Ki16425 is completely antagonising LPAR signalling.

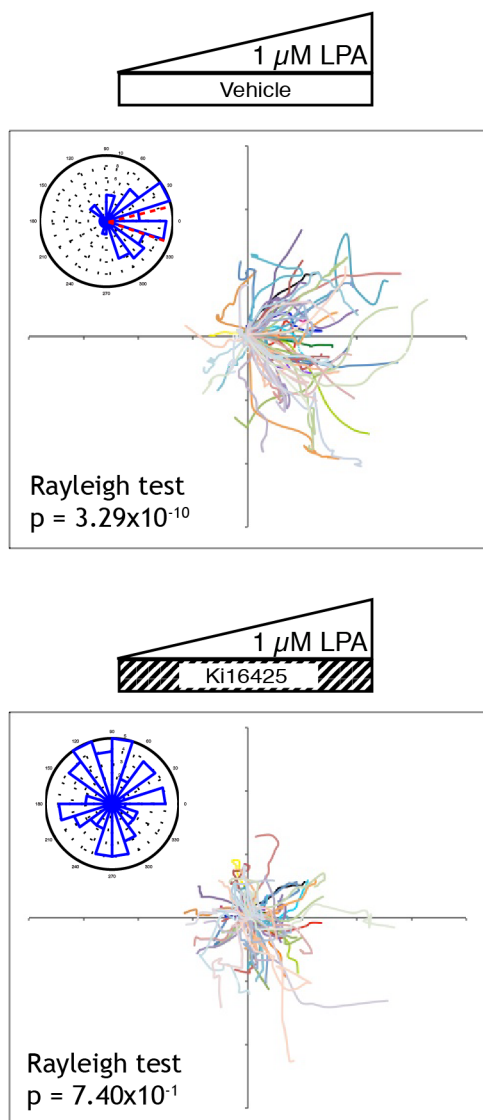


Figure 4-8 Confirmation of the effect of Ki16425 on LPA chemotaxis.

Insall chamber standard assay data generated from experiments comparing the effect of Ki16425 and vehicle on 1 μ M LPA chemotaxis of WM239A MM cells. The spider and rose plots are presented with their respective Rayleigh tests.

Following the manufacturer's protocol with pre-treatment and treatment throughout the duration of the experiment, a series of 3 experimental repeats was performed (Fig. 9). All 3 vehicle controlled experiments demonstrated strong chemotaxis but in the inhibitor treated experiments, all measures of chemotaxis were consistently and profoundly inhibited.

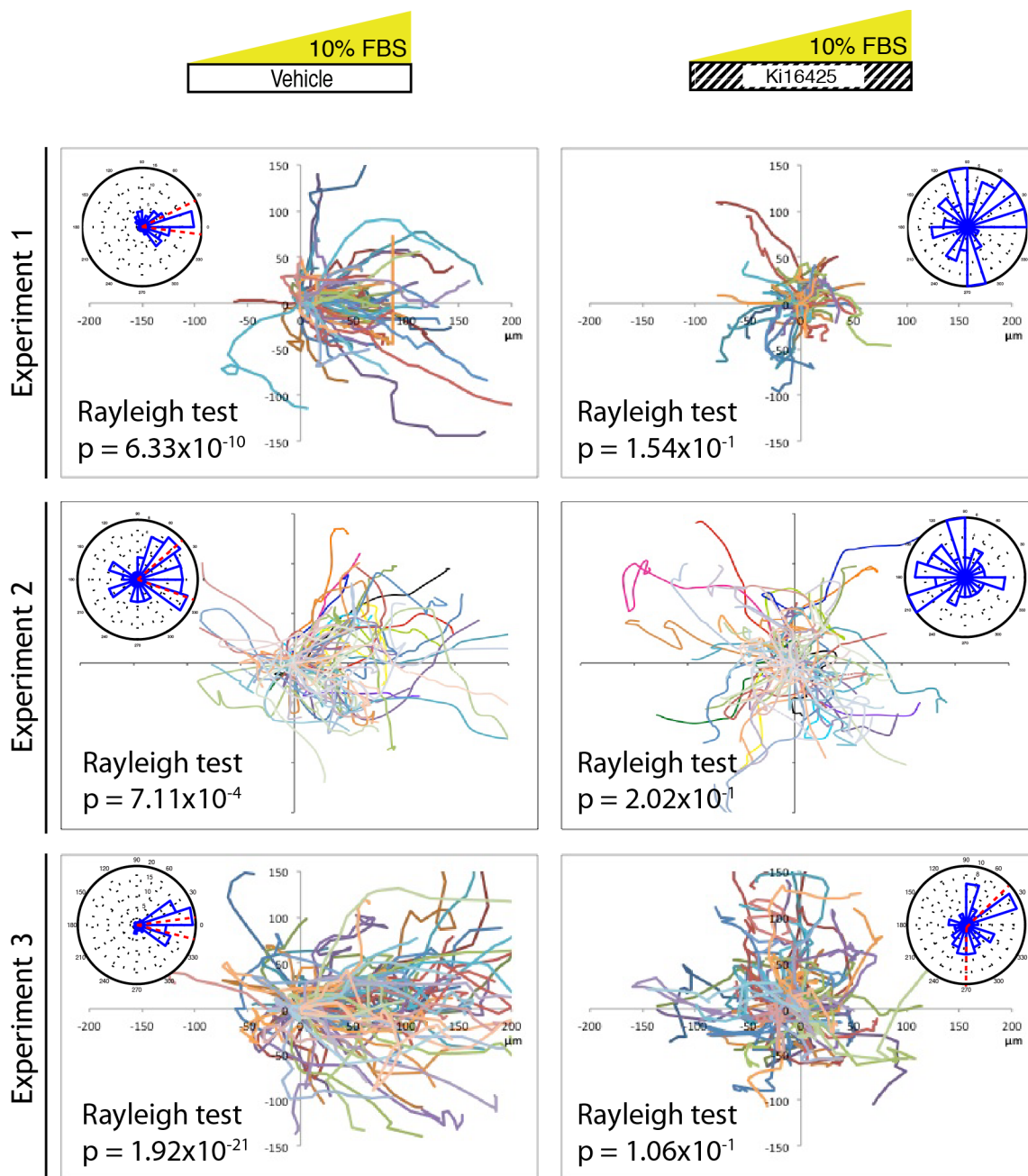


Figure 4-9 The effect of Ki16425 on WM239A serum chemotaxis.

Insall chamber standard assay data generated from 3 independent experiments investigating the chemotaxis responses of WM239A MM cells to 10% FBS +/- Ki16425. The cells were pre-treated and treated throughout the duration of the experiments. The spider and rose plots with Rayleigh tests are presented for Ki16425 and vehicle controls.

Further quantitative assessment of the impact of the inhibitor indicated that the movement of the 10% FBS plus inhibitor treated group is almost identical to the SFM experiment, although the track lengths are longer in the inhibitor group (Fig. 10A). The CI plot again highlights the excellent concordance between experimental repeats and the pooled result clearly demonstrates that Ki16425 not only reduces chemotaxis, but it completely inhibits this response with a $CI \approx 0$

(Fig. 10B). This is compared to the pooled vehicle treated cells that perform accurate chemotaxis with a CI >0.4. One sample t tests confirm that the CI for the pooled vehicle treated cells is significant ($p < 0.0001$), and there is a significant difference between the CI for the pooled vehicle and pooled Ki16425 group. Examples of cells moving in the presence of Vehicle (Movie S7) and Ki16425 (Movie S8) are provided.

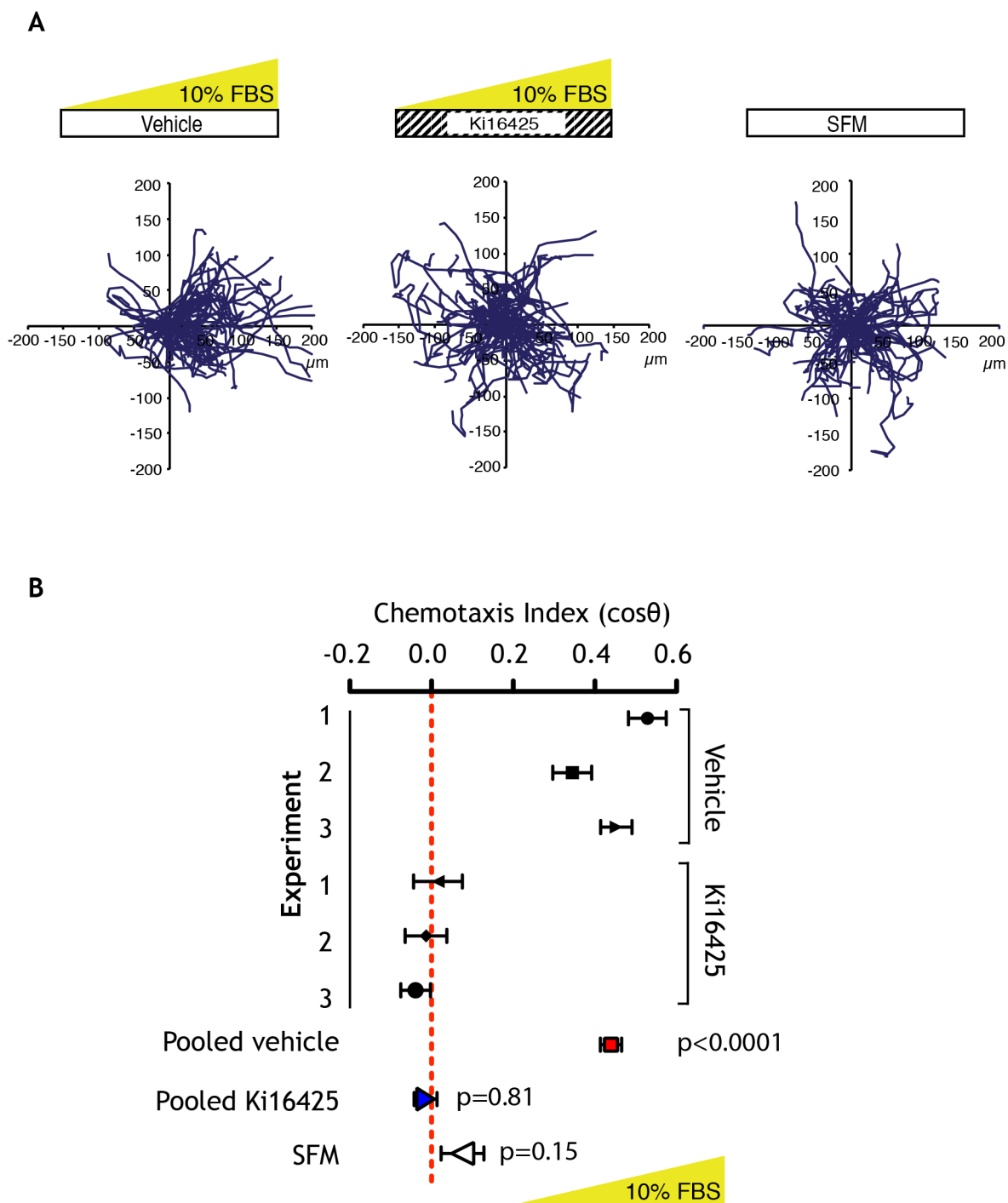


Figure 4-10 The quantitative effect of Ki16425 on WM239A serum chemotaxis.

A Representative spider plots from the experiments in Fig. 7 alongside a SFM control. **B** Chemotaxis index plot for all 3 experiments individually and pooled, alongside the SFM control. The results of one sample t tests are marked adjacent to the corresponding result, each comparing the chemotaxis index mean to the theoretical mean of 0.

To confirm that the inhibitor was not abolishing chemotaxis through other effects on cell motility, I examined the impact on speed in more detail. The results showed a slight initial reduction in speed in the Ki16425 treated group compared with the vehicle treated group (Fig. 11A). However, the reduction in speed is only temporary until 12 hours, when the cells then continue to migrate with an average speed similar to the vehicle treated group. Importantly, this difference is not significant during the window period of assessment (Fig. 11B).

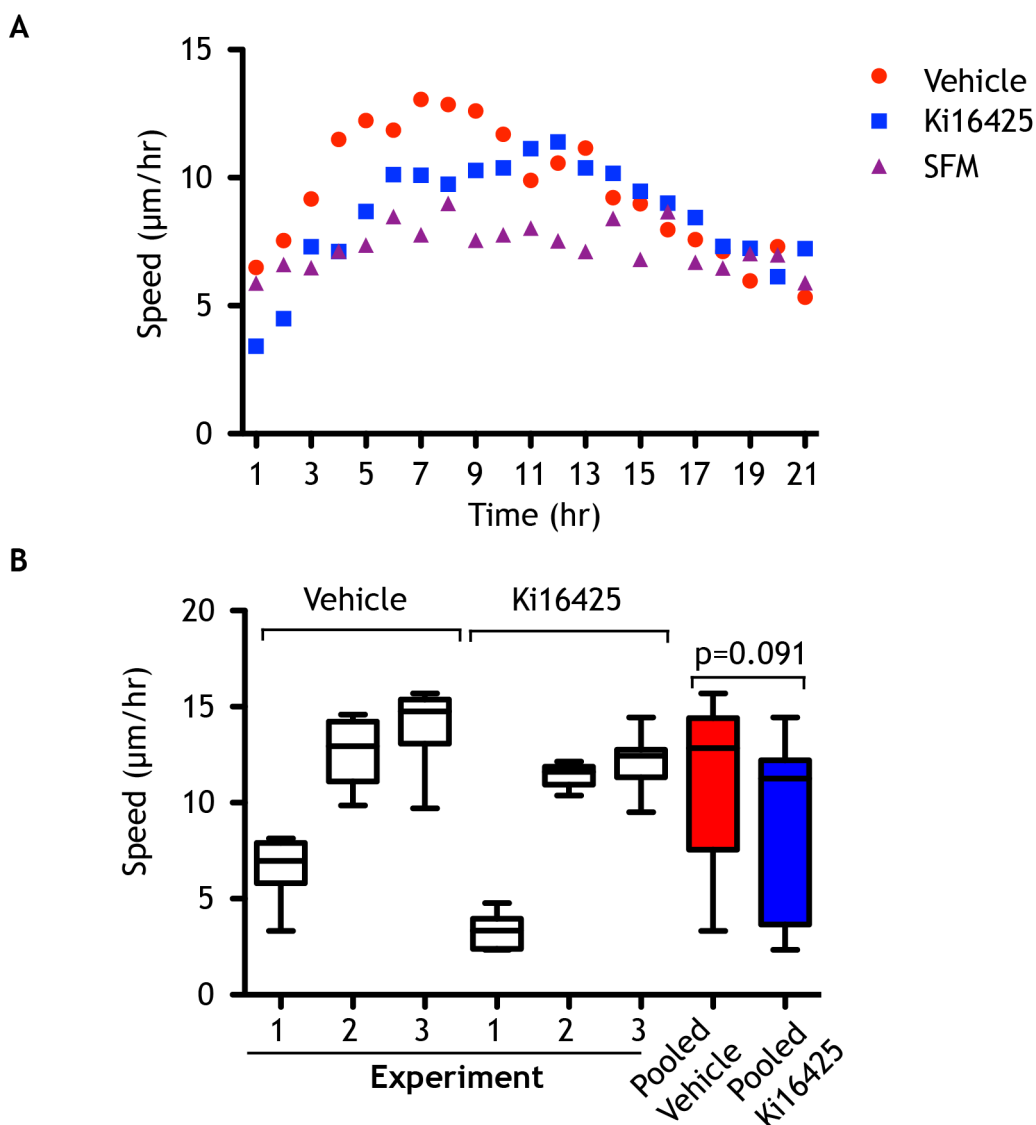


Figure 4-11 The effect of Ki16425 on the speed of cells.

The data from the experiments in Figs. 7 & 8 has been further analysed to compare the speed of cells in the presence of Ki16425 or vehicle. **A** Mean speed is plotted against time for vehicle and Ki16425 treated conditions, alongside a SFM control throughout the duration of the 21 hour assay. **B** Speed during the 6-12 hour window is presented as box and whisker plots and the pooled vehicle and Ki16425 treated conditions are compared using an unpaired t test.

These data support the inhibition of chemotaxis to serum as the primary effect of Ki16425 with a relatively minor effect on chemokinesis. In the context of Ki16425 inhibiting chemotaxis in the presence of serum it can be concluded that LPA is necessary to drive chemotaxis towards serum in WM239A metastatic melanoma cells.

4.1.7 LPA is necessary to drive chemotaxis to serum consistently across multiple melanoma cell lines

To test whether LPA is the major attractant in serum in all stages of melanoma, I investigated the effect of Ki16425 with the panel of melanoma cells presented in Fig. 2 & 3. All three chemotaxis parameters were significantly reduced or abolished as a result of Ki16425 treatment in RGP and VGP cells (Fig. 12) as well as MM cells (Fig. 13).

Comparing the effects of the inhibitor using the quantitative CI plot largely concurs with the above findings (Fig. 14A). The degree of chemotaxis is in keeping with the qualitative findings described earlier in Fig. 2 & 3, with WM278 being the least chemotactic cell line overall and WM852 the least chemotactic MM cell line. The inhibitor has a profound effect on the chemotactic responses of WM35, WM98-1, WM239A and WM1158. Interestingly, the inhibitor had least effect on the cell lines that were performing the least efficient chemotaxis i.e. WM278 (VGP) and WM852 (MM). These data suggest that if cells are chemotaxing inefficiently towards serum, then they are less likely to respond to the LPA inhibitor and raises the question of differential LPAR expression.

Filtering these data by melanoma stage confirms that the inhibitor is effective across all stages (Fig. 14B). Although there is a mild residual chemotactic response in the inhibitor treated MM group ($p=0.004$), this is markedly reduced compared to the corresponding MM vehicle treated group. The residual chemotaxis is not a surprise considering the method of action of Ki16425, acting as a competitive antagonist.

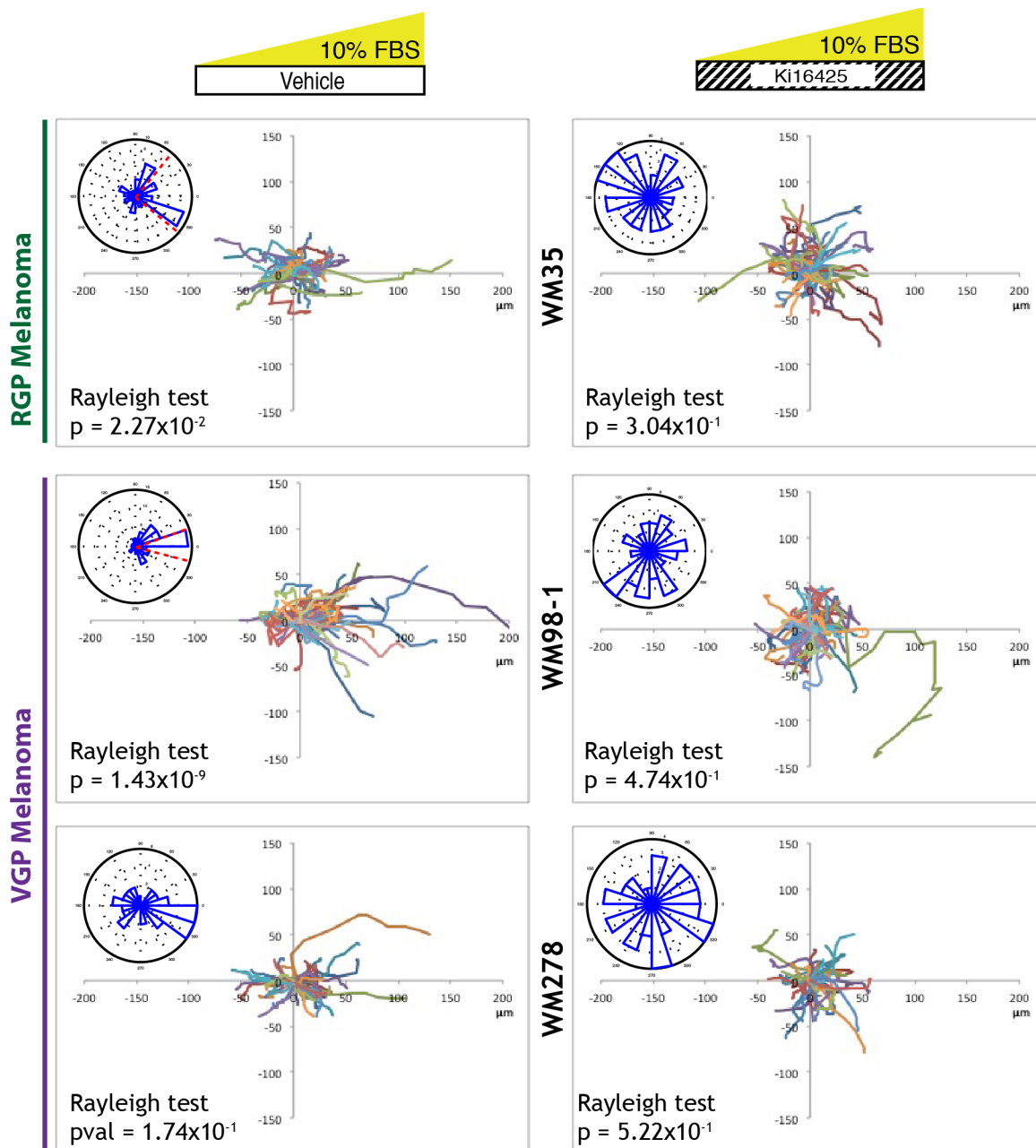


Figure 4-12 The effect of Ki16425 on primary melanoma chemotaxis.

The chemotactic responses of 3 different primary melanoma cell lines (1xRGP(green) and 2xVGP(purple)) were tested +/- Ki16425 in the presence of 10% FBS employing the standard Insall chamber assay. The spider and rose plots are presented with their respective Rayleigh tests.

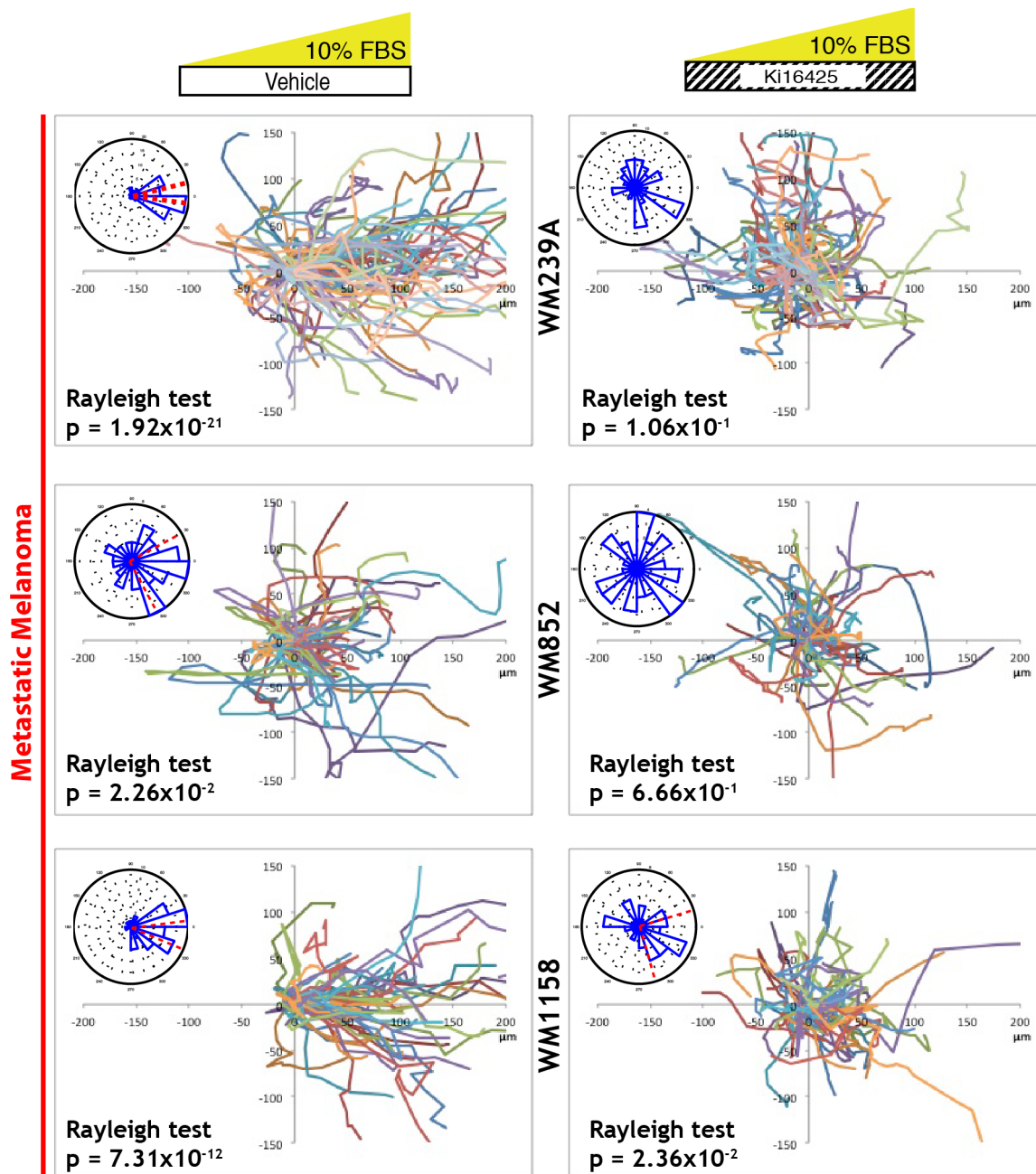


Figure 4-13 The effect of Ki16425 on metastatic melanoma chemotaxis.

The chemotactic responses of 3 different metastatic melanoma cell lines (red) were tested +/- Ki16425 in the presence of 10% FBS employing the standard Insall chamber assay. The spider and rose plots are presented with their respective Rayleigh tests.

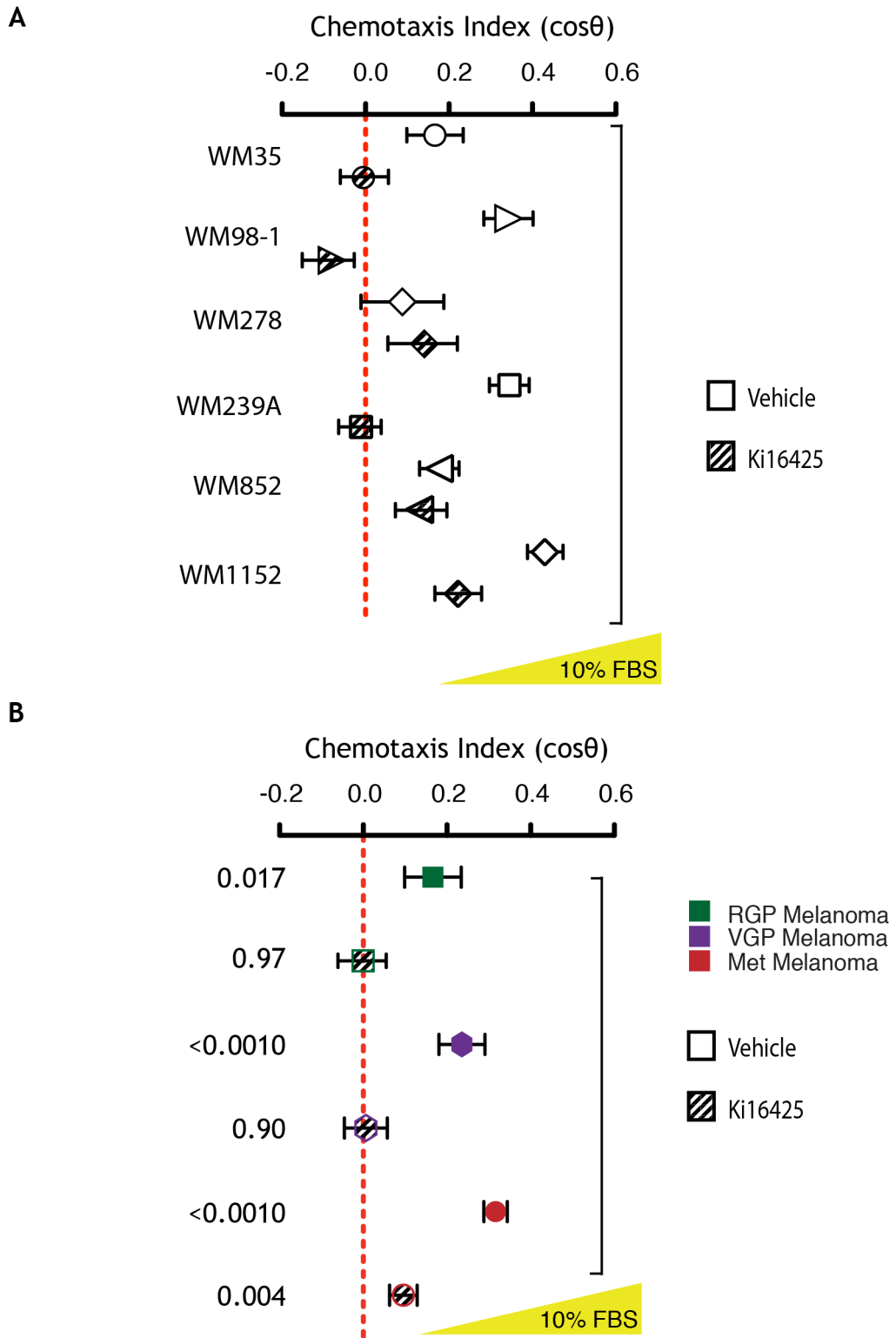


Figure 4-14 The quantitative effect of Ki16425 on chemotaxis of primary and metastatic melanoma cells.

The chemotaxis indices of all cells from Figs. 11 & 12 are presented by cell line (A) and melanoma stage (B). The results of one-sample t tests are marked adjacent to the corresponding results in (B).

4.1.8 LPA is necessary for invasion into 3D organotypic assays

The data thus far have confirmed that LPA is necessary and sufficient for chemotaxis of melanoma cells in 2D. Next I wished to examine whether LPA is also necessary for invasion into the more complex environment of a 3D organotypic matrix. I previously discussed the rationale for investigating cell biology mechanisms in both 2D and 3D due to the biological variances in behaviour that can be observed (Baker and Chen, 2012; Meyer et al., 2012; Petrie and Yamada, 2013; Tang et al., 2013).

Not all cells that are motile in 2D will invade in 3D. This is due to cell lines showing unique growth and invasive patterns, depending on the derived cell line (Meier et al., 2000). The panel of melanoma cells were seeded on organotypic assays and I identified WM98-1 (VGP) and WM1158 (MM) as the most invasive cell lines, which I used to study the effect of Ki16425.

Representative images from organotypic assays seeded with 2×10^5 cells and then harvested after 12 days at the air-liquid interface are shown in Fig. 15A. The assays were either treated with vehicle or Ki16425 $10 \mu\text{M}$. There is a marked contrast in the degree of invasion of the melanoma cells treated with the inhibitor. Both cell lines are capable of invading into the vehicle treated gels, but almost completely fail to invade into the Ki16425 treated gels. Quantifying the degree of invasion (Fig. 15B), there is a highly significant reduction in invasion in both cell lines.

These data strongly support the invasion of cancer cells into 3D organotypic matrices arising after the induction of a chemotactic gradient. I hypothesise that the gradient formation is self-generated by the overlying cancer cells through an as yet unidentified mechanism. The central result is that LPA is necessary for invasion into 3D organotypic matrices.

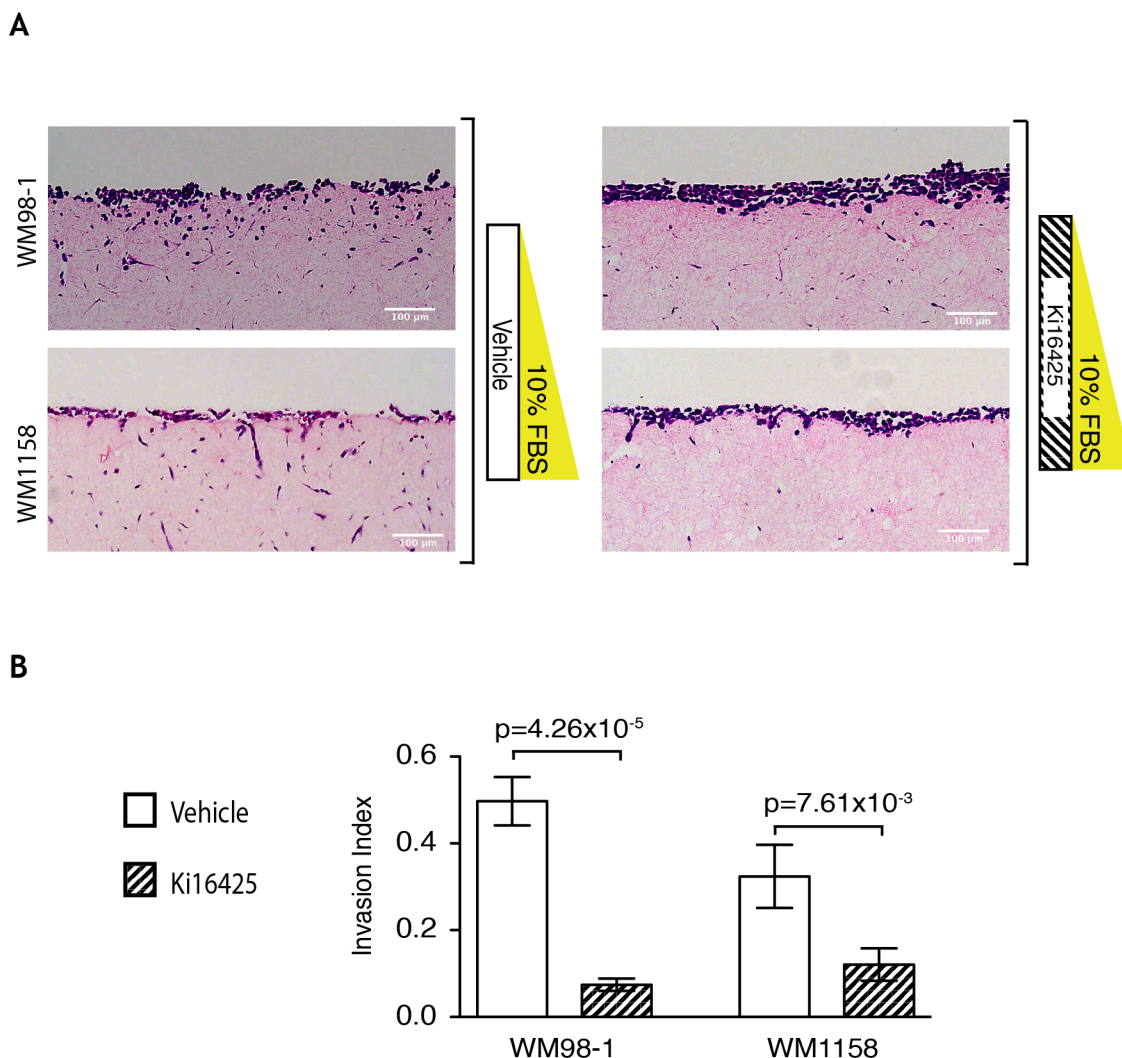


Figure 4-15 LPA is necessary for invasion into 3D organotypic assays.

A Panels of representative images of organotypic assays seeded with 2×10^5 cells of WM98-1 and WM1158 are shown +/- Ki16425. **B** Invasion index was calculated as the percentage of total cells on the organotypic matrix that invaded beyond $\sim 30 \mu\text{m}$ as a ratio of cells on top of the matrix. >1000 cells were counted per condition plotted and the results demonstrate a significant reduction in invasion with Ki16425 in both cell lines.

The role of Growth factors in LPA chemotaxis

I have demonstrated that GFs drive chemokinesis and I next asked whether they play a role in LPA chemotaxis?

4.1.9 Growth factors act as accessory factors to enhance LPA chemotaxis

To test whether GFs can modulate LPA chemotaxis I designed an experiment combining GFs with $1 \mu\text{M}$ LPA (Fig. 16). The combination of GFs with LPA produced not only longer cell tracks, suggesting greater speed, but more tightly

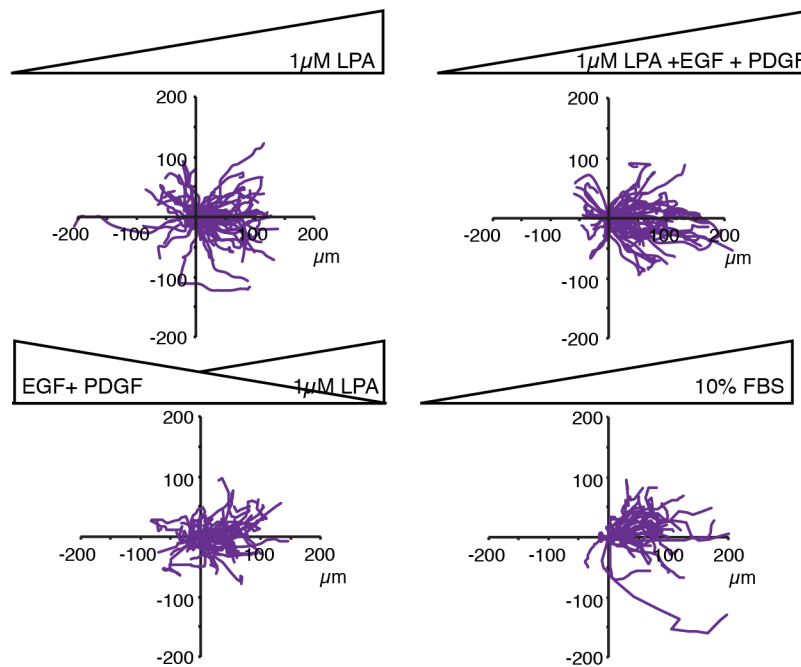
bunched tracks in the direction of the gradient when compared to 1 μ M LPA alone, indicating enhanced chemotaxis (Movie S9). There are fewer tracks in the opposite direction to the gradient in the combined GF LPA group. Based on the evidence supporting the role of GFs as chemokinetic agents, I then performed a competition experiment, with cells able to move freely in opposing gradients of LPA (gradient increasing to the right) and GFs (gradient increasing to the left). The spider plot for this experiment shows a track pattern very similar to LPA alone, although with slightly enhanced chemotaxis accuracy.

The chemotactic responses are quantified for comparison in the CI plot (Fig. 16 B). There is a trend towards the addition of growth factors enhancing the chemotaxis response to LPA but this was not statistically significant. Most interesting is the result for the opposing gradients of LPA and GFs. Again there is a trend towards enhanced chemotaxis towards LPA.

The speed data for these GF plus LPA experiments are presented in comparison to the SFM and FBS controls (Fig. 17). The chemokinetic effect of LPA alone compared to SFM is statistically highly significant ($p < 0.001$). The effect of the GFs can again be seen over and above the chemokinetic effect of LPA alone. LPA + PDGF is statistically significant compared to LPA alone ($p = 0.049$) and the graph of mean speed against time also highlights that for the majority of the 21 hour assay, these cells are migrating with greater speed.

In summary, these data indicate that GFs act as accessory factors and enhance the accuracy and speed of chemotaxis towards LPA. The competition experiment clearly demonstrates the potency of LPA as a chemoattractant in comparison to GFs.

A



B

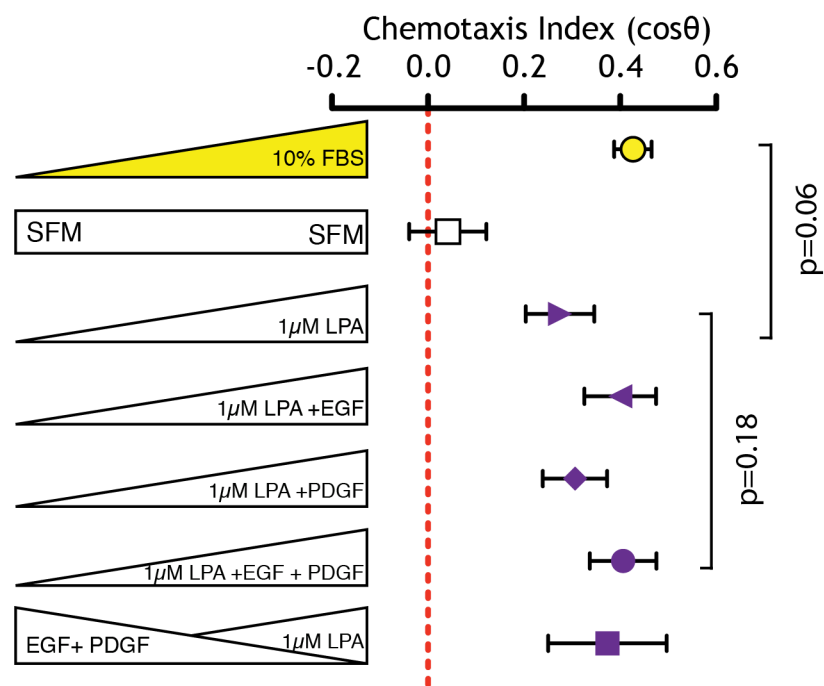


Figure 4-16 The effect of combining GFs with LPA on melanoma cell chemotaxis.

A Spider plots of the WM239A cells chemotaxing in gradients of LPA, LPA+EGF+PDGF (top) and LPA v a negative gradient of EGF +PDGF alongside a 10% FBS control. **B** Plot of chemotaxis index for the experiment in A, plus the additional experiments combining LPA with EGF and PDGF as single agents. This allows the comparison of chemotactic accuracy. Statistical comparisons are performed using the unpaired student t test.

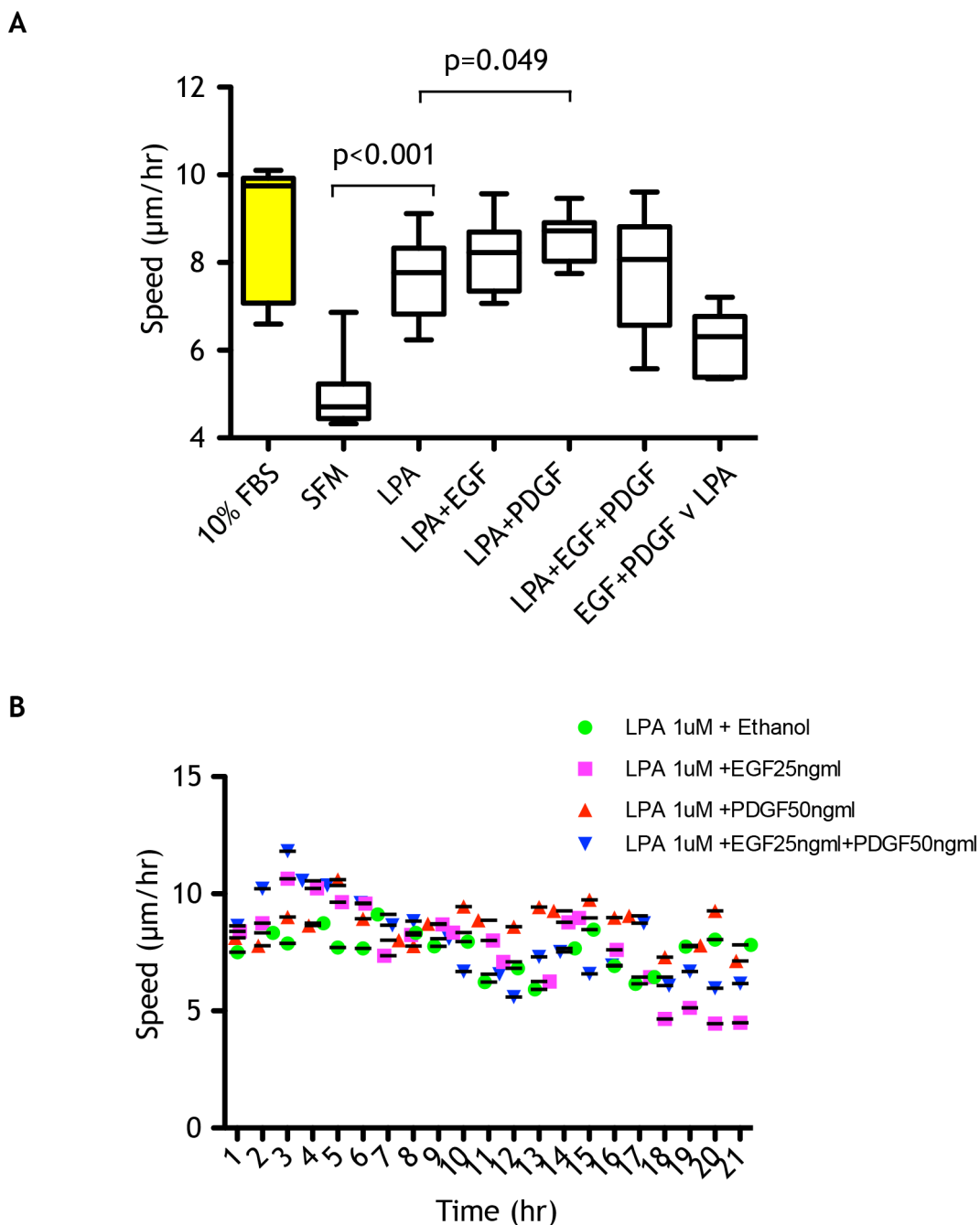


Figure 4-17 The effect of combining GFs with LPA on melanoma cell speed.

The speed data extracted from the experiments in Fig. 17 are presented for each condition along with SFM and 10% FBS controls. Statistical comparisons are performed using the unpaired student t test. (A) box and whisker plots from the time window with statistical comparisons performed using the unpaired student t test. (B) mean cell speed over time.

Discussion

The model of efficient chemotaxis driven invasion as a paradigm has been gaining greater appreciation in recent years (Condeelis et al., 1992; Hughes-Alford and Lauffenburger, 2012). I sought to comprehensively explore the relationship between the chemotactic behaviour of melanoma cells at different

stages of progression and demonstrated that even primary melanoma cells possess significant chemotactic ability. In the context of melanoma this may explain why primary melanomas are capable of metastasising so early in disease progression.

The major difference between primary and metastatic melanoma cells was the doubling of speed. Cell motility is known to be a pre-requisite for cancer cell invasion and metastasis (Bravo-Cordero et al., 2012; Liotta, 1986; Olson and Sahai, 2009; Provenzano et al., 2009). It is not clear if this results in earlier metastasis and is therefore of clinical relevance.

A major aim of this thesis was to identify the key drivers of melanoma cell chemotaxis. I found that the inflammatory signal LPA was not only the principal attractant, it was also active across all tumour stages. I also found LPA to be both sufficient and necessary for chemotaxis in both 2D and 3D assays.

The failure of all melanoma cells to produce a chemotactic response to serum in the presence of Ki16425 highlights the importance of LPARs 1 (and to a lesser extent 3) in transducing the signal necessary for chemotaxis. This is the first time an LPAR inhibitor has been used in direct visualisation studies and been shown to unequivocally abolish chemotaxis. Previous studies using indirect techniques were only able to conclude that Ki16425 reduced motility and diminished chemotaxis. It would be interesting to identify what LPAR receptors are expressed by all the cells and in particular WM278 and WM852 that revealed the weakest chemotactic response to serum. One would hypothesise that they have a different expression profile of LPARs, with less LPAR 1 & 3 in particular.

My data indicate that growth factors, which are frequently described as tumour chemoattractants, are in fact primarily chemokinetic agents in my conditions. All the GFs tested failed to induce a significant chemotactic response. Investigating the role of GFs in melanoma chemotaxis has qualified an earlier report that questioned whether they are truly chemotactic (Zicha and Dunn, 1995). I also found similar results, with trends towards unimodal directionality away from the gradient direction. Interestingly, EGF has been demonstrated to increase LPA production in ovarian cancer cells and this raises the question of whether this could be responsible for the autocrine and paracrine signalling

described (Snider et al., 2010) PDGF has also been shown to induce LPA production in fibroblasts following only 20 minutes of stimulation (Fukami and Takenawa, 1992).

One explanation for the lack of any response induced by GFs may be that the cell line investigated does not overexpress for example, the EGFR, which has been shown to enhance chemotaxis in cancer cells (Blaine et al., 2009; Hyun et al., 2011; Phillips et al., 2005; Smirnova et al., 2012). Conversely, the cells I tested did exhibit a chemokinetic response to EGF and given the strong chemotactic response induced by LPA across the majority of melanoma cell lines tested, I consider that EGFR overexpression is unlikely to be of such significance or equal importance.

However, I did identify a role for GFs acting as accessory factors, potentiating the chemoattractant activity of LPA. The addition of growth factors not only increases the speed during LPA chemotaxis, but it enhances the chemotactic accuracy to that of 10% FBS, even when a reverse gradient of GF is applied.

4.1.10 Conclusion

My data support LPA chemotaxis as a major driver of melanoma invasion across multiple cell lines from all biological stages of development. I also show how GFs, which are frequently described as tumour chemoattractants, are in fact primarily chemokinetic agents, and are capable of potentiating LPA's chemoattractant activity. It has been well documented that LPA is released from activated platelets and my finding therefore implicate the clotting system in the invasion of melanoma (Eichholtz et al., 1993; Tomas et al., 2003). The mechanism and physiological relevance of these findings will be explored in subsequent chapters.

Chapter 5:

The Self-Generation of LPA Gradients Drives Melanoma Cell Dispersal

Introduction

Having identified LPA chemotaxis as a key driver of melanoma motility and invasion, I wished to verify that this is responsible for the outward migration of cells from the primary tumour. I considered the three main modes of directed motility driving the cells to invade: positive chemotaxis (towards a gradient of chemoattractant), negative chemotaxis (away from a chemorepellent) and contact inhibition of migration. I excluded contact inhibition as a driver of invasion in 3D because this would still have been evident in the submerged cells. This also needs to be confirmed in 2D as well as exploring the possibilities of either positive or negative chemotaxis.

During standard Insall chamber assays I occasionally performed experiments with uniform serum in addition to uniform SFM controls. Interestingly, in the presence of serum, cells consistently migrated towards the nearest edge of the bridge (Fig. 1; Movie S10). This figure shows cells dispersing from the centre of the bridge, towards the nearest edge. This is most clearly seen from the spider plots for each half of the bridge and this finding highlights the importance of directly observing the cells and even then, not relying on the standard spider plot alone, which conceals this observation.

This dispersal effect has been termed the “edge-effect” and is acknowledged in the chemotaxis literature (Zigmond et al., 2001). It has been described in experiments when differing concentrations of a chemoattractant are used in either well rather than uniform concentration. This was hypothesised to be due either to the consumption of a chemoattractant within the medium, thereby generating a gradient of the chemoattractant towards one edge of the bridge, or the production of a chemorepellent driving cells to the nearest edge. In uniform SFM experiments I have already presented data to show that cells move randomly over the bridge and this supports the gradient consumption hypothesis. These effects arise in the Insall chamber due to the relatively small volume of fluid present over the bridge compared to the wells. The cells and media over the bridge are in other words, spatially restricted. This is an important feature in keeping with the complex restricted environment cells co-habit *in vivo* (Chioni and Grose, 2008).

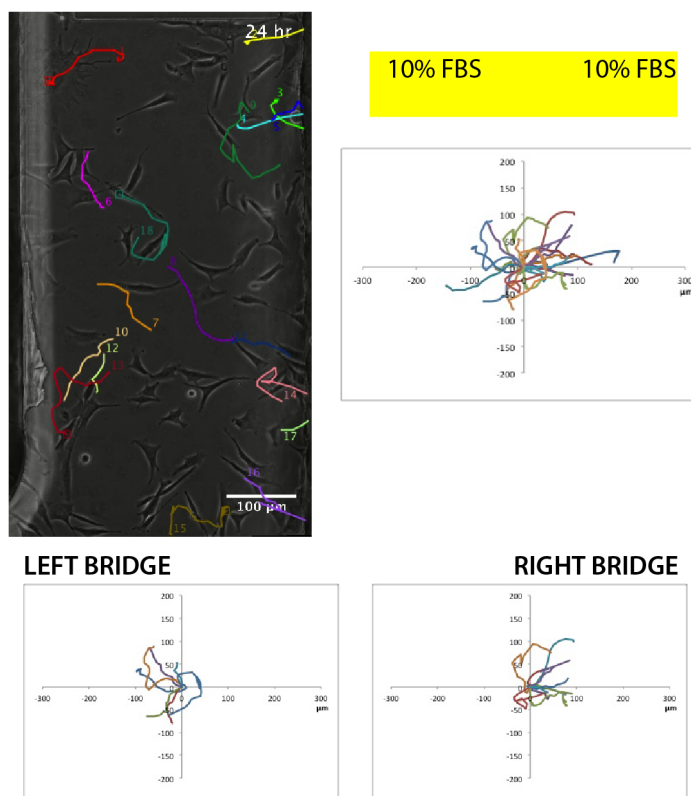


Figure 5-1 Observing the behaviour of cells in uniform serum.

With the Insall chamber standard assay, WM239A cells were added to the chamber in the presence of uniform serum (10% FBS in both inner and outer wells). These cells were imaged for 24 hours. The bridge was divided into 2 equal halves longitudinally and the cells were tracked based on their starting location into the 2 sub-groups: left of right. The upper spider plot combines all the cell tracks and the smaller spider plots present the tracks based on the starting position of the cells.

Whilst establishing the Insall chamber standard assay, I also observed that at very low cell densities, chemotaxis to serum was poor and the edge effect was less marked in uniform serum experiments. This suggests that melanoma cells are capable of exerting a communal effect on the response, supporting the hypothesis that they are capable of modifying the gradient or producing a new one. I therefore asked the question of whether this dispersal effect is also driven by positive LPA chemotaxis? And if so, how is it generated?

Melanoma cells disperse in serum by positive chemotaxis

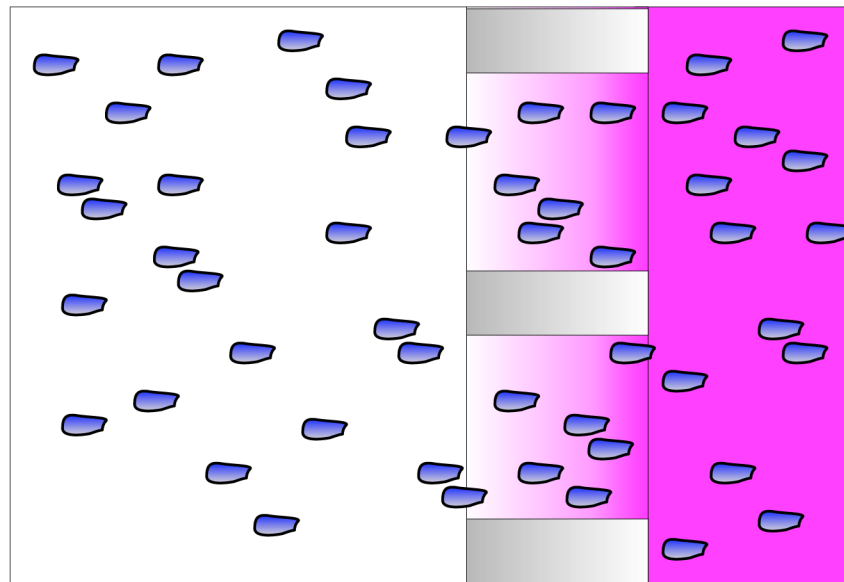
5.1.1 Melanoma cells disperse in uniform 10% FBS media

To test the mode of the dispersal effect, we devised the “centre well assay”, which is useful for observing the behaviour and initial response of cells to an undisturbed chemoattractant (Muinonen-Martin et al., In Press). A comparison with the standard assay can be seen in figure (Fig. 2). Importantly, there are no cells on the bridge that can modify the gradient. It therefore allows the observation of single and multicellular migration patterns over the entire distance of the bridge, thus allowing the probing of mechanism of migration with greater clarity. Another important difference to the standard assay is that cells can only move initially in a 180° arc directed towards the bridge and this can therefore be considered to be a simplified model of the dispersal of cells from a tumour. This assay was established by Prof David Knecht (Dept Molecular & Cell Biology, University of Connecticut) and the experiments that have been carried out by him are marked accordingly in the figure legends. All the work has been generated with our joint intellectual input.

We attempted to generate the equivalent of the edge-effect response in the centre well assay. We did this by establishing the centre well assay with WM239A MM cells in centre well immersed in uniform 10% FBS and observed their response over the course of 18 hours. The experiment was successful and cells actively migrated onto the bridge (Fig. 3). A refined example of this experiment has been performed by Olivia Susanto who compared migration of WM239A cells in uniform serum (Movie S11) and 0-10% FBS (Movie S12) in the centre well assay. This process of autonomous cell dispersal will now be investigated in further detail.

A

Standard Assay

**B**

Centre-well assay

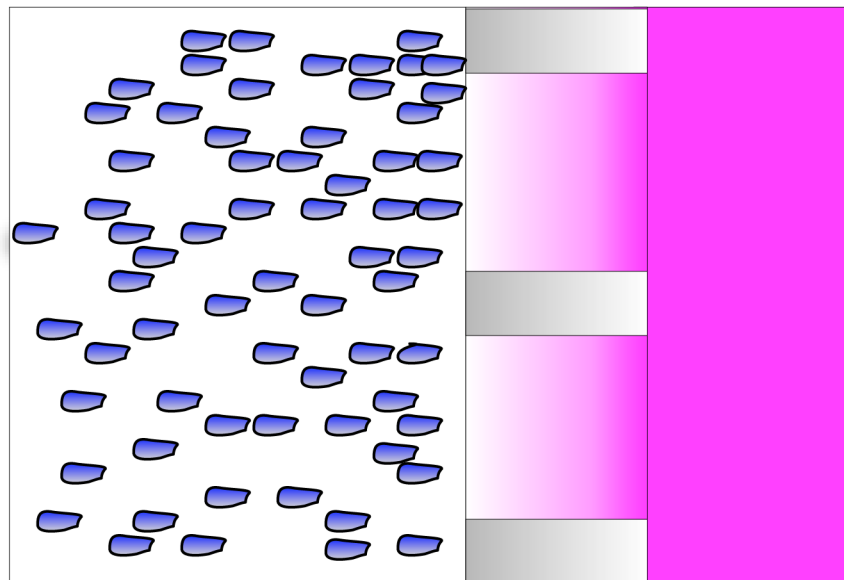


Figure 5-2 Two Insall chamber assays for investigating chemotaxis.

A The standard assay starts with cells spread evenly and predominantly singly across a coverslip and therefore throughout the chemotactic gradient on the bridges. **B** The centre-well assay is set-up with all the cells originating in the centre-well from which they can emerge into an undisturbed gradient (over the viewing bridges).

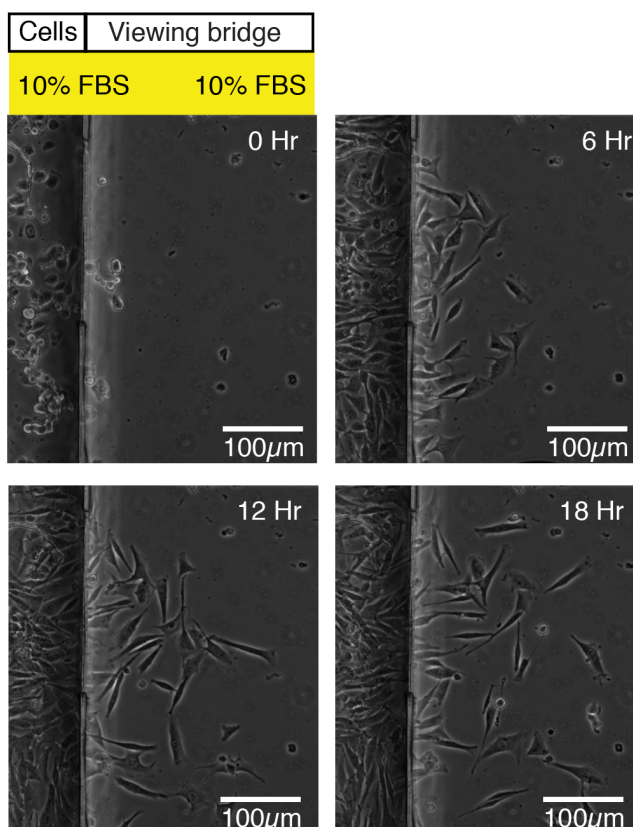


Figure 5-3 Cell migration in the centre-well assay

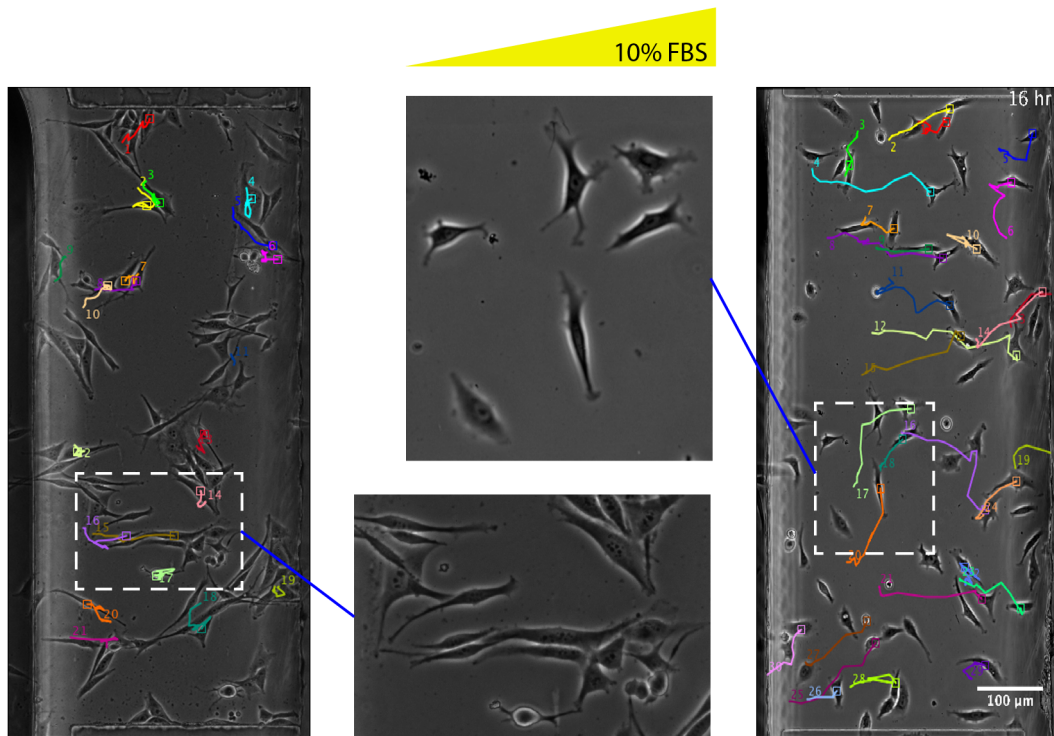
Images of WM239A melanoma cells spreading from the Insall chamber centre well assay in wave formation across the bridge over 18 hours duration. Panels represent time-lapse images taken every 6 hours during this window.

5.1.2 Melanoma cells do not disperse by contact inhibition of locomotion in 2D or 3D

To investigate which mode of directional migration is the underlying driver of the dispersal effect, we first investigated contact inhibition of locomotion using the centre well assay with uniform medium (Fig. 4). In the presence of a 10% FBS gradient cells can be seen to be dispersing whether or not they are in contact with one-another and cells can also be seen migrating in a chain out from the centre well (Movie S13). These observations confirm that contact

inhibition of locomotion is not the mechanism driving melanoma cell dispersal in these 2D assays.

A



B

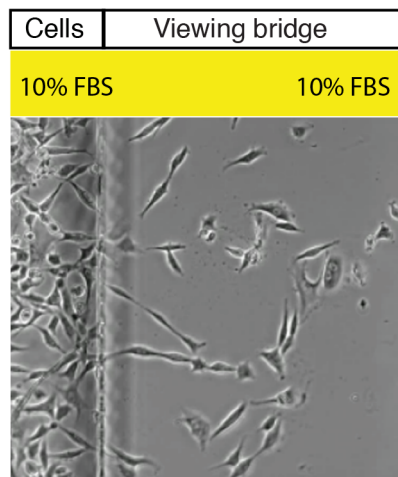


Figure 5-4 Observing the mode of migration in 2D

A Images of the standard assay with a 10% FBS gradient with 2 different experiments with WM35 cells shown in the large panel on the left and WM1158A cells on the right. There are exploded views with cells contacting in one image and migrating singly in the other **B** Images of WM1158 melanoma cells spreading during an Insall chamber centre-well assay. This latter experiment was performed by Prof David Knecht.

Investigating the mode of dispersal in 3D organotypic matrices is more challenging because of the more complex environment. There is also no proven mechanism by which cells disperse in the assay. The accepted dogma revolves around the induction of a chemotactic gradient that drives invasion generated by raising the gel to the air-liquid interface (Timpson et al., 2011). This assumption is generally accepted within the field, although there is neither evidence for how this gradient is generated, nor any confirmation that a gradient exists (Berking and Herlyn, 2001; Meier et al., 2000).

If one considers the situation where a gel is lifted to the air-liquid interface without any cells seeded over the upper surface, one would postulate that the gel would remain saturated due to the large pool of serum under the gel with no sink. No gradient would therefore be formed assuming the serum pool was regularly replenished with frequent fresh CGM changes (Zicha et al., 1991). Therefore the key factor involved in generating the gradient must be the addition of cells seeded onto the surface of the gel. Friedl et al postulated that contact inhibition of locomotion may maintain a high degree of polarity in cells invading collectively and this process would contribute to the directional persistence of motility even in the absence of a chemotactic gradient (Friedl et al., 1995). If the gels are kept submerged with a layer of cells on the upper surface, a gradient cannot form due to the saturating level of serum surrounding the matrix and cells. I therefore performed a simple experiment comparing the invasion of cells kept submerged versus the invasion of cells on gels lifted to the air-liquid interface to test the role of contact inhibition of locomotion in 3D.

Keeping the gels submerged resulted in complete failure of invasive cells to breach the integrity of the gel (Fig. 5). This result clearly rejects the hypothesis that invasion is driven by contact inhibition, which would predict invasion in both circumstances. However, it supports the theory that chemotaxis is the main mechanism by which cells invade into the gels, but direct evidence for positive or negative chemotaxis has yet to be identified. I speculate that once the gel is raised to the air-liquid interface, an LPA gradient is produced in a self-generated fashion by the overlying cancer cells and this steers their invasion.

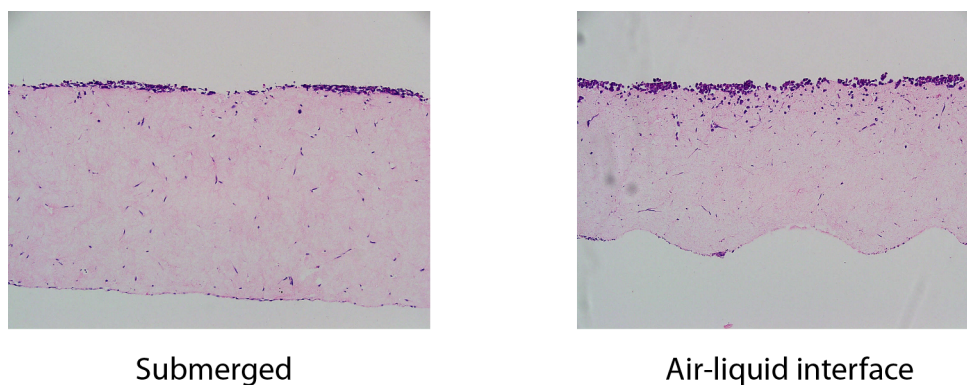


Figure 5-5 Observing the mode of migration in 3D

Representative images of organotypic assays seeded with 2×10^5 WM98-1 cells and either kept submerged (left) or raised to the air-liquid interface (right) for 14 days.

5.1.3 Melanoma cell dispersal is density dependent

To test the assertion that dispersal is density dependent, we seeded cells at different densities in the centre well assay. Representative images are shown at the same 17 hour time point for each density (Fig. 6A). It is clear from the images that as the cell density increases, the number of cells migrating onto the bridge increases (Fig. 6B,C). Not only does the number of cells migrating onto the bridge increase, but the distance migrated and the proportion of total cells migrating onto the bridge also increases. This implies that the cells are cooperating with one another to disperse more efficiently and this supports cell dispersal as a density dependent autonomous process.

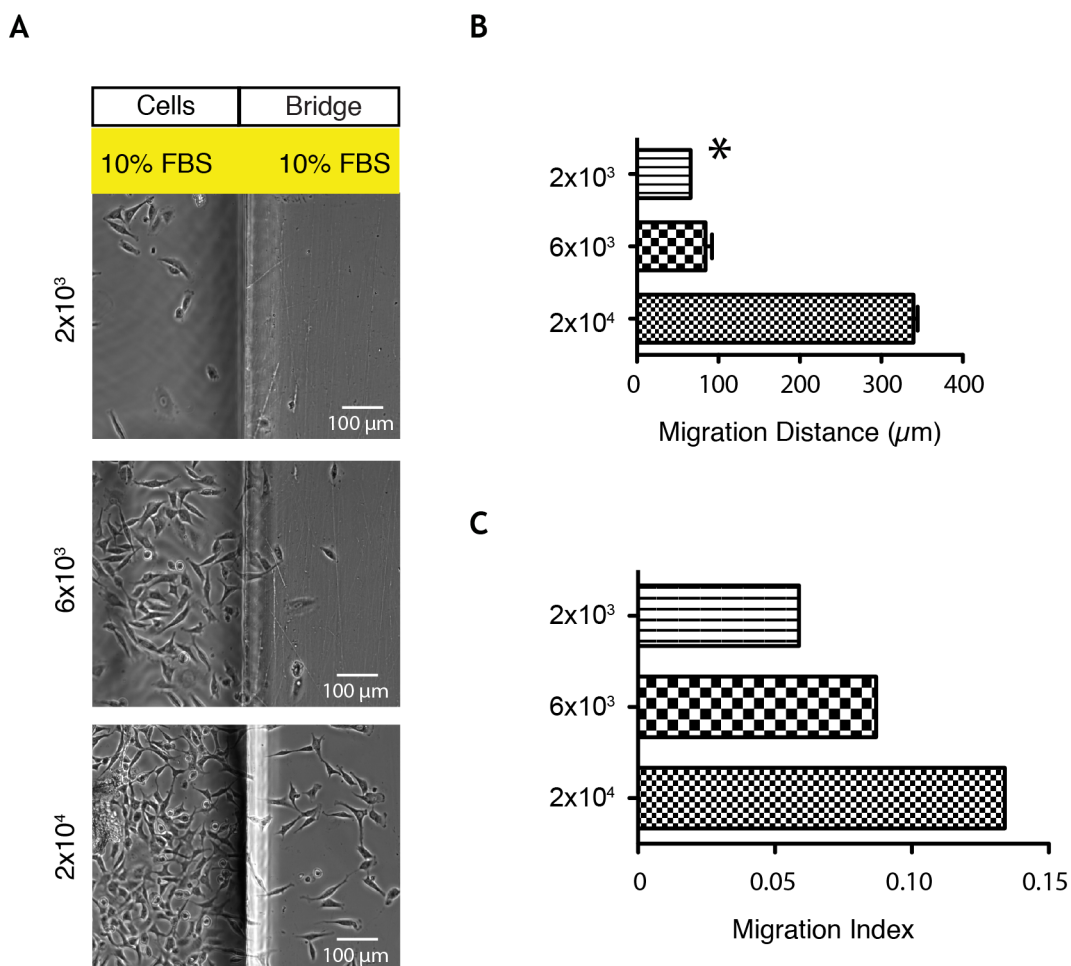


Figure 5-6 The effect of increasing cell density on autonomous cell dispersal.

A Images of the uniform media centre well assay with 3 different cell densities of the MM cell line WM1158/ well: 2×10^3 , 6×10^3 and 2×10^4 . The images represent the same 17 hour time point in each assay. These data are quantified by **(B)** distance travelled by the furthest 3 cells and **(C)** migration index (the proportion of cells on the bridge relative to the total number of cells in the field of view). This experiment was performed by Prof David Knecht.

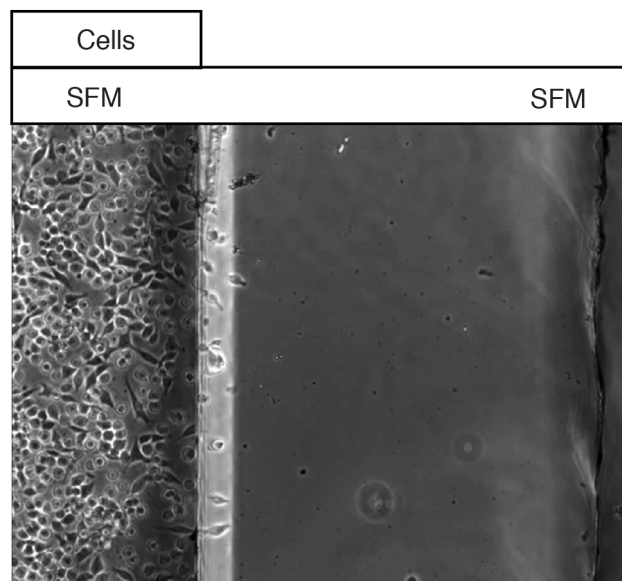
5.1.4 Melanoma cell dispersal is overwhelmingly driven by positive chemotaxis through depletion of a serum factor(s)

To investigate dispersal via positive or negative chemotaxis, we performed the centre well assay with WM1158 cells in the absence of serum (Fig. 7A). Over the time course of 17 hours, the cells completely failed to migrate onto the bridge. The result of this experiment argues against the hypothesis that cell dispersal is driven by negative chemotaxis (the production of a chemorepellent) and combined with the results from previous uniform medium experiments, indicates that there is a factor within serum that is necessary for dispersal.

This suggests that the directed migration in uniform serum arises as a result of breaking down a serum factor(s) acting as the chemoattractant(s). This process

of degrading the factor(s) generates a gradient to which the cells can chemotax. We then asked the question of whether the application of a pre-formed outward gradient of serum would drive dispersal?

A



B

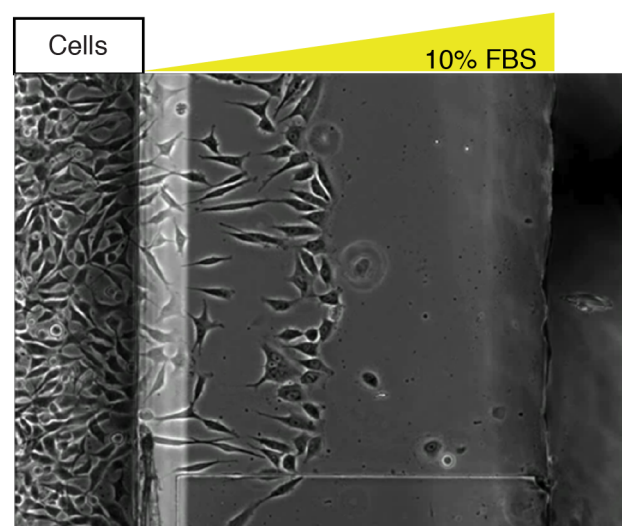


Figure 5-7 Examining the mechanism of dispersal +/- 10% FBS gradient.

A Image of Insall chamber centre-well assay demonstrating WM1158 cells spreading to the nearest edge on the bridge seen clearly on the spider plots (overall and subdivided into cells starting on left or right sides of the viewing bridge). **B** WM239A cells in the centre well assay in the presence of an artificially generated 10% FBS gradient. These experiments were performed by Prof David Knecht.

Repeating the centre-well assay, but this time adding an external outward gradient of 10% FBS (Fig. 7B), the WM1158 cells dispersed with at least equivalent efficiency onto the bridge during the same 17 hour time frame compared to the experiment in uniform serum (See Movies S11 & 12). This further supports the depletion of a serum factor, with the chemotaxis in uniform serum appearing very similar to the positive chemotaxis arising when an externally applied gradient is applied.

Melanoma cells degrade LPA to generate gradients driving dispersal

5.1.5 Degradation of a serum factor(s) drives chemotaxis

I reasoned that conditioning fresh media with melanoma cells would result in degradation of the serum factor(s). Establishing a standard assay with fresh media in one well and conditioned media in the other would in effect generate an external gradient towards the fresh media. Melanoma cells should therefore migrate in the direction of the fresh media.

The result of the migration analysis comparing fresh media mock conditioned for 0 hours (T0) to fresh media conditioned for 48 hours (T48) overall produced a spider plot with accurate chemotaxis towards the T0 media (Fig. 8). Compare control experiment (Movie S14) to conditioned experiment (Movie S15). This is indicative of the efficient chemotaxis seen towards LPA and serum. Sub-dividing the data into the half of the bridge that the cells originated from confirmed that cells starting on both sides migrated with similar efficiency towards the control side. The data for all the conditioned media time points are available (see appendix 5).

This result supports the hypothesis that melanoma cells perform chemotaxis in uniform serum by depleting a serum factor. Based on the results in chapter 4 showing that LPA is the major driver of melanoma chemotaxis I hypothesised that it is the depletion of LPA that drives this response.

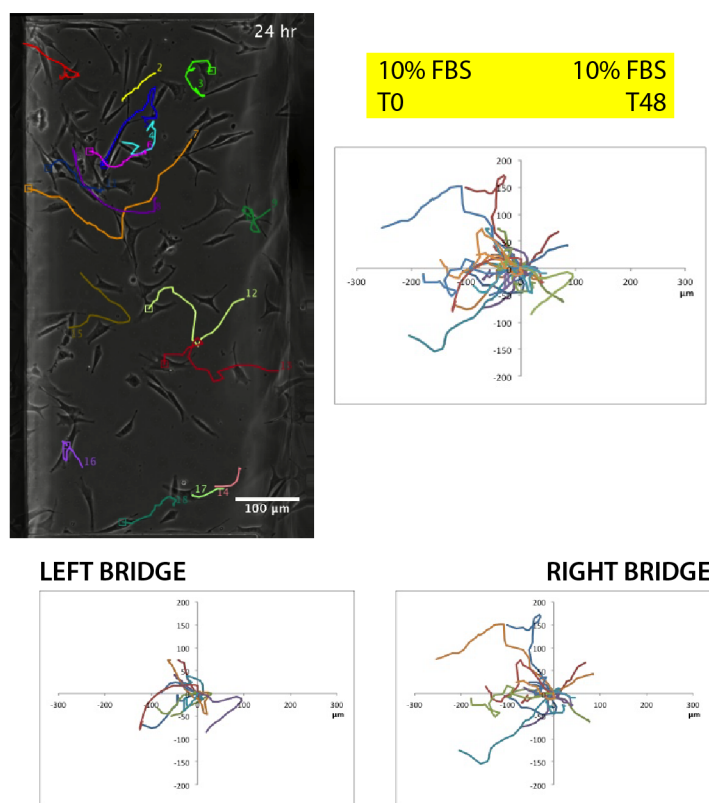


Figure 5-8 The effect of conditioning media on the dispersal effect of serum. Image of the standard assay cells with 10% FBS T0 (No conditioning) and 10% FBS T48 (Prior conditioning in the presence of WM239A cells for 48 hours) in opposing wells. The large spider represents all the tracks and the sub-divided data based on side of the bridge is below.

5.1.6 LPA is depleted in melanoma cell conditioned medium

To determine whether the LPA levels were modified by conditioning, we quantified the concentration of LPA in all the samples that I tested. The same conditioned media used in the Insall chamber assays along with SFM conditioned media was analysed by LC-MS by my collaborator (Prof. Mike Wakelam) to quantify the total and sub-species of LPA. The total LPA fell in both FBS conditioned media experiments over time with the rate of depletion being faster for FBS conditioned media 2 than FBS conditioned media 1 (Fig. 9A). This can be explained by the greater number of cells (approximately 10 times more at 24 hours) used to condition FBS conditioned media 2. The SFM conditioned media LPA concentration remained consistently negligible and did not vary over the duration of conditioning.

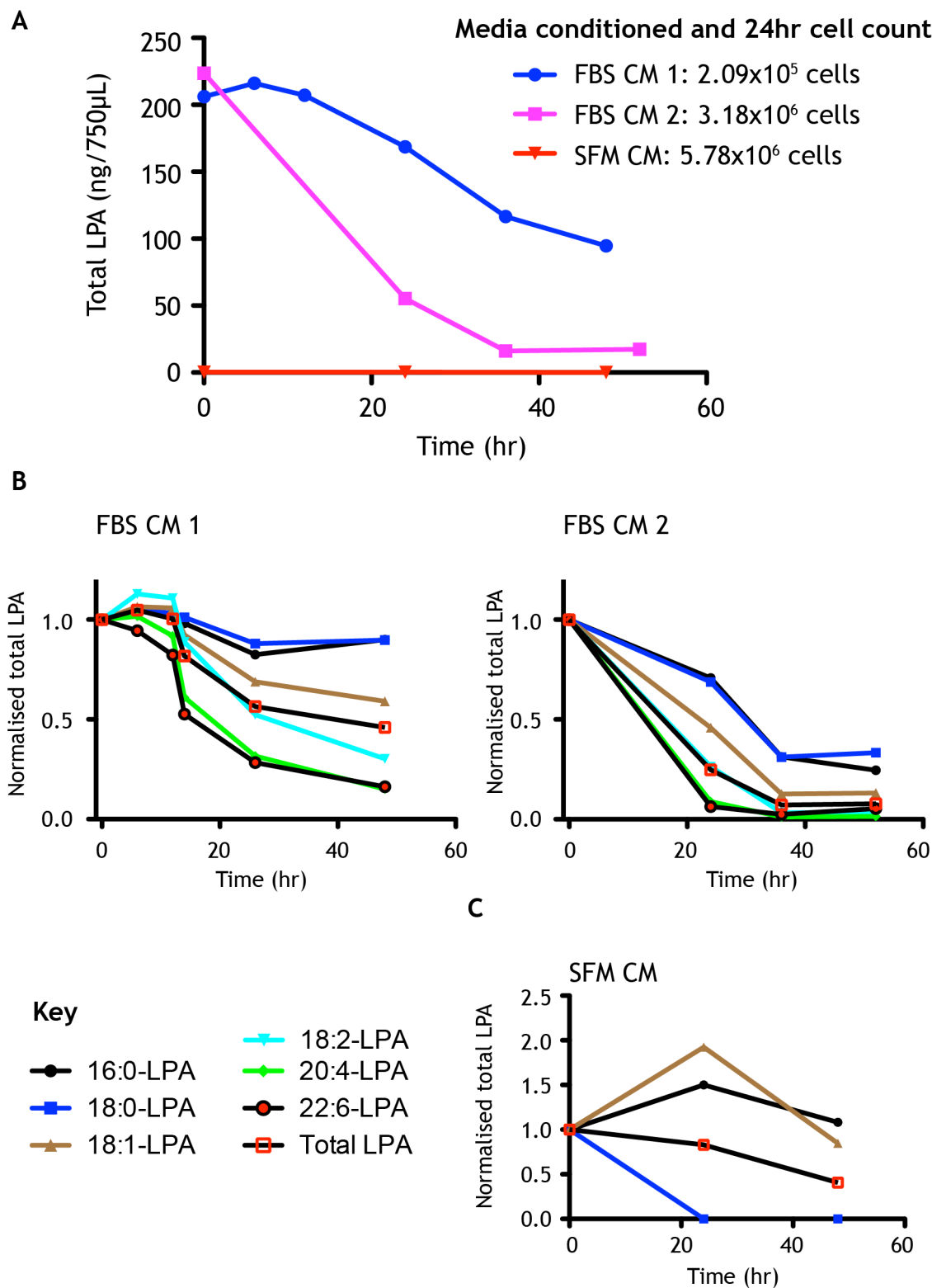


Figure 5-9 LC-MS quantification of the [LPA] within media conditioned by WM239A cells. The fresh media conditioned by WM239A melanoma cells in Fig. 6 was analysed by LC-MS to quantify the total LPA. This experiment was repeated twice with fresh media: FBS CM1 and 2. SFM media was also conditioned with WM239A cells with the same technique. Samples were immediately frozen on dry ice to prevent the sample from degradation. **A** Line graph representing the total LPA (mean \pm SEM) against conditioning time. The total LPA is presented normalised to the volume of CM analysed (750µL). The cell counts at 24 hours are marked. Line graphs of (mean \pm SEM) for LPA subspecies and total LPA normalised to T0 for the **(B)** FBS and **(C)** SFM experiments.

These data confirm that LPA is quantifiable and present at significant levels and is depleted over time by the WM239A MM cells. The rate of degradation correlates with the number of cells conditioning the media. The conclusion from the SFM conditioned media result is that there is no net production of LPA over time, although the cells may require LPC in serum. These data therefore show that melanoma cells are capable of generating a gradient of LPA over time and in a density dependent manner.

5.1.7 Biologically active LPA species are preferentially depleted

The biological activity of LPA is known to vary with its structure. In particular, there is a positive correlation with the biological activity of LPA and acyl chain length (Jalink et al., 1995; Moolenaar, 1995; Van Corven et al., 1992). We therefore quantified the subspecies present in the samples.

Analysing the subspecies following normalisation to the T0 result (Fig. 9B), there is a clear trend towards the longer chain and polyunsaturated sub-species of LPA being degraded most efficiently in both experiments. There was a very small quantity of LPA quantifiable in the SFM experiment, but not all the sub species were identifiable and there was no overall trend (Fig. 9C).

The finding that the different LPA species are preferentially depleted with the most biologically active species creating the steepest gradients is therefore significant. To the best of my knowledge, these are the first data to reveal that the most biologically active species of LPA are preferentially degraded.

This raises important questions regarding the specificity of the different LPA degrading enzymes (LPPs) for their substrate LPA. Is the slightly enhanced chemotactic response generated by MM cells related to differential expression of LPPs? One could hypothesise that they are capable of degrading the most biologically active LPA species more efficiently.

5.1.8 LPA is sufficient to generate a dispersal effect

Having demonstrated the ability of melanoma cells to deplete LPA over time, I asked whether a uniform concentration of LPA is sufficient to generate a dispersal or “edge-effect”? I tested the ability of a uniform 1 μ M LPA to generate the dispersal effect in the standard Insall chamber assay (Fig. 10).

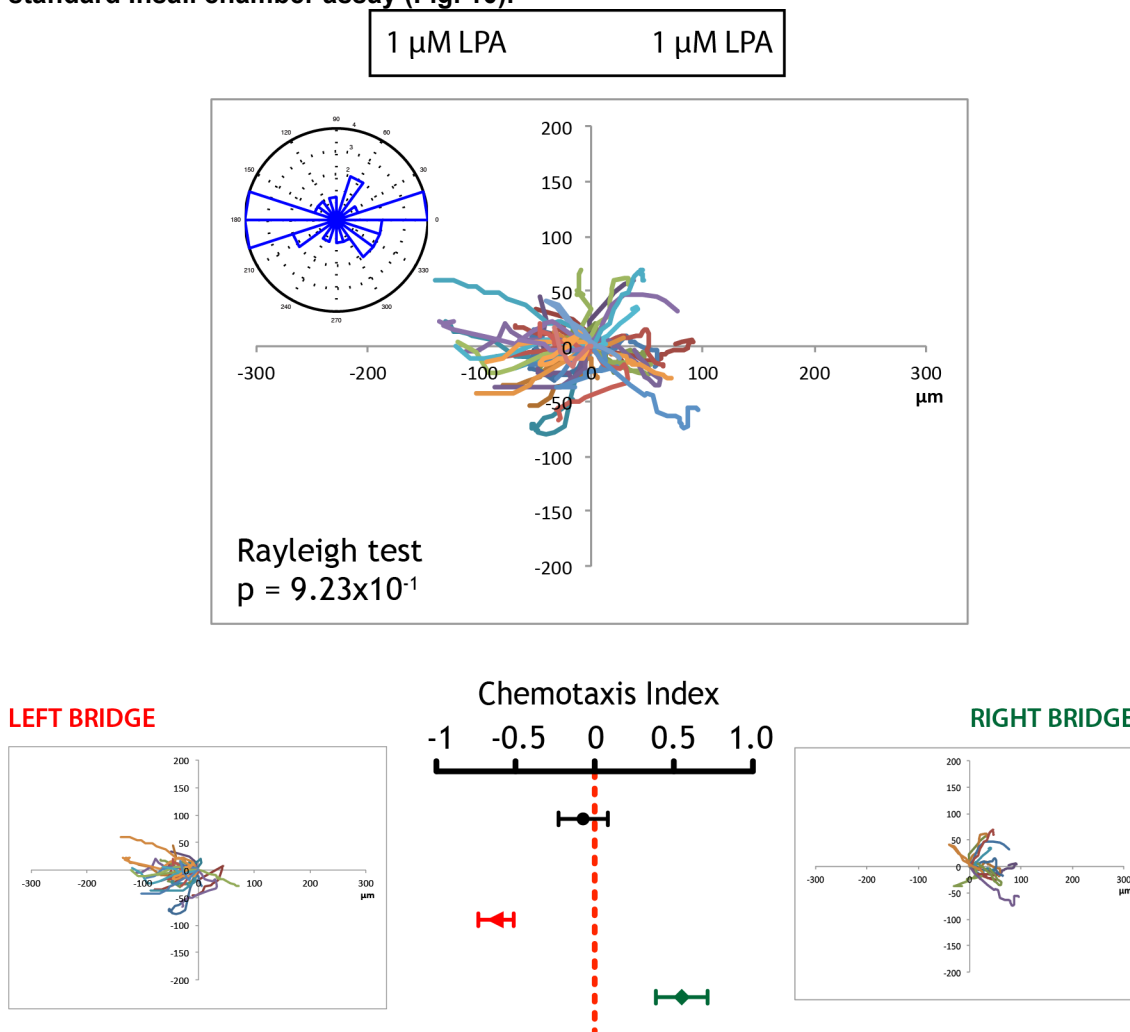


Figure 5-10 Examining the ability of 1 μ M LPA to generate an “edge-effect”.

With the Insall chamber standard assay, WM239A cells were added to the chamber in the presence of uniform 1 μ M LPA (1 μ M LPA in both inner and outer wells). These cells were imaged for 24 hours. The bridge was divided into 2 equal halves longitudinally and the cells were tracked based on their starting location into the 2 sub-groups: left of right. The upper spider plot, rose plot and Rayleigh test are calculated based on all the cell tracks and the smaller spider plots present the tracks based on the starting position of the cells. The chemotaxis index plot is calculated for all 3 scenarios.

Whilst the overall spider plot reveals no trend and the Rayleigh test is highly non-significant. The rose plot suggests there are 2 populations of cells moving directionally towards the edges of the bridges. Sub-analysing the data based on initial bridge position, the data unambiguously reveal a dispersal effect. I can therefore conclude from these data that LPA is sufficient to generate a dispersal effect.

5.1.9 LPA is necessary to generate a dispersal effect

I then wished to question whether LPA is necessary for the dispersal effect in serum? This experiment involved comparing the dispersal effects of WM239A cells in the presence or absence of the LPA inhibitor Ki16425.

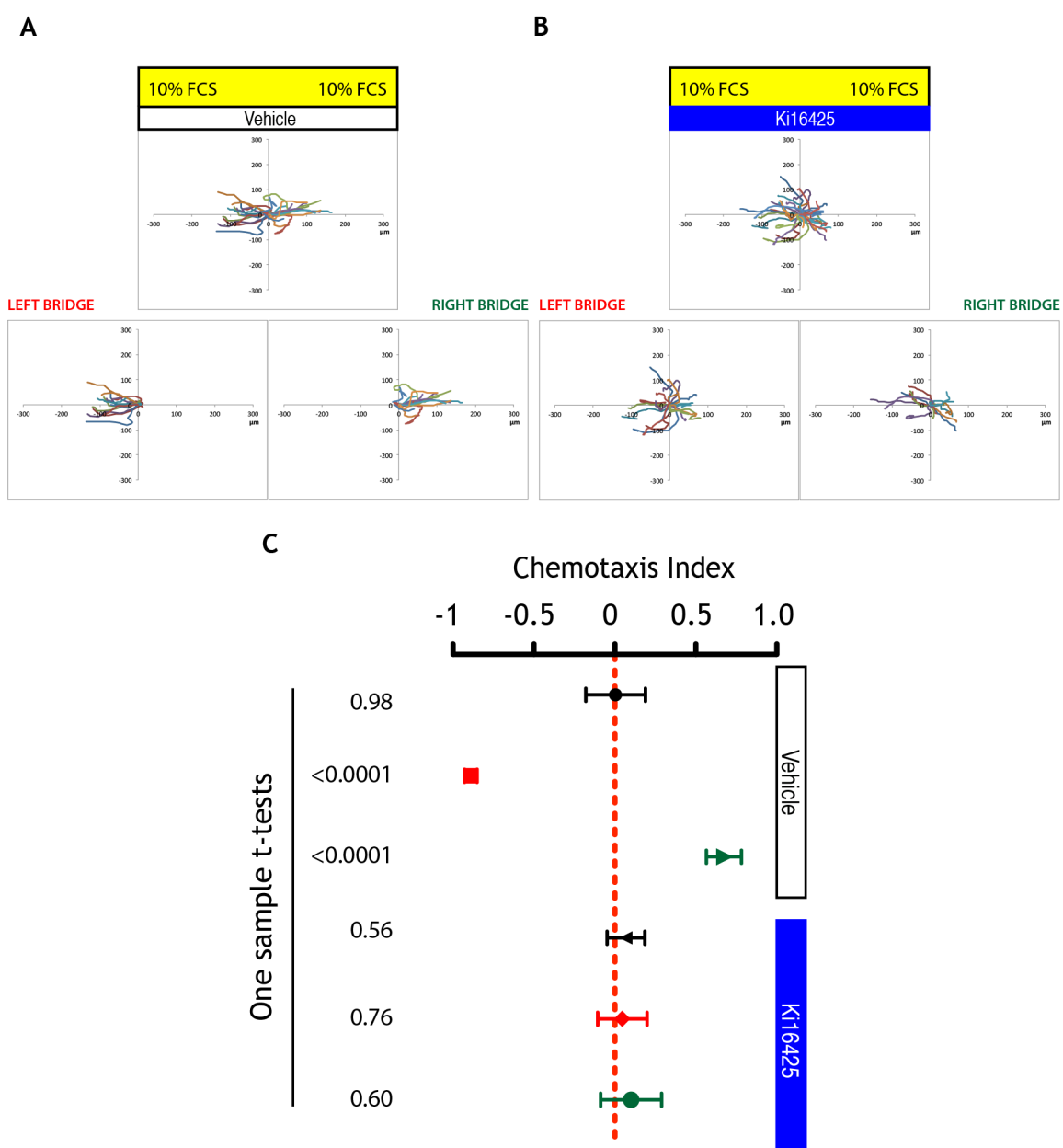


Figure 5-11 Examining the effect of Ki16425 on the “edge-effect”.

With the Insall chamber standard assay, WM239A cells were added to the chamber in the presence of uniform serum (10% FBS in both inner and outer wells) with vehicle (**A**) of the LPA inhibitor Ki16425 (**B**). These cells were imaged for 24 hours. The bridge was divided into 2 equal halves longitudinally and the cells were tracked based on their starting location into the 2 sub-groups: left of right. The upper spider plot in each combines all the cell tracks and the smaller spider plots present the tracks based on the starting position of the cells. **C** The chemotaxis index is calculated for all 6 scenarios and tested for deviation from a CI=0 with one sample t tests.

The vehicle controlled experiment (Fig. 11A; Movie S16) demonstrates a strong dispersal effect with a bipolar bias as seen previously. The addition of Ki16425 generates a completely random overall plot (Fig. 11B; Movie S17). Sub-analysing the data based on starting position on the bridge reveals spider plots that appear entirely random on both sides of the bridge. These results are presented with greatest clarity on the CI plot (Fig. 11C). The robust and highly significant dispersal effect in the vehicle treated group is completely abolished in the inhibitor treated group, with the CIs all failing to deviate from 0.

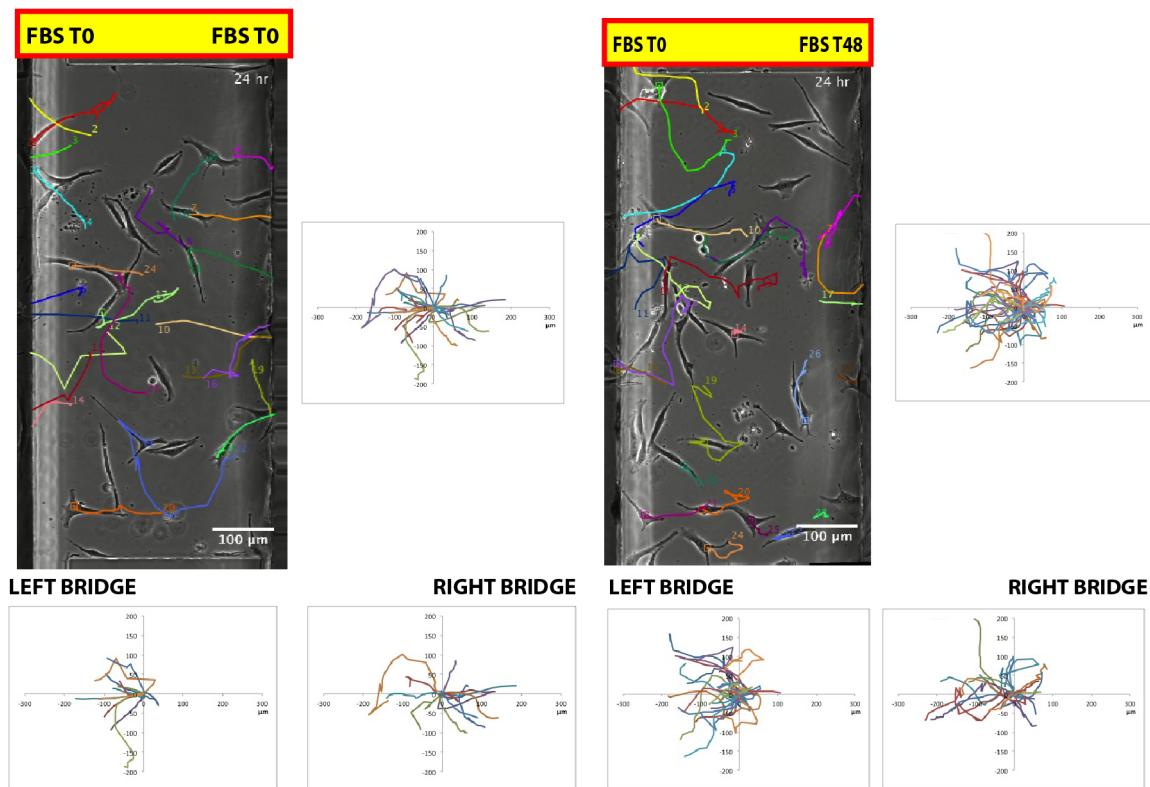
These data firstly confirm that LPA is necessary for the edge effect. Secondly, they implicate LPARs 1 and 3 in the transduction of the signal required to respond to the self-generated gradients.

Fibroblasts and keratinocytes also degrade LPA

I was interested to see whether other skin cells have the ability to degrade LPA or whether this was a melanoma specific phenomenon. I therefore conditioned media with Tiff fibroblasts and HaCaT keratinocytes. The functional chemotactic effects of these media on WM239A cells were compared using the standard assay with exactly the same technique as for the melanoma (WM239A) conditioned media experiments.

Both the fibroblast (Fig. 12A upper left) and keratinocyte (Fig. 12B lower left) mock conditioned media produced edge-effects when uniformly distributed. The dispersal effect was strongest with the keratinocyte conditioned media. Adding T48 conditioned media to the wells on the right hand side resulted in strong chemotaxis to the mock conditioned media. This confirms that other host cells are capable of self-generating gradients.

A



B

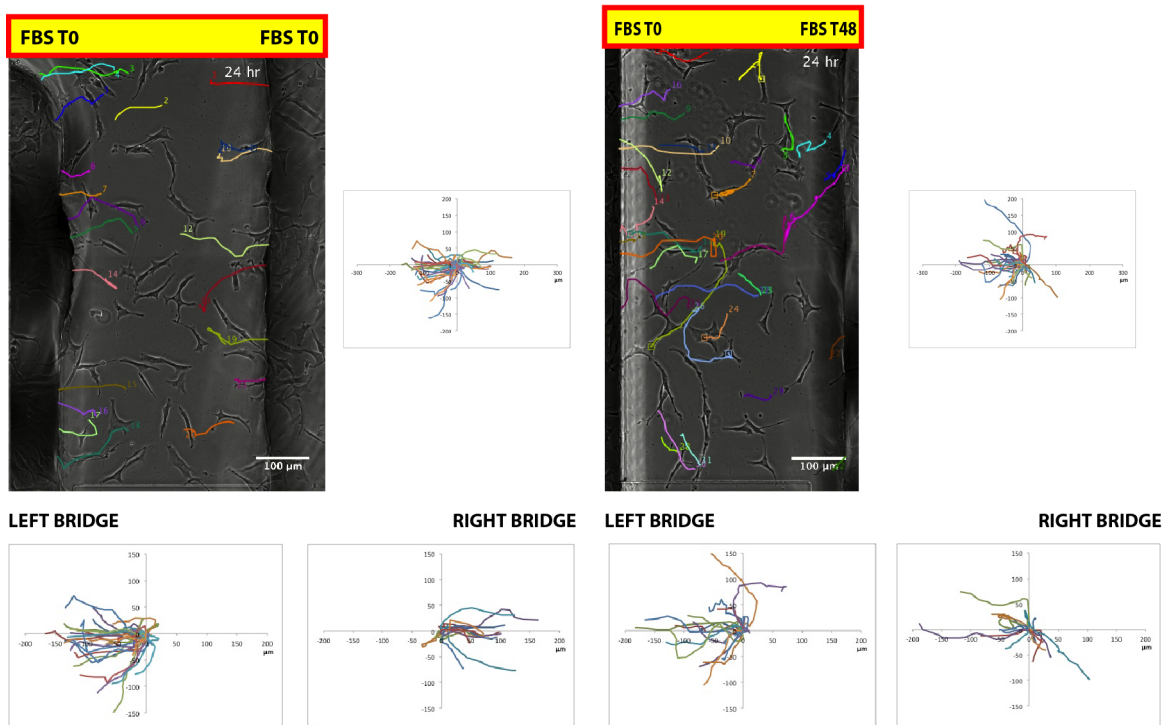


Figure 5-12 Investigating the effect of keratinocyte and fibroblast conditioned media on the dispersal of melanoma cells.

A Fibroblast and **B** keratinocyte CM was used to investigate their respective effects on the dispersal of WM239A melanoma cells. The conditioning was performed as per the melanoma cell CM. The panels on the left represent the positive control experiments with T0 CM both sides and the T0 – T48 CM experiments are on the right. The larger plots to the right of the images represent the pooled tracks and the smaller plots present the tracks based on the starting position of the cells.

Patterning associated with self-generated gradients

5.1.10 *A wave precedes the patterning of the bridge with evenly spaced cells*

Reviewing the movies of cells dispersing in uniform 10% FBS, a wave passes to the nearest edge in the standard assay (Movie S16), or more strikingly, across the bridge in the centre-well assay (Movie S11). This wave is moving independently of the mass of cells in the centre well. Of particular interest is the way in which cells dropping off the back of the way are left relatively motionless, dendritic in morphology and evenly spread across the bridge. This finding is reproducible when *Dictyostelium* cells migrate in uniform folate in the under agar assay (equivalent to the centre-well assay; Movie S18).

Discussion

In this chapter, I have shown that the dispersal of melanoma cells in uniform serum is driven by positive chemotaxis, which is serum dependent. The process of positive chemotaxis is driven by the ability of cells to deplete LPA from the immediate microenvironment to generate outward gradients that drive the dispersal of cells. Cells are therefore capable of dispersing in uniform serum, but the effect is amplified by applying an external gradient. This is almost certainly due to LPAR saturation in uniform media and following a period of LPA degradation, the LPA concentration falls to around the K_d of its receptor (Hulme and Trevethick, 2010; Tabchy et al., 2011). Near this concentration, the LPAR receptors are able to sense the gradient and transduce the signal with subsequent chemotaxis. With an externally applied gradient, the LPA concentration is already nearer to the K_d for the receptor producing a much greater and more rapid chemotactic response.

I noted that there was a time delay before dispersal in the conditioned media experiments, potentially corresponding to this initial period of receptor saturation. I hypothesised that there would therefore be a shorter delay before dispersal with increased duration of conditioning. An attempt was made to quantify this by comparing the delay with media conditioned for increasing durations, but the result was inconsistent and this line of investigation was not

pursued (see appendix 5). Alternatively, this lack of correlation may be explained by receptor adaptation after a period of saturation. LPA degradation by LPPs is very rapid and LPA has a short half life of only 3 minutes in plasma. Therefore it is likely that a gradient is established relatively quickly (regardless of the duration of conditioning) in the Insall chamber and the delay is in fact due to the time it takes for the receptors to adapt and sense the gradient following the fall below the receptor saturation concentration. To investigate this more accurately, the Insall chamber could be further modified by installing a micropump to provide a continual source of fresh media to further investigate the role of self-generated gradients. I hypothesise that cells would fail to disperse in the centre well assay if 10% FBS was being constantly replenished, because the ability of cells to generate a gradient would be overwhelmed by the supply of LPA.

The scattering/ dispersal of cells in response to LPA was first described in keratinocytes (Jourquin et al., 2006). Interestingly, this response was enhanced by a period of serum starvation. The finding was confirmed with gastrointestinal cancer cells and was shown to be dependent on LPAR1 receptor expression with cells only expressing LPAR2 unable to perform this. The underlying mechanism behind the dispersal effect of LPA was not elucidated (Shin et al., 2009). However, these experiments were performed in a standard cell culture dish with overlying media and all the cells were in contact in small colonies. It is likely therefore that this is an entirely different mechanism, reliant on alterations in adherens junctions rather than the dispersal of individual cells through self-generated gradients. In keeping with the scattering effect being dependent on LPAR 1 signalling, I found that LPAR 1+/- LPAR 3 were also necessary for the dispersal effect elicited in the Insall chamber with the use of Ki16425.

I have shown that LPA is both sufficient and necessary for the dispersal or “edge-effect”, acting through the mechanism of self-generated gradients. With the cell conditioning experiments, I have demonstrated that the greater the number of cells, the higher the rate of LPA depletion. This density dependent finding translates well to the ability of a larger proportion of melanoma cells to disperse further in higher cell densities. Applying the same mechanism to human melanoma invasion one would expect larger melanomas, containing a higher cell number, to be more invasive and produce a disproportionate number of

circulating tumour cells. Although, the current model supports depth of invasion as the best predictive marker for metastasis, there is evidence to support tumour volume as a better predictive marker (Friedman et al., 1991; Marghoob et al., 2000; Payette et al., 2009). This evaluation is currently considered impractical compared to a simple one dimensional measurement, although it would provide an even closer approximation to the model I am proposing.

LPA has been shown to promote wound healing in skin (Balazs et al., 2001), healing of the intestinal epithelium (Sturm et al., 1999), healing of corneal ulceration (Xu et al., 2007) and it has been recovered from blister fluid (Mazereeuw-Hautier et al., 2005). It also promotes keratinocyte chemotaxis and cell motility using transwell chambers (Jans et al., 2013; Sauer et al., 2004). The mechanism by which LPA induces keratinocytes to migrate across a wound is not yet known and the finding that keratinocytes can generate gradients may explain the mechanism by which they produce wound re-epithelisation. Supportive of this hypothesis is the finding that LPARs 1-3 are expressed in keratinocytes, which enables transduction of the LPA signal (Anliker and Chun, 2004).

Fibroblasts have been shown to migrate towards wounds in response to LPA (Balazs et al., 2001). *In vitro* wound remodelling and contraction is directed by LPA in experiments measuring the contraction of 3D organotypic gels (Lee et al., 2003). This mechanism again may well be directed through LPAR1. Fibroblasts are known to express LPAR1 (Ohta et al., 2003; Hama et al., 2004) and Ki16425 has been shown to significantly reduce motility in scratch assays (Tanaka et al., 2009) and Boyden chamber assays (Hama et al., 2004), but LPA chemotaxis has not been quantified using a direct visualisation method. It would therefore be interesting to see the effect of the conditioned medium on the chemotactic responses of fibroblasts and keratinocytes. The evidence from my conditioned media experiments and the literature suggests that self-generated gradients may explain the predicted chemotactic response to serum or LPA by both cell types.

The fact that numerous cells can degrade LPA complicates the emerging model, although regardless of the cell type breaking down the LPA, the process will remain density dependent. Therefore one would hypothesise that a primary melanoma will disproportionately breakdown LPA compared to keratinocytes and

fibroblasts in particular. The keratinocytes may play a role in distorting the LPA gradient above a melanoma, given their relative abundance.

Following the observation that WM239A cells preferentially break down the more biologically active LPA species, it will be important to repeat this result in other MM cell lines and to compare the results with the sub-species profile generated in conditioned media from RGP and VGP cells. This raises the question of whether strongly serum responsive melanoma cells are capable of degrading the most biologically active LPA species more efficiently than weakly responsive cells? We will need to identify the LPP and LPAR expression profile by the different cells (or stage).

Finally, the patterning of cells observed in our final experiments in this chapter is created by an advancing wave of cells driven by a self-generated gradient. The cells at the back of the wave then drop off the back in an evenly spaced distribution. The fact this finding is consistent in both *Dictyostelium* and mammalian cells suggests it may be an important conserved mechanism for the equal spreading or patterning of cells. I hypothesise that the number of cells in the wave could be maintained by a mitotic rate equal to the rate of cells lost from the back of the wave. When cells show a defect in melanoblast migration during development, one of the phenotypes they produce is a white belly, whereby the cells fail to migrate around the trunk (Li et al., 2011). It is interesting to hypothesise whether this arises due to a lack of chemoattractant, a failure to generate gradients or a slowing of growth. The latter would result in the wave petering out or slowing before critical survival signals result in the melanoblasts invading the epidermis wherever they had reached and interestingly, defects in cell-cycle progression and cytokinesis have been confirmed in these Rac1 deficient mice.

5.1.11 Conclusion:

Through the use of a direct visualisation assay, we show that the dispersal of melanoma cells is overwhelmingly driven by positive chemotaxis. Melanoma cells deplete LPA in their immediate vicinity to generate gradients of LPA that drive positive chemotaxis. I hypothesise that this process may also be the mechanism employed by other cell types resulting in wound closure by keratinocytes or

ensuring the even distribution of melanoblasts during development. The efficiency of the mechanism is enhanced by the preferential degradation of biologically active LPPs. I hypothesise that self-generated LPA gradients will drive the invasion of melanoma cells *in vivo* and the efficiency of this process may depend on the LPP expression profile.

Chapter 6:

The Identification of LPA Gradients Across the Margins of Melanomas *In Vivo*

Introduction

The data presented in chapter 4 indicates that the inflammatory signal LPA is the key chemoattractant in serum. To demonstrate the physiological relevance of this finding I hypothesised that a gradient of LPA will exist across the margin or invasive front of a melanoma *in vivo*. The data presented thus far would suggest that this gradient is a marker for active LPA chemotactic invasion and may therefore represent a much needed prognostic marker for the risk of metastasis (Mackie, 2000).

To test this hypothesis, I decided to sample the LPA concentration across the margin of a melanoma. I first considered the shape and nature of the gradient. It would be important to prove that there exists an outward gradient of LPA from the melanoma, ie. lower within the tumour and higher outside the tumour. This would provide the key signal to melanoma cells at the periphery of the tumour to invade and indicate that the melanoma cells are actively self-generating a gradient. This outward gradient should be present in all directions, and would act as a tumour-centric dispersive force that drives outward invasive migration in all directions. This could explain the pagetoid (upward) spread commonly associated with invasive melanoma (Brenn, 2012; Petronic-Rosic et al., 2004; Trotter, 2011) and the lateral spread necessitating wide local excisions to excise these micrometastases following initial excision of the primary melanoma (Marsden et al., 2010). The source of LPA in this model arises from within the tumour as a result of inflammation and platelet activation. The final chapter will discuss this further as this hypothesis has not formerly been tested.

The presence of LPA has only been investigated in human skin on one previous occasion (Mazereeuw-Hautier et al., 2005). This study quantified the presence of LPA in serous blister fluid from patients with a range of bullous dermatoses using a simple and highly sensitive radioenzymatic assay (Saulnier-Blache et al., 2000). LPA was detected in the blisters of all 24 patients at physiological concentrations ($0.60 \pm 0.0087 \mu\text{M}$). LPA is now detectable by liquid chromatography-mass spectrometry (LC-MS) and I opted to use this highly accurate technique in collaboration with Prof Mike Wakelam to quantify the concentration of LPA in the tumour and surrounding skin (Wakelam et al., 2008;

Wakelam and Clark, 2011). I therefore acquired fresh melanoma tissue from murine models of melanoma to pilot and validate the technique. These models are considered highly representative of human disease and cancer (Van Dyke and Jacks, 2002).

To the best of my knowledge, the existence of a chemotactic gradient across a tumour has never been demonstrated *in vivo* and the discovery of this gradient would further support the chemotactic driven invasion paradigm. In particular it would improve understanding about the generation of chemotactic gradients *in vivo*, provide important information about the tumour microenvironment's sphere of influence and perhaps pave the way to develop a novel prognostic marker.

The generation of murine melanomas

6.1.1 The *Tyr::CreER^{T2} BRAF^{V600E/+} PTEN^{lox/+}* mouse melanoma model

The *Tyr::CreER^{T2} BRAF^{V600E/+} PTEN^{lox/+}* melanoma model has been described in the introductory chapter. Based on the McMahon model, it was generated and maintained by Dr. Colin Lindsay, Dr. William Faller, through the breeding programme of Prof Sansom and Prof Ozanne at the Beatson Institute (Dankort et al., 2009).

6.1.2 Suitability & characterisation of the *Tyr::CreER^{T2} BRAF^{V600E/+} PTEN^{lox/+}* mouse melanoma model for sampling LPA gradients

This model has been thoroughly characterised in Dr Lindsay's PhD thesis (Lindsay, 2012). The specific details about the alleles used in the model and the method of induction are covered in chapter 2. The results in this section on suitability and characterisation were obtained by Dr Lindsay and are presented with his express permission.

A comparison of overall survival between the *Tyr::CreER^{T2} BRAF^{V600E/+} PTEN^{lox/+}* model and the *Tyr::CreER^{T2} BRAF^{V600E/+} PTEN^{lox/lox}* model, revealed that the latter's survival was considerably shortened. This was due to the extremely

rapid overgrowth and ulceration of the tumours and so the model using the PTEN heterozygote allele was considered a more faithful representation of the human disease. Importantly, this melanoma model is driven by the BRAF^{V600E} mutation. This is the most common mutation found in approximately 50% of human melanomas and is therefore highly desirable to study from a translational perspective (Broekaert et al., 2010; Ellerhorst et al., 2011). An NRAS model was less desirable for the reasons outlined in the introduction.

Histologically, the tumours generated demonstrated a nodular melanoma (NM) morphology with, which is typical of mouse melanoma models. Epithelioid and spindle cells are found intradermally and most of the tumours were amelanotic with pigmented cells predominantly found in the dermis. Following induction with tamoxifen, the median time to melanoma induction was approximately 10 weeks and by 22 weeks, all mice have developed a primary melanoma. Following melanoma induction, the median time until death was approximately 3 weeks.

Macroscopically, 19/23 melanomas demonstrated ulceration at a median diameter of 7mm and 2 mice in the cohort were not assessed. Morphologically, the melanomas are clearly delineated and after shaving the skin, it is easy to identify where the tumour margin resides. As the skin on the back is activated with tamoxifen, the majority of tumours are located on this very accessible and easy to sample area.

6.1.3 Incorporation of the 3Rs: replacement, reduction and refinement

The project had already explored and utilised “replacement” alternatives in the work described in chapter 4, particularly with the use of 3D organotypic assays. Advancing the understanding a stage further and discovering whether LPA gradients are physiologically relevant by proving their existence *in vivo* was considered potentially of great scientific and medical importance.

The Tyr::CreER^{T2} BRAF^{V600E/+} PTEN^{lox/+} murine model has been developed and “refined” for generating melanomas. Importantly, the fact they were being bred for another simultaneous project meant that no extra animals were

required for this work. Having incorporated the 3Rs in the experimental proposal, I considered the proposed work ethically sound.

Sampling & quantifying LPA *in vivo*

6.1.4 Quantification of LPA

A collaboration was established with Prof. Mike Wakelam (Babraham Institute, Cambridge) who has pioneered the use of high-sensitivity liquid chromatography-mass spectrometry (LC-MS) technology to rapidly and comprehensively measure the levels of lipids in a wide range of cells, tissues and tumours (Wakelam, 2013). This robust technique has been used to quantify the LPA concentration within different tissues. The key factors to consider were firstly that the sensitivity of the technique necessitated that at least 1 mg of tissue was required per sample. Secondly, LPA is known to have a short half-life of only 3 minutes in plasma and therefore all biopsies were attempted within this time frame (Samadi et al., 2011). Therefore, to ensure that no LPA is lost through enzymatic degradation, the samples were snap frozen in liquid nitrogen and transported to the Babraham Institute on dry ice for LPA extraction and quantification.

6.1.5 Sampling methodology

Ideally, I wished to measure the LPA gradient downwards in the y-plane across the invasive front because this is known to correspond to the key prognostic marker for primary melanomas, the Breslow thickness (Balch et al., 2009; Haass and Smalley, 2009; Mackie, 2000; Marghoob et al., 2000). However, slicing the core sample in the y-plane would provide insufficient material to measure the LPA due to the limited thickness of the skin (Lee and Hwang, 2002). Based on the hypothesis of the “global outward LPA gradient model”, I instead sampled across the edge of the melanoma in the x-plane.

For reproducibility, I opted to sample the tumour and surrounding skin using a punch biopsy technique. This technique is commonly employed by dermatologists for biopsying cutaneous neoplasms or inflammatory dermatoses and involves taking a cylindrical core of tissue of a set diameter by rotating the circular blade down through the epidermis and dermis, and into the

subcutaneous fat (Zuber, 2002). The punch biopsies employed by dermatologists commonly vary between 3-6mm in diameter and the tools are available in 1mm increments.

By sampling at points within, at the margin and outside the tumour I planned to demonstrate a gradient of LPA across the margin of the melanoma (Fig. 1). For mice that developed more than one melanoma, the melanomas were sampled in a direction that was equidistant from other melanomas to reduce the risk of contamination from the microenvironment of these other tumours.

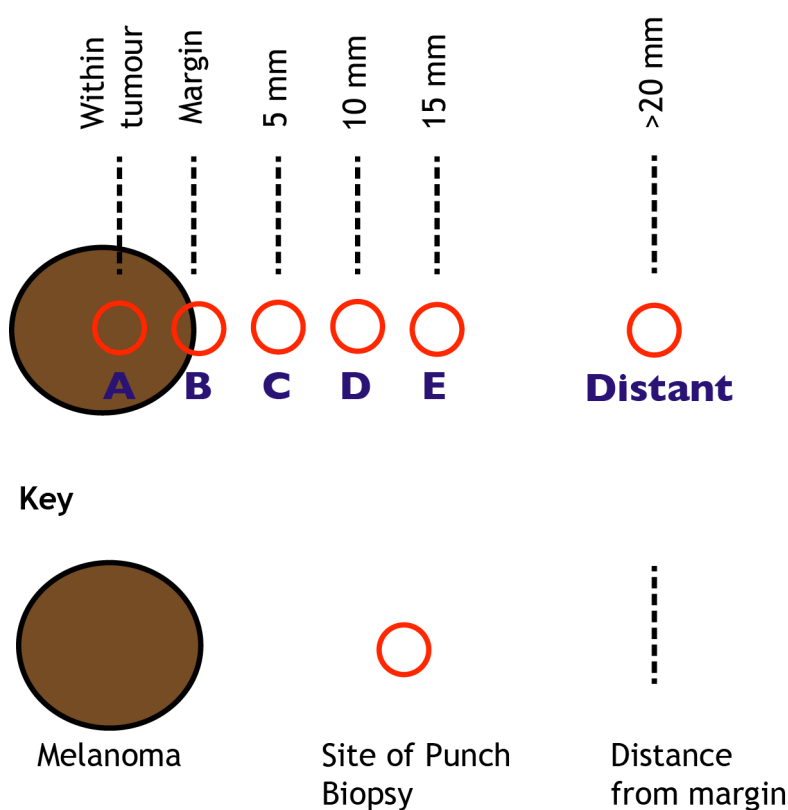


Figure 6-1 Schematic of *in vivo* melanoma sampling methodology.

This schematic represents the locations of the punch biopsies (red ring) for sampling tissue for LPA quantification in relation to the melanoma (brown filled circle). The distance from the tumour margin is marked by a dashed line.

The identification of LPA gradients across murine melanomas

6.1.6 LPA gradients exists across the margins of non-ulcerated murine melanomas

Only mice with non-crusted and non-ulcerated tumours were included in this analysis (Fig. 2A). 6 melanomas were analysed from 3 separate mice. All the melanomas demonstrated a clear outward gradient of total LPA (Fig. 2B). The concentration of LPA was lowest in the tumour, slightly higher at the margin and much higher outside the tumour and this was extremely reproducible and statistically significant.

Analysis was performed after normalising the data to position A for subspecies of LPA relative to the total LPA (Fig. 2C). The signalling LPAs all generated steeper gradients than the non-signalling, saturated LPA subspecies.

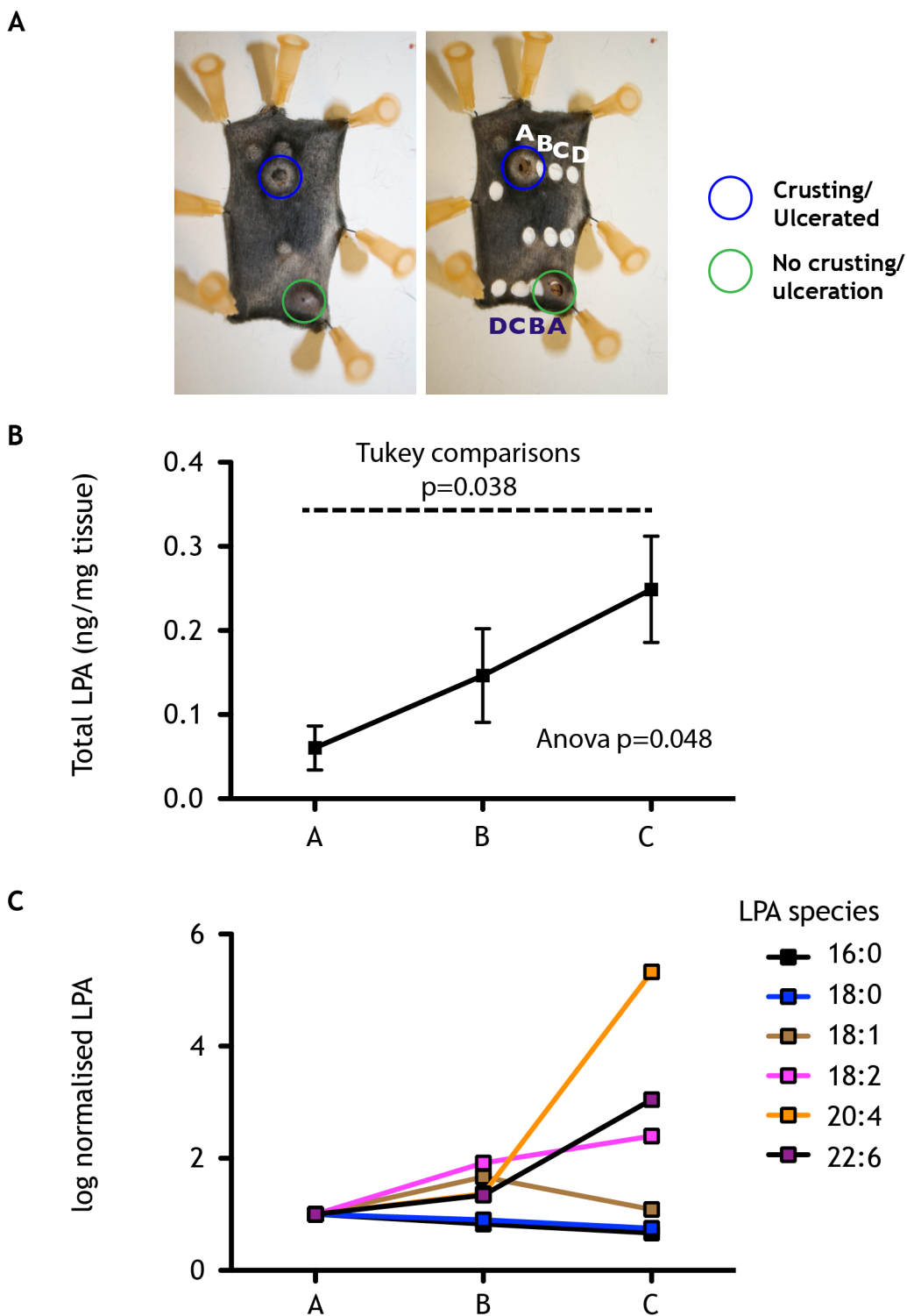


Figure 6-2 Quantification of [LPA] across the margins of non-ulcerated murine melanomas

A Photographs of murine melanomas following dissection of a large area of dorsal skin down to the subcutaneous layer, before and after sampling the tumours with a 6mm punch biopsy tool, within 5 mins of the mouse being sacrificed. The melanomas are generated with the Tyr::CreER^{T2} BRAF^{V600E/+} PTEN^{lox/+} melanoma model. This example highlights the phenotypic difference between normal melanomas and crusting/ ulcerated melanomas (green and blue rings respectively). Crusting/ ulcerated melanomas were excluded from this analysis. The position of the biopsy is noted from A-D **B** Line graph representing the *in vivo* concentration of LPA (mean +/- SEM) across the margins of 6 melanomas in 3 mice. The total LPA (ng/mg tissue) was quantified by mass spectrometry after weighing the snap frozen specimens and extracting the LPA. Statistical comparisons have been performed by anova and tukey comparison of the means **C** log scale plot of (mean +/- SEM) for LPA subspecies and total LPA normalised to the value at position A and plotted across positions B and C.

6.1.7 Inverse LPA gradients exists across the margins of ulcerated murine melanomas

The previous figure showed photographs of a mouse with mixed non-ulcerated and ulcerated tumours. The mouse shown here developed 2 distinct ulcerated melanomas over its back (Fig. 3A). Again, these were sampled in an orientation to control for and reduce the risk of contamination from the microenvironment from the other melanoma.

In total, 3 ulcerated/ crusted melanomas were sampled across 2 mice. In complete contrast to the non-ulcerated melanomas, the gradient of LPA was inverted, from high within the tumour to low outside, which was statistically significant (Fig. 3B). Interestingly, the level of LPA at C was lower still than nearer to the tumour, suggesting that the source of LPA is derived from or within the immediate microenvironment of the tumours.

Interestingly, the data for sub-species of LPA, the trend towards steeper gradients of signalling LPAs was not evident in ulcerated melanomas (Fig. 3C). Although, the most shallow gradient belonged to 18:0, 16:0 produced a steep gradient. LPA quantification for individual murine melanomas is available (appendix 6).

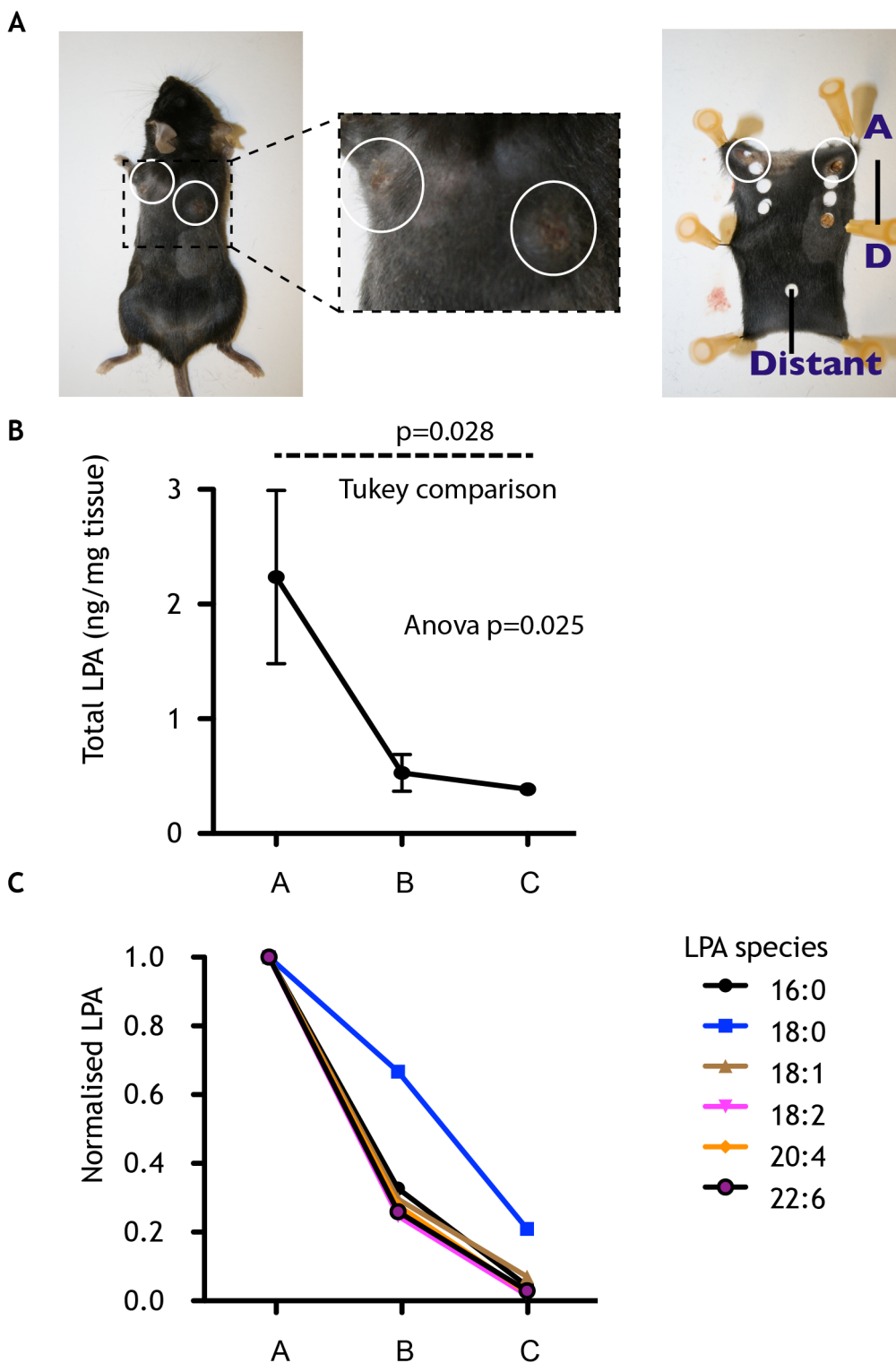


Figure 6-3 Quantification of [LPA] across the margins of ulcerated murine melanomas

A The photographs show an example of 2 ulcerated/ crusted melanomas arising on the dorsal aspect of one mouse. These are seen more clearly with the exploded view. The photograph on the right depicts the dissected skin after the punch biopsy samples were acquired. In addition to the standard samples, a sample was taken at a site distant to both melanomas. **B** Line graph representing the *in vivo* concentration of LPA (mean \pm SEM) across the margins of 3 ulcerated/ crusted melanomas in 2 mice. The total LPA (ng/mg tissue) was quantified by mass spectrometry after weighing the snap frozen specimens and extracting the LPA. **C** Line graph of (mean \pm SEM) for LPA subspecies and total LPA normalised to the value at position A and plotted across positions B and C.

6.1.8 Steady LPA levels exist across normal murine skin

To investigate the concentration of LPA across normal skin, mice with the same genetic background (Tyr::CreER^{T2} BRAF^{V600E/+} PTEN^{lox/+}) were also treated with tamoxifen to activate the alleles. The same sampling technique was used and 3 replicates were taken per mouse (Fig. 4A). In total, normal skin from 2 mice, with 2 replicate series in each was used for LPA quantification.

The result showed no evidence of a gradient and instead revealed a stable and reproducible concentration of LPA across the skin (Fig. 4B). Further analysing the data based on normalised sub-species of LPA, revealed no trend base on signalling LPAs (Fig. 4C). Performing statistical analyses, there was no significant difference between sites A, B or C.

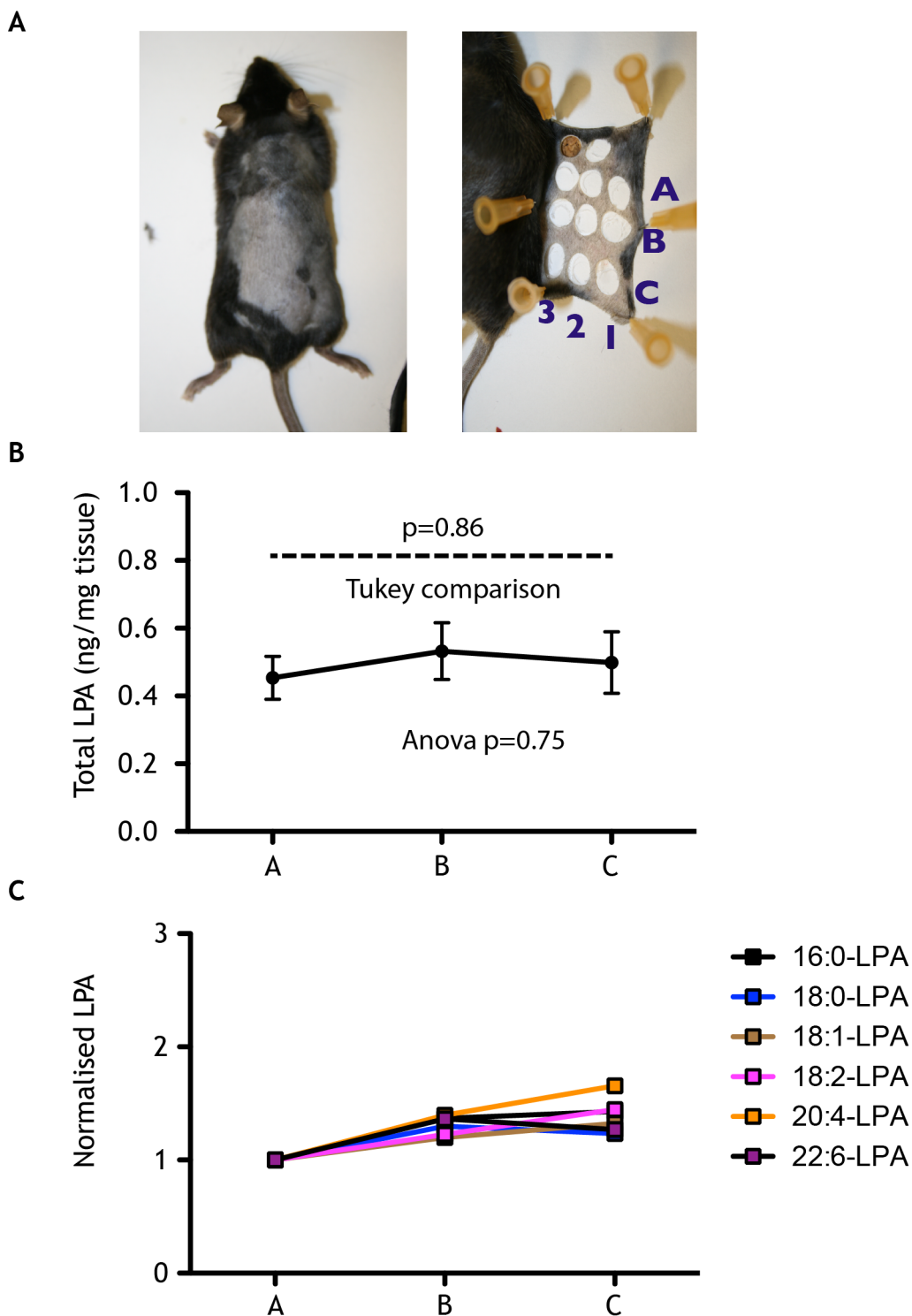


Figure 6-4 Quantification of [LPA] in normal murine skin *in vivo*.

A The photographs show an example of normal skin on the dorsal aspect of one mouse. This skin is sampled from the same Tyr::CreER^{T2} BRAF^{V600E/+} PTEN^{lox/+} melanoma model, which has been activated with tamoxifen, but not yet developed any melanomas at the time of tissue sampling. The photograph on the right depicts the dissected skin after the punch biopsy samples were acquired. Samples A-C (each separated by 5mm) are used for comparison with 3 experimental replicates acquired per mouse. **B** Line graph representing the *in vivo* concentration of LPA (mean +/- SEM) across the positions A-C on a sample of normal skin from 2 mice, with 2 replicate series in each. The total LPA (ng/mg tissue) was quantified by mass spectrometry after weighing the snap frozen specimens and extracting the LPA. **C** Line graph of (mean +/- SEM) for LPA subspecies and total LPA normalised to the value at position A and plotted across positions B and C.

The identification of LPA gradients across a human melanoma

There are concerns about translating the results from murine models to the human disease due to anatomical differences (Becker et al., 2010; Walker and Hayward, 2002). From a pigment cell perspective, mouse melanocytes are distributed in the hair follicles, rather than the hair follicles and the inter-follicular skin along the dermo-epidermal junction as found in humans (Billingham and Silvers, 1971; Buac and Pavan, 2007). Having successfully shown gradients of LPA across the margins of murine melanomas I established ethical approval to collect fresh primary human melanomas for analysis to investigate the presence of an LPA gradient with exactly the same methodology as for murine melanomas.

A suitable subject was identified meeting the minimum criteria for the width of the primary lesion (see Chapter 2: materials and methods). The 81-year-old female patient presented with an ulcerated nodule arising in a long standing naevus and the overall lesion measured 4.5 cm. The central nodule was biopsied confirming the diagnosis of an ulcerated superficial spreading melanoma (SSM) with a Breslow thickness of 22 mm. Following informed consent, the lesion was photographed in situ prior to a 3cm wide-local excision (Fig. 5A). Following excision, the lesion was immediately examined by the attending consultant pathologist and following his approval, samples A-E were taken, along with a sample of the sub-cutaneous tissue within 5 minutes of the excision.

The line graph of the total LPA from each site within this melanoma showed features in keeping with both ulcerated and non-ulcerated melanomas (Fig. 5B). The sample within the tumour (A) was higher than the margin (B) in keeping with an ulcerated melanoma, but then the LPA gradient increased between the margin (B) and 5mm outside (C). This melanoma was sampled further out to provide as much detail as possible and the gradient continues to increase to 10mm (D), before falling at 15mm (E).

Analysing the data by sub-species of LPA following normalisation fails to show any clear bias for signalling over non-signalling LPAs (Fig. 5C).

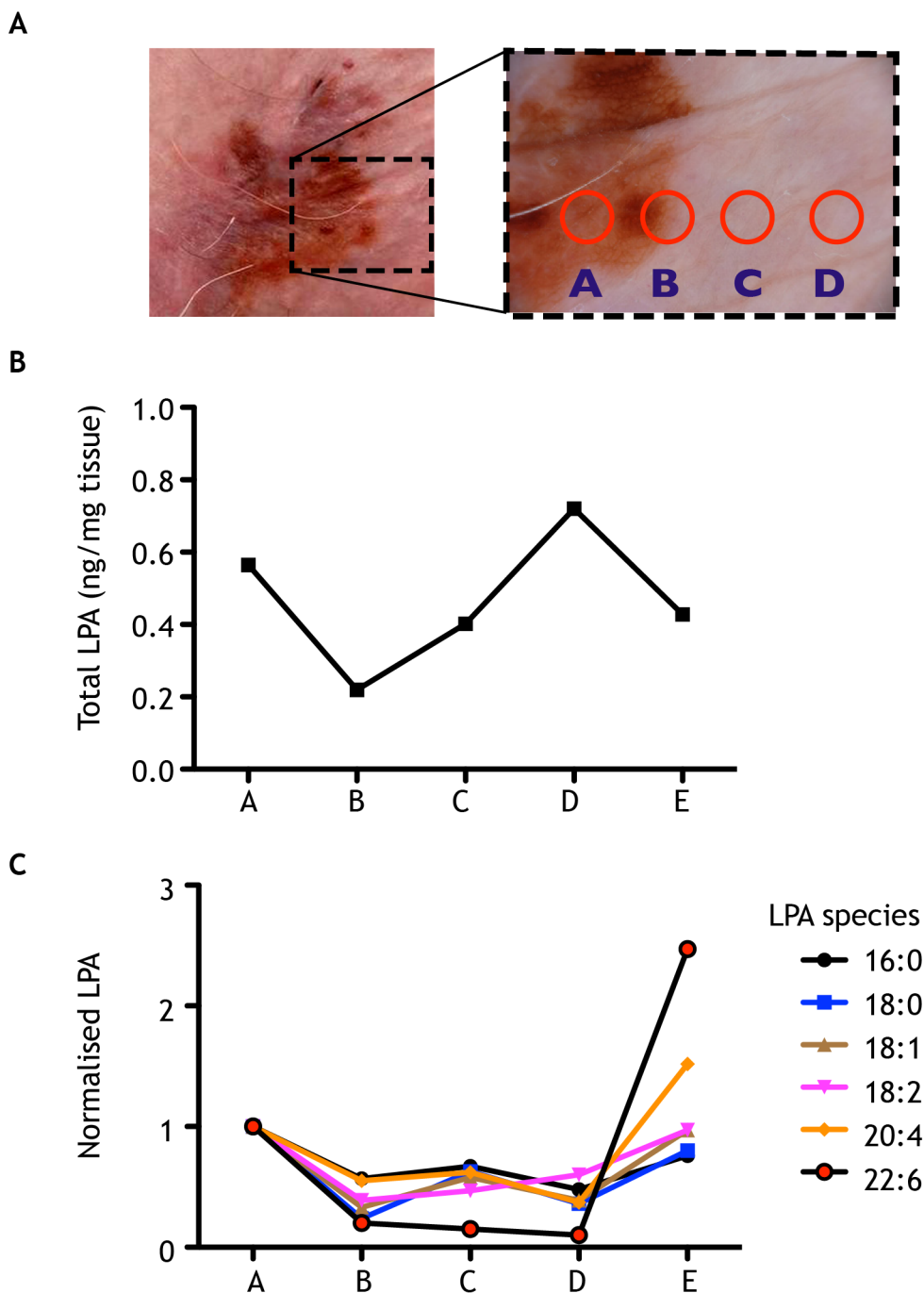


Figure 6-5 Quantification of [LPA] across the margin of a human melanoma.

A Photographs of the human melanoma printed with the consent of the patient. The image on the left demonstrates the overall morphology and the exploded view is a dermatoscopic (10x) image. The latter is marked with 4 of the 5, locations sampled with a 3mm punch biopsy. These included, positions A-E. **B** Line graph representing the *in vivo* concentration of LPA (mean) across the margin of 1 human melanoma. The total LPA (ng/mg tissue) was quantified by mass spectrometry after weighing the snap frozen specimens and extracting the LPA. **C** Line graph of (mean) for LPA subspecies and total LPA normalised to the value at position A and plotted across positions A-E.

Discussion

The introductory chapter highlighted work by the Condeelis lab who pioneered an *in vivo* needle assay to collect tumour cells that migrate into a pipette by

chemotaxis (Wyckoff et al., 2000). This technique has enabled the collection of cells by chemotaxis *in vivo*. These cells can then be isolated and studied in further detail. This has generated data supporting the chemotaxis driven *in vivo* invasion of breast cancer cells towards EGF produced by macrophages (Goswami et al., 2005; Patsialou et al., 2009; Wyckoff et al., 2004). One caveat with these *in vivo* chemotaxis studies is that it is not possible to know whether the soluble factors remain soluble or bind to some degree to the ECM. Their lab therefore defined chemotaxis *in vivo* as directional migration to either soluble or solid state gradients (Roussos et al., 2011).

Studying chemotaxis responses *in vivo* has therefore resulted in important insights into the role of stromal cells in the tumour microenvironment. The functional effects of chemotaxis (or chemokinesis/ haptotaxis) have therefore been demonstrated *in vivo*, but there remains no direct evidence for the EGF gradients proposed. To the best of my knowledge, the work carried out in this chapter is the first evidence to support the existence of any chemoattractant gradient across a tumour *in vivo*, thereby demonstrating the physiological relevance of my findings.

It is clear from the data in this chapter that melanomas influence their immediate microenvironment by shaping LPA gradients in this field. The nature and extent of the LPA gradient is dependent on the presence or absence of ulceration. Without a tumour, the LPA concentration remains steady across normal skin.

One can muse on the results produced for the ulcerated murine and human samples when considering the model for LPA generation. Both show that distant sites have a lower concentration of LPA than proximal sites. This supports the idea that the LPA detected is tumour-centric in origin. Taken a stage further, following a period of inflammation or more specifically increased platelet activation, that may be exacerbated by ulceration, one would hypothesise that a surge of LPA would be released from the tumour (Peyton et al., 1998; Ruiter et al., 2002). Alternatively, there is evidence that platelet activation leads to ulceration and may be an independent marker of elevated LPA (Tao et al., 1995). This LPA could subsequently diffuse in all directions into the tumour micro-environment.

The previous chapter supports the self-generation of an outward gradient. One would hypothesise that following a surge in LPA generated by ulceration, there follows a period of gradient generation by the melanoma cells. This would explain why there was a high concentration of LPA in the tumour and an outward gradient from the margin of the tumour in the human sample (Fig. 5B). I would hypothesise based on my results in chapter 5, that the period of gradient generation would be instructive, acting as a signal to promote outward migration/ invasion, assuming the cells express LPAR 1 and possibly LPAR 3.

The data presented in this chapter and the strength of the results are limited by the relatively low number of melanomas sampled. The main limitation has been the number of mice with the correct genotype that have been bred by my collaborators during the period of study. The technique employed is fairly crude, particularly trying to determine a more complex gradient shape than a simple linear or exponential curve. We would ideally have sampled in a bread slicing fashion both outward and downward from the tumour but this was not technically feasible due to the quantity of material required.

A limitation has been the dependence on a murine melanoma model that more closely resembles human NM than the more commonly occurring SSM subtype. Ideally I would repeat this experiment with a different murine model with SSM pattern, although these are still being developed and there are concerns that these models are less representative of human melanoma from an oncogene perspective. *In vivo* studies with correlative histopathological analysis have suggested that compared to SSM, NM is more vertically invasive with less horizontal growth relative to Breslow thickness and has a tendency to ulcerate (Liu et al., 2006; Segura et al., 2008; Shaikh et al., 2012). This perhaps explains why it is also the most aggressive form in humans. These characteristics have generated the hypothesis that NMs may arise from dermal melanocytes (Longo et al., 2013). However, NMs are the fastest growing sub-category making this a useful model in the available time frame (Zalaudek et al., 2008).

It has proved particularly challenging to access fresh human primary melanomas. This is mainly due to the tough criteria that are understandably set by the pathology team. This is to ensure that the process of sampling the melanomas in no way risks impairing the diagnostic and prognostic information. Unfortunately,

by setting the minimum melanoma diameter to 25mm, it is selecting a group of melanomas that are not only rare, but are almost certainly behaving in a different biological fashion (Kopf et al., 1982). The one sample collected has supported my hypothesis and it will be important to build on this unique discovery.

Ignoring the one human sample, there is a trend towards steeper gradients of biologically active LPA species with outward gradients and no pattern with inverse gradients. I would hypothesise that the former is arising as a result of differential LPA species degradation, with the more biologically active species being degraded faster. The latter is arising as a result of diffusion from the tumour and therefore, one would not hypothesise any differential alterations in gradient with sub-species because the process does not require active enzymatic degradation.

The result from the human melanoma highlights the extent of the microenvironmental zone of tissue that is under the influence of LPA. It is promising that this subject's gradient tailed off within the confines of the wide-local excision and it would be interesting to correlate not only the peak gradient, but the width of the gradient with the risk of metastasis. This then raises the possibility of using LPA gradient detection as a prognostic test and this will be covered in the final chapter.

6.1.9 Conclusion

I have presented data supporting the presence of *in vivo* gradients of LPA across the margins of melanomas, supporting the physiological relevance of my earlier work. I discovered outward gradients of LPA in non-ulcerated murine melanomas, inverse gradients in ulcerated melanomas and no LPA imbalance in normal skin. Combined with my earlier results, I conclude that LPA chemotaxis drives melanoma invasion. However, rather than LPA acting as a direct signal, it is the LPA gradient that drives invasion. Cells from all melanoma stages of disease progression are chemotactic, but the ability to create a gradient is density-dependent. Therefore, the size of the tumour will determine its ability to promote metastasis providing there is an adequate source of LPA.

Chapter 7:

Discussion

A summary of key findings generated by this thesis

7.1.1 The Insall chamber is a robust assay for investigating chemotaxis

We have developed two assays for investigating cancer cell chemotaxis: 1) the “standard assay”, which acts as a model for single cell tumour invasion, and 2) the “centre-well assay”, which acts as a model for collective/ single cell invasion from the tumour periphery. In addition to ongoing work investigating the findings from this thesis, the assay is optimised for detailed higher resolution work, for example, investigating pseudopod dynamics and intracellular signalling with fluorescent probes in mammalian and *Dictyostelium* cells.

7.1.2 LPA chemotaxis is a key driver of melanoma dispersal and invasion across all stages

This thesis conclusively demonstrates the importance of LPA signalling in the chemotactic responses of melanoma cells to serum, demonstrating that LPA is sufficient as well as necessary for highly accurate chemotaxis and invasion. This further supports the paradigm of chemotaxis driven invasion and identifies LPA as a key driver of melanoma invasion. LPA signalling through LPAR 1 has previously been shown to be important in cell motility and invasion (Hama et al., 2004; Shida et al., 2003; Yamada et al., 2004). The data presented in this thesis provide further support for the involvement of this signalling pathway in melanoma invasion. My findings in ulcerated melanomas in particular implicate the inflammatory response in the metastatic process.

7.1.3 Growth factors act as accessory factors enhancing LPA chemotaxis

To the best of my knowledge, this study and one other by Zicha and Dunn are the only two to investigate the role of Growth Factors in long-term direct visualisation assays of cancer cell motility (Zicha and Dunn, 1995). My findings concur with their outcome that Growth Factors are primarily chemokinetic agents, but, I also conclude that combined with LPA, the efficiency of chemotaxis is enhanced. I therefore propose that this combination may potentiate invasion and requires further study.

7.1.4 Melanoma cells perform positive chemotaxis through the self-generation of outward gradients

I conclude that melanoma cells self-direct their invasion through a programme of LPA gradient generation *in vitro* and *in vivo*. The self-generation of chemotactic gradients generates a cell dispersal effect and thus provides a mechanism for the “edge-effect”, or dispersal of cells to the nearest edge, which was first described by Zigmond in her eponymous direct visualisation chamber (Zigmond et al., 2001). This gradient generation behaviour was observed through the direct visualisation of chemotaxis. Using this approach, I demonstrated that the ability of cells to locally degrade LPA and generate a gradient acts as the signal driving melanoma cell migration and invasion. The ability of cells to self-generate gradients and migrate by positive chemotaxis has important implications for melanoma metastasis and the broader cell motility field. This model dictates that provided with a supply of chemoattractant and a high enough cell density to efficiently degrade the attractant, the cells will efficiently disperse. Therefore the source of LPA within the microenvironment and the growth of the tumour are likely to be the rate limiting factors in the dispersal of melanoma cells.

Key questions & future perspectives

Throughout this thesis I have discussed the direct implications of the results at the end of each chapter. This section aims to cohesively expand on these by bringing together many of the concepts highlighted in the summary of key findings. In doing so, I will discuss the implications of this work on the fields of chemotaxis and melanoma biology. The implications of this work in relation to clinical practice are of particular importance and are therefore discussed in detail. Together these raise important questions and I therefore highlight several key experiments that are necessary to answer them and expand on the knowledge and test the hypotheses generated from this thesis. It is envisaged that these will be performed by a combination of researchers with ongoing work by colleagues in the laboratory, and future work by a clinical fellow(s) as well as personal ongoing research.

7.1.5 The role of platelets in LPA generation and metastasis

7.1.5.1 Are platelets the primary source of LPA and does its presence correlate with the risk of metastasis?

The source of LPA *in vivo* is not known. In many cancer sub-types, including melanoma, the increased expression of Autotaxin has been associated with tumour progression (Saunders et al., 2008). As discussed in the introductory chapter, LPA is produced via the autocrine action of Autotaxin on Lysophosphatidylcholine (LPC). The LPA produced from Autotaxin would therefore be tumour centric, which after diffusion would create inward-facing gradients (ie. a gradient highest in the tumour and lowest outside the tumour). Rather than promoting tumour dispersal, my data suggest this would drive inward chemotaxis, tending to prevent the escape of tumour cells. Contrary to this, I found that there was a net loss of LPA in conditioned media experiments, despite the relative abundance of the substrate LPC in serum once the cell density reaches a critical point. My work is consistent with the initial tumour-centric production of LPA following ulceration, but suggests that this LPA is subsequently modified after its diffusion through the microenvironment to generate outward-facing gradients (ie. a gradient lowest in the tumour and highest outside the tumour). The effect of this outward-facing gradient is to drive cell dispersal by positive chemotaxis.

Current evidence supports two main pathways for LPA production as reviewed in detail in the introduction. The concentration of LPA in the immediate environment is dependent on the homeostatic cellular mechanisms controlling extra-cellular LPA concentrations, with Autotaxin producing a net gain and the Lipid phosphate phosphatases (LPPs) producing a net loss of LPA (Brindley and Pilquill, 2009), My data clearly show an outward gradient of LPA and therefore suggest that there is a relative reduction in Autotaxin activity compared to that of the LPPs. If Autotaxin activity is low, I hypothesise that LPA is instead being generated via the alternative pathway from platelets. Phosphatidic acid (PA) is hydrolysed by sPLA₂ to produce LPA and both the substrate and the enzyme are secreted from platelets in membrane microvesicles following platelet activation (Eichholtz et al., 1993; Fourcade et al., 1995). This process is reinforced by positive feedback, with LPA inducing further platelet aggregation and activation, thereby generating an LPA rich microenvironment. Current *in vivo* evidence

suggests that there is slowing of platelets in the tumour microcirculation. Although thrombus formation is not evident, modelling supports slow enough flow to allow for localised release of platelet vesicles (Manegold et al., 2003).

The association between platelets and cancer was initially cited by Trousseau who observed the increased risk of venous thrombosis in cancer (Rak et al., 2006). Platelet activation is amplified in cancer and thrombocytosis is one amongst several aberrantly activated markers representing the hypercoagulable state (Gay LL, 2011). There is limited evidence that the activation of the coagulation and fibrinolytic system potentiates invasiveness and metastasis (Gabazza et al., 1993). In the setting of melanoma, patients with normal fibrinogen levels had a significant 1-year survival benefit over patients with elevated levels (87.7% v 58.4% (p=0.031) respectively; Tas et al., 2012). This group did not normalise their data based on Breslow thickness. I hypothesise that patients demonstrating elevated markers of platelet activation are at increased risk of metastasis due to increased LPA release at the tumour site. P-selectin (CD62p) is present in the α -granules of platelets and is translocated to the cell surface upon platelet activation. It is therefore a useful marker for platelet-activation and has been shown to correlate with metastasis in mouse models (Coupland et al., 2012). To the best of my knowledge, no one has yet identified the melanoma patients that are at increased risk of metastasis based on identifying markers of platelets or platelet activation in melanoma tissue or blood samples.

To test the hypothesis that platelets are the primary source of LPA *in vivo* and that this correlates with the risk of metastasis, I therefore propose the following.

- Identify markers of platelets and platelet activation within human melanomas (CD42b (Clemetson et al., 1982), CD62p (Kamath, 2001)) and blood (fibrinogen and CD62p) and correlate the findings with histological markers (Breslow thickness, mitotic rate and ulceration) and LPA concentration.
- After seeking appropriate ethical approval, this would first be piloted in human melanoma using formalin fixed paraffin embedded tissue from the

NHS pathology archive and correlated with clinical outcome data if possible to correlate these retrospective findings with metastasis. The Scottish Melanoma Group holds records of individual patient follow-up in a database that would aid this study.

7.1.5.2 Can platelet derived LPA support different stages of metastasis?

I have reviewed the classification systems for melanoma and the current move towards an improved system combining genetic and morphological information (Viros et al., 2008). These systems do not, however, include factors associated with the microenvironment that are known to influence the behaviour of cancer cells. I believe that the work included in this thesis is some of the most persuasive data to-date supporting a role for a microenvironmental factor influencing the risk of melanoma metastasis through enhanced invasion. In order to develop a reliable prognostic marker for melanoma, it will be important to identify surrogate markers for melanomas with outward gradients due to the difficulty and cost associated with quantifying LPA gradients by mass spectrometry.

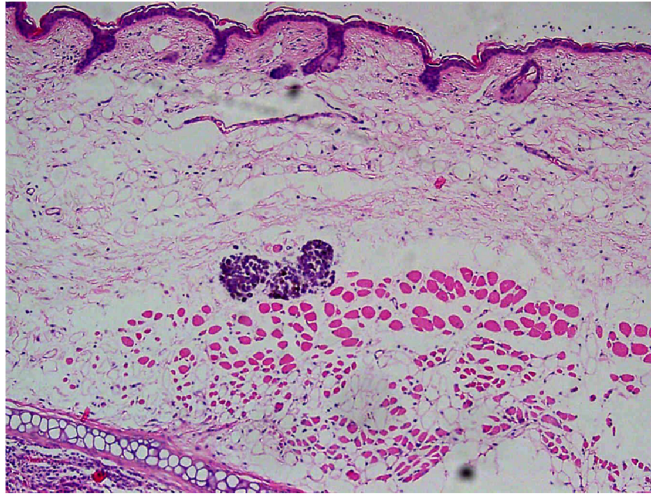
There is growing evidence to support platelets contributing to the metastatic process at later stages of the metastatic process following intravasation (Gay LL, 2011). The mechanisms aiding haematogenous metastasis are varied and include immune evasion through antigenic cloaking, to the formation of tumour-platelet heteroaggregates acting as tumour survival rafts that can mechanically lodge in distant organs. Boucharaba et al demonstrated the effects of LPA on inducing the formation of bony metastases in mice injected with metastatic breast cancer cells. This effect was shown to be mediated through LPAR 1 (Boucharaba et al., 2006). Two interesting results from an earlier paper showed that breast cancer cells did not produce LPA keeping with my results (Boucharaba et al., 2004). However, the cancer cells stimulated platelet activation and LPA release and inhibiting platelets *in vivo* with the specific integrin $\alpha\text{IIb}\beta\text{3}$ antagonist (Integrilin) produced a 70% fall in the concentration of circulating LPA and a 50% reduction in the extent of bony metastases. These results support an endogenous source of local production of LPA (Guise, 2005).

More recently, David et al reported increased osteoclast density at the site of metastasis (David et al., 2010). It is notable that osteoclasts, responsible for bone resorption and the generation of osteolytic lesions are highly motile and express LPAR 1 (Chellaiah et al., 2000; Lapierre et al., 2010). It is tempting to hypothesise that osteoclasts use the gradient generated by the platelets (platelet-tumour heteroaggregate) to aid their migration to the site of metastasis, rather than LPA acting purely as a purely mitogenic agent at this site.

My results therefore imply an additional mechanism by which platelets actively promote metastasis by driving invasion from the primary towards the bloodstream. To test the hypothesis that platelet derived LPA supports metastasis *in vivo*, I propose the following:

- First, we will establish an orthotopic murine melanoma metastasis model to better recapitulate the invasive stage based on previous attempts to produce orthotopic melanoma models (Bobek et al., 2011; Rofstad, 1994; Rozenberg et al., 2010). The main complicating factor is that the primary often outgrows the metastases, necessitating the sacrifice of the model before macrometastases have appeared. The development of a model allowing the resection of the primary is therefore essential. Here, I have demonstrated pilot experiments to generate this model using subcutaneous ear injections of melanoma cells into nude mice (Fig. 1). In the future, I also propose intradermal back injections of human melanoma cells into nude mice.
- Having established an orthotopic melanoma metastasis model, we will compare the metastatic load of vehicle vs. platelet antagonist (eg. Integrilin) treated mice. We will quantify platelet activation and the LPA concentration across the primary tumours as previously described.

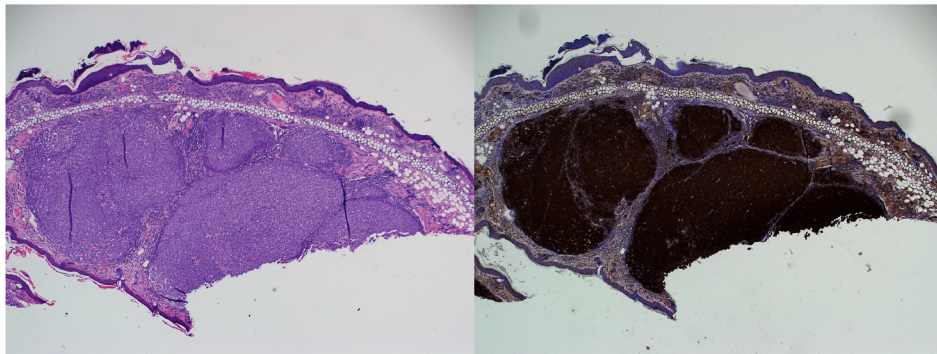
A



B



C



10x H&E Right Ear

10x S100 Right Ear

Figure 7-1 Development of an orthotopic mouse metastasis model

A H&E slide demonstrating the localisation of the xenografted cells (1×10^6 cells in $10 \mu\text{L}$ RPMI) in the dermal/ subcutaneous space above the cartilage in the distal ear of a nude mouse. B Photograph of the mouse showing the subsequent development of a loco-regional metastasis at the base of the ear distal to the site of inoculation. C H&E and S100 stains of the locoregional metastasis confirming the tumour is a melanoma.

7.1.5.3 Is there evidence for platelet treatments reducing the risk of metastasis in humans?

There are several reports of platelet targeting treatment reducing the risk of metastasis (Bambace and Holmes, 2011). It is clear that targeting platelet activation reduces the risk of metastasis in some clinical models described in this review, but there is currently no evidence to support the reduction in metastasis occurring due to a reduction in invasion.

Prospective studies investigating the clinical outcomes for patients with cancer who have been treated with platelet inhibitors found either no effect, or in some cases, improvement in survival (Bambace and Holmes, 2011). For melanoma specifically, there are retrospective studies again showing similar outcomes (Asgari et al., 2008; Curiel-Lewandrowski et al., 2011; Harris RE, 2001; Johannesdottir et al., 2012; Joosse et al., 2009). Last year, two meta-analyses were published with the finding that aspirin has a beneficial effect on reducing the incidence and death from cancer, in addition to the beneficial effects on vascular disease (Algra and Rothwell, 2012; Rothwell et al., 2012). It is also interesting to note in these papers, that the reduction in metastasis is not found in patients receiving the anticoagulant warfarin, which does not affect platelet aggregation.

Targeting platelets in melanoma as a chemo-preventative strategy is therefore a subject that requires further study. Initial laboratory work is required to investigate the role of anti-platelet therapies at differing doses in their ability to reduce LPA production. These data could then be used to inform a melanoma chemoprevention trial.

7.1.5.4 Is there evidence to support Growth Factors acting as accessory agents *in vivo*?

Given the enhancing effect of Growth Factors on chemotaxis in the presence of LPA, one can hypothesise that cells succeeding in intravasating are more likely to have achieved this through integration of GF and LPA signalling. Well established sources of Growth Factors include host cells. The breast cancer cell loop described earlier, is driven through paracrine signalling, with EGF produced

via macrophages. Conversely, fibroblasts may potentially play a role in generating LPA in the presence of EGF through paracrine signalling.

Further support for the importance of platelets in the metastatic process is the finding that a multitude of bioactive factors in addition to LPA are released following platelet activation. These include PDGF and EGF, the Growth Factors that I have shown to be important chemotaxis accessory factors to LPA (David et al., 2010; Sierko and Wojtukiewicz, 2004).

7.1.6 The LPA-axis as a potential prognostic and or therapeutic target for metastasis

7.1.6.1 Are LPA gradients clinically significant?

I have shown that both murine and human melanomas create outward-facing LPA gradients. One could hypothesise that LPA gradients are only present in melanomas that are actively invasive and therefore the demonstration of a gradient could present a novel adverse prognostic marker. There are therefore two key questions that need to be answered. First, does the presence of a gradient predict the risk of invasion and ultimately metastasis? Second, can a more detailed analysis of the gradient profile (ie. steepness or distance over which a gradient is present) predict a highly invasive group? To answer these questions, we would need to collect samples from primary melanomas. Due to the ethical constraints regarding melanoma tissue collection, it might be wise to simplify the tissue collection regimen and sample one, or if possible, two punch biopsy samples lateral to the primary melanoma for LPA quantification. This would provide tissue for analysis without disturbing the primary melanoma. If deemed ethically sound, this approach would theoretically allow melanomas of all diameters to be sampled, which would enable a more clinically representative cohort to be assessed than has been possible during this study. A further sample taken >5cm from the primary could be used as a standard. These could be compared to samples taken proximal to benign and dysplastic naevi.

We are continuing to investigate whether there is degradation of LPA in samples stored on ice for one hour compared to samples that are snap frozen. Processing samples on ice would considerably increase the potential yield of melanomas

that could be sampled by enabling them to be conveniently processed by the consultant pathologist in the laboratory.

To investigate the clinical significance of LPA gradients, I therefore propose the following:

- To establish a prospective human study collecting fresh melanoma to calculate LPA gradients and blood samples for evidence of platelet activation and following their progress over 5 years to record the presence of loco-regional or distant metastases. The results could be normalised to current histopathological staging criteria, and Breslow thickness in particular, and an assessment could be made of whether LPA gradients act as an independent prognostic marker. During this study we would seek to obtain formalin fixed paraffin embedded tissue to identify other markers from the LPA-axis, which will be discussed next.

7.1.6.2 LPARs and LPPs as potential melanoma prognostic markers

In addition to identifying markers for the source of LPA, it would be important to investigate the known key regulators of external LPA concentrations in the microenvironment and the receptors involved in LPA signal transduction, ie. LPPs and LPARs and correlate their expression profile with metastasis and Breslow thickness.

LPARs

As summarised earlier in this chapter, my work has demonstrated the importance of LPAR 1 in the motility and chemotaxis of melanoma cells, in keeping with published data. There is data to suggest that the outcome of cell migration is dictated by the relative expression levels of individual receptors (Jongsma et al., 2011). Interestingly, Jongsma et al demonstrated that LPAR 5 expression can mediate chemorepulsion in B16 melanoma cells, which express relatively less LPAR 1. Although the mechanism behind this remains to be determined, the present findings warrant further studies on the expression patterns and clinical outcome of the LPARs in melanoma and other cancers and

the B16 cells may act as a useful negative control for LPAR 1 expression and chemotaxis towards LPA.

LPPs

Current thinking suggests that metastasis should be favoured by decreased LPP expression (and increased Autotaxin expression), which has been hypothesised to result in an increased extracellular LPA concentration (Moolenaar et al., 2004; Samadi et al., 2011). My data however support the opposite, with increased expression of LPP acting as a driver of metastasis. As discussed, there is growing evidence that the metastatic spread of melanoma is driven not by a linear increase in tumorigenic aggressiveness, but rather by switching back and forth between two different phenotypes of metastatic potential ie. strong proliferation/weak invasiveness and weak proliferation/strong invasiveness (Widmer et al., 2012). Using the gene expression-based tool generated by the Hoek group for predicting phenotype (the Heuristic Online Phenotype Prediction tool) there are statistically significant 1.8 fold and 1.9 fold increases in the expression of LPP1 (PPAP2A) and LPP3 (PPAP2B) respectively, in invasive compared to proliferative melanomas. These very recent data are therefore supportive of the model I have generated.

It is not known which of the LPPs are more important, although it may be the signature pattern of several LPP enzymes that is critical in determining the response. My data suggests that the most biologically active LPA sub-species are preferentially degraded and I would therefore seek to identify the LPPs responsible for producing this profile. I would also seek to confirm the finding that LPP activity is upregulated in advanced melanoma.

In order to investigate the expression profiles of LPARs and LPPs expression profiles, I propose:

- To perform a screen using RT-PCR across the cell lines used throughout this thesis across the various biological stages of melanoma development and also to include an assessment in melanocytes. Based on my data, I hypothesise that the WM278 cell line (demonstrating the weakest chemotaxis), may poorly express LPAR 1 or perhaps express a profile with

increased LPAR 5. Conversely, WM239A would serve as a positive control and we expect the expression signature to favour LPAR 1 and 3.

- If this is successful in identifying expression profiles consistent with chemotactic ability I would plan to investigate this further using patient samples. In the first instance I would propose to refine the technique using archival patient samples described already, before collecting tissue in a prospective manner as part of the tissue collection project described above.

7.1.6.3 Targeting the LPA-axis to inhibit invasion

Targeting cell motility to inhibit tumour cell invasion remains controversial due to the potential toxicity associated with this strategy, especially on normal cellular turnover throughout the gastrointestinal tract and skin (Wells, 2000).

The LPA inhibitor Ki16425 would be unlikely to be tolerated for any length of time as a cancer treatment because LPA homeostasis is essential for health. Its use could therefore result in a failure of homeostatic mechanisms, resulting in serious and unwanted side-effects. It will therefore be important to develop a deeper understanding of the role of the LPA-axis in metastatic progression to identify alternative strategies to blocking this pathway in melanoma progression without the unwanted side-effects.

Having screened cell lines and patient samples, I hope to discover an LPP signature consistent with LPA gradient generation and therefore invasion. By comparing this signature with those expressed by melanocytes, it may be possible to identify an LPP signature that is sufficiently different to those necessary for physiological processes. This will not only enhance the understanding of the process of gradient generation but it may identify novel elements of the LPA-axis that could enable the safer and less toxic targeting of the LPA-axis to prevention melanoma invasion.

The *in vitro* models we have used throughout this work have been optimised to produce chemotactic responses. A key finding using these models was the increased speed of the metastatic cells. It remains uncertain whether the

increased speed of migration is clinically relevant, or whether the most invasive strains will metastasise earlier, and thus be the first to be identified and may therefore represent an artefact of selection. My data suggest that even less invasive cells can generate LPA gradients, and move rapidly and accurately enough to metastasise. In order to investigate this further it will be important to integrate chemotaxis into an even more complex model that includes factors that are known to retard cell migration.

To more accurately investigate chemotaxis and the role of the LPA-axis in health and disease to identify meaningful targets, I propose the following:

- Combine keratinocytes in the 3-dimensional organotypic model to investigate whether chemotaxis overrides keratinocyte-dependence, particularly in early stage melanoma cells.
- Assess the ability of all melanocyte lineage cells, including melanoblasts and melanocytes to generate gradients and quantify the LPA concentration in or across the migrating melanoblast front in embryo skin and across naevi.
- Using siRNA, we will attempt to knockdown relevant LPARs and LPPs to quantify the effect on cell motility, chemotaxis and gradient generation, with the aim of identifying novel LPA-axis targets.
- More generally, it will be essential to assess whether these findings are relevant to other cancers.

7.1.7 A biological explanation for the adverse prognosis associated with melanoma ulceration

7.1.7.1 Do ulcerative melanomas behave more aggressively due to increased LPA production?

The biological significance of melanoma ulceration is almost completely unknown, despite its ability to act as an independent prognostic indicator by enhancing metastasis (Spatz et al., 2010). The wound paradigm in cancer research is based on the hypothesis that cancer is an aberrancy of the

physiologic processes of wound healing (Riss et al., 2006). Within hours of wounding, a fibrin-rich clot is formed containing activated platelets (Schneider IC, 2006). A multitude of biological mediators and growth factors are formed and stored in human platelets, which are released in response to an injury at the wounded site (Sauer et al., 2004). There is good evidence to support LPA in particular being released into acute wounds from serum and platelets to aid wound healing (Eichholtz et al., 1993; Mazereeuw-Hautier et al., 2005; Xu et al., 2007).

I hypothesise that a tumour with an overlying ulcer will induce an exaggerated wounding response, with increased platelet activation. In support of this, my results from sampling LPA concentrations across ulcerated melanomas indicate inward-facing gradients. All these tumours were sampled the same day the ulceration was discovered in keeping with the terms of the project license. I hypothesise that there is enhanced LPA release in a tumour centric-manner following the onset of ulceration. Over time, I would expect the tumour cells to self-generate steeper outward gradients over a longer distance compared to non-ulcerated tumours, thereby potentiating invasion.

Investigating this is challenging, because based on current UK Home Office guidance, mice must be sacrificed immediately after ulceration is discovered and therefore it is not possible to monitor the gradient evolving over time. I therefore propose the following:

- We would seek approval to wound melanomas across a cohort of mice and sample the LPA gradients over time across the cohort.
- In another identical cohort we would compare metastasis from wounded vs. non-wounded tumours. We would simultaneously quantify the LPA gradient and quantify invasion and metastasis. To confirm that the process was dependent on LPA we would perform parallel experiments +/- Ki16425.

7.1.8 Implications for diagnosis & treatment

7.1.8.1 Is tumour volume a more important prognostic indicator than Breslow thickness?

My results support the requirement of a critical tumour mass with sufficient density to generate a gradient sufficient to drive invasion. In Breslow's seminal paper, he identified maximal tumour thickness and maximal surface area as the key determinants of outcome but found maximal depth to be the most important determinant (Breslow, 1970). However, Breslow only investigated the melanomas of 98 patients and as discussed, there are more recent papers suggesting that tumour volume is more important than Breslow thickness. Given my findings, it is important to revisit his premise and design a study to accurately assess the effect of tumour volume on recurrent or metastatic disease and survival.

7.1.8.2 Could incisional biopsies promote metastasis?

Assuming the main source of LPA is derived from platelets, I hypothesise that incisional biopsies into primary melanomas may enhance the risk of metastasis by inducing further platelet activation. This is supported with the finding of increased circulating tumour cells (CTCs) shed into the blood 3-4 weeks post-operatively after complete excision (De Giorgi et al., 2010). It is not known whether these cells are clinically significant as this study found no correlation between number of CTCs and staging criteria. However, shortcomings of this study include a cohort that was possibly not large enough to show statistical significance and the follow up was only 17 months despite the fact that the majority of metastases arise over a three-year window following diagnosis (Dicker et al., 1999).

Further longitudinal studies on larger series of patients are required and in addition to CTC collection, this could be correlated with a quantitative measure of LPA with a biopsy lateral to the primary melanoma, in addition to markers of platelet activation. I would propose a similar technique to De Giorgi by detecting CTCs by performing RT-PCR for tyrosinase mRNA from samples collected in the prospective study I have described.

7.1.8.3 Could LPA gradients define the size of the WLE required?

For melanomas that have invaded less than 1mm Breslow thickness, current UK guidelines advise taking a 1cm margin and for melanomas that have invaded more than 1mm then at least a 1-3cm margin is required (Marsden et al., 2010). Assuming that an LPA gradient drives lateral invasion/ dispersal, this suggests that the effect of an LPA gradient may involve tissue up to 3cm from the primary lesion in deep melanomas. Therefore a greater understanding about the extent of the LPA gradient could potentially establish the optimal excision margin and allow tailoring of the wide local excision would reduce risk of recurrence. I propose to define the extent of the LPA gradient surrounding tumours as part of the experiments already described.

7.1.9 Self-generated gradients: a universal model for cell dispersal in morphogenesis and disease?

7.1.9.1 Evidence for self-generated gradients from other model systems.

Our data supports the migration of melanoma cells in a wave-like formation towards LPA. This is very reminiscent of the migration of dermal fibroblasts, which migrate as a population over days into a fibrin-rich clot following wounding (Schneider IC, 2006). Schneider and Haugh found that fibroblasts require a narrow range of absolute chemoattractant concentration to migrate. This necessitates a novel mechanism to enable them to migrate over distances many orders of magnitude greater than their cellular dimensions and they do this by eroding the gradient of PDGF. This erosion by a high density of fibroblast cells constantly maintains the PDGF gradient in the optimal range around the K_d of the receptor, ensuring that the front of the cells will advance “at a constant linear rate within the wound, settling into the gradient sensing sweet spot” (Schneider IC, 2006).

Researchers in the motility field are struggling to understand how attractive signals can be integrated by a migratory group (Theveneau et al., 2010). I believe that the wave formation that we have observed implies an important model. At the leading edge of the wave, it is likely that the melanoma cells propagate through a similar mechanism to fibroblasts through a coupling between gradient generation and chemoattractant sensing. It is therefore

tempting to hypothesise that dermal fibroblasts are also entering a wound in wave formation.

I hypothesise that the wave phenomena arises by the following mechanism. Cells upstream of the wave move randomly due to there being no chemotactic gradient and all their receptors being saturated until they are seemingly swept along by the wave. This is likely to occur because the cells are dense enough in the wave to self-generate a chemotactic gradient and the cells are able to sense a difference in receptor occupancy and therefore perform positive chemotaxis. However, the cells at the rear of the wave fall behind and become stationary because the chemoattractant has been degraded to the point of there being essentially uniform loss of the attractant. If this mechanism of wave-like chemotaxis is a key biological mechanism for the migration of populations of cells then it is important to seek examples across different species and organisms. It is therefore even more convincing that we observed the exact same behaviour in *Dictyostelium* cells migrating in the presence of a uniform gradient of chemoattractant (data generated by Prof. D Knecht).

Rather than the linear motility response observed by dermal fibroblasts, it may be that melanoma cells are able to respond across a wider concentration range with LPPs acting to degrade LPA in proportion to its physiological concentration (Brindley and Pilquill, 2009). Moolenaar predicted that LPP activity would serve to prevent receptor downregulation and concluded that future studies should substantiate the relative importance of ligand degradation versus receptor desensitisation in controlling LPA signal duration and strength (Moolenaar et al., 2004). I concur and reflecting on the model of tumour cell dispersal I have generated and the wave formation I have observed, I conclude that the chemoattractant message resides in the gradient, which drives cell dispersal, rather than the absolute concentration of LPA predicted by the Autotaxin and other traditional chemoattractant models.

7.1.9.2 Can melanoblast spreading and patterning be explained by the same mechanism?

As discussed in the previous section, cells intermittently fall off the back of the wave and this was consistently observed in videos of melanoma and

Dictyostelium cells migrating in wave formation from an area of high density in uniform chemoattractant conditions. After the wave has spread across the bridge, these residual cells remain immotile and evenly dispersed. This mechanism of spreading and the resulting patterning has to the best of my knowledge not been described previously and therefore presents a fascinating starting point from where to examine whether this model can explain the even patterning of melanocytes found after the melanoblasts have completed their dorso-lateral migration.

We know that SCF has an important role in determining when melanoblasts migrate into the epidermis, along with spatio-temporal expression patterns of cadherins, but little is known about signals that control directionality. Based on the response I have seen from melanoma cells to LPA, I hypothesise that either this or another factor(s) acting through the same G-protein subunits may therefore be responsible. Data to support a role for LPA has been generated by Ohuchi et al who described the spatial and temporal expression patterns of different LPAR genes during embryogenesis (Ohuchi et al., 2008). They found that LPAR 1 is expressed where migratory neural crest cells would be expected to reside around E8.5 at exactly the time when they commence dorso-lateral migration. LPAR 1 expression therefore has the correct spatial and temporal credentials. One might therefore expect a pigimentary phenotype in the LPAR 1 deficient mouse, but this has not been described. The lack of pigimentary phenotype in the LPAR 1 deficient mouse may well occur as a result of functional redundancy due to perhaps compensation by LPAR 3 signalling (Contos et al., 2000; Mills and Moolenaar, 2003). It is also possible that the system is extremely robust with many more cells commencing dorso-lateral migration than are actually required to evenly cover the embryo.

The most convincing data supporting a role for LPA in the *in vivo* migration of cells is derived from LPP knockout models in *Drosophila*, which show impaired germ cell migration. LPPs belong to a large phosphatase family that includes Wunen proteins in *Drosophila* (Samadi et al., 2011). *Drosophila* expresses two Wunen proteins, *wun* and *wun2*, that are homologous to LPP 3. In germ cells they act redundantly as repellent factors that disperse migrating germ cells in *Drosophila* embryos to the gonads (Renault et al., 2010). The repellent effect is hypothesised to result from the spatially restricted degradation of an unknown

lipid factor that guides the germ cells and acts as a survival factor (Brindley and Pilquill, 2009).

In mice, disruption of the gene encoding LPP 3 caused a very severe phenotype [Escalante-Alcalde et al., 2003]. These LPP 3 deficient mouse embryos failed to form a chorio-allantoic placenta and yolk sac vasculature. However, as with the LPAR knock-out mice, no pigmentary defect was seen, but as with the *Drosophila* models this may be due to functional redundancy.

I therefore hypothesise that LPA plays an important role in guiding melanoblast dispersal and patterning. To investigate this further I propose the following:

- To investigate the role of LPA signalling in melanoblast dispersal *in vivo* using an explant assay +/- Ki16425. If this fails, then we would explore treating the mother with Ki16425 at different times during dorso-lateral melanoblast migration from E8.5 and 10.5.

7.1.9.3 What is the mechanism behind the preferential degradation of biologically active LPA subspecies?

Leading researchers in the field of lipid metabolism have highlighted that further work is needed to establish how the individual LPPs differentially control the metabolism of exogenous and endogenous lipid phosphates and thereby elicit their different functions in regulating cell signalling (Brindley and Pilquill, 2009). A correlation between increasing disease activity and increasing LPA polyunsaturation was identified from LPA species detected in bronchoalveolar lavage fluids after induction of allergic airway inflammation (Georas et al., 2007). The authors concluded that LPPs generated this profile but further research was required to investigate the significance. This raises the question of whether strongly serum responsive melanoma cells are capable of degrading the most biologically active LPA species more efficiently than weakly responsive cells. It will therefore be important to confirm the LPP and LPAR expression profiles of the different cells and identify whether there is a signature associated with enhanced degradation of the most biologically active LPA species that may point towards specific LPPs associated with melanoma invasion.

Model for melanoma invasion

To summarise the key findings in this thesis, I have generated an enhanced model of melanoma invasion based on the schematic of the biological stages of melanoma development in chapter 1. This model assumes that LPA is derived from platelets and is released at a saturating concentration around the melanoma. (Fig. 2)

This model will require ongoing refinement to incorporate the effect of other host cells in shaping the LPA rich field.

Summary

The aim of this project was to investigate the role of chemotaxis in melanoma cell invasion. I have shown that chemotaxis has a central, if not essential, role in the invasion of melanoma cells and LPA has been identified as a key driver of this response. The challenges and complexities of cancer research have meant that the final aim of identifying a novel prognostic and therapeutic marker remains at the hypothesis stage. However, given the novelty and apparent importance of the data I have generated, it will be essential to interrogate the role of the LPA-axis in this process. Similarly, I hypothesise that this model can be applied to melanoblast dispersal during embryogenesis and therefore the role of the LPA-axis in this context requires rigorous investigation. The implication that the inflammatory response and, in particular, platelet activation plays an essential role in melanoma progression is an area that requires particular attention.

This thesis has generated results that challenge current concepts about how populations of cells migrate, highlighting their ability to perform chemotaxis to self-generated gradients. Detailed work will therefore be required to validate the hypotheses generated through this work in respect to not only pigment cells, but also to other cell types more generally. Finally, it would appear essential to investigate whether these findings are translatable across other cancer types.

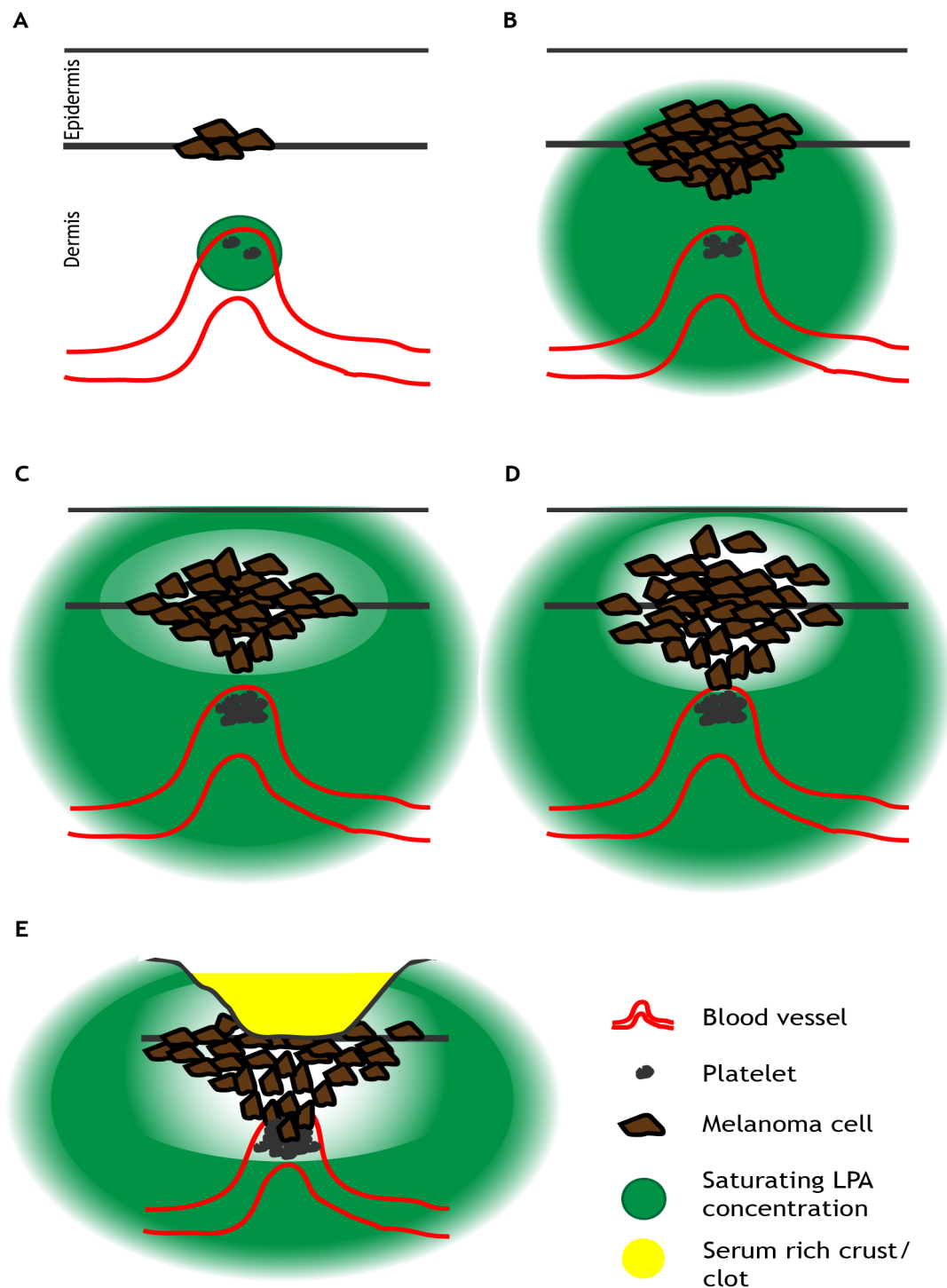


Figure 7-2 Model for LPA driven melanoma invasion

This schematic represents the different stages of melanoma progression. It should be stressed that the source of LPA and the effect of ulceration remain speculative at this stage. **A** An early melanoma initiates an inflammatory response with platelet activation and subsequent LPA release. **B** The melanoma continues to proliferate with increasing platelet activation and greater LPA release, saturating all the melanoma cell LPA receptors. **C** The melanoma reaches a critical density whereby it is able to degrade the local LPA. These self-generated gradients thereby drive outward dispersal and as the cells remain keratinocyte dependent the tumour spreads radially migrate (RGP melanoma). **D** The melanoma undergoes further mutations rendering it keratinocyte independent and the cells are now able to continue degrading the local LPA and spread or invade vertically (VGP melanoma). **E** If the melanoma ulcerates LPA rich serum is released into the wound following enhanced platelet activation and this surge of LPA diffuses from the tumour to extend further than prior to ulceration. It is subsequently degraded by the cells and they invade more aggressively.

References

- Abercrombie, M. (1970) Contact inhibition in tissue culture. *In Vitro*, **6**, 128-142.
- Ackermann, J. et al. (2005) Metastasizing melanoma formation caused by expression of activated N-RasQ61K on an INK4a-deficient background. *Cancer Res*, **65**, 4005-4011.
- Albini, A. et al. (1987) A rapid in vitro assay for quantitating the invasive potential of tumour cells. *Cancer Res*, **47**, 3239-3245.
- Algra, A.M. & Rothwell, P.M. (2012) Effects of regular aspirin on long-term cancer incidence and metastasis: a systematic comparison of evidence from observational studies versus randomised trials. *The Lancet Oncology*, **13**, 518-527.
- Alikhan, A., Ibrahimi, O.A. & Eisen, D.B. (2012) Congenital melanocytic nevi: Where are we now?: Part I. Clinical presentation, epidemiology, pathogenesis, histology, malignant transformation, and neurocutaneous melanosis. *J Am Acad Dermatol*, **67**, 495.e1-495.e17.
- Amatschek, S. et al. (2011) CXCL9 induces chemotaxis, chemorepulsion and endothelial barrier disruption through CXCR3-mediated activation of melanoma cells. *Br J Cancer*, **104**, 469-479.
- Andrew, N. & Insall, R.H. (2007) Chemotaxis in shallow gradients is mediated independently of PtdIns 3-kinase by biased choices between random protrusions. *Nat Cell Biol*, **9**, 193-200.
- Anliker, B. & Chun, J. (2004) Cell surface receptors in lysophospholipid signalling. *Semin Cell Dev Biol*, **15**, 457-465.
- Aoki, J., Inoue, A. & Okudaira, S. (2008) Two pathways for lysophosphatidic acid production. *Biochim Biophys Acta*, **1781**, 513-518.
- Aoki, J. et al. (2002) Serum lysophosphatidic acid is produced through diverse phospholipase pathways. *J Biol Chem*, **277**, 48737-48744.

- Aota, S., Nagai, T. & Yamada, K.M. (1991) Characterization of regions of fibronectin besides the arginine-glycine-aspartic acid sequence required for adhesive function of the cell-binding domain using site-directed mutagenesis. *J Biol Chem*, **266**, 15938-15943.
- Argenziano, G. et al. (2012) Early diagnosis of melanoma: what is the impact of dermoscopy? *Dermatol Ther*, **25**, 403-409.
- Arrington, J.H.r. et al. (1977) Plantar lentiginous melanoma: a distinctive variant of human cutaneous malignant melanoma. *Am J Surg Pathol*, **1**, 131-143.
- Asgari, M.M., Maruti, S.S. & White, E. (2008) A large cohort study of nonsteroidal anti-inflammatory drug use and melanoma incidence. *J Natl Cancer Inst*, **100**, 967-971.
- Atkins, M.B. (1997) The treatment of metastatic melanoma with chemotherapy and biologics. *Curr Opin Oncol*, **9**, 205-213.
- Aznavoorian, S. et al. (1990) Signal transduction for chemotaxis and haptotaxis by matrix molecules in tumour cells. *J Cell Biol*, **110**, 1427-1438.
- Baicu, S.C. & Taylor, M.J. (2002) Acid-base buffering in organ preservation solutions as a function of temperature: new parameters for comparing buffer capacity and efficienc. *Cryobiology*, **45**, 33-48.
- Bailly, M. et al. (1998) Regulation of protrusion shape and adhesion to the substratum during chemotactic responses of mammalian carcinoma cells. *Exp Cell Res*, **241**, 285-299.
- Baker, B.M. & Chen, C.S. (2012) Deconstructing the third dimension: how 3D culture microenvironments alter cellular cues. *J Cell Sci*, **125**, 3015-3024.
- Balazs, L. et al. (2001) Topical application of the phospholipid growth factor lysophosphatidic acid promotes wound healing in vivo. *Am J Physiol Regul Integr Comp Physiol*, **280**, R466-72.

- Balch, C.M. et al. (2009) Final version of 2009 AJCC melanoma staging and classification. *J Clin Oncol*, **27**, 6199-6206.
- Bambace, N.M. & Holmes, C.E. (2011) The platelet contribution to cancer progression. *J Thromb Haemost*, **9**, 237-249.
- Bandoh, K. et al. (2000) Lysophosphatidic acid (LPA) receptors of the EDG family are differentially activated by LPA species. Structure-activity relationship of cloned LPA receptors. *FEBS Lett*, **478**, 159-165.
- Bathena, S.P. et al. (2011) Quantitative determination of lysophosphatidic acids (LPAs) in human saliva and gingival crevicular fluid (GCF) by LC-MS/MS. *J Pharm Biomed Anal*, **56**, 402-407.
- Baynash, A.G. et al. (1994) Interaction of endothelin-3 with endothelin-B receptor is essential for development of epidermal melanocytes and enteric neurons. *Cell*, **79**, 1277-1285.
- Becker, J.C. et al. (2010) Mouse models for melanoma: a personal perspective. *Exp Dermatol*, **19**, 157-164.
- Belmadani, A. et al. (2009) The chemokine SDF-1/CXCL12 regulates the migration of melanocyte progenitors in mouse hair follicles. *Differentiation*, **77**, 395-411.
- Belmadani, A. et al. (2005) The chemokine stromal cell-derived factor-1 regulates the migration of sensory neuron progenitors. *J Neurosci*, **25**, 3995-4003.
- Bennett, D.C. (2003) Human melanocyte senescence and melanoma susceptibility genes. *Oncogene*, **22**, 3063-3069.
- Bennett, D.C. (2008) How to make a melanoma: what do we know of the primary clonal events? *Pigment Cell Melanoma Res*, **21**, 27-38.
- Berens, P. (2009) CircStat: A MATLAB Toolbox for Circular Statistics. *J Stat Software*, **31**, 1-21.

- Berking, C. & Herlyn, M. (2001) Human skin reconstruct models: a new application for studies of melanocyte and melanoma biology. *Histol Histopathol*, **16**, 669-674.
- Billingham, R.E. & Silvers, W.K. (1971) A biologist's reflections on dermatology. *J Invest Dermatol*, **57**, 227-240.
- Bishop, D.T. et al. (2009) Genome-wide association study identifies three loci associated with melanoma risk. *Nat Genet*, **41**, 920-925.
- Bittner, M. et al. (2000) Molecular classification of cutaneous malignant melanoma by gene expression profiling. *Nature*, **406**, 536-540.
- Bjorkelund, H., Gedda, L. & Andersson, K. (2011) Comparing the epidermal growth factor interaction with four different cell lines: intriguing effects imply strong dependency of cellular context. *PLoS One*, **6**, e16536.
- Blaine, S.A. et al. (2009) Epidermal growth factor receptor regulates pancreatic fibrosis. *Am J Physiol Gastrointest Liver Physiol*, **297**, G434-41.
- Blokx, W.A., van Dijk, M.C. & Ruiter, D.J. (2010) Molecular cytogenetics of cutaneous melanocytic lesions - diagnostic, prognostic and therapeutic aspects. *Histopathology*, **56**, 121-132.
- Bobek, V. et al. (2011) Tail spontaneous metastatic mouse model: comparison of metastatic potential of orthotopic and heterotopic models imaged by GFP and RFP protein. *In Vivo*, **25**, 849-852.
- Bobek, V. et al. (2010) A clinically relevant, syngeneic model of spontaneous, highly metastatic B16 mouse melanoma. *Anticancer Res*, **30**, 4799-4803.
- Bogenrieder, T. & Herlyn, M. (2003) Axis of evil: molecular mechanisms of cancer metastasis. *Oncogene*, **22**, 6524-6536.
- Bosenberg, M. et al. (2006) Characterization of melanocyte-specific inducible Cre recombinase transgenic mice. *Genesis*, **44**, 262-267.

- Bot, M. et al. (2013) Lysophosphatidic Acid Triggers Mast Cell-driven Atherosclerotic Plaque Destabilization by Increasing Vascular Inflammation. *J Lipid Res*,
- Boucharaba, A. et al. (2004) Platelet-derived lysophosphatidic acid supports the progression of osteolytic bone metastases in breast cancer. *J Clin Invest*, **114**, 1714-1725.
- Boucharaba, A. et al. (2006) The type 1 lysophosphatidic acid receptor is a target for therapy in bone metastases. *Proc Natl Acad Sci U S A*, **103**, 9643-9648.
- Boukamp, P. et al. (1988) Normal keratinization in a spontaneously immortalized aneuploid human keratinocyte cell line. *J Cell Biol*, **106**, 761-771.
- Box, N.F. et al. (2001) MC1R genotype modifies risk of melanoma in families segregating CDKN2A mutations. *Am J Hum Genet*, **69**, 765-773.
- Brash, D.E. et al. (1991) A role for sunlight in skin cancer: UV-induced p53 mutations in squamous cell carcinoma. *Proc Natl Acad Sci U S A*, **88**, 10124-10128.
- Bravo-Cordero, J.J., Hodgson, L. & Condeelis, J. (2012) Directed cell invasion and migration during metastasis. *Curr Opin Cell Biol*, **24**, 277-283.
- Brenn, T. (2012) Pitfalls in the evaluation of melanocytic lesions. *Histopathology*, **60**, 690-705.
- Brenner, M. & Hearing, V.J. (2008) The protective role of melanin against UV damage in human skin. *Photochem Photobiol*, **84**, 539-549.
- Breslow, A. (1970) Thickness, cross-sectional areas and depth of invasion in the prognosis of cutaneous melanoma. *Ann Surg*, **172**, 902-908.
- Brindley, D.N. (2004) Lipid phosphate phosphatases and related proteins: signalling functions in development, cell division, and cancer. *J Cell Biochem*, **92**, 900-912.

- Brindley, D.N. & Pilquill, C. (2009) Lipid phosphate phosphatases and signalling. *J Lipid Res*, **50 Suppl**, S225-30.
- Broekaert, S.M. et al. (2010) Genetic and morphologic features for melanoma classification. *Pigment Cell Melanoma Res*, **23**, 763-770.
- Buac, K. & Pavan, W.J. (2007) Stem cells of the melanocyte lineage. *Cancer Biomark*, **3**, 203-209.
- CRUK. (2013) Skin cancer incidence statistics:<http://www.cancerresearchuk.org/cancer-info/cancerstats/types/skin/incidence/uk-skin-cancer-incidence-statistics>. *UK Statistics*,
- Carvajal, R.D. et al. (2011) KIT as a therapeutic target in metastatic melanoma. *JAMA*, **305**, 2327-2334.
- Chang, Y.M. et al. (2009) Sun exposure and melanoma risk at different latitudes: a pooled analysis of 5700 cases and 7216 controls. *Int J Epidemiol*, **38**, 814-830.
- Chapman, P.B. et al. (2011) Improved survival with vemurafenib in melanoma with BRAF V600E mutation. *N Engl J Med*, **364**, 2507-2516.
- Chellaiah, M.A. et al. (2000) Rho-A is critical for osteoclast podosome organization, motility, and bone resorption. *J Biol Chem*, **275**, 11993-12002.
- Chioni, A.M. & Grose, R. (2008) Organotypic modelling as a means of investigating epithelial-stromal interactions during tumourigenesis. *Fibrogenesis Tissue Repair*, **1**, 8.
- Choi, J.W. et al. (2010) LPA receptors: subtypes and biological actions. *Annu Rev Pharmacol Toxicol*, **50**, 157-186.

- Clark, W.H.J. et al. (1984) A study of tumour progression: the precursor lesions of superficial spreading and nodular melanoma. *Hum Pathol*, **15**, 1147-1165.
- Clark, W.H.J. et al. (1969) The histogenesis and biologic behavior of primary human malignant melanomas of the skin. *Cancer Res*, **29**, 705-727.
- Clemetson, K.J. et al. (1982) Characterization of the platelet membrane glycoprotein abnormalities in Bernard-Soulier syndrome and comparison with normal by surface-labeling techniques and high-resolution two-dimensional gel electrophoresis. *J Clin Invest*, **70**, 304-311.
- Commandeur, S. et al. (2009) An in vitro three-dimensional model of primary human cutaneous squamous cell carcinoma. *Exp Dermatol*, **18**, 849-856.
- Condeelis, J., Jones, J. & Segall, J. (1992) Chemotaxis of metastatic tumour cells: clues to mechanisms from the Dictyostelium paradigm. *Cancer Met Revs*, **11**, 55-68.
- Condeelis, J., Singer, R.H. & Segall, J.E. (2005) The great escape: when cancer cells hijack the genes for chemotaxis and motility. *Annu Rev Cell Dev Biol*, **21**, 695-718.
- Contos, J.J. et al. (2000) Requirement for the lpA1 lysophosphatidic acid receptor gene in normal suckling behavior. *Proc Natl Acad Sci U S A*, **97**, 13384-13389.
- Coory, M. et al. (2006) Trends for in situ and invasive melanoma in Queensland, Australia, 1982-2002. *Cancer Causes Control*, **17**, 21-27.
- Coupland, L.A., Chong, B.H. & Parish, C.R. (2012) Platelets and P-selectin control tumour cell metastasis in an organ-specific manner and independently of NK cells. *Cancer Res*, **72**, 4662-4671.

- Curiel-Lewandrowski, C. et al. (2011) Long-term use of nonsteroidal anti-inflammatory drugs decreases the risk of cutaneous melanoma: results of a United States case-control study. *J Invest Dermatol*, **131**, 1460-1468.
- Dankort, D. et al. (2009) Braf(V600E) cooperates with Pten loss to induce metastatic melanoma. *Nat Genet*, **41**, 544-552.
- David, M. et al. (2010) Cancer cell expression of autotaxin controls bone metastasis formation in mouse through lysophosphatidic acid-dependent activation of osteoclasts. *PLoS One*, **5**, e9741.
- Davies, H. et al. (2002) Mutations of the BRAF gene in human cancer. *Nature*, **417**, 949-954.
- De Giorgi, V. et al. (2010) Application of a Filtration- and Isolation-by-Size Technique for the Detection of Circulating Tumor Cells in Cutaneous Melanoma. *J Invest Dermatol*, **130**, 2440-2447.
- de Vries, E. & Coebergh, J.W. (2004) Cutaneous malignant melanoma in Europe. *Eur J Cancer*, **40**, 2355-2366.
- Dennis, L.K. (1999) Analysis of the melanoma epidemic, both apparent and real: data from the 1973 through 1994 surveillance, epidemiology, and end results program registry. *Arch Dermatol*, **135**, 275-280.
- Desmarais, V. et al. (2009) N-WASP and cortactin are involved in invadopodium-dependent chemotaxis to EGF in breast tumour cells. *Cell Motil Cytoskeleton*, **66**, 303-316.
- Deuel, T.F. et al. (1981) Human platelet-derived growth factor. Purification and resolution into two active protein fractions. *J Biol Chem*, **256**, 8896-8899.
- Devitt, B. et al. (2011) Clinical outcome and pathological features associated with NRAS mutation in cutaneous melanoma. *Pigment Cell Melanoma Res*, **24**, 666-672.

- Dhomen, N. et al. (2009) Oncogenic Braf induces melanocyte senescence and melanoma in mice. *Cancer Cell*, **15**, 294-303.
- Dicker, T.J. et al. (1999) A rational approach to melanoma follow-up in patients with primary cutaneous melanoma. Scottish Melanoma Group. *Br J Dermatol*, **140**, 249-254.
- DiMilla, P.A. (1992) Adsorption and elution of extracellular matrix proteins on non-tissue culture polystyrene Petri dishes. *J Colloid Interface Sci*, **153**, 212-225.
- DiMilla, P.A. et al. (1993) Maximal migration of human smooth muscle cells on fibronectin and type IV collagen occurs at an intermediate attachment strength. *J Cell Biol*, **122**, 729-737.
- Dimitrow, E. et al. (2009) Sensitivity and specificity of multiphoton laser tomography for in vivo and ex vivo diagnosis of malignant melanoma. *J Invest Dermatol*, **129**, 1752-1758.
- Doherty, V.R. & MacKie, R.M. (1988) Experience of a public education programme on early detection of cutaneous malignant melanoma. *BMJ*, **297**, 388-391.
- Dong, C. et al. (2002) In vitro characterization and micromechanics of tumour cell chemotactic protrusion, locomotion, and extravasation. *Ann Biomed Eng*, **30**, 344-355.
- Dorsam, R.T. & Gutkind, J.S. (2007) G-protein-coupled receptors and cancer. *Nat Rev Cancer*, **7**, 79-94.
- Easty, D.J. et al. (2011) Receptor tyrosine kinases and their activation in melanoma. *Pigment Cell Melanoma Res*, **24**, 446-461.
- Easty, D.J., Herlyn, M. & Bennett, D.C. (1995) Abnormal protein tyrosine kinase gene expression during melanoma progression and metastasis. *Int J Cancer*, **60**, 129-136.

- Eichholtz, T. et al. (1993) The bioactive phospholipid lysophosphatidic acid is released from activated platelets. *Biochem J*, **291**, 677-680.
- Eichinger, L. et al. (2005) The genome of the social amoeba *Dictyostelium discoideum*. *Nature*, **435**, 43-57.
- Ellerhorst, J.A. et al. (2011) Clinical correlates of NRAS and BRAF mutations in primary human melanoma. *Clin Cancer Res*, **17**, 229-235.
- Emmett, M.S. et al. (2011) CCR7 mediates directed growth of melanomas towards lymphatics. *Microcirculation*, **18**, 172-182.
- Eton, O. et al. (1998) Prognostic factors for survival of patients treated systemically for disseminated melanoma. *J Clin Oncol*, **16**, 1103-1111.
- Falchi, M. et al. (2009) Genome-wide association study identifies variants at 9p21 and 22q13 associated with development of cutaneous nevi. *Nat Genet*, **41**, 915-919.
- Fang, L. et al. (2008) CCR7 regulates B16 murine melanoma cell tumorigenesis in skin. *J Leukoc Biol*, **84**, 965-972.
- Fidler, I.J. (2003) The pathogenesis of cancer metastasis: the 'seed and soil' hypothesis revisited. *Nat Rev Cancer*, **3**, 453-458.
- Fidler, I.J. & Nicolson, G.L. (1976) Organ selectivity for implantation survival and growth of B16 melanoma variant tumour lines. *J Natl Cancer Inst*, **57**, 1199-1202.
- Fingleton, B. (2006) Matrix metalloproteinases: roles in cancer and metastasis. *Front Biosci*, **11**, 479-491.
- Fischer, A.H. et al. (2008) Preparation of slides and coverslips for microscopy. *CSH Protoc*, **2008**, pdb.prot4988.
- Fitzpatrick, T.B. & Breathnach, A.S. (1963) The epidermal melanin unit system. *Dermatol Wochenschr*, **147**, 481-489.

- Flaherty, K.T., Hodi, F.S. & Fisher, D.E. (2012a) From genes to drugs: targeted strategies for melanoma. *Nat Rev Cancer*, **12**, 349-361.
- Flaherty, K.T. et al. (2012b) Combined BRAF and MEK inhibition in melanoma with BRAF V600 mutations. *N Engl J Med*, **367**, 1694-1703.
- Flaherty, K.T. et al. (2012c) Improved survival with MEK inhibition in BRAF-mutated melanoma. *N Engl J Med*, **367**, 107-114.
- Fourcade, O. et al. (1995) Secretory phospholipase A2 generates the novel lipid mediator lysophosphatidic acid in membrane microvesicles shed from activated cells. *Cell*, **80**, 919-927.
- Franke, J. & Kessin, R. (1977) A defined minimal medium for axenic strains of *Dictyostelium discoideum*. *Proc Natl Acad Sci U S A*, **74**, 2157-2161.
- Friedl, P. & Gilmour, D. (2009) Collective cell migration in morphogenesis, regeneration and cancer. *Nat Rev Mol Cell Biol*, **10**, 445-457.
- Friedl, P. et al. (1997) Migration of highly aggressive MV3 melanoma cells in 3-dimensional collagen lattices results in local matrix reorganization and shedding of alpha2 and beta1 integrins and CD44. *Cancer Res*, **57**, 2061-2070.
- Friedl, P. et al. (1995) Migration of coordinated cell clusters in mesenchymal and epithelial cancer explants in vitro. *Cancer Res*, **55**, 4557-4560.
- Friedman, R.J., Rigel, D.S. & Kopf, A.W. (1985) Early detection of malignant melanoma: the role of physician examination and self-examination of the skin. *CA Cancer J Clin*, **35**, 130-151.
- Friedman, R.J. et al. (1991) Volume of malignant melanoma is superior to thickness as a prognostic indicator. Preliminary observation. *Dermatol Clin*, **9**, 643-648.

- Fukami, K. & Takenawa, T. (1992) Phosphatidic acid that accumulates in platelet-derived growth factor-stimulated Balb/c 3T3 cells is a potential mitogenic signal. *J Biol Chem*, **267**, 10988-10993.
- Fukunaga-Kalabis, M. et al. (2006) CCN3 controls 3D spatial localization of melanocytes in the human skin through DDR1. *J Cell Biol*, **175**, 563-569.
- Gabazza, E.C. et al. (1993) Evaluating prethrombotic state in lung cancer using molecular markers. *Chest*, **103**, 196-200.
- Gaetano, C.G. et al. (2009) Inhibition of autotaxin production or activity blocks lysophosphatidylcholine-induced migration of human breast cancer and melanoma cells. *Mol Carcinog*, **48**, 801-809.
- Gaggioli, C. & Sahai, E. (2007) Melanoma invasion - current knowledge and future directions. *Pigment Cell Res*, **20**, 161-172.
- Gandini, S. et al. (2005a) Meta-analysis of risk factors for cutaneous melanoma: I. Common and atypical naevi. *Eur J Cancer*, **41**, 28-44.
- Gandini, S. et al. (2005b) Meta-analysis of risk factors for cutaneous melanoma: II. Sun exposure. *Eur J Cancer*, **41**, 45-60.
- Gandini, S. et al. (2005c) Meta-analysis of risk factors for cutaneous melanoma: III. Family history, actinic damage and phenotypic factors. *Eur J Cancer*, **41**, 2040-2059.
- Garibyan, L. & Fisher, D.E. (2010) How sunlight causes melanoma. *Curr Oncol Rep*, **12**, 319-326.
- Gay LL, F.-H.B. (2011) Contribution of platelets to tumour metastasis. *Nature Rev Cancer*, **11**, 123.
- Georas, S.N. et al. (2007) Lysophosphatidic acid is detectable in human bronchoalveolar lavage fluids at baseline and increased after segmental allergen challenge. *Clin Exp Allergy*, **37**, 311-322.

- Gerisch, G. & Keller, H.U. (1981) Chemotactic reorientation of granulocytes stimulated with micropipettes containing fMet-Leu-Phe. *J Cell Sci*, **52**, 1-10.
- Gilchrest, B.A. et al. (1999) The pathogenesis of melanoma induced by ultraviolet radiation. *N Engl J Med*, **340**, 1341-1348.
- Giuliano, A.E., Cochran, A.J. & Morton, D.L. (1982) Melanoma from unknown primary site and amelanotic melanoma. *Semin Oncol*, **9**, 442-447.
- Gogas, H.J., Kirkwood, J.M. & Sondak, V.K. (2007) Chemotherapy for metastatic melanoma: time for a change? *Cancer*, **109**, 455-464.
- Goswami, S. et al. (2005) Macrophages promote the invasion of breast carcinoma cells via a colony-stimulating factor-1/epidermal growth factor paracrine loop. *Cancer Res*, **65**, 5278-5283.
- Grinnell, F. & Feld, M.K. (1979) Initial adhesion of human fibroblasts in serum-free medium: possible role of secreted fibronectin. *Cell*, **17**, 117-129.
- Gudbjartsson, D.F. et al. (2008) ASIP and TYR pigmentation variants associate with cutaneous melanoma and basal cell carcinoma. *Nat Genet*, **40**, 886-891.
- Guise, T.A. (2005) Thromboembolism to metastasis: The platelet-lysophosphatidic acid connection. *IBMS BoneKEy*, **2**, 12-16.
- Guitera, P. & Menzies, S.W. (2011) State of the art of diagnostic technology for early-stage melanoma. *Expert Rev Anticancer Ther*, **11**, 715-723.
- Gupta, P.B. et al. (2005) The melanocyte differentiation program predisposes to metastasis after neoplastic transformation. *Nat Genet*, **37**, 1047-1054.
- Haass, N.K. & Herlyn, M. (2005) Normal human melanocyte homeostasis as a paradigm for understanding melanoma. *J Invest Dermatol Symp Proc*, **10**, 153-163.

- Haass, N.K. & Smalley, K.S. (2009) Melanoma biomarkers: current status and utility in diagnosis, prognosis, and response to therapy. *Mol Diagn Ther*, **13**, 283-296.
- Hama, K. et al. (2004) Lysophosphatidic acid and autotaxin stimulate cell motility of neoplastic and non-neoplastic cells through LPA1. *J Biol Chem*, **279**, 17634-17639.
- Harris RE (2001) Inverse association of non-steroidal anti-inflammatory drugs and malignant melanoma among women. *Onc Reports*,
- Haugh, J.M. et al. (1999) Effect of epidermal growth factor receptor internalization on regulation of the phospholipase C-gamma1 signalling pathway. *J Biol Chem*, **274**, 8958-8965.
- Healsmith, M.F. et al. (1994) An evaluation of the revised seven-point checklist for the early diagnosis of cutaneous malignant melanoma. *Br J Dermatol*, **130**, 48-50.
- Hecht, J.H. et al. (1996) Ventricular zone gene-1 (vzg-1) encodes a lysophosphatidic acid receptor expressed in neurogenic regions of the developing cerebral cortex. *J Cell Biol*, **135**, 1071-1083.
- Hegerfeldt, Y. et al. (2002) Collective cell movement in primary melanoma explants: plasticity of cell-cell interaction, beta1-integrin function, and migration strategies. *Cancer Res*, **62**, 2125-2130.
- Herlyn, M. (1990) Human melanoma: development and progression. *Cancer Metastasis Rev*, **9**, 101-112.
- Herlyn, M. (2009) Driving in the melanoma landscape. *Exp Dermatol*, **18**, 506-508.
- Herlyn, M. et al. (1985a) Primary melanoma cells of the vertical growth phase: similarities to metastatic cells. *J Natl Cancer Inst*, **74**, 283-289.

- Herlyn, M. & Fukunaga-Kalabis, M. (2010) What is a good model for melanoma? *J Invest Dermatol*, **130**, 911-912.
- Herlyn, M. et al. (1990) Growth-regulatory factors for normal, premalignant, and malignant human cells in vitro. *Adv Cancer Res*, **54**, 213-234.
- Herlyn, M. & Shih, I.M. (1994) Interactions of melanocytes and melanoma cells with the microenvironment. *Pigment Cell Res*, **7**, 81-88.
- Herlyn, M. et al. (1985b) Characteristics of cultured human melanocytes isolated from different stages of tumour progression. *Cancer Res*, **45**, 5670-5676.
- Hirayama, R. et al. (1984) Different metastatic modes of malignant melanoma implanted in the ear of young and old mice. *Cancer Immunol Immunother*, **18**, 209-214.
- Hodgson, L., Henderson, A.J. & Dong, C. (2003) Melanoma cell migration to type IV collagen requires activation of NF-kappaB. *Oncogene*, **22**, 98-108.
- Hodis, E. et al. (2012) A landscape of driver mutations in melanoma. *Cell*, **150**, 251-263.
- Hoek, K.S. et al. (2008) In vivo switching of human melanoma cells between proliferative and invasive states. *Cancer Res*, **68**, 650-656.
- Hoek, K.S. & Goding, C.R. (2010) Cancer stem cells versus phenotype-switching in melanoma. *Pigment Cell Melanoma Res*,
- Hoeller, O. & Kay, R.R. (2007) Chemotaxis in the absence of PIP3 gradients. *Curr Biol*, **17**, 813-817.
- Hoos, A. et al. (2010) Development of ipilimumab: contribution to a new paradigm for cancer immunotherapy. *Semin Oncol*, **37**, 533-546.
- T, H. (1995) Melanocyte Mitogens Induce both melanocyte chemokinesis and chemotaxis. *JID*, **104**, 256-259.

- Horn, S. et al. (2013) TERT promoter mutations in familial and sporadic melanoma. *Science*, **339**, 959-961.
- Hotary, K. et al. (2006) A cancer cell metalloprotease triad regulates the basement membrane transmigration program. *Genes Dev*, **20**, 2673-2686.
- Hsieh, R. et al. (2012) The CDKN2A and MAP Kinase Pathways: Molecular Roads to Primary Oral Mucosal Melanoma. *Am J Dermatopathol*,
- Huang, R.Y. et al. (2008) Lysophosphatidic acid induces ovarian cancer cell dispersal by activating Fyn kinase associated with p120-catenin. *Int J Cancer*, **123**, 801-809.
- Huang, S.K. et al. (2009) LC/MS-based quantitative proteomic analysis of paraffin-embedded archival melanomas reveals potential proteomic biomarkers associated with metastasis. *PLoS One*, **4**, e4430.
- Hughes-Alford, S.K. & Lauffenburger, D.A. (2012) Quantitative analysis of gradient sensing: towards building predictive models of chemotaxis in cancer. *Curr Opin Cell Biol*, **24**, 284-291.
- Hulme, E.C. & Trevethick, M.A. (2010) Ligand binding assays at equilibrium: validation and interpretation. *Br J Pharmacol*, **161**, 1219-1237.
- Hyun, S.W. et al. (2011) Diverse injurious stimuli reduce protein tyrosine phosphatase- μ expression and enhance epidermal growth factor receptor signalling in human airway epithelia. *Exp Lung Res*, **37**, 327-343.
- Ibarra, N. et al. (2006) Nap1 regulates Dictyostelium cell motility and adhesion through SCAR-dependent and -independent pathways. *Curr Biol*, **16**, 717-722.
- Imamura, F. et al. (1993) Induction of in vitro tumour cell invasion of cellular monolayers by lysophosphatidic acid or phospholipase D. *Biochem Biophys Res Commun*, **193**, 497-503.

- Inaba, M., Yamanaka, H. & Kondo, S. (2012) Pigment pattern formation by contact-dependent depolarization. *Science*, **335**, 677.
- Inoue, A. et al. (2011) LPA-producing enzyme PA-PLA(1) α regulates hair follicle development by modulating EGFR signalling. *EMBO J*, **30**, 4248-4260.
- Insall, R.H. (2010a) Understanding eukaryotic chemotaxis: a pseudopod-centred view. *Nat Rev Mol Cell Biol*, **11**, 453-458.
- Insall, R.H. (2010b) Understanding eukaryotic chemotaxis: a pseudopod-centred view. *Nature Rev Mol Cell Bio*,
- Insall, R.H. & Machesky, L.M. (2009a) Actin dynamics at the leading edge: from simple machinery to complex networks. *Dev Cell*, **17**, 310-322.
- Insall, R.H. & Machesky, L.M. (2009b) Actin dynamics at the leading edge: from simple machinery to complex networks. *Dev Cell*, **17**, 310-322.
- Jalink, K. et al. (1995) Lysophosphatidic acid-induced Ca²⁺ mobilization in human A431 cells: structure-activity analysis. *Biochem J*, **307**, 609-616.
- Jalink, K., Moolenaar, W.H. & Van Duijn, B. (1993) Lysophosphatidic acid is a chemoattractant for Dictyostelium discoideum amoebae. *Proc Natl Acad Sci U S A*, **90**, 1857-1861.
- Jalink, K. et al. (1994) Inhibition of lysophosphatidate- and thrombin-induced neurite retraction and neuronal cell rounding by ADP ribosylation of the small GTP-binding protein Rho. *J Cell Biol*, **126**, 801-810.
- Jans, R. et al. (2013) Lysophosphatidic Acid Promotes Cell Migration through STIM1- and Orai1-Mediated Ca(2+)(i) Mobilization and NFAT2 Activation. *J Invest Dermatol*, **133**, 793-802.
- Jechlinger, M. et al. (2006) Autocrine PDGFR signalling promotes mammary cancer metastasis. *J Clin Invest*, **116**, 1561-1570.

- Jensen, A.R. et al. (2011) Fyn is downstream of the HGF/MET signalling axis and affects cellular shape and tropism in PC3 cells. *Clin Cancer Res*, **17**, 3112-3122.
- Jerant, A.F. et al. (2000) Early detection and treatment of skin cancer. *Am Fam Physician*, **62**, 357-68, 375-6, 381-2.
- Ji, Z., Flaherty, K.T. & Tsao, H. (2010) Molecular therapeutic approaches to melanoma. *Mol Aspects Med*, **31**, 194-204.
- Johannesdottir, S.A. et al. (2012) Nonsteroidal anti-inflammatory drugs and the risk of skin cancer: A population-based case-control study. *Cancer*, **118**, 4768-4776.
- Jongsma, M. et al. (2011) LPA is a chemorepellent for B16 melanoma cells: action through the cAMP-elevating LPA5 receptor. *PLoS One*, **6**, e29260.
- Joose, A. et al. (2009) Non-steroidal anti-inflammatory drugs and melanoma risk: large Dutch population-based case-control study. *J Invest Dermatol*, **129**, 2620-2627.
- Jordan, S.A. & Jackson, I.J. (2000a) A late wave of melanoblast differentiation and rostrocaudal migration revealed in patch and rump-white embryos. *Mech Dev*, **92**, 135-143.
- Jordan, S.A. & Jackson, I.J. (2000b) MGF (KIT ligand) is a chemokinetic factor for melanoblast migration into hair follicles. *Dev Biol*, **225**, 424-436.
- Jourquin, J. et al. (2006) Dispersal of epithelial cancer cell colonies by lysophosphatidic acid (LPA). *J Cell Physiol*, **206**, 337-346.
- Jowhar, D. et al. (2010) Open access microfluidic device for the study of cell migration during chemotaxis. *Integr Biol (Camb)*,
- Kamath, S.. (2001) Platelet activation: assessment and quantification. *Eur Heart J*, **22**, 1561-1571.

- Kanagasundaram, V., Jaworowski, A. & Hamilton, J.A. (1996) Association between phosphatidylinositol-3 kinase, Cbl and other tyrosine phosphorylated proteins in colony-stimulating factor-1-stimulated macrophages. *Biochem J*, **320**, 69-77.
- Kay, R.R. et al. (2008) Changing directions in the study of chemotaxis. *Nat Rev Mol Cell Biol*, **9**, 455-463.
- Kedrin, D. et al. (2007) Cell motility and cytoskeletal regulation in invasion and metastasis. *J Mammary Gland Biol Neoplasia*, **12**, 143-152.
- Kelsh, R.N. et al. (2009) Stripes and belly-spots -- a review of pigment cell morphogenesis in vertebrates. *Semin Cell Dev Biol*, **20**, 90-104.
- Kim, M. et al. (2010) CXCR4 signalling regulates metastasis of chemoresistant melanoma cells by a lymphatic metastatic niche. *Cancer Res*, **70**, 10411-10421.
- Kim, M.Y. et al. (2009) Tumor self-seeding by circulating cancer cells. *Cell*, **139**, 1315-1326.
- King, J.S. & Insall, R.H. (2009) Chemotaxis: finding the way forward with Dictyostelium. *Trends Cell Biol*, **19**, 523-530.
- Kiowski, G. et al. (2011) Engineering Melanoma Progression in a Humanized Environment In Vivo. *J Invest Dermatol*,
- Kittler, H. et al. (2002) Diagnostic accuracy of dermoscopy. *Lancet Oncol*, **3**, 159-165.
- Kleinman, H.K. et al. (1982) Isolation and characterization of type IV procollagen, laminin, and heparan sulfate proteoglycan from the EHS sarcoma. *Biochemistry*, **21**, 6188-6193.
- Klominek, J., Sumitran Karuppan, S. & Hauzenberger, D. (1997) Differential motile response of human malignant mesothelioma cells to fibronectin,

- laminin and collagen type IV: the role of beta1 integrins. *Int J Cancer*, **72**, 1034-1044.
- Kondo, S. & Miura, T. (2010) Reaction-diffusion model as a framework for understanding biological pattern formation. *Science*, **329**, 1616-1620.
- Kopf, A.W. et al. (1982) "Small" melanomas: relation of prognostic variables to diameter of primary superficial spreading melanomas. *J Dermatol Surg Oncol*, **8**, 765-770.
- Korn, E.L. et al. (2008) Meta-analysis of phase II cooperative group trials in metastatic stage IV melanoma to determine progression-free and overall survival benchmarks for future phase II trials. *J Clin Oncol*, **26**, 527-534.
- Krauthammer, M. et al. (2012) Exome sequencing identifies recurrent somatic RAC1 mutations in melanoma. *Nat Genet*, **44**, 1006-1014.
- Kumagai, A. et al. (1989) Regulation and function of G alpha protein subunits in Dictyostelium. *Cell*, **57**, 265-275.
- Kwok, E. et al. (2012) FES Kinase promotes mast cell recruitment to mammary tumours via the stem cell factor/kit receptor signalling axis. *Mol Cancer Res*, **10**, 881-891.
- Lachiewicz, A.M. et al. (2008) Epidemiologic support for melanoma heterogeneity using the surveillance, epidemiology, and end results program. *J Invest Dermatol*, **128**, 1340-1342.
- Lanati, S. et al. (2010) Chemotrap-1: an engineered soluble receptor that blocks chemokine-induced migration of metastatic cancer cells in vivo. *Cancer Res*,
- Lancaster, H.O. (1956) Some geographical aspects of the mortality from melanoma in Europeans. *Med J Aust*, **43**, 1082-1087.

- Langley, R.R. & Fidler, I.J. (2011) The seed and soil hypothesis revisited--the role of tumour-stroma interactions in metastasis to different organs. *Int J Cancer*, **128**, 2527-2535.
- Lapierre, D.M. et al. (2010) Lysophosphatidic acid signals through multiple receptors in osteoclasts to elevate cytosolic calcium concentration, evoke retraction, and promote cell survival. *J Biol Chem*, **285**, 25792-25801.
- Larue, L., de Vuyst, F. & Delmas, V. (2012) Modeling melanoblast development. *Cell Mol Life Sci*,
- Lee, D.J., Ho, C.H. & Grinnell, F. (2003) LPA-stimulated fibroblast contraction of floating collagen matrices does not require Rho kinase activity or retraction of fibroblast extensions. *Exp Cell Res*, **289**, 86-94.
- Lee, J.T. & Herlyn, M. (2007) Microenvironmental influences in melanoma progression. *J Cell Biochem*, **101**, 862-872.
- Lee, K.C. & Weinstock, M.A. (2009) Melanoma is up: are we up to this challenge? *J Invest Dermatol*, **129**, 1604-1606.
- Lee, S.J. & Yun, C.C. (2010) Colorectal cancer cells - Proliferation, survival and invasion by lysophosphatidic acid. *Int J Biochem Cell Biol*, **42**, 1907-1910.
- Lee, Y. & Hwang, K. (2002) Skin thickness of Korean adults. *Surg Radiol Anat*, **24**, 183-189.
- Lemmon, M.A. & Schlessinger, J. (2010) Cell signalling by receptor tyrosine kinases. *Cell*, **141**, 1117-1134.
- Lesche, R. et al. (2002) Cre/loxP-mediated inactivation of the murine Pten tumour suppressor gene. *Genesis*, **32**, 148-149.
- Li Jeon, N. et al. (2002) Neutrophil chemotaxis in linear and complex gradients of interleukin-8 formed in a microfabricated device. *Nat Biotechnol*, **20**, 826-830.

- Li, A. et al. (2012) Activated mutant NRas(Q61K) drives aberrant melanocyte signalling, survival, and invasiveness via a Rac1-dependent mechanism. *J Invest Dermatol*, **132**, 2610-2621.
- Li, A. et al. (2011) Rac1 drives melanoblast organization during mouse development by orchestrating pseudopod- driven motility and cell-cycle progression. *Dev Cell*, **21**, 722-734.
- Lin, J. et al. (2008) Genetics of melanoma predisposition. *Br J Dermatol*, **159**, 286-291.
- Lindsay, C.R. (2012) An Investigation of the Roles of Two Novel Cancer Targets, P-Rex1 and FAK, in Genetically Modified Models of Melanoma. Ph.D. thesis, University of Glasgow.
- Lindsay, C.R. et al. (2011) P-Rex1 is required for efficient melanoblast migration and melanoma metastasis. *Nat Commun*, **2**, 555.
- Liotta, L.A. et al. (1986) Tumor cell autocrine motility factor. *Proc Natl Acad Sci U S A*, **83**, 3302-3306.
- Liotta, L.A. (1986) Tumor invasion and metastases—role of the extracellular matrix: Rhoads Memorial Award lecture. *Cancer Research*, **46**, 1-7.
- Liu, W. et al. (2006) Rate of growth in melanomas: characteristics and associations of rapidly growing melanomas. *Arch Dermatol*, **142**, 1551-1558.
- Longo, C. et al. (2013) Can noninvasive imaging tools potentially predict the risk of ulceration in invasive melanomas showing blue and black colors? *Melanoma Res*,
- Lugassy, C. et al. (2007) C16 laminin peptide increases angiotropic extravascular migration of human melanoma cells in a shell-less chick chorioallantoic membrane assay. *Br J Dermatol*, **157**, 780-782.

- Lv, G.M. et al. (2011) Lysophosphatidic acid (LPA) and endothelial differentiation gene (Edg) receptors in human pancreatic cancer. *J Surg Oncol*, **104**, 685-691.
- Machesky, L.M. & Sansom, O.J. (2012) Rac1 in the driver's seat for melanoma. *Pigment Cell Melanoma Res*, **25**, 762-764.
- Mackesky, L.M. & Li, A. (2010) Fascin: invasive filopodia promoting metastasis. *Comm Integrative Bio*, **3**, 263-270.
- Mackie, R.M. (2000) Malignant melanoma: clinical variants and prognostic indicators. *Clin Dermatol*, **25**, 471-475.
- Mackie, R.M., Clelland, D.B. & Skerrow, C.J. (1989) Type IV collagen and laminin staining patterns in benign and malignant cutaneous lesions. *J Clin Pathol*, **42**, 1173-1177.
- Magalhaes, M.A. et al. (2011) Cortactin phosphorylation regulates cell invasion through a pH-dependent pathway. *J Cell Biol*, **195**, 903-920.
- Maheshwari, G. & Lauffenburger, D.A. (1998) Deconstructing (and reconstructing) cell migration. *Microsc Res Tech*, **43**, 358-368.
- Maheshwari, G. et al. (1999) Biophysical integration of effects of epidermal growth factor and fibronectin on fibroblast migration. *Biophys J*, **76**, 2814-2823.
- Makova, K. & Norton, H. (2005) Worldwide polymorphism at the MC1R locus and normal pigmentation variation in humans. *Peptides*, **26**, 1901-1908.
- Mandrekar, S.J. & Sargent, D.J. (2011) All-comers versus enrichment design strategy in phase II trials. *J Thorac Oncol*, **6**, 658-660.
- Manegold, P.C. et al. (2003) Platelet-endothelial interaction in tumour angiogenesis and microcirculation. *Blood*, **101**, 1970-1976.

- Marghoob, A.A. et al. (2000) Breslow thickness and clark level in melanoma: support for including level in pathology reports and in American Joint Committee on Cancer Staging. *Cancer*, **88**, 589-595.
- Marsden, J.R. et al. (2010) Revised U.K. guidelines for the management of cutaneous melanoma 2010. *Br J Dermatol*, **163**, 238-256.
- Maury, E. et al. (2000) Identification of two secreted phospholipases A2 in human epidermis. *J Invest Dermatol*, **114**, 960-966.
- Mayer, T.C. (1973) The migratory pathway of neural crest cells into the skin of mouse embryos. *Dev Biol*, **34**, 39-46.
- Mazereeuw-Hautier, J. et al. (2005) Production of lysophosphatidic acid in blister fluid: involvement of a lysophospholipase D activity. *J Invest Dermatol*, **125**, 421-427.
- McCarthy, S.W. & Scolyer, R.A. (2004) Melanocytic lesions of the face: diagnostic pitfalls. *Ann Acad Med Singapore*, **33**, 3-14.
- McCluggage, W.G. (2006) My approach to the interpretation of endometrial biopsies and curettings. *J Clin Pathol*, **59**, 801-812.
- Meerschaert, K. et al. (1998) Gelsolin and functionally similar actin-binding proteins are regulated by lysophosphatidic acid. *EMBO J*, **17**, 5923-5932.
- Meier, F. et al. (2000) Human melanoma progression in skin reconstructs : biological significance of bFGF. *Am J Pathol*, **156**, 193-200.
- Mercer, K. et al. (2005) Expression of endogenous oncogenic V600E-raf induces proliferation and developmental defects in mice and transformation of primary fibroblasts. *Cancer Res*, **65**, 11493-11500.
- Metcalf, J.S. (1996) Melanoma: criteria for histological diagnosis and its reporting. *Semin Oncol*, **23**, 688-692.

- Meyer, A.S. et al. (2012) 2D protrusion but not motility predicts growth factor-induced cancer cell migration in 3D collagen. *J Cell Biol*, **197**, 721-729.
- Micalizzi, D.S., Farabaugh, S.M. & Ford, H.L. (2010) Epithelial-mesenchymal transition in cancer: parallels between normal development and tumour progression. *J Mammary Gland Biol Neoplasia*, **15**, 117-134.
- Michaloglou, C. et al. (2005) BRAFE600-associated senescence-like cell cycle arrest of human naevi. *Nature*, **436**, 720-724.
- Mills, G.B. & Moolenaar, W.H. (2003) The emerging role of lysophosphatidic acid in cancer. *Nat Rev Cancer*, **3**, 582-591.
- Monypenny, J. et al. (2009) Cdc42 and Rac family GTPases regulate mode and speed but not direction of primary fibroblast migration during platelet-derived growth factor-dependent chemotaxis. *Mol Cell Biol*, **29**, 2730-2747.
- Moolenaar, W.H. (1994) LPA: a novel lipid mediator with diverse biological actions. *Trends Cell Biol*, **4**, 213-219.
- Moolenaar, W.H. (1995) LPA, a Multifunctional Phospholipid Messenger. *J Biol Chem*, **270**, 12949-12952.
- Moolenaar, W.H. & Hla, T. (2012) SnapShot: Bioactive Lysophospholipids. *Cell*, **148**, 378-378.e2.
- Moolenaar, W.H. & Perrakis, A. (2011) Insights into autotaxin: how to produce and present a lipid mediator. *Nat Rev Mol Cell Biol*, **12**, 674-679.
- Moolenaar, W.H., van Meeteren, L.A. & Giepmans, B.N. (2004) The ins and outs of lysophosphatidic acid signalling. *Bioessays*, **26**, 870-881.
- Morton, C.A. & Mackie, R.M. (1998) Clinical accuracy of the diagnosis of cutaneous malignant melanoma. *Br J Dermatol*, **138**, 283-287.

- Moustafa, A.S. & Nicolson, G.L. (1997) Breast cancer metastasis-associated genes: prognostic significance and therapeutic implications. *Oncol Res*, **9**, 505-525.
- Mueller-Klieser, W. (2000) Tumor biology and experimental therapeutics. *Crit Rev Oncol Hematol*, **36**, 123-139.
- Muinonen-Martin, A.J. et al. (2013) Measuring Chemotaxis Using Direct Visualisation Microscope Chambers. *Methods Mol Biol*, 1046:307-21 (Ed, CouttsAS) Springer,
- Muinonen-Martin, A.J. et al. (2010) An improved chamber for direct visualisation of chemotaxis. *PLoS One*, **5**, e15309.
- Munro, J. et al. (2001) Human fibroblast replicative senescence can occur in the absence of extensive cell division and short telomeres. *Oncogene*, **20**, 3541-3552.
- Murata, J. et al. (1992) Differences in chemotaxis to fibronectin in weakly and highly metastatic tumour cells. *Jpn J Cancer Res*, **83**, 1327-1333.
- Naber, H.P. et al. (2011) Spheroid assay to measure TGF-beta-induced invasion. *J Vis Exp*,
- Nakamasu, A. et al. (2009) Interactions between zebrafish pigment cells responsible for the generation of Turing patterns. *Proc Natl Acad Sci U S A*, **106**, 8429-8434.
- Nam, S.W. et al. (2000) A sensitive screening assay for secreted motility-stimulating factors. *Cell Motil Cytoskeleton*, **46**, 279-284.
- Newton-Bishop, J.A. et al. (2010) Melanocytic nevi, nevus genes, and melanoma risk in a large case-control study in the United Kingdom. *Cancer Epidemiol Biomarkers Prev*, **19**, 2043-2054.

- Nishigaki, T. et al. (2006) Stroboscopic illumination using light-emitting diodes reduces phototoxicity in fluorescence cell imaging. *Biotechniques*, **41**, 191-197.
- Nishimura, E.K. et al. (1999) Regulation of E- and P-cadherin expression correlated with melanocyte migration and diversification. *Dev Biol*, **215**, 155-166.
- Noonan, F.P. et al. (2001) Neonatal sunburn and melanoma in mice. *Nature*, **413**, 271-272.
- Nystrom, M.L. et al. (2005) Development of a quantitative method to analyse tumour cell invasion in organotypic culture. *J Pathol*, **205**, 468-475.
- Oberholzer, P.A. et al. (2012) RAS mutations are associated with the development of cutaneous squamous cell tumours in patients treated with RAF inhibitors. *J Clin Oncol*, **30**, 316-321.
- Ohta, H. et al. (2003) Ki16425, a subtype-selective antagonist for EDG-family lysophosphatidic acid receptors. *Mol Pharmacol*, **64**, 994-1005.
- Ohuchi, H. et al. (2008) Expression patterns of the lysophospholipid receptor genes during mouse early development. *Dev Dyn*, **237**, 3280-3294.
- Olson, M.F. & Sahai, E. (2009) The actin cytoskeleton in cancer cell motility. *Clin Exp Metastasis*, **26**, 273-287.
- Ono, K. et al. (2006) Involvement of hepatocyte growth factor in the development of bone metastasis of a mouse mammary cancer cell line, BALB/c-MC. *Bone*, **39**, 27-34.
- Onsum, M. & Rao, C.V. (2007) A mathematical model for neutrophil gradient sensing and polarization. *PLoS Comput Biol*, **3**, e36.
- Otsuka, T. et al. (1998) c-Met autocrine activation induces development of malignant melanoma and acquisition of the metastatic phenotype. *Cancer Res*, **58**, 5157-5167.

- Paget, s. (1889) The distribution of secondary growths in cancer of the breast. *Lancet Oncol*, **1**, 571-573.
- Palmer, J.S. et al. (2000) Melanocortin-1 receptor polymorphisms and risk of melanoma: is the association explained solely by pigmentation phenotype? *Am J Hum Genet*, **66**, 176-186.
- Patsialou, A. et al. (2009) Invasion of human breast cancer cells in vivo requires both paracrine and autocrine loops involving the colony-stimulating factor-1 receptor. *Cancer Res*, **69**, 9498-9506.
- Payette, M.J., Katz, M.r. & Grant-Kels, J.M. (2009) Melanoma prognostic factors found in the dermatopathology report. *Clin Dermatol*, **27**, 53-74.
- Payne, A.S. & Cornelius, L.A. (2002) The role of chemokines in melanoma tumour growth and metastasis. *J Invest Dermatol*, **118**, 915-922.
- Peak, J.G. & Peak, M.J. (1991) Comparison of initial yields of DNA-to-protein crosslinks and single-strand breaks induced in cultured human cells by far- and near-ultraviolet light, blue light and X-rays. *Mutat Res*, **246**, 187-191.
- Peters, J. (2008) Nikon Instruments TiE-PFS Dynamic Focusing System. *Nat Methods: Application notes*,
- Petrie, R.J. & Yamada, K.M. (2013) At the leading edge of three-dimensional cell migration. *J Cell Sci*,
- Petronic-Rosic, V., Shea, C.R. & Krausz, T. (2004) Pagetoid melanocytosis: when is it significant? *Pathology*, **36**, 435-444.
- Peyton, B.D. et al. (1998) Patients with venous stasis ulceration have increased monocyte-platelet aggregation. *J Vasc Surg*, **27**, 1109-15; discussion 1115-6.
- Philippar, U. et al. (2008) A Mena invasion isoform potentiates EGF-induced carcinoma cell invasion and metastasis. *Dev Cell*, **15**, 813-828.

- Phillips, R.J. et al. (2005) Epidermal growth factor and hypoxia-induced expression of CXC chemokine receptor 4 on non-small cell lung cancer cells is regulated by the phosphatidylinositol 3-kinase/PTEN/AKT/mammalian target of rapamycin signalling pathway and activation of hypoxia inducible factor-1alpha. *J Biol Chem*, **280**, 22473-22481.
- Piazza, G.A., Ritter, J.L. & Baracka, C.A. (1995) Lysophosphatidic acid induction of transforming growth factors alpha and beta: modulation of proliferation and differentiation in cultured human keratinocytes and mouse skin. *Exp Cell Res*, **216**, 51-64.
- Pierce, J.H. et al. (1991) Oncogenic potential of erbB-2 in human mammary epithelial cells. *Oncogene*, **6**, 1189-1194.
- Pierschbacher, M.D. & Ruoslahti, E. (1984) Cell attachment activity of fibronectin can be duplicated by small synthetic fragments of the molecule. *Nature*, **309**, 30-33.
- Pinner, S. et al. (2009) Intravital imaging reveals transient changes in pigment production and Brn2 expression during metastatic melanoma dissemination. *Cancer Res*, **69**, 7969-7977.
- Pinner, S. & Sahai, E. (2008) PDK1 regulates cancer cell motility by antagonising inhibition of ROCK1 by RhoE. *Nat Cell Biol*, **10**, 127-137.
- Pirkmajer, S. & Chibalin, A.V. (2011) Serum starvation: caveat emptor. *Am J Physiol Cell Physiol*, **301**, C272-9.
- Plesance, E.D. et al. (2009) A comprehensive catalogue of somatic mutations from a human cancer genome. *Nature*,
- Pollard, J.W. (2008) Macrophages define the invasive microenvironment in breast cancer. *J Leukoc Biol*, **84**, 623-630.
- Pollock, P.M. et al. (2003) High frequency of BRAF mutations in nevi. *Nat Genet*, **33**, 19-20.

- Pradere, J.P. et al. (2007) LPA1 receptor activation promotes renal interstitial fibrosis. *J Am Soc Nephrol*, **18**, 3110-3118.
- Provenzano, P.P., Eliceiri, K.W. & Keely, P.J. (2009) Shining new light on 3D cell motility and the metastatic process. *Trends Cell Biol*, **19**, 638-648.
- Pryczynicz, A. et al. (2008) Expression of EGF and EGFR strongly correlates with metastasis of pancreatic ductal carcinoma. *Anticancer Res*, **28**, 1399-1404.
- Quinones, L.G. & Garcia-Castro, I. (2004) Characterization of human melanoma cell lines according to their migratory properties in vitro. *In Vitro Cell Dev Biol Anim*, **40**, 35-42.
- Rak, J. et al. (2006) Oncogenes, trousseau syndrome, and cancer-related changes in the coagulome of mice and humans. *Cancer Res*, **66**, 10643-10646.
- Rancoule, C. et al. (2011) Lysophosphatidic acid-1-receptor targeting agents for fibrosis. *Expert Opin Investig Drugs*, **20**, 657-667.
- Raz, A. & Ben-Ze'ev, A. (1987) Cell-contact and -architecture of malignant cells and their relationship to metastasis. *Cancer Metastasis Rev*, **6**, 3-21.
- Rebecca, V.W., Sondak, V.K. & Smalley, K.S. (2012) A brief history of melanoma: from mummies to mutations. *Melanoma Res*, **22**, 114-122.
- Renault, A.D., Kunwar, P.S. & Lehmann, R. (2010) Lipid phosphate phosphatase activity regulates dispersal and bilateral sorting of embryonic germ cells in *Drosophila*. *Development*, **137**, 1815-1823.
- Rhodes, J.M. (1982) Measurement of chemotaxis in Boyden chamber filter assays. Is the checkerboard correction valid? *J Immunol Methods*, **49**, 235-236.
- Ridky, T.W. et al. (2010) Invasive three-dimensional organotypic neoplasia from multiple normal human epithelia. *Nat Med*, **16**, 1450-1455.

- Ridley, A.J. & Hall, A. (1992) The small GTP-binding protein rho regulates the assembly of focal adhesions and actin stress fibers in response to growth factors. *Cell*, **70**, 389-399.
- Rigel, D.S., Russak, J. & Friedman, R. (2010) The evolution of melanoma diagnosis: 25 years beyond the ABCDs. *CA Cancer J Clin*, **60**, 301-316.
- Riss, J. et al. (2006) Cancers as wounds that do not heal: differences and similarities between renal regeneration/repair and renal cell carcinoma. *Cancer Res*, **66**, 7216-7224.
- Rofstad, E.K. (1994) Orthotopic human melanoma xenograft model systems for studies of tumour angiogenesis, pathophysiology, treatment sensitivity and metastatic pattern. *Br J Cancer*, **70**, 804-812.
- Romano, E. et al. (2011) Treatment implications of the emerging molecular classification system for melanoma. *Lancet Oncol*,
- Rothwell, P.M. et al. (2012) Short-term effects of daily aspirin on cancer incidence, mortality, and non-vascular death: analysis of the time course of risks and benefits in 51 randomised controlled trials. *Lancet*, **379**, 1602-1612.
- Roussos, E.T. et al. (2011a) Mena invasive (MenaINV) promotes multicellular streaming motility and transendothelial migration in a mouse model of breast cancer. *J Cell Sci*, **124**, 2120-2131.
- Roussos, E.T., Condeelis, J.S. & Patsialou, A. (2011b) Chemotaxis in cancer. *Nat Rev Cancer*, **11**, 573-587.
- Rozenberg, G.I. et al. (2010) Metastasis in an orthotopic murine model of melanoma is independent of RAS/RAF mutation. *Melanoma Res*, **20**, 361-371.
- Ruiter, D. et al. (2002) Melanoma-stroma interactions: structural and functional aspects. *Lancet Oncol*, **3**, 35-43.

- Saadi, W. et al. (2006) A parallel-gradient microfluidic chamber for quantitative analysis of breast cancer cell chemotaxis. *Biomed Microdevices*, **8**, 109-118.
- Sahai, E. & Marshall, C.J. (2003) Differing modes of tumour cell invasion have distinct requirements for Rho/ROCK signalling and extracellular proteolysis. *Nat Cell Biol*, **5**, 711-719.
- Saito, N. et al. (2009) Laminin-421 produced by lymphatic endothelial cells induces chemotaxis for human melanoma cells. *Pigment Cell Melanoma Res*, **22**, 601-610.
- Samadi, N. et al. (2011) Regulation of lysophosphatidate signalling by autotaxin and lipid phosphate phosphatases with respect to tumour progression, angiogenesis, metastasis and chemo-resistance. *Biochimie*, **93**, 61-70.
- Sanders, D.S. et al. (1999) Alterations in cadherin and catenin expression during the biological progression of melanocytic tumours. *Mol Pathol*, **52**, 151-157.
- Sano, T. et al. (2002) Multiple mechanisms linked to platelet activation result in lysophosphatidic acid and sphingosine 1-phosphate generation in blood. *J Biol Chem*, **277**, 21197-21206.
- Santiago-Walker, A. et al. (2009) Melanocytes: from morphology to application. *Skin Pharmacol Physiol*, **22**, 114-121.
- Sanz-Moreno, V. et al. (2011) ROCK and JAK1 signalling cooperate to control actomyosin contractility in tumour cells and stroma. *Cancer Cell*, **20**, 229-245.
- Satyamoorthy, K. et al. (1997) Melanoma cell lines from different stages of progression and their biological and molecular analyses. *Melanoma Res*, **7 Suppl 2**, S35-42.

- Satyamoorthy, K. et al. (2003) Constitutive mitogen-activated protein kinase activation in melanoma is mediated by both BRAF mutations and autocrine growth factor stimulation. *Cancer Res*, **63**, 756-759.
- Sauer, B. et al. (2004) Lysophosphatidic acid interacts with transforming growth factor-beta signalling to mediate keratinocyte growth arrest and chemotaxis. *J Invest Dermatol*, **123**, 840-849.
- Saulnier-Blache, J.S. et al. (2000) A simple and highly sensitive radioenzymatic assay for lysophosphatidic acid quantification. *J Lipid Res*, **41**, 1947-1951.
- Saunders, L.P. et al. (2008) Identification of small-molecule inhibitors of autotaxin that inhibit melanoma cell migration and invasion. *Mol Cancer Ther*, **7**, 3352-3362.
- Schachtner, H. et al. (2013) Megakaryocytes assemble podosomes that degrade matrix and protrude through basement membrane. *Blood*,
- Schaffer, J.V. et al. (2004) Cutaneous melanoma--past, present, and future. *J Am Acad Dermatol*, **51**, S65-9.
- Schenk, P.W. et al. (2001) Lysophosphatidic acid- and Gbeta-dependent activation of Dictyostelium MAP kinase ERK2. *Biochem Biophys Res Commun*, **282**, 765-772.
- Schneider IC, H.J.M. (2006) Mechanisms of Gradient Sensing and Chemotaxis. *Cell cycle*, **5**, 1130-1134.
- Scope, A. et al. (2008) The "ugly duckling" sign: agreement between observers. *Arch Dermatol*, **144**, 58-64.
- Scoyler, R.A. et al. (2012) Recent advances and important issues in melanoma pathology: an update for oncologists. *CancerForum*, **36**,
- Segura, S. et al. (2008) In vivo microscopic features of nodular melanomas: dermoscopy, confocal microscopy, and histopathologic correlates. *Arch Dermatol*, **144**, 1311-1320.

- Seiberg, M. (2001) Keratinocyte-melanocyte interactions during melanosome transfer. *Pigment Cell Res*, **14**, 236-242.
- Sethi, N. & Kang, Y. (2011) Unravelling the complexity of metastasis - molecular understanding and targeted therapies. *Nat Rev Cancer*, **11**, 735-748.
- Shaikh, W.R., Xiong, M. & Weinstock, M.A. (2012) The contribution of nodular subtype to melanoma mortality in the United States, 1978 to 2007. *Arch Dermatol*, **148**, 30-36.
- Shida, D. et al. (2003) Lysophosphatidic acid (LPA) enhances the metastatic potential of human colon carcinoma DLD1 cells through LPA1. *Cancer Res*, **63**, 1706-1711.
- Shin, K.J. et al. (2009) Lysophosphatidic acid signalling through LPA receptor subtype 1 induces colony scattering of gastrointestinal cancer cells. *J Cancer Res Clin Oncol*, **135**, 45-52.
- Sierko, E. & Wojtukiewicz, M.Z. (2004) Platelets and angiogenesis in malignancy. *Semin Thromb Hemost*, **30**, 95-108.
- Sinha, R. et al. (2012) Cutaneous adverse events associated with vemurafenib in patients with metastatic melanoma: practical advice on diagnosis, prevention and management of the main treatment-related skin toxicities. *Br J Dermatol*, **167**, 987-994.
- Sladden, M.J. et al. (2009) Surgical excision margins for primary cutaneous melanoma. *Cochrane Database Syst Rev*, CD004835.
- Slamon, D.J. et al. (2001) Use of chemotherapy plus a monoclonal antibody against HER2 for metastatic breast cancer that overexpresses HER2. *N Engl J Med*, **344**, 783-792.
- Slingluff, C.L.J. & Seigler, H.F. (1992) "Thin" malignant melanoma: risk factors and clinical management. *Ann Plast Surg*, **28**, 89-94.

- Sluder, G. et al. (2007) A sealed preparation for long-term observations of cultured cells. *CSH Protoc*, **2007**, pdb.prot4660.
- Smalley, K.S. & Sondak, V.K. (2010) Melanoma--an unlikely poster child for personalized cancer therapy. *N Engl J Med*, **363**, 876-878.
- Smirnova, T. & Segall, J.E. (2007) Amoeboid chemotaxis: future challenges and opportunities. *Cell Adh Migr*, **1**, 165-170.
- Smirnova, T. et al. (2012) Phosphoinositide 3-kinase signalling is critical for ErbB3-driven breast cancer cell motility and metastasis. *Oncogene*, **31**, 706-715.
- Smyth, S.S. et al. (2003) Lipid phosphate phosphatases regulate lysophosphatidic acid production and signalling in platelets: studies using chemical inhibitors of lipid phosphate phosphatase activity. *J Biol Chem*, **278**, 43214-43223.
- Snider, A.J. et al. (2010) Epidermal growth factor increases lysophosphatidic acid production in human ovarian cancer cells: roles for phospholipase D2 and receptor transactivation. *Am J Physiol Cell Physiol*, **298**, C163-70.
- Soon, L. et al. (2005) Description and characterization of a chamber for viewing and quantifying cancer cell chemotaxis. *Cell Motil Cytoskeleton*, **62**, 27-34.
- Soon, L.L. (2007) A discourse on cancer cell chemotaxis: where to from here? *IUBMB Life*, **59**, 60-67.
- Sourjik, V. & Berg, H.C. (2002) Receptor sensitivity in bacterial chemotaxis. *PNAS*, **99**, 123-127.
- Spatz, A., Batist, G. & Eggermont, A.M. (2010) The biology behind prognostic factors of cutaneous melanoma. *Curr Opin Oncol*, **22**, 163-168.
- Stahle, M. et al. (2003) Mechanisms in LPA-induced tumour cell migration: critical role of phosphorylated ERK. *J Cell Sci*, **116**, 3835-3846.

- Stathopoulos, G.T. et al. (2008) Host nuclear factor-kappaB activation potentiates lung cancer metastasis. *Mol Cancer Res*, **6**, 364-371.
- Steeg, P.S. & Theodorescu, D. (2008) Metastasis: a therapeutic target for cancer. *Nat Clin Pract Oncol*, **5**, 206-219.
- Stewart, D.J., Whitney, S.N. & Kurzrock, R. (2010) Equipose lost: ethics, costs, and the regulation of cancer clinical research. *J Clin Oncol*, **28**, 2925-2935.
- Stracke, M.L. et al. (1989) The type I insulin-like growth factor receptor is a motility receptor in human melanoma cells. *J Biol Chem*, **264**, 21544-21549.
- Stracke, M.L. et al. (1992) Identification, purification, and partial sequence analysis of autotaxin, a novel motility-stimulating protein. *J Biol Chem*, **267**, 2524-2529.
- Sturge, J. et al. (2003) GPI-anchored uPAR requires Endo180 for rapid directional sensing during chemotaxis. *J Cell Biol*, **162**, 789-794.
- Sturm, A. et al. (1999) Modulation of intestinal epithelial wound healing in vitro and in vivo by lysophosphatidic acid. *Gastroenterology*, **117**, 368-377.
- Subramanian, P. et al. (2010) Lysophosphatidic acid receptors LPA1 and LPA3 promote CXCL12-mediated smooth muscle progenitor cell recruitment in neointima formation. *Circ Res*, **107**, 96-105.
- Sussman, M. et al. (1967) The effect of actinomycin D on cellular slime mold morphogenesis. *Biochem Biophys Res Commun*, **26**, 353-359.
- Svobodova, A. & Vostalova, J. (2010) Solar radiation induced skin damage: review of protective and preventive options. *Int J Radiat Biol*, **86**, 999-1030.
- Swaney, J.S. et al. (2010) A novel, orally active LPA(1) receptor antagonist inhibits lung fibrosis in the mouse bleomycin model. *Br J Pharmacol*, **160**, 1699-1713.

- Swetter, S.M. et al. (2005) Increasing incidence of lentigo maligna melanoma subtypes: northern California and national trends 1990-2000. *J Invest Dermatol*, **125**, 685-691.
- Tabchy, A., Tigyi, G. & Mills, G.B. (2011) Location, location, location: a crystal-clear view of autotaxin saturating LPA receptors. *Nat Struct Mol Biol*, **18**, 117-118.
- Taketo, M.M. (2012) Roles of stromal microenvironment in colon cancer progression. *J Biochem*, **151**, 477-481.
- Tanaka, T. et al. (2009) Formation of lysophosphatidic acid, a wound-healing lipid, during digestion of cabbage leaves. *Biosci Biotechnol Biochem*, **73**, 1293-1300.
- Tang, A. et al. (1994) E-cadherin is the major mediator of human melanocyte adhesion to keratinocytes in vitro. *J Cell Sci*, **107**, 983-992.
- Tang, H. et al. (2013) Loss of Scar/WAVE Complex Promotes N-WASP- and FAK-Dependent Invasion. *Curr Biol*, **23**, 107-117.
- Tao, Y., Bazan, H.E. & Bazan, N.G. (1995) Platelet-activating factor induces the expression of metalloproteinases-1 and -9, but not -2 or -3, in the corneal epithelium. *Invest Ophthalmol Vis Sci*, **36**, 345-354.
- Tas, F. et al. (2012) Clinical and prognostic significance of coagulation assays in melanoma. *Melanoma Res*, **22**, 368-375.
- Taylor, M.L. et al. (2001) The Kit-activating mutation B816V enhances stem cell factor--dependent chemotaxis. *Blood*, **98**, 1195-1199.
- Theveneau, E. et al. (2010) Collective chemotaxis requires contact-dependent cell polarity. *Dev Cell*, **19**, 39-53.
- Theveneau, E. & Mayor, R. (2012) Neural crest delamination and migration: from epithelium-to-mesenchyme transition to collective cell migration. *Dev Biol*, **366**, 34-54.

- Tigyi, G. & Miledi, R. (1992) Lysophosphatidates bound to serum albumin activate membrane currents in *Xenopus* oocytes and neurite retraction in PC12 pheochromocytoma cells. *J Biol Chem*, **267**, 21360-21367.
- Timpson, P. et al. (2011) Spatial regulation of RhoA activity during pancreatic cancer cell invasion driven by mutant p53. *Cancer Res*, **71**, 747-757.
- Toetsch, S. et al. (2009) The evolution of chemotaxis assays from static models to physiologically relevant platforms. *Integr Biol (Camb)*, **1**, 170-181.
- Tomas, M. et al. (2003) Protective effects of lysophosphatidic acid (LPA) on chronic ethanol-induced injuries to the cytoskeleton and on glucose uptake in rat astrocytes. *J Neurochem*, **87**, 220-229.
- Torisawa, Y.S. et al. (2010) Microfluidic platform for chemotaxis in gradients formed by CXCL12 source-sink cells. *Integr Biol (Camb)*, **2**, 680-686.
- Tortora, G., Ciardiello, F. & Gasparini, G. (2008) Combined targeting of EGFR-dependent and VEGF-dependent pathways: rationale, preclinical studies and clinical applications. *Nat Clin Pract Oncol*, **5**, 521-530.
- Trotter, M.J. (2011) Melanoma margin assessment. *Clin Lab Med*, **31**, 289-300.
- Troxel, D.B. (2004) Error in surgical pathology. *Am J Surg Pathol*, **28**, 1092-1095.
- Tucker, M.A. (2009) Melanoma epidemiology. *Hematol Oncol Clin North Am*, **23**, 383-95, vii.
- Ullrich, A. & Schlessinger, J. (1990) Signal transduction by receptors with tyrosine kinase activity. *Cell*, **61**, 203-212.
- Uong, A. & Zon, L.I. (2010) Melanocytes in development and cancer. *J Cell Physiol*, **222**, 38-41.
- Valverde, P. et al. (1995) Variants of the melanocyte-stimulating hormone receptor gene are associated with red hair and fair skin in humans. *Nat Genet*, **11**, 328-330.

- Van Corven, E.J. et al. (1989) Lysophosphatidate-induced cell proliferation: identification and dissection of signalling pathways mediated by G proteins. *Cell*, **59**, 45-54.
- Van Corven, E.J. et al. (1992) Mitogenic action of lysophosphatidic acid and phosphatidic acid on fibroblasts. Dependence on acyl-chain length and inhibition by suramin. *Biochem J*, **281**, 163-169.
- Van der Bend, R.L. et al. (1992) Identification of a putative membrane receptor for the bioactive phospholipid, lysophosphatidic acid. *EMBO J*, **11**, 2495-2501.
- Van Dijk, M.C. et al. (2008) Expert review remains important in the histopathological diagnosis of cutaneous melanocytic lesions. *Histopathology*, **52**, 139-146.
- Van Dyke, T. & Jacks, T. (2002) Cancer modeling in the modern era: progress and challenges. *Cell*, **108**, 135-144.
- Van Haastert, P.J. & Devreotes, P.N. (2004) Chemotaxis: signalling the way forward. *Nat Rev Mol Cell Biol*, **5**, 626-634.
- Van Meeteren, L.A. et al. (2006) Autotaxin, a secreted lysophospholipase D, is essential for blood vessel formation during development. *Mol Cell Biol*, **26**, 5015-5022.
- Van Muijen, G.N. et al. (1991) Establishment and characterization of a human melanoma cell line (MV3) which is highly metastatic in nude mice. *Int J Cancer*, **48**, 85-91.
- Veltman, D.M. & Van Haastert, P.J. (2008) The role of cGMP and the rear of the cell in Dictyostelium chemotaxis and cell streaming. *J Cell Sci*, **121**, 120-127.
- Viros, A. et al. (2008) Improving melanoma classification by integrating genetic and morphologic features. *PLoS Med*, **5**, e120.

- Volk, T., Geiger, B. & Raz, A. (1984) Motility and adhesive properties of high- and low-metastatic murine neoplastic cells. *Cancer Res*, **44**, 811-824.
- Vultur, A. & Herlyn, M. (2009) Cracking the system: melanoma complexity demands new therapeutic approaches. *Pigment Cell Melanoma Res*, **22**, 4-5.
- Wakelam, M.J. (2013) Systems biology of phosphatidic-acid-mediated signalling.
- Wakelam, M.J. & Clark, J. (2011) Methods for analyzing phosphoinositides using mass spectrometry. *Biochim Biophys Acta*, **1811**, 758-762.
- Wakelam, M.J., Powner, D.J. & Pettitt, T.R. (2008) Determination of phospholipase D, lysophospholipase D and DG kinase signalling pathways in disease states by mass spectrometry. *Adv Enzyme Regul*, **48**, 254-260.
- Walker, G.J. & Hayward, N.K. (2002) Pathways to Melanoma Development: Lessons from the mouse. *JID*, **119**, 783-792.
- Walker, G.J. et al. (2011) Modelling melanoma in mice. *Pigment Cell Melanoma Res*, **24**, 1158-1176.
- Wang, S.J. et al. (2004a) Differential effects of EGF gradient profiles on MDA-MB-231 breast cancer cell chemotaxis. *Exp Cell Res*, **300**, 180-189.
- Wang, W. et al. (2004b) Identification and testing of a gene expression signature of invasive carcinoma cells within primary mammary tumours. *Cancer Res*, **64**, 8585-8594.
- Wang, W. et al. (2002) Single cell behavior in metastatic primary mammary tumours correlated with gene expression patterns revealed by molecular profiling. *Cancer Res*, **62**, 6278-6288.
- Ware, M.F., Wells, A. & Lauffenburger, D.A. (1998) Epidermal growth factor alters fibroblast migration speed and directional persistence reciprocally and in a matrix-dependent manner. *J Cell Sci*, **111**, 2423-2432.

- Warren, R. et al. (1991) Age, sunlight, and facial skin: a histologic and quantitative study. *J Am Acad Dermatol*, **25**, 751-760.
- Watts, T.L. & Cui, R. (2012) Malignant melanoma induces migration and invasion of adult mesenchymal stem cells. *Laryngoscope*, **122**, 2769-2772.
- Weaver, V.M. et al. (1997) Reversion of the malignant phenotype of human breast cells in three-dimensional culture and in vivo by integrin blocking antibodies. *J Cell Biol*, **137**, 231-245.
- Wehrle-Haller, B. (2003) The role of Kit-ligand in melanocyte development and epidermal homeostasis. *Pigment Cell Res*, **16**, 287-296.
- Wells, A. (2000) Tumor invasion: role of growth factor-induced cell motility. *Adv Cancer Res*, **78**, 31-101.
- Wells, A. et al. (1998) Epidermal growth factor receptor-mediated motility in fibroblasts. *Microsc Res Tech*, **43**, 395-411.
- Wetzel, R. et al. (1980) Temperature behaviour of human serum albumin. *Eur J Biochem*, **104**, 469-478.
- Weyers, W. et al. (1999) Classification of cutaneous malignant melanoma: a reassessment of histopathologic criteria for the distinction of different types. *Cancer*, **86**, 288-299.
- Wich, L.G. et al. (2009) Developing a multidisciplinary prospective melanoma biospecimen repository to advance translational research. *Am J Transl Res*, **1**, 35-43.
- Widmer, D.S. et al. (2012) Systematic classification of melanoma cells by phenotype-specific gene expression mapping. *Pigment Cell Melanoma Res*, **25**, 343-353.
- Wilkie, A.L., Jordan, S.A. & Jackson, I.J. (2002) Neural crest progenitors of the melanocyte lineage: coat colour patterns revisited. *Development*, **129**, 3349-3357.

- Wolf, K. et al. (2003) Compensation mechanism in tumour cell migration: mesenchymal-amoeboid transition after blocking of pericellular proteolysis. *J Cell Biol*, **160**, 267-277.
- Wu, L. et al. (1995) The G protein beta subunit is essential for multiple responses to chemoattractants in Dictyostelium. *J Cell Biol*, **129**, 1667-1675.
- Wyckoff, J. et al. (2004) A paracrine loop between tumour cells and macrophages is required for tumour cell migration in mammary tumours. *Cancer Res*, **64**, 7022-7029.
- Wyckoff, J.B. et al. (2000a) A critical step in metastasis: in vivo analysis of intravasation at the primary tumour. *Cancer Res*, **60**, 2504-2511.
- Wyckoff, J.B., Segall, J.E. & Condeelis, J.S. (2000b) The collection of the motile population of cells from a living tumour. *Cancer Res*, **60**, 5401-5404.
- Wyckoff, J.B. et al. (2007) Direct visualization of macrophage-assisted tumour cell intravasation in mammary tumours. *Cancer Res*, **67**, 2649-2656.
- Xu, K.P., Yin, J. & Yu, F.S. (2007) Lysophosphatidic acid promoting corneal epithelial wound healing by transactivation of epidermal growth factor receptor. *Invest Ophthalmol Vis Sci*, **48**, 636-643.
- Xue, C. et al. (2006) Epidermal growth factor receptor overexpression results in increased tumour cell motility in vivo coordinately with enhanced intravasation and metastasis. *Cancer Res*, **66**, 192-197.
- Xue, J. et al. (2010) Effects of lysophosphatidic acid and its receptors LPA(1/3) on radiation pneumonitis. *Oncol Rep*, **24**, 1515-1520.
- Yamada, K.M. & Cukierman, E. (2007) Modeling tissue morphogenesis and cancer in 3D. *Cell*, **130**, 601-610.

- Yamada, T. et al. (2004) Lysophosphatidic acid (LPA) in malignant ascites stimulates motility of human pancreatic cancer cells through LPA1. *J Biol Chem*, **279**, 6595-6605.
- Ye, Q., Kantonen, S. & Gomez-Cambronero, J. (2012) Serum Deprivation Confers the MDA-MB-231 Breast Cancer Line with an EGFR/JAK3/PLD2 System That Maximizes Cancer Cell Invasion. *J Mol Biol*,
- Yoshida, K. & Soldati, T. (2006) Dissection of amoeboid movement into two mechanically distinct modes. *J Cell Sci*, **119**, 3833-3844.
- Zaki, M., Andrew, N. & Insall, R.H. (2006) Entamoeba histolytica cell movement: a central role for self-generated chemokines and chemorepellents. *Proc Natl Acad Sci U S A*, **103**, 18751-18756.
- Zalaudek, I. et al. (2008) Three Roots of Melanoma. *Arch Dermatol*, **144**, 1375-1379.
- Zbytek, B. et al. (2008) Current concepts of metastasis in melanoma. *Expert Rev Dermatol*, **3**, 569-585.
- Zengel, P. et al. (2011) mu-Slide Chemotaxis: a new chamber for long-term chemotaxis studies. *BMC Cell Biol*, **12**, 21.
- Zhang, T. et al. (2006) Preferential involvement of CX chemokine receptor 4 and CX chemokine ligand 12 in T-cell migration toward melanoma cells. *Cancer Biol Ther*, **5**, 1304-1312.
- Zicha, D. et al. (1998) Chemotaxis of macrophages is abolished in the Wiskott-Aldrich syndrome. *Br J Haematol*, **101**, 659-665.
- Zicha, D., Dunn, G. & Jones, G. (1997) Analyzing chemotaxis using the Dunn direct-viewing chamber. *Methods Mol Biol*, **75**, 449-457.
- Zicha, D. & Dunn, G.A. (1995) Are growth factors chemotactic agents? *Exp Cell Res*, **221**, 526-529.

- Zicha, D., Dunn, G.A. & Brown, A.F. (1991) A new direct-viewing chemotaxis chamber. *J Cell Sci*, **99**, 769-775.
- Zigmond, S.H. (1977) Ability of polymorphonuclear leukocytes to orient in gradients of chemotactic factors. *J Cell Biol*, **75**, 606-616.
- Zigmond, S.H., Foxman, E.F. & Segall, J.E. (2001) Chemotaxis assays for eukaryotic cells. *Curr Protoc Cell Biol*, **Chapter 12**, Unit 12.1.
- Zigmond, S.H. & Hirsch, J.G. (1973) Leukocyte locomotion and chemotaxis. New methods for evaluation, and demonstration of a cell-derived chemotactic factor. *J Exp Med*, **137**, 387-410.
- Zuber, T.J. (2002) Punch Biopsy of the Skin. *Am Family Phys*, **65**, 1155-1158.

Appendices

Cell line	Age	Sex	Subtype & Site	Breslow thickness (mm)	Biological stage	BRAF	PTEN	N-ras	c-KIT	CDK4
WM35	24	Female	SSM Scalp	0.69	RGP	V600E	Mu	WT	WT	WT
WM278	62	Female	Nodular M	3.7	VGP	V600E	Hem Del	WT	WT	WT
WM98-1	N/A	N/A	N/A	N/A	VGP	N/A	N/A	N/A	N/A	N/A
WM239A	N/A	N/A	Groin lymph node	N/A	MM	N/A	N/A	N/A	N/A	N/A
WM852	60	Male	Skin metastasis	1.2	MM	WT	Hem Del	61R	WT	WT
WM1158	32	Male	Lymph node	2.75	MM	V600E	Hem Del	WT	WT	WT

Figure 9-1 Appendix: Cell line characterisation

Cell lines acquired from collaborator Prof Dot Bennett through the Wellcome Trust Genomics Cell Bank. Sequencing performed by K Nathanson Lab. Information presented here adapted from Meenhard Herlyn's and Dot Bennet's cell bank holding websites.



Research & Development
R&D Management Office
1st Floor, Tennent Institute
Western Infirmary
GLASGOW G11 6NT
Tel: 0141 232 9447

Our Ref: EP/BR
Enquiries to: Dr Erica Packard
Direct Line: 0141 211 8544
e-mail: Erica.packard@ggc.scot.nhs.uk

4th June 2010

Dr Robert Jones
Consultant Medical Oncologist
BWoSCC
1053 Great Western Road
Glasgow
G12 0YN

R&D Management Approval

Dear Dr Jones

R&D Reference: GN09ON587

GG&C Sites: Western Infirmary, Southern General Hospital, Glasgow Royal Infirmary, Gartnavel General Hospital, Stobhill Hospital and Victoria Infirmary

Chief Investigator: Dr R Jones

Project Title: A pilot study investigating chemotaxis and its effect on the motility of human skin cancer cells: A Clinical Sample Collection Programme

Protocol No: Version 2.0, dated 12th February 2010

I am pleased to confirm that Greater Glasgow & Clyde Health Board is now able to grant **Management Approval** for the above study.

As a condition of this approval the following information is required during the lifespan of the project:

1. SAES/SUSARS – If the study is a **Clinical Trial** as defined by the Medicines for Human Use Clinical Trial Regulations, 2004 (CTIMP only)
2. Recruitment Numbers on a quarterly basis (not required for commercial trials)
3. Any change of Staff working on the project named on the ethics form
4. Change of CI
5. Amendments – Protocol/CRF etc
6. Notification of when the Trial / study has ended
7. Final Report
8. Copies of Publications & Abstracts

Please add this approval to your study file as this letter may be subject to audit and monitoring.

Yours sincerely


Dr Erica Packard
Research Co-ordinator

Cc: Liz-Anne Lewsley, Project Manager, BWoSCC
Jan Wallis, Regulatory Administrator, BWoSCC

Delivering better health

www.nhs.gov.uk

Figure 9-2 Appendix: R&D project approval
R&D approval letter for fresh melanoma tissue collection

9.1.1 DECLARATION OF HELSINKI

9.1.2 WORLD MEDICAL ASSOCIATION DECLARATION OF HELSINKI

9.1.3 Ethical Principles for Medical Research Involving Human Subjects

Adopted by the 18th WMA General Assembly
Helsinki, Finland, June 1964
and amended by the
29th WMA General Assembly, Tokyo, Japan, October 1975
35th WMA General Assembly, Venice, Italy, October 1983
41st WMA General Assembly, Hong Kong, September 1989
48th WMA General Assembly, Somerset West, Republic of South Africa, October 1996
and the
52nd WMA General Assembly, Edinburgh, Scotland, October 2000

9.1.4 A. INTRODUCTION

1. The World Medical Association has developed the Declaration of Helsinki as a statement of ethical principles to provide guidance to physicians and other participants in medical research involving human subjects. Medical research involving human subjects includes research on identifiable human material or identifiable data.
2. It is the duty of the physician to promote and safeguard the health of the people. The physician's knowledge and conscience are dedicated to the fulfilment of this duty.
3. The Declaration of Geneva of the World Medical Association binds the physician with the words, "The health of my patient will be my first consideration," and the International Code of Medical Ethics declares that, "A physician shall act only in the patient's interest when providing medical care which might have the effect of weakening the physical and mental condition of the patient."
4. Medical progress is based on research which ultimately must rest in part on experimentation involving human subjects.
5. In medical research on human subjects, considerations related to the well-being of the human subject should take precedence over the interests of science and society.
6. The primary purpose of medical research involving human subjects is to improve prophylactic, diagnostic and therapeutic procedures and the understanding of the etiology and pathogenesis of disease. Even the best proven prophylactic, diagnostic, and therapeutic methods must continuously be challenged through research for their effectiveness, efficiency, accessibility and quality.
7. In current medical practice and in medical research, most prophylactic, diagnostic and therapeutic procedures involve risks and burdens.
8. Medical research is subject to ethical standards that promote respect for all human beings and protect their health and rights. Some research populations are

vulnerable and need special protection. The particular needs of the economically and medically disadvantaged must be recognised. Special attention is also required for those who cannot give or refuse consent for themselves, for those who may be subject to giving consent under duress, for those who will not benefit personally from the research and for those for whom the research is combined with care.

9. Research Investigators should be aware of the ethical, legal and regulatory requirements for research on human subjects in their own countries as well as applicable international requirements. No national ethical, legal or regulatory requirement should be allowed to reduce or eliminate any of the protections for human subjects set forth in this Declaration.

9.1.5 B. BASIC PRINCIPLES FOR ALL MEDICAL RESEARCH

10. It is the duty of the physician in medical research to protect the life, health, privacy, and dignity of the human subject.

11. Medical research involving human subjects must conform to generally accepted scientific principles, be based on a thorough knowledge of the scientific literature, other relevant sources of information, and on adequate laboratory and, where appropriate, animal experimentation.

12. Appropriate caution must be exercised in the conduct of research which may affect the environment, and the welfare of animals used for research must be respected.

13. The design and performance of each experimental procedure involving human subjects should be clearly formulated in an experimental protocol. This protocol should be submitted for consideration, comment, guidance, and where appropriate, approval to a specially appointed ethical review committee, which must be independent of the investigator, the sponsor or any other kind of undue influence. This independent committee should be in conformity with the laws and regulations of the country in which the research experiment is performed. The committee has the right to monitor ongoing trials. The researcher has the obligation to provide monitoring information to the committee, especially any serious adverse events. The researcher should also submit to the committee, for review, information regarding funding, sponsors, institutional affiliations, other potential conflicts of interest and incentives for subjects.

14. The research protocol should always contain a statement of the ethical considerations involved and should indicate that there is compliance with the principles enunciated in this Declaration.

15. Medical research involving human subjects should be conducted only by scientifically qualified persons and under the supervision of a clinically competent medical person. The responsibility for the human subject must always rest with a medically qualified person and never rest on the subject of the research, even though the subject has given consent.

16. Every medical research project involving human subjects should be preceded by careful assessment of predictable risks and burdens in comparison with foreseeable benefits to the subject or to others. This does not preclude the participation of healthy volunteers in medical research. The design of all studies should be publicly available.

17. Physicians should abstain from engaging in research projects involving human subjects unless they are confident that the risks involved have been adequately assessed and can be satisfactorily managed. Physicians should cease any

investigation if the risks are found to outweigh the potential benefits or if there is conclusive proof of positive and beneficial results.

18. Medical research involving human subjects should only be conducted if the importance of the objective outweighs the inherent risks and burdens to the subject. This is especially important when the human subjects are healthy volunteers.

19. Medical research is only justified if there is a reasonable likelihood that the populations in which the research is carried out stand to benefit from the results of the research.

20. The subjects must be volunteers and informed participants in the research project.

21. The right of research subjects to safeguard their integrity must always be respected. Every precaution should be taken to respect the privacy of the subject, the confidentiality of the patient's information and to minimise the impact of the study on the subject's physical and mental integrity and on the personality of the subject.

22. In any research on human beings, each potential subject must be adequately informed of the aims, methods, sources of funding, any possible conflicts of interest, institutional affiliations of the researcher, the anticipated benefits and potential risks of the study and the discomfort it may entail. The subject should be informed of the right to abstain from participation in the study or to withdraw consent to participate at any time without reprisal. After ensuring that the subject has understood the information, the physician should then obtain the subject's freely-given informed consent, preferably in writing. If the consent cannot be obtained in writing, the non-written consent must be formally documented and witnessed.

23. When obtaining informed consent for the research project the physician should be particularly cautious if the subject is in a dependent relationship with the physician or may consent under duress. In that case the informed consent should be obtained by a well-informed physician who is not engaged in the investigation and who is completely independent of this relationship.

24. For a research subject who is legally incompetent, physically or mentally incapable of giving consent or is a legally incompetent minor, the investigator must obtain informed consent from the legally authorised representative in accordance with applicable law. These groups should not be included in research unless the research is necessary to promote the health of the population represented and this research cannot instead be performed on legally competent persons.

25. When a subject deemed legally incompetent, such as a minor child, is able to give assent to decisions about participation in research, the investigator must obtain that assent in addition to the consent of the legally authorised representative.

26. Research on individuals from whom it is not possible to obtain consent, including proxy or advance consent, should be done only if the physical/mental condition that prevents obtaining informed consent is a necessary characteristic of the research population. The specific reasons for involving research subjects with a condition that renders them unable to give informed consent should be stated in the experimental protocol for consideration and approval of the review committee. The protocol should state that consent to remain in the research should be obtained as soon as possible from the individual or a legally authorised surrogate.

27. Both authors and publishers have ethical obligations. In publication of the results of research, the investigators are obliged to preserve the accuracy of the

results. Negative as well as positive results should be published or otherwise publicly available. Sources of funding, institutional affiliations and any possible conflicts of interest should be declared in the publication. Reports of experimentation not in accordance with the principles laid down in this Declaration should not be accepted for publication.

9.1.6 C. ADDITIONAL PRINCIPLES FOR MEDICAL RESEARCH COMBINED WITH MEDICAL CARE

28. The physician may combine medical research with medical care, only to the extent that the research is justified by its potential prophylactic, diagnostic or therapeutic value. When medical research is combined with medical care, additional standards apply to protect the patients who are research subjects.

29. The benefits, risks, burdens and effectiveness of a new method should be tested against those of the best current prophylactic, diagnostic, and therapeutic methods. This does not exclude the use of placebo, or no treatment, in studies where no proven prophylactic, diagnostic or therapeutic method exists.

30. At the conclusion of the study, every patient entered into the study should be assured of access to the best proven prophylactic, diagnostic and therapeutic methods identified by the study.

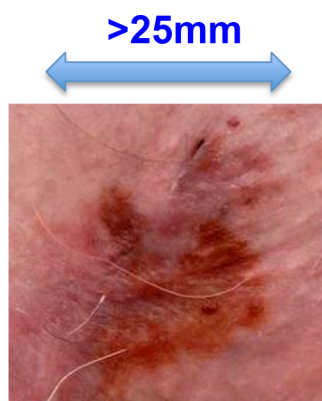
31. The physician should fully inform the patient which aspects of the care are related to the research. The refusal of a patient to participate in a study must never interfere with the patient-physician relationship.

32. In the treatment of a patient, where proven prophylactic, diagnostic and therapeutic methods do not exist or have been ineffective, the physician, with informed consent from the patient, must be free to use unproven or new prophylactic, diagnostic and therapeutic measures, if in the physician's judgment it offers hope of saving life, re-establishing health or alleviating suffering. Where possible, these measures should be made the object of research, designed to evaluate their safety and efficacy. In all cases, new information should be recorded and, where appropriate, published. The other relevant guidelines of this Declaration should be followed.

Figure 9-3 Appendix: Declaration of Helsinki

Melanoma Chemotaxis Study

An investigation into the role of chemotaxis gradients and their ability to drive melanoma cell invasion: A clinical sample collection programme



Suitable samples include any of the following:

- 1) Primary melanoma >25mm diameter
- 2) Any cutaneous melanoma metastasis
- 3) Melanomas that have been diagnosed by incisional biopsy and require referral to a Plastic Surgeon for excision

If you identify a suitable sample then please contact the study co-ordinator Dr Andy Muinonen-Martin: andrew.muinonen-martin@glasgow.ac.uk or 0141 330 3698/ 07973 441738. Please do not email patient information. I will contact you back directly to discuss the case in more detail in order to consider whether the subject is suitable for the study.

This research will be carried out under the direction of a Consultant Dermatopathologist to ensure that there is no risk of undermining the patient's diagnosis and management. The acquisition process will follow GGC policy and procedures for the use of human tissue in research with the assistance of the GGC Bio-repository staff.

Figure 9-4 Appendix: Melanoma tissue collection advert with inclusion criteria

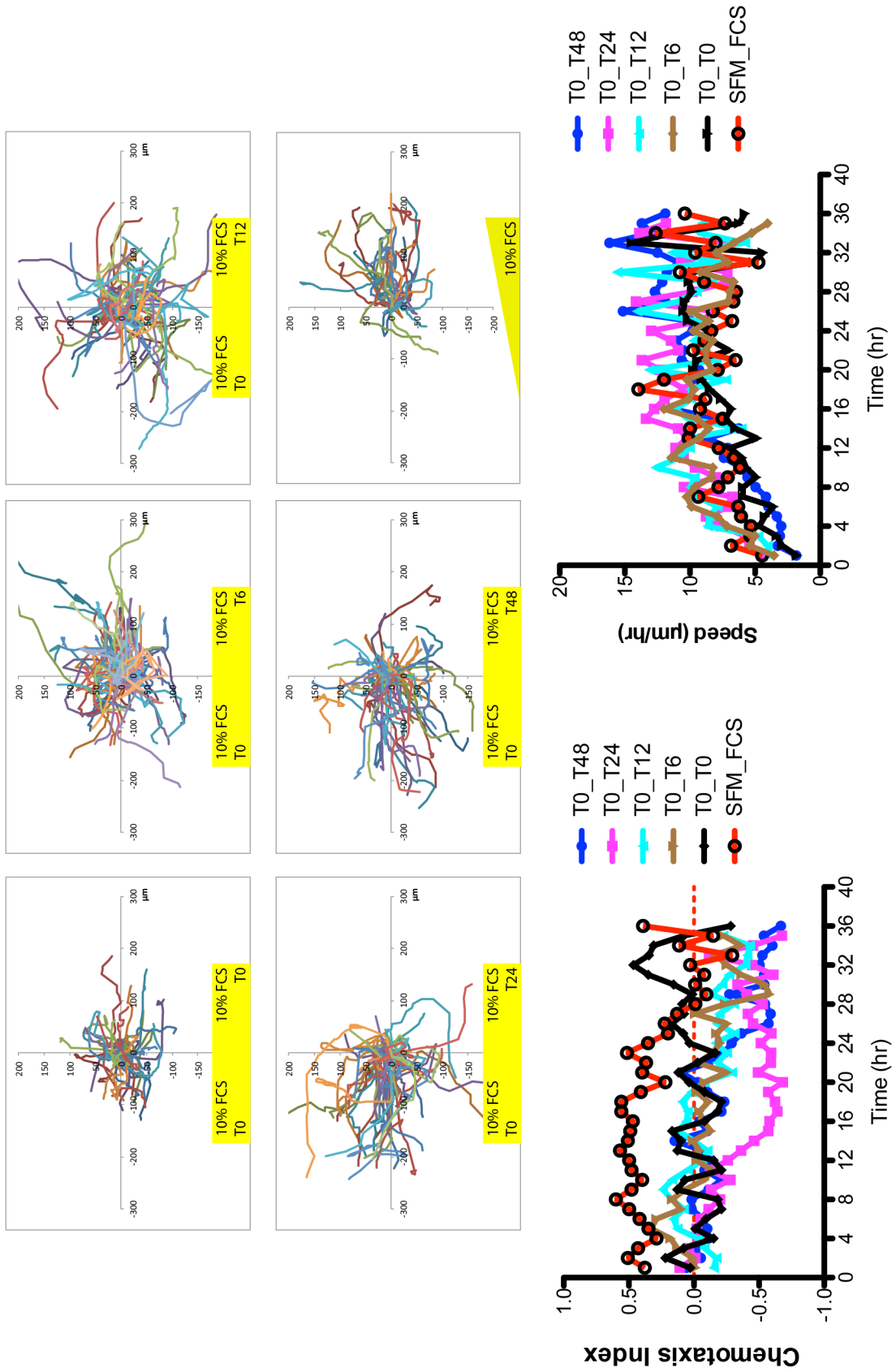


Figure 9-5 Appendix: WM239A dispersal in conditioned media – all time-points

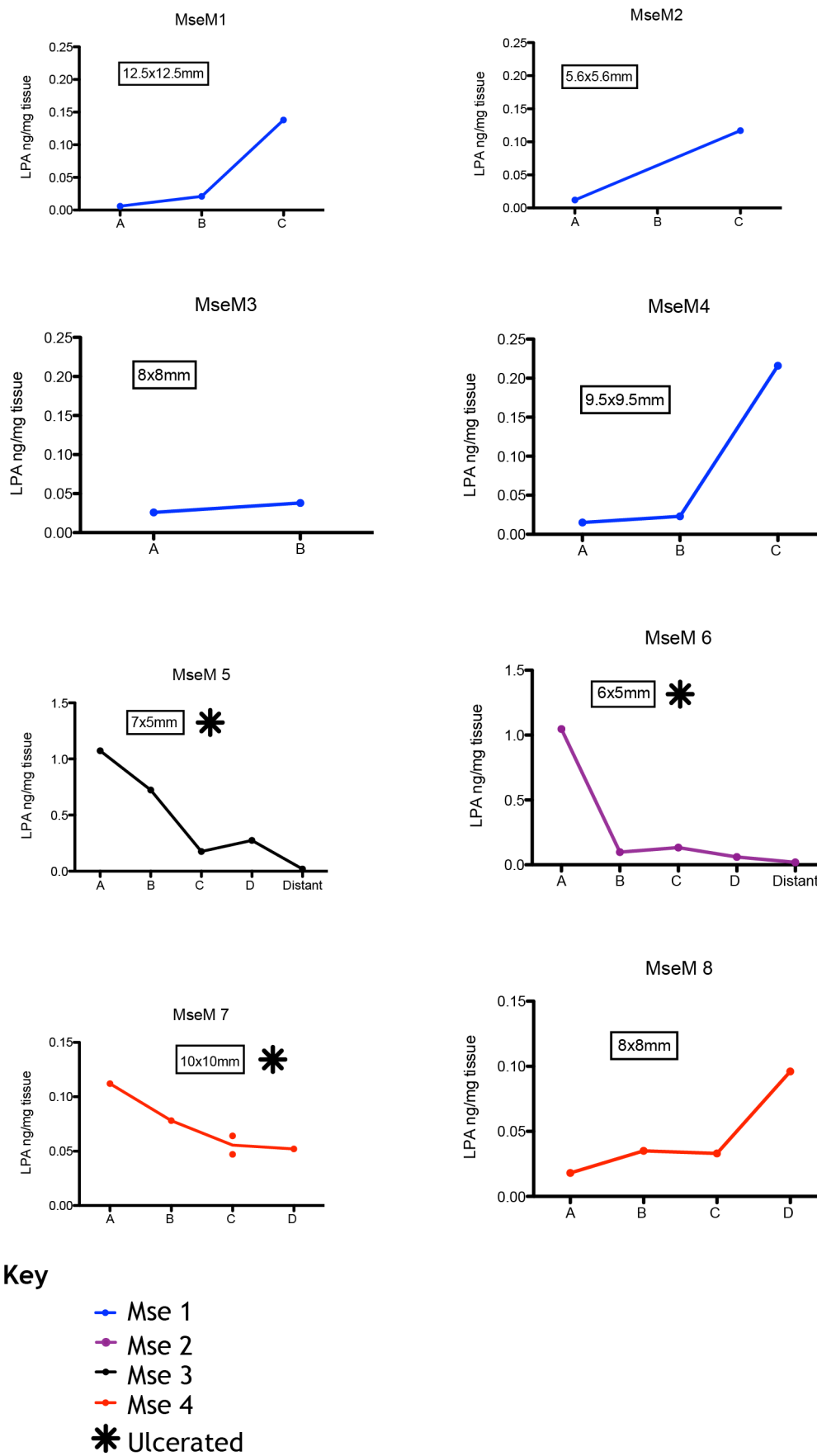


Figure 9-6 Appendix: Individual murine melanoma LPA quantification